

1-1-1997

**Synthesis of organic-inorganic hybrids via ozone chemistry :
synthesis, characterization and mechanical properties of
polystyrene-polyetherimide ABA block copolymers.**

Anthony G. Karandinos
University of Massachusetts Amherst

Follow this and additional works at: https://scholarworks.umass.edu/dissertations_1

Recommended Citation

Karandinos, Anthony G., "Synthesis of organic-inorganic hybrids via ozone chemistry : synthesis, characterization and mechanical properties of polystyrene-polyetherimide ABA block copolymers." (1997). *Doctoral Dissertations 1896 - February 2014*. 971.
<https://doi.org/10.7275/vfss-sh77> https://scholarworks.umass.edu/dissertations_1/971

This Open Access Dissertation is brought to you for free and open access by ScholarWorks@UMass Amherst. It has been accepted for inclusion in Doctoral Dissertations 1896 - February 2014 by an authorized administrator of ScholarWorks@UMass Amherst. For more information, please contact scholarworks@library.umass.edu.



312066 0264 0764 7

SYNTHESIS OF ORGANIC-INORGANIC HYBRIDS VIA OZONE
CHEMISTRY;
SYNTHESIS, CHARACTERIZATION AND MECHANICAL PROPERTIES
OF POLYSTYRENE-POLYETHERIMIDE ABA BLOCK COPOLYMERS

A Dissertation Presented

by

ANTHONY G. KARANDINOS

Submitted to the Graduate School of the University of Massachusetts Amherst
in partial fulfillment of the requirements for the degree of

DOCTOR OF PHILOSOPHY

September 1997

Polymer Science and Engineering

© Copyright by Anthony George Karandinos 1997

All Rights Reserved

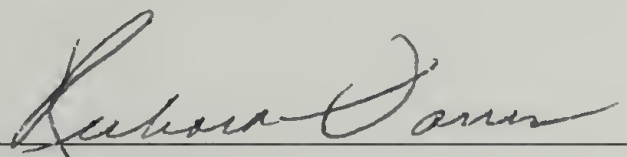
SYNTHESIS OF ORGANIC-INORGANIC HYBRIDS VIA OZONE
CHEMISTRY;
SYNTHESIS, CHARACTERIZATION AND MECHANICAL PROPERTIES
OF POLYSTYRENE-POLYETHERIMIDE ABA BLOCK COPOLYMERS

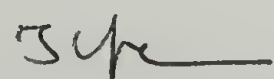
A Dissertation Presented

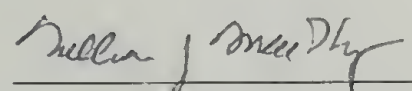
by

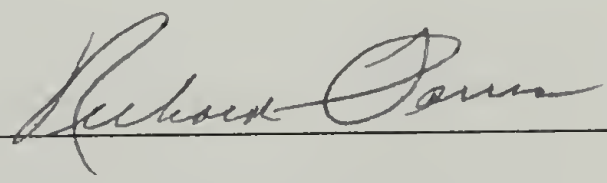
ANTHONY G. KARANDINOS

Approved as to style and content by:


Richard J. Farris, Co-Chair


Thomas J. McCarthy, Co-Chair


William J. MacKnight, Member


Richard J. Farris, Head Polymer
Science and Engineering

This dissertation is dedicated with all my love to the best mother of all,
my Mother

ACKNOWLEDGEMENTS

By the time that these lines will have been laid down on this piece of paper, the end of my career as a graduate student will have commenced. It has been a long scientific odyssey with a plethora of exciting and inspiring moments. I had not realized how lucky I was when I was given the opportunity to attend this program at the University of Massachusetts. It is only now five years later that I look back and I feel content. It is now after five years that I ask myself what I would do if I could turn back the hands of time and the answer is always the same. I would start all over again, at this University, in this program, with exactly the same advisors.

Indeed, the satisfaction I feel today is attributed largely to my advisors. Both Professor Farris (now head of the department) and Professor McCarthy helped me grow as a scientist and as a person. Their patience and their kindness, their criticism and their encouragement, their trust and their understanding helped me to overcome the many frustrations and setbacks that naturally occur on a perplexing journey like this. I could not have chosen better people and better scientists to advise me all these years. The addition of Professor MacKnight as a member of my thesis committee strengthened the scientific circle around me. His advice and comments were always appreciated. I thank them very much. They will always be in my thoughts.

When I came to Amherst to pursue my graduate career, I did not know a single soul. Today, five years later, I have the feeling that there is not anyone that I do not know. Together with classmates, colleagues and friends I shared many good and some not so wonderful times. My classmates (Frank, Bob, Joan, Joanne (the crazy Irish), Alice,

Volker) and many others willing to extend their distinctive individual qualities created a small community that survived through the years. We studied together, we partied together and we worked together. I thank them all. They are embedded in my memory forever.

The many discussions, comments and remarks with my colleagues (Brant, Damo, Erdem, Jahu, Scott, Erik, Geni, Jim, Raul, Kapil), and all the others from Dr. Farris' and Dr. McCarthy's group were always gladly received and appreciated. Jack's help was always there when it was needed. My special friend Socratis occupies a special place in my heart. I thank them all. They will never be forgotten.

My family's love and support has been monumental. I don't know who to thank first and who to thank the most. My mother (Νίκη) has been the light in my life. Her unmatched endurance through the hardship of life, her wisdom, her unsurpassed willingness to sacrifice herself for me and my brother have earned my everlasting respect. Her dreams were not fulfilled until now. My son (Γιώργος, currently in his eighth year) was my best buddy all these years. He always wanted to be a part of my work, to participate in the group meetings, seminars and in the laboratory. His passion to be with me, however, was never completely gratified and I am really regretful for this. His unconditional love and faith in me was always a motivation for achievement. My younger brother (Τάσος) always reassured me that he would be there for me if I ever needed anything. He kept telling me that no distance is far enough to keep us apart in times of need. In fond memory, I would like to point out that it would have been very difficult to be here today without my father-in-law's (Νίκο) endless support. Unfortunately, his life was cut short before his dream (to attend my graduation ceremony)

became a reality. My wife's (Ματα) help, support and comfort was graciously accessible to me all the time. Her warmth and her constant struggle to overcome the overwhelming obstacles I put in front of her every single day, reminded me what marriage is all about. The countless lonely nights she endured all these years, when I was totally absorbed in school, is an illustration of her character, her love and understanding. I thank them so very much. They have shaped my future and they will be in my heart and a part of this work forever.

ABSTRACT

SYNTHESIS OF ORGANIC-INORGANIC HYBRIDS VIA OZONE
CHEMISTRY;

SYNTHESIS, CHARACTERIZATION AND MECHANICAL PROPERTIES
OF POLYSTYRENE-POLYETHERIMIDE ABA BLOCK COPOLYMERS

SEPTEMBER 1997

ANTHONY G. KARANDINOS, B.S., UNIVERSITY OF ALABAMA

BIRMINGHAM

M.S., UNIVERSITY OF MASSACHUSETTS AMHERST

Ph.D., UNIVERSITY OF MASSACHUSETTS AMHERST

Co-directed by: Professor Richard J. Farris and Professor Thomas J. McCarthy

This thesis is divided in two independent parts. The work described in the first part involves the development of a new system for the synthesis of organic-inorganic hybrids utilizing ozone and silicon chemistry.

Polydimethylsiloxane proved to be resistant to ozone over 24 hr. This indicates that the Si-CH₃ group is resistant to ozone attack. Investigation of the ozonization of phenyl-containing siloxane copolymers (PSX-80) suggested that ozone attack takes place in two steps. In the first step ozone attacks and breaks the aromatic ring attached to silicon and subsequently the weakened Si-C moiety is cleaved to form the siloxane group.

Mixtures of phenylsilane with several hydrosiloxanes having variable amount of hydride content were oxidized in order to effect hybridization. Ozonization of phenylsilane (PhSiH_3) generates the inorganic component of the hybrid material, while the organic constituent is due to the siloxane polymers. The ability to vary the hydride concentration on the polymer backbone enables the control of the inorganic content of the hybrid. The hybrid materials exhibit low surface polarity and high thermal stability which depends on the inorganic content of the material.

Application of ozonized hydrosiloxanes as coatings for cellulose paper was investigated. Contact angle and tensile testing data suggested that even the smallest amount of silicone coating dramatically affects the surface behavior and the wet strength of the cellulose paper.

In the second part of this document the mechanical properties of oriented elastomers at low temperatures are investigated. A dramatic increase, to the levels of high performance plastics, was observed in the modulus and strength of the oriented elastomers (~ 32 GPa, 1.2 GPa).

A polyetherimide-b-polystyrene ABA type block copolymer was synthesized and its properties were examined. The weak and brittle behavior of the copolymer indicated that a higher molecular weight soft segment (polystyrene) is necessary in order to perform tensile testing in the elongated state.

TABLE OF CONTENTS

	Page
ACKNOWLEDGMENTS	v
ABSTRACT	viii
LIST OF TABLES	xvi
LIST OF FIGURES	xx
LIST OF SCHEMES	xxix

PART I

SYNTHESIS OF ORGANIC-INORGANIC HYBRIDS VIA OZONE CHEMISTRY

CHAPTER

1.	INTRODUCTION	2
	1.1 Ozone: General discussion	2
	1.2 The ozone molecule: physical and chemical properties	3
	1.3 Organosilicon chemistry	9
	1.4 Research objective and motivation	14
	REFERENCES	17
2.	BACKGROUND	20
	2.1 Ozonization of organosilicon compounds	20

2.2 Synthesis of organic-inorganic hybrids containing silicon; sol-gel chemistry	23
--	----

REFERENCES	30
------------------	----

3. OZONIZATION OF DIMETHYLSILOXANE POLYMERS AND PHENYL CONTAINING COPOLYMERS	32
--	----

3.1 Introduction.....	32
-----------------------	----

3.2 Experimental	33
------------------------	----

3.2.1 Materials	33
-----------------------	----

3.2.2 Experimental setting	36
----------------------------------	----

3.2.3 Analytical techniques and methods	38
---	----

3.2.4 Ozonization of polydimethylsiloxanes	41
--	----

3.2.5 Ozonization of phenyl-containing siloxanes.....	43
---	----

3.2.6 Thin layer chromatography of the isolated solid by-product formed during the ozonization of (80 %) dimethyl-(20 %)-diphenylsiloxane (PSX 80).....	46
---	----

3.2.7 Synthesis of the 2,4-dinitrophenylhydrazone derivatives	47
---	----

3.2.8 Thin layer chromatography of the carbonyl containing by-products formed during the ozonization of (80 %) dimethyl-(20 %)-diphenylsiloxane (PSX 80).....	49
---	----

3.2.9 Ozonization of phenyltrimethylsilane.....	49
---	----

3.3 Results and discussion	50
----------------------------------	----

3.3.1 Polydimethylsiloxanes	50
-----------------------------------	----

3.3.2 (80 %) dimethyl-(20 %)-diphenylsiloxane (PSX 80)	55
--	----

3.3.3 Phenyltrimethylsilane	68
-----------------------------------	----

3.4 Conclusions.....	75
----------------------	----

REFERENCES	79
------------------	----

4. OZONIZATION OF HYDRIDE FUNCTIONALIZED SILOXANES: SYNTHESIS OF ORGANIC-INORGANIC HYBRIDS.....	81
---	----

4.1 Introduction.....	81
-----------------------	----

4.2 Experimental.....	83
4.2.1 Materials	83
4.2.2 Analytical techniques and methods	85
4.2.3 Ozonization of phenylsilane	86
4.2.4 Ozonization of polydimethylsiloxane hydride-terminated(PDMS-H)	89
4.2.5 Ozonization of polydimethylsiloxane-hydride terminated (PDMS-H)/phenylsilane (PhSiH ₃)	89
4.2.6 Condensation of the PDMS-H/PhSiH ₃ mixtures	90
4.2.7 Ozonization of mixtures of poly(dimethyl methylhydro-siloxanes), trimethylsilyl-terminated (PDMMHS) copolymers, and methylhydrosiloxane (PMHS) trimethylsilyl-terminated polymer with various amounts of phenylsilane (PhSiH ₃)	92
4.2.8 Nitrogen adsorption (B.E.T experiments) for surface area calculations.....	94
4.2.9 Qualitative picture of the surface polarity differences between a hybrid powder (PMHS ⁴¹) and an inorganic powder (silica gel).....	95
4.2.10 Determination of activation energy from thermogravimetric analysis for the organic-inorganic hybrids	97
4.3 Results and discussion: Analysis	98
4.3.1 Phenylsilane	98
4.3.2 Polydimethylsiloxane hydride-terminated (PDMS-H)	99
4.3.3 Polydimethylsiloxane hydride-terminated (PDMS-H)/phenylsilane (PhSiH ₃)	107
4.3.4 Poly (dimethyl methylhydrosiloxanes), trimethylsilyl-terminated (PDMMHS) copolymers, and methylhydrosiloxane (PMHS) trimethylsilyl-terminated polymers with various amounts of phenylsilane (PhSiH ₃).....	110
4.4 Results and discussion: Properties.....	118
4.5 Conclusions and future work	143
REFERENCES	145
5. POLYMETHYLHYDROSILOXANE: WET STRENGTHENING COATING FOR PAPER	147
5.1 Introduction.....	147

5.2 Experimental.....	150
5.2.1 General.....	150
5.2.2 Sample preparation	151
5.2.3 Ozonization of the cellulose paper strips impregnated with PMHS.....	153
5.3 Results and discussion	155
5.4 Conclusions.....	182
REFERENCES	184

PART II

SYNTHESIS, CHARACTERIZATION AND MECHANICAL PROPERTIES OF POLYSTYRENE-POLYETHERIMIDE ABA BLOCK COPOLYMER

6. INTRODUCTION	187
6.1 The major routes for obtaining high performance polymers	187
6.1.1 Processing of flexible polymers.....	189
6.1.2 The rigid chains	194
6.2 Objective.....	198
REFERENCES	201
7. BACKGROUND	204
7.1 Rubber and rubberlike materials.....	204
7.2 Phase separation and morphological characteristics for elastomeric block copolymers	206
7.3 Properties of block copolymers	207
7.3.1 Glass transition	207

7.3.2	Modulus-temperature behavior.....	211
7.3.3	Stress-strain behavior and mechanical properties.....	212
7.4	Conclusions	213
	REFERENCES	216
8.	MECHANICAL PROPERTIES OF ORIENTED ELASTOMERS AT LIQUID NITROGEN TEMPERATURES	218
8.1	Introduction.....	218
8.2	Experimental.....	220
8.3	Results and discussion	223
8.4	Conclusions and future work	230
	REFERENCES	240
9.	SYNTHESIS AND CHARACTERIZATION OF POLY (ETHERIMIDE- <i>b</i> -STYRENE) ABA TYPE COPOLYMERS.....	241
9.1	Introduction.....	241
9.2	Materials	242
9.3	Synthesis of the polyetherimide- <i>b</i> -polystyrene copolymer.....	244
9.4	Characterization	248
9.4.1	Thin layer chromatography	248
9.4.2	Fourier transform infrared spectroscopy (FT-IR)	249
9.4.3	¹ H NMR spectroscopy	249
9.4.4	Solubility characteristics.....	253
9.5	Conclusions.....	253
	REFERENCES	256
10.	THERMAL AND MECHANICAL PROPERTIES OF UNORIENTED POLY (ETHERIMIDE- <i>b</i> -STYRENE) ABA COPOLYMER	258
10.1	Introduction.....	258
10.2	Thermal properties.....	259

10.3 Mechanical properties.....263

10.3.1 Sample preparation for tensile testing263

10.4 Conclusion and future work.....269

REFERENCES272

APPENDICES

A. GEL SPUN HIGH MOLECULAR WEIGHT POLY(METHYL METHACRYLATE) AND POLYSTYRENE FIBERS274

B. POLYCARBONATE-POLYETHYLENE TEREPHTHALATE COPOLYMERIZATION BY TRANSESTERIFICATION279

BIBLIOGRAPHY281

LIST OF TABLES

Table	Page
1.1 Properties that can be modified by hybridization of organic and inorganic components.	16
3.1 Relative intensity of characteristic bands of polydimethylsiloxanes normalized to the ν_{as} Si-O-Si (1030 cm^{-1}).	53
3.2 The XPS atomic concentrations of 93.7K and 250K polydimethylsiloxane copolymers in relation to ozonization times. The atomic concentrations were determined for two different XPS take-off angles (15° , 75°).	54
3.3 Thin layer chromatography of a series of standard compounds suspected in the unknown acidic mixtures produced from ozonization reactions.	60
3.4 Size Exclusion Chromatographic data for the (80%) dimethyl-(20%)-diphenylsiloxane ozonized from 13 to 43 hr.	63
4.1 Ozonization conditions of polydimethylsiloxane hydride-terminated (PDMS-H) and mixtures of PDMS-H with PhSiH_3 (phenylsilane).	90
4.2 Tested potential catalysts (dehydrating agents) for the silanol (-SiOH) condensation. All catalysts used in 2% concentration.	91
4.3 Summary of the ozonized hydrosilicones; PDMS-H: polydimethylsiloxane hydride-terminated, PDMMHS: poly(dimethyl methylhydrosiloxane) copolymers, PMHS: polymethylhydrosiloxane. The superscript indicates the weight concentration of the glass forming agent (PhSiH_3). The number at the end of each siloxane copolymer name indicates the molar concentration of methylhydro groups.	119
4.4 Nitrogen adsorption results (silica gel) for surface area calculations (B.E.T experiments). The pressure is reported in torr. The atmospheric pressure was 753.6 and the vacuum pressure 0.05. The sample weight was 0.2515 g. The calculated surface area is $285.3\text{ m}^2/\text{g}$	126

4.5	Nitrogen adsorption results (dimethyl methylhydrosiloxane mixed with 41 % phenylsilane) for surface area calculations (B.E.T experiments). The pressure is reported in torr. The atmospheric pressure was 757.5 and the vacuum pressure 0.2. The sample weight was 0.2335 g. The calculated surface area is 2.8 m ² /g.....	127
4.6	Nitrogen adsorption results (polymethylhydrosiloxane mixed with 41% phenylsilane) for surface area calculation (B.E.T experiments). The pressure is reported in torr. The atmospheric pressure was 759 and the vacuum pressure 0.0. The sample weight was 0.301 g. The calculated surface area is 2.9 m ² /g.	128
4.7	The effect of the glass forming agent (PhSiH ₃) on the T _g of the ozonized siloxanes.	131
4.8	The effect of the glass modifier (PhSiH ₃) on the decomposition temperatures of the hybrid networks. The materials were heated under nitrogen and air at 10 °C/min.....	135
4.9	Calculated activation energies for the 3% methylhydro group-containing siloxane copolymers.	140
4.10	Calculated activation energies for the 30% methylhydro group-containing siloxane copolymers.....	141
4.11	Calculated activation energies for the 50% methylhydro group-containing siloxane copolymers.....	142
5.1	PMHS solutions prepared for impregnation of the paper samples and the weight gained after impregnation and solvent evaporation.	153
5.2	Dynamic contact angle (θ_A , θ_R) dependence on PMHS content of the cellulose paper samples.	156
5.3	Relationship of coating concentration with residue left after degradation of paper samples under nitrogen. R _{mS} is the (%) residue found from the different coated samples. R _{mC} is the (%) residue due to control non ozonized sample. The residual masses were estimated at a temperature of 780 °C.	166
5.4	Increase of linear coefficient of thermal expansion (LCTE) as a function of coating concentration for paper samples.	174
5.5	Linear coefficient of thermal expansion (LCTE) for selected polymers.	178

5.6	Dry and wet tensile properties of non-coated samples (control) cut in three different (including the two principal) directions.	181
5.7	The dry and wet tensile properties of papers coated with different concentration of PMHS polymer.	182
6.1	Comparison between the theoretical and actual values of elastic moduli for selected polymers [4,5,8].	188
7.1	Examples of some elastomeric and non-elastomeric polymers at ambient temperature.	205
8.1	Mechanical properties of the polyurethane samples tested at liquid nitrogen temperature. Pre-elongation is the elongation at room temperature, ϵ : the tensile strain at break, σ : the tensile stress at break, E: the elastic modulus.	227
8.2	Mechanical properties of the Spandex fibers tested at liquid nitrogen temperature. Pre-elongation is the elongation at room temperature, ϵ : the tensile strain at break, σ : the tensile stress at break, E: the elastic modulus.....	231
8.3	Mechanical properties of natural rubber samples tested at liquid nitrogen temperature. Pre-elongation is the elongation at room temperature, ϵ : the tensile strain at break, σ : the tensile stress at break, E: the elastic modulus.....	235
8.4	Mechanical properties of low molecular weight radiation crosslinked polyethylene samples tested at liquid nitrogen temperature. Pre-elongation is the elongation at room temperature, ϵ : the tensile strain at break, σ : the tensile stress at break, E: the elastic modulus.....	237
8.5	Mechanical properties of some common polymer fibers in comparison with rubber and polyurethanes oriented at ambient and tested at liquid nitrogen temperatures.	239
9.1	The solubility characteristics of functionalized polystyrene, polyetherimide and their copolymer. Solubility characteristics were determined using 10 mg/5 ml solvent.....	255

- 10.1 The various decomposition temperatures and the weight loss for the ABA block copolymer and the homopolymers used as A and B segments, T_i : initial decomposition temperature ($\sim 2\%$ wt lost), T_d : temperature at the maximum decomposition rate, T_f : the final decomposition temperature. The W_f is the corresponding residual weight percentage. The temperatures enclosed in parenthesis correspond to the polymer blend.260
- A.1 Mechanical properties of the gel-spun (from acetonitrile) poly (methyl methacrylate) fibers.274
- A.2 Mechanical properties of the gel-spun (from methyl ethyl ketone) poly styrene fibers.279

LIST OF FIGURES

Figure		Page
3.1	Schematic diagram of the ozone generator.....	37
3.2	Schematic representation of the experimental setting. All the connections are either glass or tygon tubing. The ozonator is cooled with tap water.	39
3.3	Reactor used for the bubbling type ozonizations.....	42
3.4	The modified reactor for the “solid state” ozonization.....	44
3.5	Representative FT-IR spectra of a polydimethylsiloxane sample (Mw=770). The top is from the pure (non-ozonized) sample and the bottom is taken from the same sample ozonized for 24 hours.	52
3.6	Acidic concentration as a function of ozonization time. The ozonized material is the (80%) dimethyl-20%-diphenylsiloxane.	58
3.7	FT-IR spectra of the crude isolated by-products from the 43 hr ozonization of the (80%) dimethyl-(20%)-diphenylsiloxane (PSX 80) sample.	59
3.8	FT-IR spectra obtained from a standard sample of oxalic acid (top) and from the purified by-product isolated after the ozonization of (80%) dimethyl-(20%)- diphenylsiloxane (PSX 80) sample.	62
3.9	FT-IR spectra of the (80%) dimethyl-(20%)-diphenylsiloxane (PSX 80) at different ozonization times. The spectra shown at the top was taken from an non-ozonized PSX 80. The 6 hours ozonization spectra is shown in the middle and the 43 hours on the bottom.	64

3.10	Solid state ^{29}Si NMR of the isolated (80%) dimethyl-(20%)-diphenylsiloxane (PSX 80) ozonized for 43 hr. The peak at -23 ppm is due to unreacted $-\text{Si}(\text{CH}_3)_2$ while the peaks at -72 ppm, -82 ppm, and -87 ppm are due to trifunctional and tetrafunctional silicon.	66
3.11	Thermograms obtained from the thermal degradation of pure and ozonized copolymer. The heating rates are: $\beta_1=5\text{ }^\circ\text{C}$, $\beta_2=10\text{ }^\circ\text{C}$ and $\beta_3=20\text{ }^\circ\text{C}$. The isoconversion temperatures are T_1 , T_2 , and T_3 . The activation energy can be calculated from the plot of $\log\beta$ vs. $\log 1/T$, while the average value can be obtained from the various isoconversion plots.....	67
3.12	Ozonization of the (80%) dimethyl-(20%)-diphenylsiloxane (PSX 80). The isolated by-products are glyoxal, oxalic acid and glyoxylic acid.	70
3.13	A plausible mechanism of the ozonization of the (80%) dimethyl-(20%)-diphenylsiloxane (PSX 80). First, a nucleophilic ozone attack on silicon produces a super diperoxide which decomposes to form a peroxide. Peroxide decomposition leads to the final products.	71
3.14	A plausible mechanism of the ozonization of the (80%) dimethyl-(20%)-diphenylsiloxane (PSX 80). First, a nucleophilic ozone attack on phenyl ring produces an unstable molozonide which rearranges to form a more stable ozonide. Ozonide decomposition leads to the formation of the desired products.	72
3.15	Two possible paths for the ozone attack on phenyltrimethylsilane.	73
3.16	FT-IR spectra of the “bubbling” type ozonization (3 hours) of the phenyltrimethylsilane (PTMS). The top spectrum is taken from a non-reacted PTMS sample.	74
3.17	FT-IR spectra of the “mild” type ozonization of phenyltrimethylsilane. The recorded ozonization times are; A : 0 h, B : 1/2 h, C : 7 h, D : 20 h.	77
3.18	Proposed mechanism of the ozonization of a phenyltrimethylsilane.....	78
4.1	Modified reactor for the ozonizations of phenylsilane and hydrosiloxanes and their mixtures.	88
4.2	General procedure for the ozonization/condensation of the various hydrosiloxanes.	93
4.3	Experimental setting for nitrogen adsorption (BET method), in order to determine the surface area of the hybrid powders.	96

4.4	FT-IR spectra of phenylsilane (PhSiH_3); a: non-ozonized, b: 15 minutes ozonized, c: 180 minutes ozonized.	101
4.5	Solid state ^{29}Si NMR spectrum obtained from the phenylsilane (PhSiH_3) ozonized for 3 hours. The SiO_2 peak appears at -102 ppm. The peak at -86 ppm is due to the partial PhSiH_3 oxidation.	102
4.6	TGA thermogram of the ozone oxidized (3 hours) phenylsilane. The heating rate is $10^\circ\text{C}/\text{min}$ under air.	103
4.7	FT-IR spectra of unreacted (bottom) and reacted (top) PDMS-H. The Si-H absorption bands appear at 2128 cm^{-1} (stretching) and 913 cm^{-1} (bending).	104
4.8	Size exclusion chromatography of the ozonized PDMS-H (10% in chloroform). Ozonization time was 2 hrs. The molecular weight increases from 400 (non-ozonized siloxane) to 3,000 for the ozonized.	105
4.9	^1H NMR spectra (20% concentration in CDCl_3 containing 0.03% tetramethylsilane) of the ozonized (top) and non-ozonized (bottom) polydimethylsiloxane hydride-terminated (PDMS-H). The Si-H peak appears at 4.69 ppm and the doublet due to the $-\text{Si}(\text{CH}_3)_2$ at 0.19 and 0.16 ppm.	106
4.10	Representative FT-IR spectra of the ozonized (top) and non-ozonized (bottom) hydride-terminated polydimethylsiloxane mixed with 41% phenylsilane (PDMS-H^{41}).	108
4.11	Solid state ^{29}Si NMR spectrum taken from the PDMS-H^{41} sample. The peak at -23 ppm is due to the $\text{Si}(\text{CH}_3)$ the SiO_2 peak appear at -111 ppm. The peak at -102 ppm is possibly due to some unreacted phenyl residue.	109
4.12	FT-IR spectra of the 3% methylhydrosiloxane copolymer (PDMMHS^3 -3).	113
4.13	Representative FT-IR spectra of three different ozonized hydrosilicones. The top spectrum is taken from the PMHS^{41} ; the one in the middle is due to PDMMHS^{41} -50 and the PDMMHS^{41} -30 spectrum is depicted on the bottom.	114
4.14	Solid state ^{29}Si NMR spectrum of the PDMMHS^{12} -3 sample. The peak at -23 ppm is due to difunctional silicon, $(\text{CH}_3)_2\text{SiO}_2$; the -52 ppm, -68 ppm, -82 ppm and -86 ppm peaks are due to the trifunctional part (RSiO_3).	115

4.15	Solid state ^{29}Si NMR spectrum of the PDMMHS ²⁵ -30 sample. The peak at -23 ppm is due to difunctional silicon, $(\text{CH}_3)_2\text{SiO}_2$; the -40 ppm, -70 ppm, -82 ppm and -88 ppm peaks are due to the trifunctional part (RSiO_3). The peak of the SiO_2 appears at -113 ppm.....	116
4.16	Solid state ^{29}Si NMR spectrum of the PMHS ¹² sample. The peak at -23 ppm is due to difunctional silicon, $(\text{CH}_3)_2\text{SiO}_2$; the -67 ppm, RSiO_3 and the peak at -108 ppm is due to SiO_2	117
4.17	Scanning electron micrograph obtained from a PDMMHS ³ -3 film. The ductile fracture indicates the rubbery nature of the polymer film.....	122
4.18	Scanning electron micrograph obtained from a PDMS-H ⁴¹ film. The polymer film behaves as a hard rubber.	123
4.19	Scanning electron micrograph obtained from a PMHS ⁴¹ film. The brittle and almost featureless fracture is an indication of the high inorganic content.....	124
4.20	Scanning electron microscopy micrographs obtained from silica gel (top) and the hybrid PMHS ⁴¹ powder (bottom).....	125
4.21	Qualitative test for the surface polarity of the hybrid powder. A drop of water colored with potassium permanganate is placed on the surface of a silica gel and the PMHS ⁴¹ hybrid powder. The wetting of the surface is observed with time.....	129
4.22	The effect of the phenylsilane on the glass transition temperature of the various siloxanes. The heating rate was 10 °C/min under N_2	130
4.23	The effect of the glass modifier (PhSiH_3) on the weight loss of the hybrid networks heated under N_2 at 10 °C/min.	132
4.24	Thermogravimetric analysis of the PDMMHS-30/ PhSiH_3 mixtures. The heating rate was 10 °C/min under N_2	133
4.25	Thermogravimetric analysis of the PDMMHS-30/ PhSiH_3 hybrids. The heating rate was 10 °C/min under air.....	134
4.26	The effect of the glass modifier (PhSiH_3) on the decomposition temperature, T_d , of the PDMMHS-30 hybrid networks heated under N_2 and air at 10 °C/min.	136

4.27	The effect of the glass modifier (PhSiH ₃) on the decomposition temperature, T _d , of the PMHS hybrid networks heated under N ₂ and air at 10 °C/min.	137
4.28	Example of isoconversional analysis of TGA thermograms in order to study the kinetics of thermal degradation. The heating rates are, β ₁ : 1°C/min, β ₂ : 5 °C/min, β ₃ : 10 °C/min and β ₄ : 20 °C/min. For a given conversion, four different temperatures are determined (T ₁ , T ₂ , T ₃ , T ₄) and the activation energy can be calculated from a plot of log β vs. 1/T.	138
4.29	Plots of log β (heating rate) vs. 1/T for various conversions (0.1-0.9) during the thermal degradation of the PDMMHS ³ -3, PDMMHS ³ -30 and PDMMHS ³ -50. The activation energy is calculated from the slopes and is averaged over the chosen conversions.	139
5.1	Experimental setting for humidity control. The CH ₃ COOK is the preconditioning salt (22 ± 1% RH) and the K ₂ CO ₃ is the conditioning salt (43 ± 0% RH). Temperature range 25 ± 3 °C.....	154
5.2	ATR-IR spectra of the control (non-impregnated) paper strip. The absence of carbonyl absorption bands indicates that no appreciable ozonization takes place.	158
5.3	The ATR-IR spectra of the 48.1% polymethylhydrosiloxane-impregnated paper sample, before and after ozonization. There is a significant reduction of the characteristic absorption band at 2168 cm ⁻¹ due to Si-H. There is also a notable reduction of the absorption bands at 2969 cm ⁻¹ , 1428 cm ⁻¹ and 1271 cm ⁻¹ due to SiCH ₂ -H.....	159
5.4	Several drops of water colored with potassium permanganate are placed on the surface of two pieces of paper in order to demonstrate the results obtained from contact angle experiments. The hydrophobic paper is coated with 1% polymethylhydrosiloxane (PMHS).	160
5.5	Scanning electron micrographs (SEM) at two different magnifications of pure cellulose paper (control) samples.	161
5.6	Scanning electron micrographs (SEM) of paper samples. The top micrograph is obtained from a control sample while the bottom is taken from the 16.2% PMHS coated paper. It is noticeable, from the bottom micrograph, that the coating does not eliminate the porosity of the filter paper.	162

5.7	Scanning electron micrographs (SEM) of two PMHS coated paper samples. The top micrograph shows the porous surface of the 16.2% coated sample. In contrast, PMHS in the 48.1% sample has formed a continuous coating (sandwich) which completely destroy the surface porosity.	163
5.8	A TGA thermogram of a control (non-coated) sample. The sample was heated under air to 800 °C at a rate of 10 °C/min. The first degradation started at 266 °C and the second at 358 °C. There is no residue left at the end of the second degradation (490 °C).	167
5.9	A series of TGA thermograms of several samples heated under N ₂ at 10 °C/min., a: is the control non-ozonized sample, b: the 1%, c: the 7%, d: the 16.7%, e: the 48.1% PMHS-coated sample. The differential thermogram at the top indicates that coating does not affect the thermal stability of the substrate.	168
5.10	Scanning electron micrographs (SEM) at two different magnifications of a control (non-coated) sample heated under N ₂ to 800 °C at 10 °C/min. The residue left in a fiber form is a result of incomplete pyrolysis.	169
5.11	Scanning electron micrographs (SEM) at two different magnifications of the 16.7% PMHS-coated sample heated under N ₂ at 10 °C/min.	170
5.12	Scanning electron micrographs (SEM) of two different samples, a: non-heated control sample, b: 16.7% coated sample heated under air to 800 °C at 10 °C/min. The residue left is due only to the coating and appears as the footprints of the pyrolyzed cellulose fibers.	171
5.13	Low resolution X-ray photoelectron (XPS) spectra obtained from a control (top) and the 0.2% PMHS coated sample.	172
5.14	High resolution X-ray photoelectron spectra (XPS) obtained from a series of samples. The high binding energy carbon (C _{1s}) peak at 289 eV is due to substrate C-O and O-C-O. The lower binding energy carbon (C _{1s}) peak at 286 eV is due to coating (Si-C). The intensity of the Si-C peak increases as the concentration of the coating increases.	175
5.15	High resolution X-ray photoelectron spectra (XPS) obtained from a series of highly coated samples. The high binding energy carbon (C _{1s}) peak at 289 eV due to substrate vanishes above 5.7% PMHS. Only the carbon peak (C _{1s}) at 286 eV (Si-C) due to coating is detected.	176
5.16	Deconvoluted high resolution X-ray photoelectron spectra (XPS) obtained from a series of coated samples.	177

5.17	Typical thermomechanical analysis plot of dimensional change vs. temperature. The linear coefficient of thermal expansion (LCTE) can be calculated from the slope of the second heating.	179
5.18	Plot of linear coefficient of thermal expansion (LCTE) as a function of PMHS (%) concentration.....	180
6.1	Modulus dependence on the draw ratio for drawn polyethylene sheets. The S1, S2, A, and Q are different starting materials [47].	193
6.2	Stress-strain behavior of various yarns. Strain rate was 10% min ⁻¹ at 23 °C [10].....	197
7.1	Morphological model of a physical network formed in poly(styrene-b-butadiene) copolymers. Polystyrene has molecular weight ~10 ⁴ and polybutadiene ~7x10 ⁴ [11].....	208
7.2	Schematic representation of morphological forms in block copolymers [5].....	209
7.3	Dependence of modulus-temperature curves on block copolymer morphology: (a) A and B units are fully compatible giving one phase system, (b) bundling of units without phase separation, (c) phase separation with diffuse phase boundaries, (d) phase separation with boundaries between phases. Curves A and B correspond to the pure homopolymers (reproduced from Ref. 9).	210
7.4	A typical stress-strain plot for rubber or rubber-like materials. The orientation of polymer chains increases with elongation.....	215
8.1	A typical stress-strain plot for an elastomeric material at ambient temperatures. A strain hardening can be observed, at very high elongation.	219
8.2	A schematic representation of the experimental set-up. The instron tester was modified to accommodate testing at liquid nitrogen temperatures.....	221
8.3	Schematic representation of the specially made grips for the testing of the spandex fibers. The fiber was passed through the two perpendicular openings and pressed against the stationary flat aluminum surface with the use of a mobile screw.....	225

8.4	The modulus pre-elongation relationship for polyurethane samples tested at liquid nitrogen temperatures.	226
8.5	SEM micrographs depict the direction of crack propagation in the tested polyurethane samples, pre-elongated 640% at room temperature. It is shown that the crack propagates preferably in the direction of the applied load. The two micrographs represent the same sample at two different magnifications at room temperature.	228
8.6	Stress-strain curves for the polyurethane samples tested at liquid nitrogen temperature. The different curves correspond to different pre-elongation at ambient temperature. Increase of the pre-elongation increases the linear stress-strain response.....	229
8.7	Stress-strain curves for the spandex fibers tested at liquid nitrogen temperatures. The different curves correspond to different pre-elongation at ambient temperature. Increase of the pre-elongation increases the linear stress-strain response.....	232
8.8	The modulus pre-elongation relationship for natural rubber samples tested at liquid nitrogen temperature.	233
8.9	Stress-strain curves for the natural rubber samples tested at liquid nitrogen temperature. The different curves correspond to different pre-elongation at ambient temperature. Increases of the pre-elongation increases the linear stress-strain response.....	234
8.10	The modulus pre-elongation relationship for radiation crosslinked low molecular weight polyethylene samples tested at liquid nitrogen temperature.	236
8.11	Stress-strain curves for the low molecular weight radiation crosslinked polyethylene samples tested at liquid nitrogen temperature. The different curves correspond to different pre-elongation at ambient temperature. Increase of the pre-elongation increases the linear stress-strain response.	238
9.1	A general model for the morphology of the (AB) _n type copolymers [4].	244
9.2	FT-IR spectra of the two pure homopolymers and their copolymer. The spectrum shown at the top is taken from the dicarboxyl-terminated polystyrene. The middle spectrum represents the copolymer and the one shown at the bottom is obtained from diamino-terminated polyetherimide.	250

9.3	FT-IR spectra for the two pure homopolymers and their copolymer. The copolymer spectrum appears in the middle. The carbonyl peaks at 1780 cm^{-1} and 1724 cm^{-1} and the aromatic C-C peak at 1620 cm^{-1} are due to polyimide. The polystyrene segment is identified from the strong overtones and the aromatic C-C at 1584 and 1602 cm^{-1}	251
9.4	^1H NMR spectra of the two pure homopolymers (polystyrene and polyimide) and their isolated block copolymer.....	252
10.1	At the top are thermograms (TGs) of the polystyrene homopolymer (—•—), polyetherimide (—) and the block copolymer (—). At the bottom are the differential thermograms (DTGs) of the same polymers.	262
10.2	Differential thermograms (DTGs) of a dicarboxyl-terminated polystyrenediamino-terminated polyetherimide blend and of the block copolymer.	264
10.3	DSC thermograms of the two homopolymer components and the block copolymer. The thermogram at the top is obtained from the polyetherimide ($T_g=197^\circ\text{C}$), the bottom is from the polystyrene ($T_g=92^\circ\text{C}$) homopolymer. The copolymer thermogram is depicted in the middle ($T_{gA}=102$, $T_{gB}=210$).....	265
10.4	Dynamic mechanical thermal analysis (DMTA) of the block copolymer and the two homopolymer segments. The variation of the dynamic moduli is displayed on the top. The change in dumping factor, $\tan \delta$, is illustrated at the bottom.	267
10.5	Dependence of fracture stress, σ_f , upon molar mass for polystyrene. The “zero” stress molar mass, M_0 , is 50,000.	270
10.6	Dependence of fracture energy G_i upon molar mass for polystyrene and poly(methylmethacrylate). M_0 is the “zero” stress molar mass.	271

LIST OF SCHEMES

Scheme	Page
1.1 Geometric characteristics and resonance description of ozone [16].....	5
1.2 The 1,3-dipole-type of ozone attack at an olefin double bond.	6
1.3 The electrophilic attack of ozone at a tetrachloro-substituted olefin.....	7
1.4 An example of the nucleophilic attack of ozone to cyclohexanone.....	10
1.5 A proposed reaction of ozone with C-H group.....	11
1.6 Base-catalyzed reactions of Si-H and C-H groups. The SiH group is based catalyzed while the CH is not..	13
2.1 Mechanism of ozonization of tetraethylsilane.	21
2.2 Mechanism of ozonization of trisubstituted silanes.....	24
2.3 Mechanism of ozonization of disilanes proposed by Spialter and Austin.....	25
2.4 Hydrosilation reaction used to incorporate trimethoxysilyl moieties into the polydimethylsiloxane oligomer.....	27
2.5 Synthesis of PDMS-SiO ₂ organic-inorganic networks.	28
2.6 The use of isocyanate reactions to facilitate the incorporation of trialkoxysilyl moieties into a cellulose polymer.	29
3.1 The reaction of glyoxal and glyoxylic acid with 2,4-dinitrophenyl- hydrazines. The 2,4-dinitrophenylhydrazone formed from glyoxal is orange and melts at 328 °C. The glyoxylic acid derivative shows no melting (sublimes at 175 °C).	48
4.1 Ozonization of phenylsilane.	100
4.2 Ozonization of a polydimethylsiloxane hydride-terminated (PDMS-H) mixed with phenylsilane (PhSiH ₃). The concentration of (PhSiH ₃) varies from 3 to 41%.	111

4.3 Ozonization of poly(dimethyl methylhydrosiloxane) copolymers
(PDMMHS) and polymethylhydrosiloxane polymer (PMHS). 112

5.1 Ozonization of polymethylhydrosiloxane coated cellulose. 149

9.1 Poly(styrene-b-etherimide) ABA type copolymer. 246

PART I

SYNTHESIS OF ORGANIC-INORGANIC HYBRIDS VIA OZONE CHEMISTRY

CHAPTER 1

INTRODUCTION

1.1 Ozone: General discussion

Ozone is as old as life itself. The characteristic odor of ozone in the air during thunder and lightning has been observed since ancient times. Homer in his Iliad and Odyssey talks about the “sulfurous” smell and the “freshness” of the air after a storm. The characteristic smell was associated with a chemical substance in 1840 [1] and this substance was named ozone (after the Greek word οζειν, to smell). Early after its discovery, ozone was recognized to be a very powerful oxidant with many applications in organic and inorganic chemistry. One of the most important people in the area of ozone chemistry was Harries in the early 1900s. He not only established ozonolysis as one of the classical reactions in organic chemistry but also pioneered most of the known reactions of ozone with organics [2]. It was professor Criegee however, that is considered to be the father of modern organic chemistry of ozone [2]. His work in the 1950s resulted in the establishment of an understanding of the mechanism of ozone attack.

Considerable interest has been developed during the last two decades due to the emergence of new and re-established uses and technologies. Ozone has proved to be a very powerful and useful oxidizing agent in the chemical industry [3]. It has been used

extensively and for a long time in the purification of water and industrial wastes [4]. In addition, ozone has been used as a very effective bleach for many organic liquids (oils, esters, acids, and solvents) [9]. Textile and paper industries are using ozone for bleaching as well [4,9]. Furthermore, due to its biological activity, ozone has been used in the food and agricultural industry as an antiseptic and preservative [10]. Numerous other applications of ozone exist or are developing [4-8]. Most ozone applications are relying on the fact that ozone is highly reactive toward all kind of organic substances. For example, it reacts with olefins to form carbonyl and carboxyl compounds; acetylenic compounds; aromatic rings (both carbocyclic and heterocyclic); various nucleophilic groups (amines, phosphines, sulfides, etc.); carbon-sulfur and carbon-nitrogen double bonds; carbonyl groups; carbon-hydrogen bonds; silicon and other organometallic compounds; small or polymeric substances. Ozone can react with all these groups, some much more rapidly than others and some to the exclusion of others, when more than one group is present in the same system [11].

1.2 The ozone molecule: physical and chemical properties

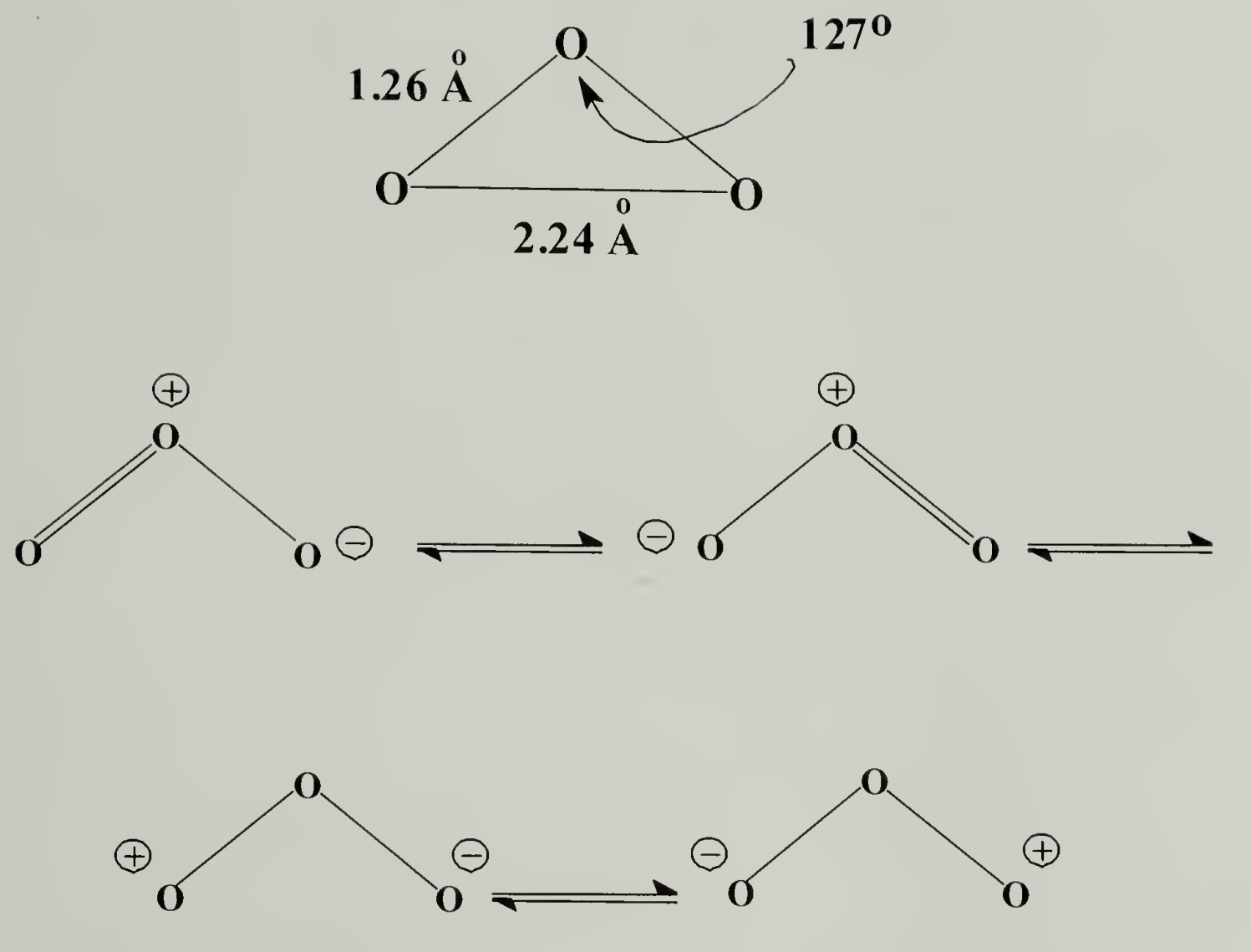
A knowledge of the structure and the properties of ozone itself is essential in order to understand the reactions of ozone with organic and inorganic compounds. In the gaseous form, ozone is colorless, whereas liquid ozone is almost non-transparent (bluish-black) and in the solid state forms violet-blue crystals. The melting point is $-193\text{ }^{\circ}\text{C}$ and the boiling point is $-112\text{ }^{\circ}\text{C}$ [12,13]. The critical points are $T_{\text{cr}}=12\text{ }^{\circ}\text{C}$, $P_{\text{cr}}=5.5\text{ MPa}$,

$d_{cr}=0.432\text{ g cm}^{-3}$ [14]. In each of its three states ozone is extremely sensitive to sudden variations of pressure and temperature [12]. Extremely violent explosion can occur even at room temperature with a sudden compression. Explosions have been recorded also as a result of a small but sudden rise of temperature. Ozone is extremely toxic and can have various physiological effects on all living organisms. Ozone inhalation causes a wide range of symptoms, from an unpleasant smell to pulmonary edema or lethal poisoning. The sharp odor of ozone can be detected in concentrations of about 0.1 ppm which is about ten times less than the permissible concentration (1 ppm) [15].

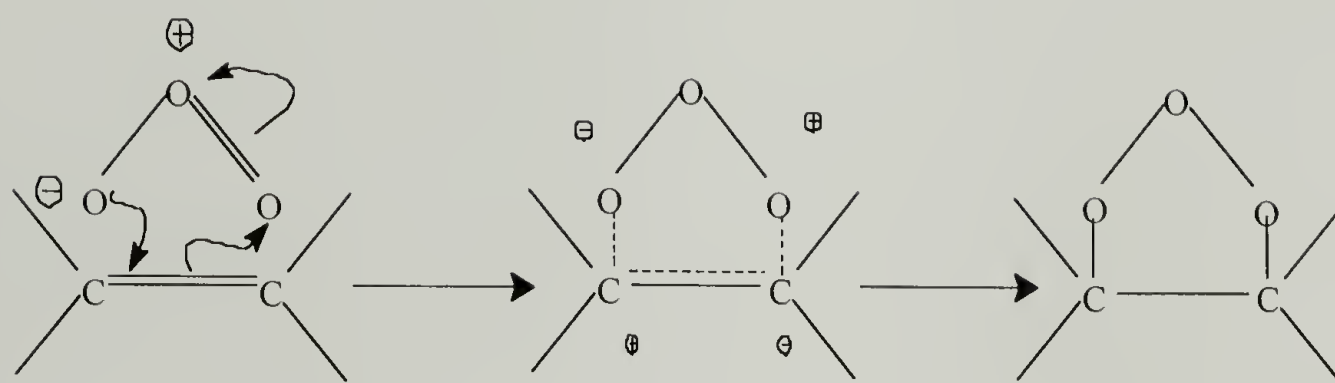
For a long time, it was believed that the ozone molecule had a ring structure where all three oxygen atoms were equivalent. Electron diffraction studies however, have revealed that the three oxygens in ozone form an isosceles triangle with a vertex angle of 127° , the length of the equal sides being 0.126 nm and the base being 0.224 nm [17], scheme 1.1.

It was mentioned earlier that ozone reacts with virtually all organic compounds. On the basis of the resonance description of the ozone molecule described in scheme 1.1, it is expected that ozone should function as a 1,3- dipole, as an electrophile, or as a nucleophile. It can also function as a diradical [18].

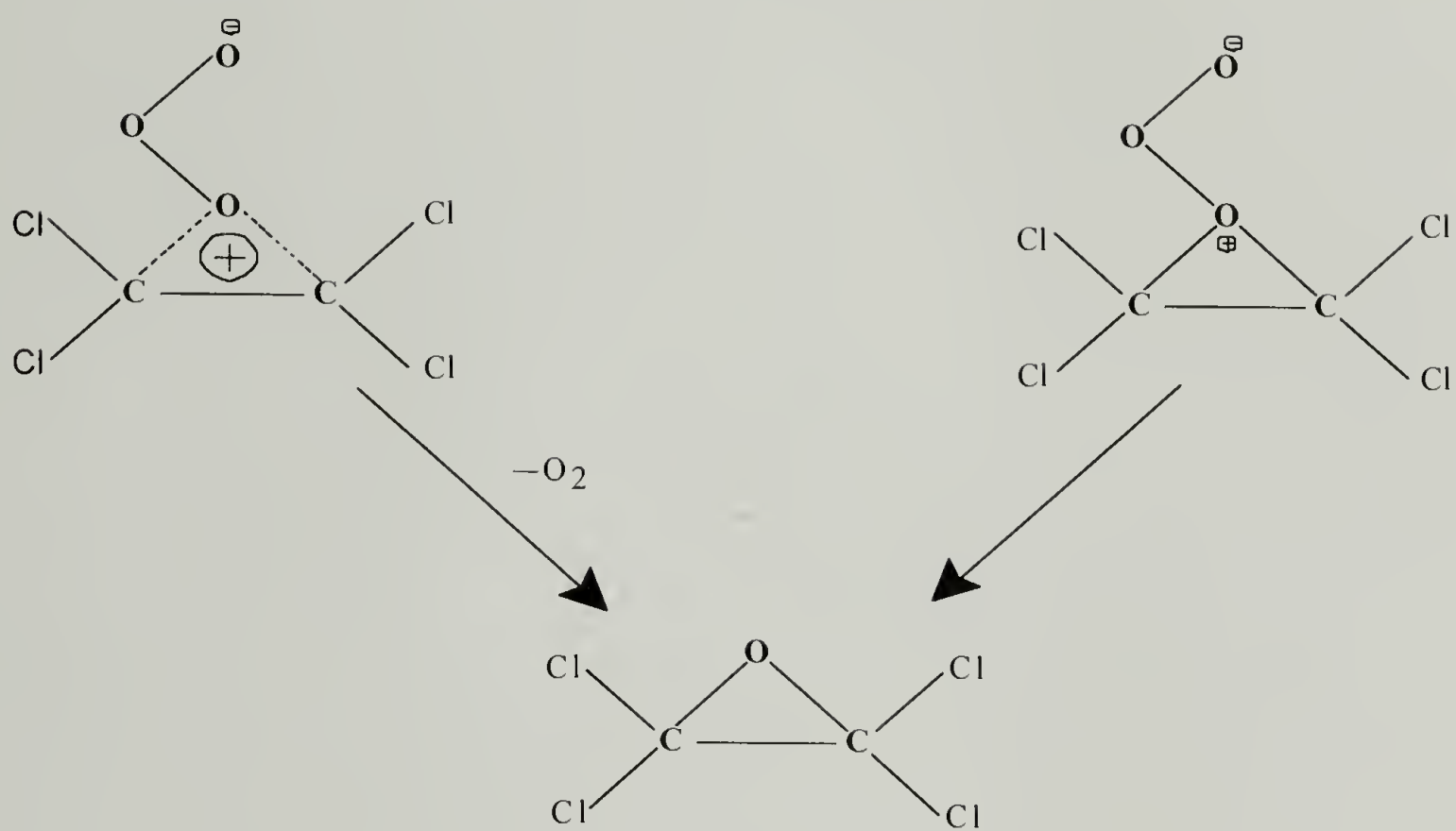
The 1,3-dipolar cycloaddition occurs when ozone attacks an olefinic double bond. The attack is a stereospecific, one step reaction, in which a reversible π -complex might be formed initially [19], scheme 1.2. There are many examples of olefins that react with only one atom of the ozone molecule. An example of this electrophilic attack is described in scheme 1.3.



Scheme 1.1. Geometric characteristics and resonance description of ozone [16].



Scheme 1.2. The 1,3 - dipole-type of ozone attack at an olefin double bond.



Scheme 1.3. The electrophilic attack of ozone at a tetrachloro-substituted olefin.

Molecular oxygen is released along with the formation of epoxides and products of an epoxide [20]. In addition, it has been stated that ozone should be able to react as a nucleophile when the right reaction conditions exist [18], scheme 1.4. Several examples are cited in the literature; reactions with certain carbon-oxygen double bonds, certain heterocycles, and ozonization in "super acids", are thought to follow the nucleophilic route.

The diradical form of ozone had been an ongoing controversy for many years. Recently however, it seems that there is agreement that ozone can have a character ranging from diradical to zwitterion. Radical-type ozonization can be encountered in the reaction with a C-H bond [21], scheme 1.5.

It has been reported in the literature that ozone interacts with many synthetic and natural polymers [22]. Because of its reactivity with polymers, ozone has been used in polymer qualitative and quantitative analysis, polymer modification and polymer degradation. In addition, ozonization of polysaccharides and other natural polymers has been widely studied. Even though the importance of ozone reactions with organic compounds is well accepted, the inorganic chemistry of ozone has re-surfaced in recent years due primarily to environmental factors [23, 24].

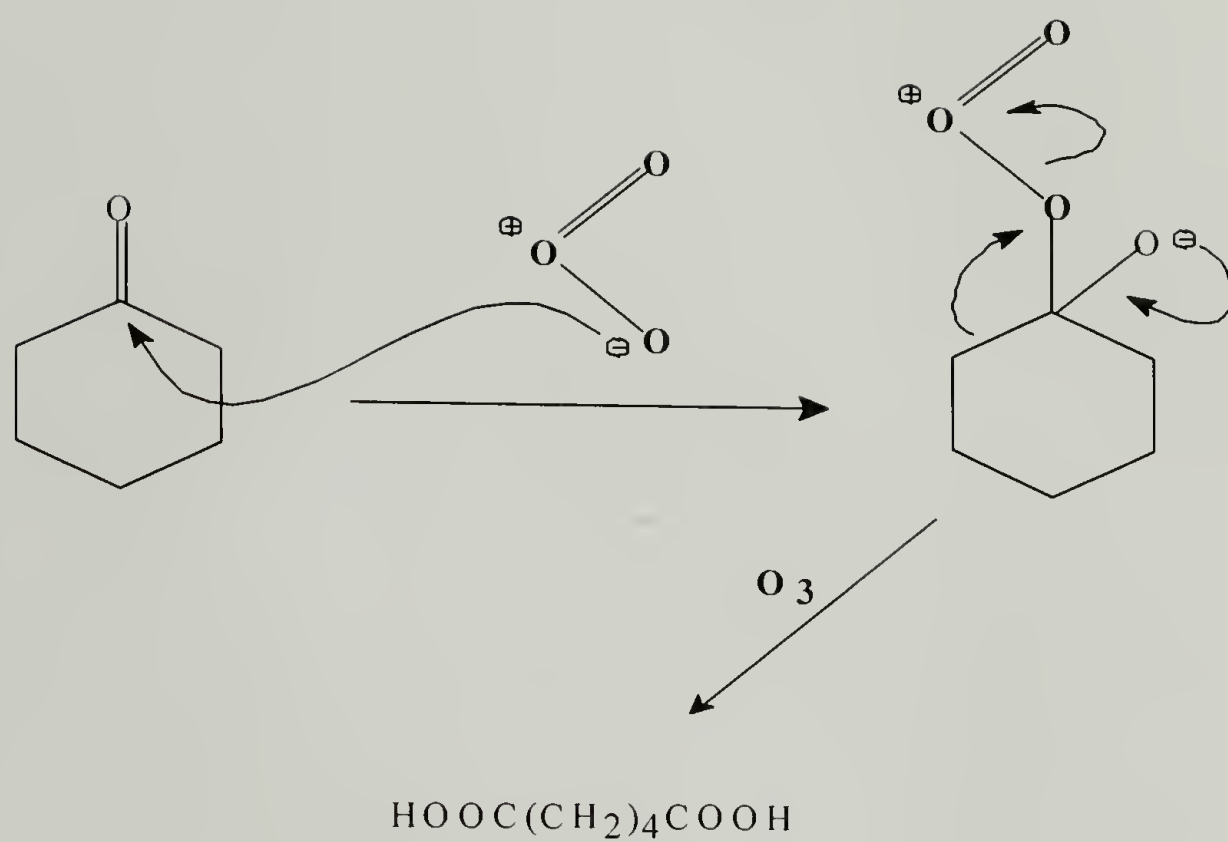
Ozone takes part in inorganic reactions as an exceptionally powerful oxidizing agent. It oxidizes all metals except gold, platinum, and iridium [25]. There are many important reactions of ozone with inorganic substances, some of the most important are the following [26]:



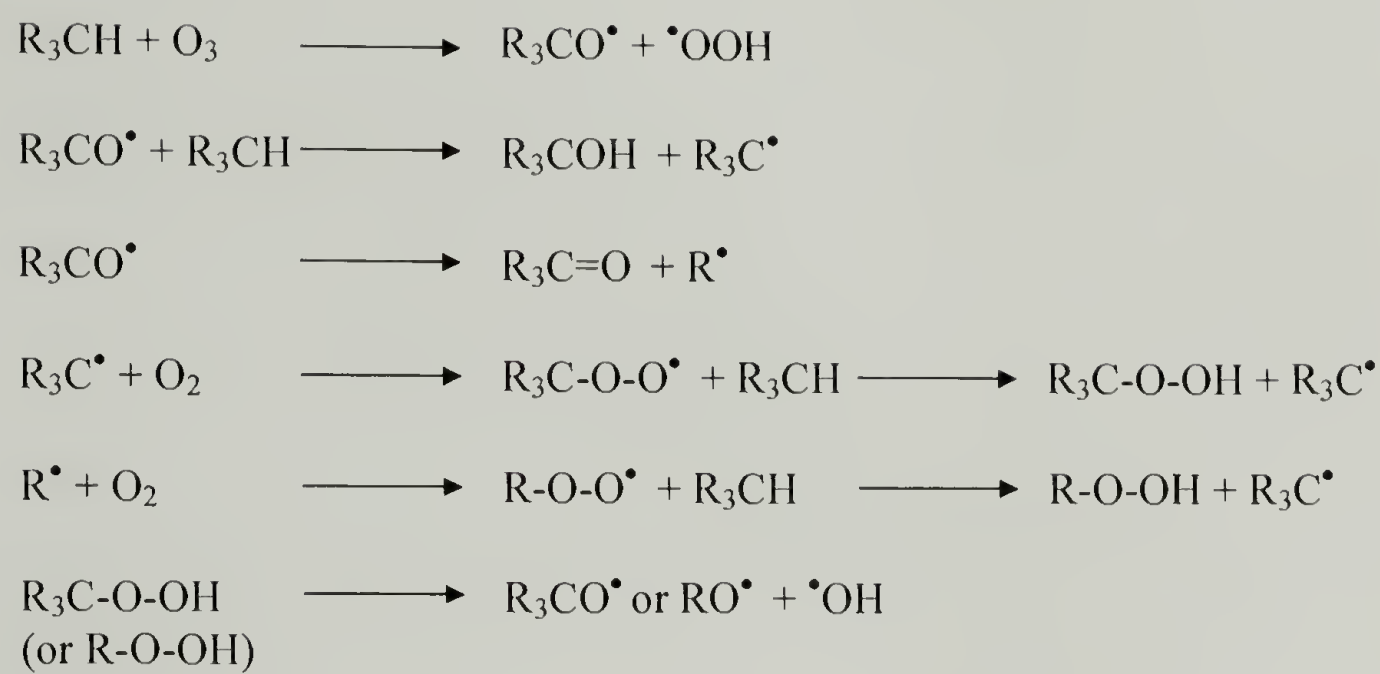
1.3 Organosilicon chemistry

Next to oxygen, silicon is the most abundant element in the lithosphere (27.5%). There are no natural organic silicon compounds: all of them have been created in the laboratory. Even though both carbon and silicon are members of group IV of the periodic table, there are some striking differences in their chemistry. The chemistry of silicon is affected by the availability of empty 3d orbitals, the energy of which is not much higher than the silicon 3s and 3p orbitals. These make it easy for silicon to form 5- and 6-coordinated complexes. The electronegativity of silicon is 1.74 [27] (O, 3.50; H, 2.20; C, 2.50). The silicon compounds used in this work are compounds containing O, H and C. It is useful therefore to examine some chemical properties of silicon bonds with these elements.

Only one kind of silicon-oxygen direct bond is known for each natural compound of silicon. The linkage of the oxygen free electron pair with the free d-orbital of silicon increases the strength of the bond. The oxides of silicon (SiO_2) form a 3D-network of



Scheme 1.4. An example of the nucleophilic attack of ozone on cyclohexanone.

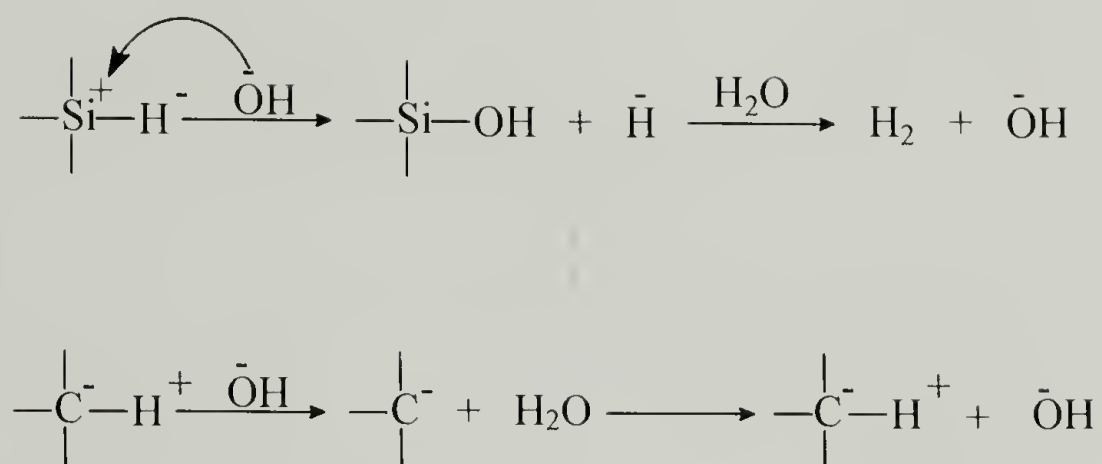


Scheme 1.5. A proposed reaction of ozone with C-H group.

highly polymerized material with high melting points. Orthosilicic acid, $\text{Si}(\text{OH})_4$, is easily condensed to SiO_2 . All silicon bonds spontaneously convert to silicon-oxygen bonds. The reverse, even though it is possible, is difficult and not spontaneous.

The SiH bond is also thermodynamically stable [28]. The dissociation energy is ~ 377 kJ/mol (C-H, 438 kJ/mol in methane). Since the electronegativity is $\text{Si} < \text{H} < \text{C}$ the chemical properties of the Si-H are inverse of the C-H. For example, hydrosilanes can react with bases, whereas the hydrocarbons can not, scheme 1.6.

The silicon-carbon bond is nearly as strong as a C-C single bond. The dissociation energy of Si-C bond in $\text{Si}(\text{CH})_4$ is ~ 374 kJ/mol and of C-C in paraffins is up to ~ 356 kJ/mol. The simplest silicon-carbon compound (silicon carbide) is especially stable ($T_m = 2700^\circ\text{C}$). The organic silicon compounds are not as stable as silicon carbide. Nevertheless, tetraorganosilanes are thermally and chemically stable. However, heterolytic fission of Si-C occurs more readily than the C-C bond because it is more polar. Therefore, the Si-C bond is more susceptible to ionic attack. The Si-C bond is always polarized and depending on the substituent groups on silicon and carbon, the polarization may be increased or decreased. For example, the Si-C bond weakens when an electronegative functional group is attached to an α , or β , position to the silicon. Stabilization of the Si-C bond occurs when more electropositive atoms than C are attached to the carbon, and more electronegative atoms than Si are attached to the silicon. The optimum effect of the stabilizing - non stabilizing substitution is shown in poly(dimethylsiloxane). On the other hand, the Si-C in $\text{R}_3\text{Si-CF}_3$ can be removed even with cold hydrolysis. Silicon can also form double bonds with carbon but only if certain rather bulky groups are substituents of the carbon.



Scheme 1.6. Base-catalyzed reactions of Si-H and C-H groups. The SiH group is base catalyzed while the CH is not.

1.4 Research objective and motivation

In order to meet the challenges of the rapid evolution of new industrial applications and the need for new materials, scientists have been vigorously engaged in the development of new systems for producing them. One recent approach, for the development of new materials with unique properties, has been the preparation of organic-inorganic hybrids: that is combining organic and inorganic components at the molecular level [29]. The combination of organic and inorganic parts has led to the development of fundamentally new types of materials with unique and extraordinary properties that can be useful in a wide range of applications. Table 1.1 shows some of the properties of one component materials (either organic or inorganic) that can be modified by combining them at the molecular level [31, 32].

For the synthesis of this hybrid materials, chemical or physical methods must be used since mechanical mixing in microscale becomes impossible [33]. In addition, if organic components have to be incorporated, low temperature syntheses must be employed.

A recent strategy for the preparation of new hybrid systems involves sol-gel chemistry [30]. In this approach inorganic metal alkoxides, organic oligomers and polymers are combined. Several limitations of the sol-gel strategy have been reported in the literature [31, 34]. For example, one limitation is that shrinking and cracking can occur during drying or heating. Other limitations are the complexity of the reactions involved (hydrolysis, condensation) and the poor solubility of most polymers in water. More details about the sol-gel process will be given in the next chapter.

This research is directed toward the development of a new system for the hybridization of organic and inorganic components. The new system under development utilizes ozonization chemistry. In contrast to sol-gel methods, the ozonization approach allows the hybrid network to form directly from silicone polymers or oligomers. The ozonization method utilizes the reactivity of the Si-H and Si-Ar moieties toward ozone. The glass forming agent is phenylsilane and the network forming material is hydride-containing siloxanes.

A background about the ozonization of organosilicon compounds will be presented in chapter two. In addition, in this chapter, the synthesis of organic-inorganic hybrids via sol-gel routes will be discussed briefly.

Chapter three presents the ozone reactions with polydimethylsiloxane, (79-82 %) polydimethyl (18-21 %)-diphenylsiloxane (PSX 80) and trimethylsilane.

The ozonization of hydride terminated polydimethylsiloxane and hydrosiloxanes as well as their mixtures with phenylsilane is described in chapter four.

Chapter five examines the possibility of applying hydrosiloxane polymers as hydrophobic coatings.

Table 1.1. Properties that can be modified by hybridization of organic and inorganic components.

Modified	Modified
Inorganic Glasses	Organic Polymer
Optical properties	Elasticity, plasticity
Temperature resistance	Low temperature resistance
Low impact strength	Toughness, Strength
High glass transition, T _g	Low glass transition, T _g
Low thermal expansion	High thermal expansion
Surface polarity modification	Electrical properties modification
High density, strong materials	Low density, high modulus materials
Diffusion modification	Low scratch resistance

REFERENCES

1. Schonbein, C. F., C. R. Hebd. Seances Acad. Sci. **10**, 706 (1840)
2. Bailey, P. S., "Ozonization in Organic Chemistry," Vol. I, p. 3, Academic Press Inc., New York, 1970
3. Anonymous, Chem. Eng. (N. Y.) **59**, No. 9, 246 (1952)
4. Horvath, M., Bilitzky, L. and Huttner, J., "Ozone," ch. V, p. 257-291, Akademiai Kiado, Budapest, 1985
5. Platz, G. M., and C. K. Hersh, Ind. Eng. Chem., **48**, 742 (1956)
6. Bowman, R. L., and N. Alexander, Science, **154**, 1454 (1966)
7. Laroque, R. L., Engineering Digest, **21**, No. 4, 37 (1975)
8. Arnold, L. B., Chemistry and Industry, **22**, No. 16, 899 (1974)
9. "Basic Manual of Applications and Laboratory Ozonization Techniques," The Welsbach Corporation, Ozone Process Division.
10. Billion, M. J., Revue Generale du Froid, **27**, No. 10, 1093 (1973)
11. Bailey, P. S., "Ozonization in Organic Chemistry," Vol. II, p. 1, Academic Press Inc., New York, 1982
12. Schumacher, H. L., Anales de la Asociación Quimica Argentina, **41**, p. 197-264 (1953); J. R. C. Brown, A. W. Berger and C. K. Hersh, J. Chem. Phys., **22**, 1151 (1954)
13. Jenkins, A. C., and F. S. DiPaolo, J. Chem. Phys., **25**, 2 (1956)
14. Birdsall, C. M., and A. C. Jenkins, J. Chem. Phys., **20**, 1158 (1952)
15. "Basic Manual of Applications and Laboratory Ozonization Techniques," p. 2, The Welsbach Corporation, Ozone Process Division.
16. Horvath, M., Bilitzky, L. and Huttner, J., "Ozone" ch. I, p. 13, Akademiai Kiado, Budapest, 1985

17. Durrant, P. J., and B. Durrant, Introduction to Advanced Inorganic Chemistry 2nd ed., p. 800, 806 and 954, Longmans, 1970
18. Bailey, P. S., "Ozonization in Organic Chemistry," Vol. II, Academic Press Inc., New York, 1982
19. Bailey, P. S., "Ozonization in Organic Chemistry," Vol. I, pg 19-24, Academic Press Inc., New York, 1970.
20. Bailey, P. S., "Ozonization in Organic Chemistry," Vol. I, ch. XI, Academic Press Inc., New York, 1970.
21. Bailey, P. S., "Ozonization in Organic Chemistry," Vol. II, ch. IX, Academic Press Inc., New York, 1982
22. Lofquist, R. A., and J. C. Haylock, in "Ozone Chemistry and Technology: A Review of the Literature 1961-1974," ch. 9, eds. J. S. Murphy and Janet R. Orr, The Franklin Institute Press, Philadelphia, 1975
23. Graedel, T. E., L. A. Farrow, in "Ozone Chemistry and Technology: A Review of the Literature 1961-1974," ch. 6, eds. J. S. Murphy and Janet R. Orr, The Franklin Institute Press, Philadelphia, 1975
24. Johnston, H. S., Science, **173**, 3996, 1971
25. Horvath, M., Bilitzky, L. and Huttner, J., "Ozone," chi. II, p. 44, Akademiai Kiado, Budapest, 1985
26. Edwards, J. O., in "Ozone Chemistry and Technology: A Review of the Literature 1961-1974," ch. 7, eds. J. S. Murphy and Janet R. Orr, The Franklin Institute Press, Philadelphia, 1975
27. Allred, A. L., and E. G. Rochow, J. Inorg. and Nucl. Chem. **5**, 264 (1958)
28. Walsh, R., Accts. Chem. Res., **14**, 246 (1981)
29. Karandinos, G. A.; Farris, R. J.; McCarthy, T. J. Polymer Preprints, **35**, 1, 695, 1994
30. Wilkes, G. L., Huang, H. H., Glaser, H. R., in "Silicon-Based Polymer Science-A comprehensive Resource, Zeigler, M. J.; Fearon, G. F. W. eds. American Chemical Society: Washington, D. C., 1990
31. Novak, B. M., Adv. Mater. **5**, No. 6, 1993

32. Schmidt, H., in "Ultrastructure Processing of Advanced Materials," p. 409, eds. D. R. Uhlmann and D. R. Ulrich, John Wiley & Sons, Inc., N. Y., 1992
33. Schmidt, H., "Better Ceramics Through Chemistry IV", p. 961, eds. B. J. J. Zelinski, C. J. Brinker, D. E. Clark, D. R. Ulrich, MRS, Pittsburgh. PA, 1990
34. Garino, J., "Better Ceramics Through Chemistry IV", p. 497, eds. B. J. J. Zelinski, C. J. Brinker, D. E. Clark, D. R. Ulrich, MRS, Pittsburgh. PA, 1990

CHAPTER 2

BACKGROUND

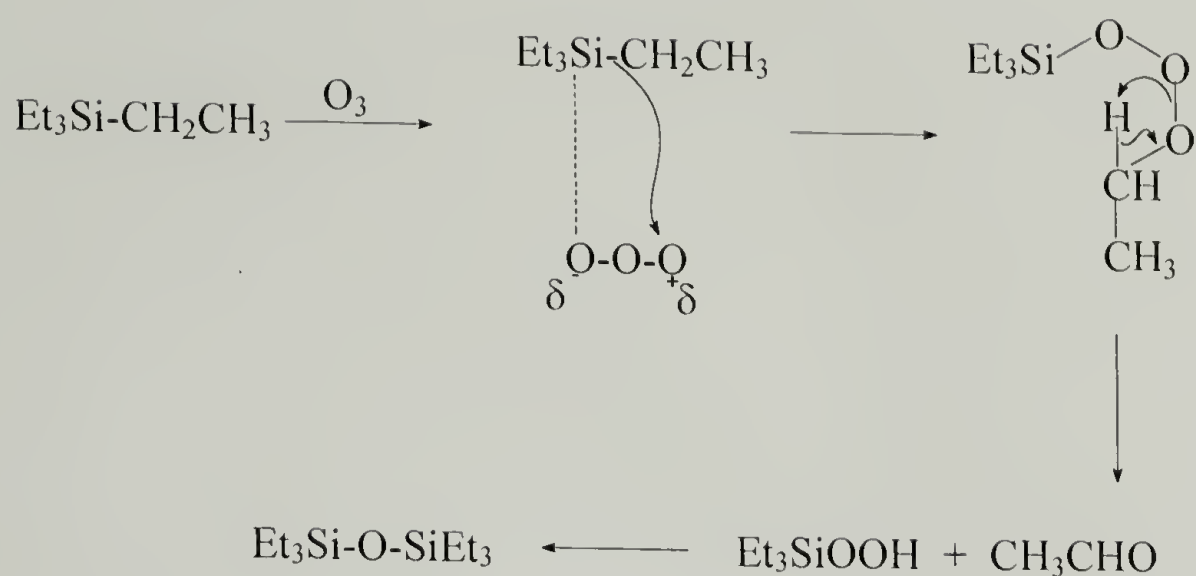
2.1 Ozonization of organosilicon compounds

The versatility and power of ozone as an oxidizing agent are evident from the discussion in the previous chapter. This chapter will cover the major characteristics of the ozonization of organosilicon compounds. The ozonolysis of vinyl silanes dates back to 1953 [1, 2]. Ozone reacts with vinyltrichlorosilane to form the ozonide. Hydrolysis of the ozonide with dilute hydrogen peroxide results in cleavage of the carbon-silicon bond and formation of silica. This hydrolytic cleavage indicates that carbonyl groups attached to silicon are unstable [1].

The first reports of the ozonization of saturated silanes appeared in 1958 [3, 4]. It is reported that the conversion of a tetrasubstituted silane during ozonization yields not only ozonolysis products but also a disiloxane, eq. 2.1. It is not clear whether the disiloxane arises directly, eq. 2.1 or whether the silanol is formed first.



According to Aleksandov [9-11], ozonization of tetraethylsilane yields initially hydroperoxide and acetaldehyde which can be further oxidized to acetic acid scheme 2.1.



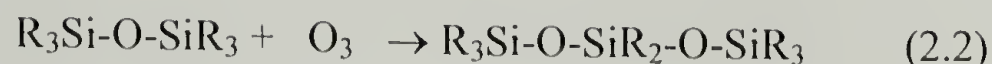
Scheme 2.1. Mechanism of ozonization of tetraethylsilane.

The ozonization is first order, both in regard to the silane and to ozone [10, 11].

Following the initial coordination, an ethyl carbanion transfer takes place and a super-peroxide is formed. The super-peroxide decomposes to give acetaldehyde and hydroperoxide which further decomposes to produce disiloxane. Even though scheme 2.2 depicts a hydrogen transfer, it is not clear whether a proton, a hydrogen atom, or a hydride anion is transferred [17].

From trisubstituted silanes are obtained, in high yield, the corresponding hydrosiloxanes which react further to produce siloxanes eq. 2.2 [6, 10]. The most complete and detailed mechanistic studies on the ozonization of trisubstituted organosilicon compounds have been made by Spialter [5-8] and Quellette and Marks [12]. The trisubstituted silanes undergo exclusive silicon-hydrogen bond cleavage. The

ozonization has been shown to be first order with respect to silane and ozone [13-15], scheme 2.2.



The first step involves a nucleophilic attack of ozone followed by electrophilic coordination with the hydride and abstraction via a transition state. This 1,3-dipolar insertion is the rate limiting step. The resulting super-peroxide can lose oxygen to afford trisubstituted silanol or it can decompose via a radical decomposition[13, 14, 16].

The silicon-silicon bond cleavage has not been clarified mechanistically. It has been suggested [6], however, a simple insertion via a transition state, as shown in scheme 2.3.

The mechanisms for the ozonization of silane hydroxides and alkoxides have not been reported in the literature. The conversion of silanol to siloxane, eq. 2.2, has been described simply as dehydration, although the presence of ozone appears to be required [13, 14].

The kinetics of the ozonization of various organosilicon compounds have been reported [6]. Competitive studies have shown that the reactivity and bond cleavage is in the following order:

Most reactive

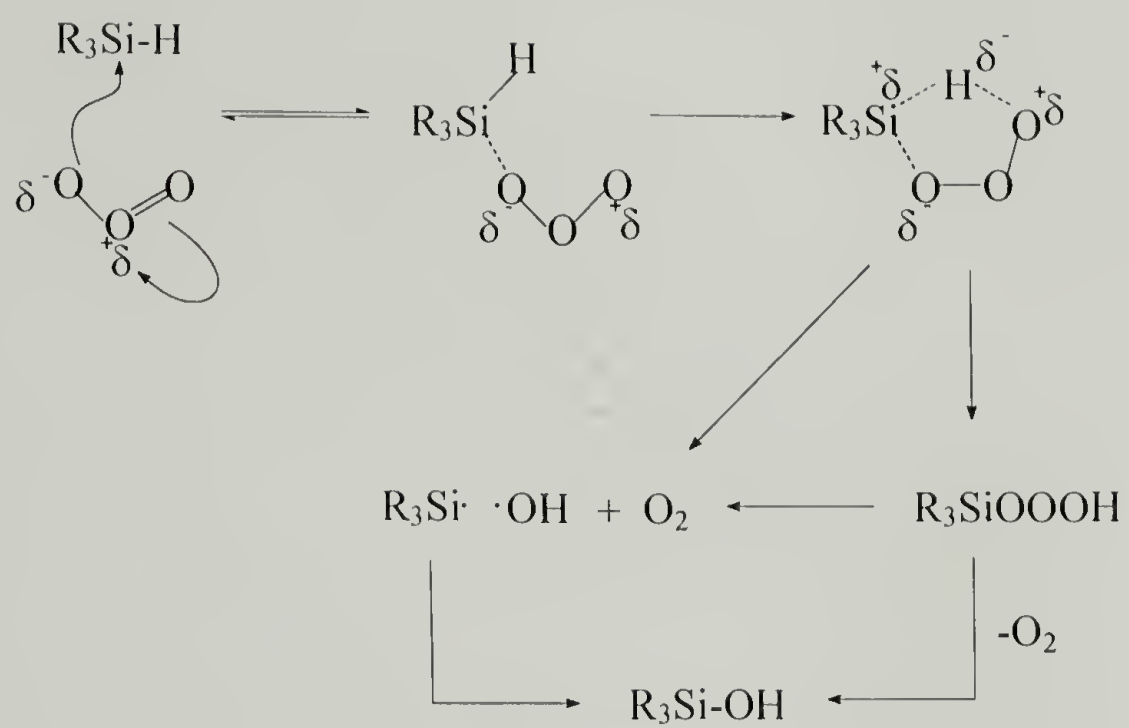
Least reactive



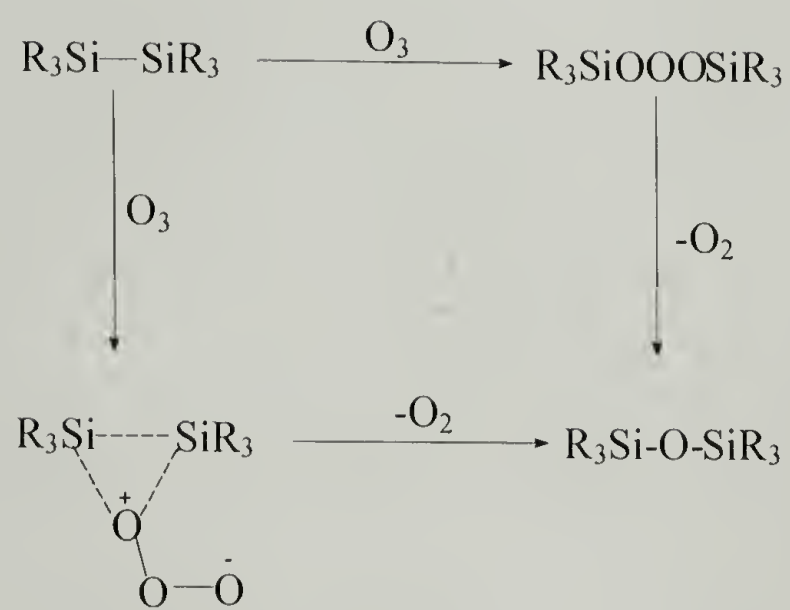
2.2 Synthesis of organic-inorganic hybrids containing silicon; sol-gel chemistry

Sol-gel is a useful process to generate glasses at low temperatures. In addition, as was mentioned in chapter one, this process has been used to synthesize ORMOCERS (organic modified ceramics) and CERAMERS (ceramic modified polymers). These materials can be divided into five major classes based on their macromolecular structure and phase connectivity [18].

- Soluble, preformed organic polymers embedded in an inorganic network
- Embedded, preformed organic polymers possessing covalent bonds to the inorganic network
- Mutually interpenetrating organic-inorganic networks
- Mutually interpenetrating organic-inorganic networks with covalent bonds between the organic and inorganic phases
- “Non-shrinking” sol-gel composite materials



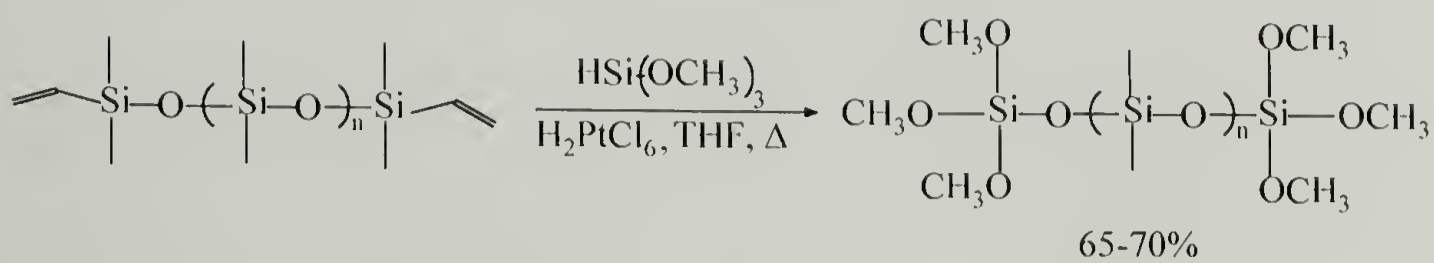
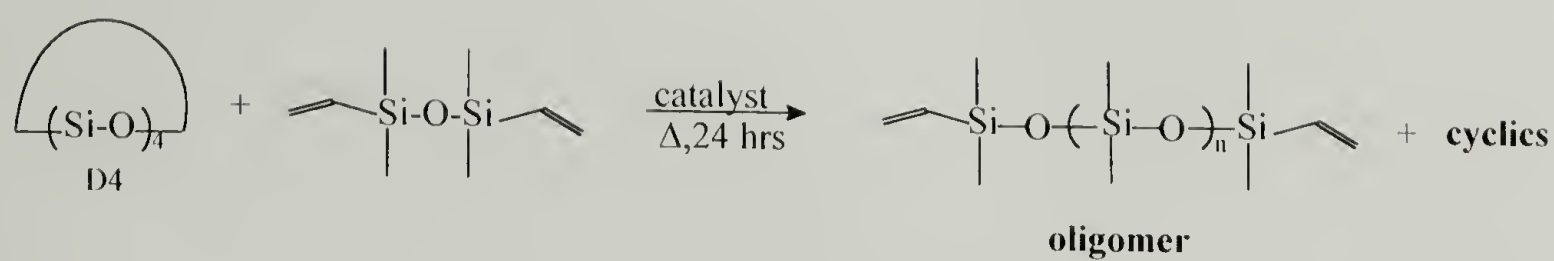
Scheme 2.2. Mechanism of ozonization of trisubstituted silanes



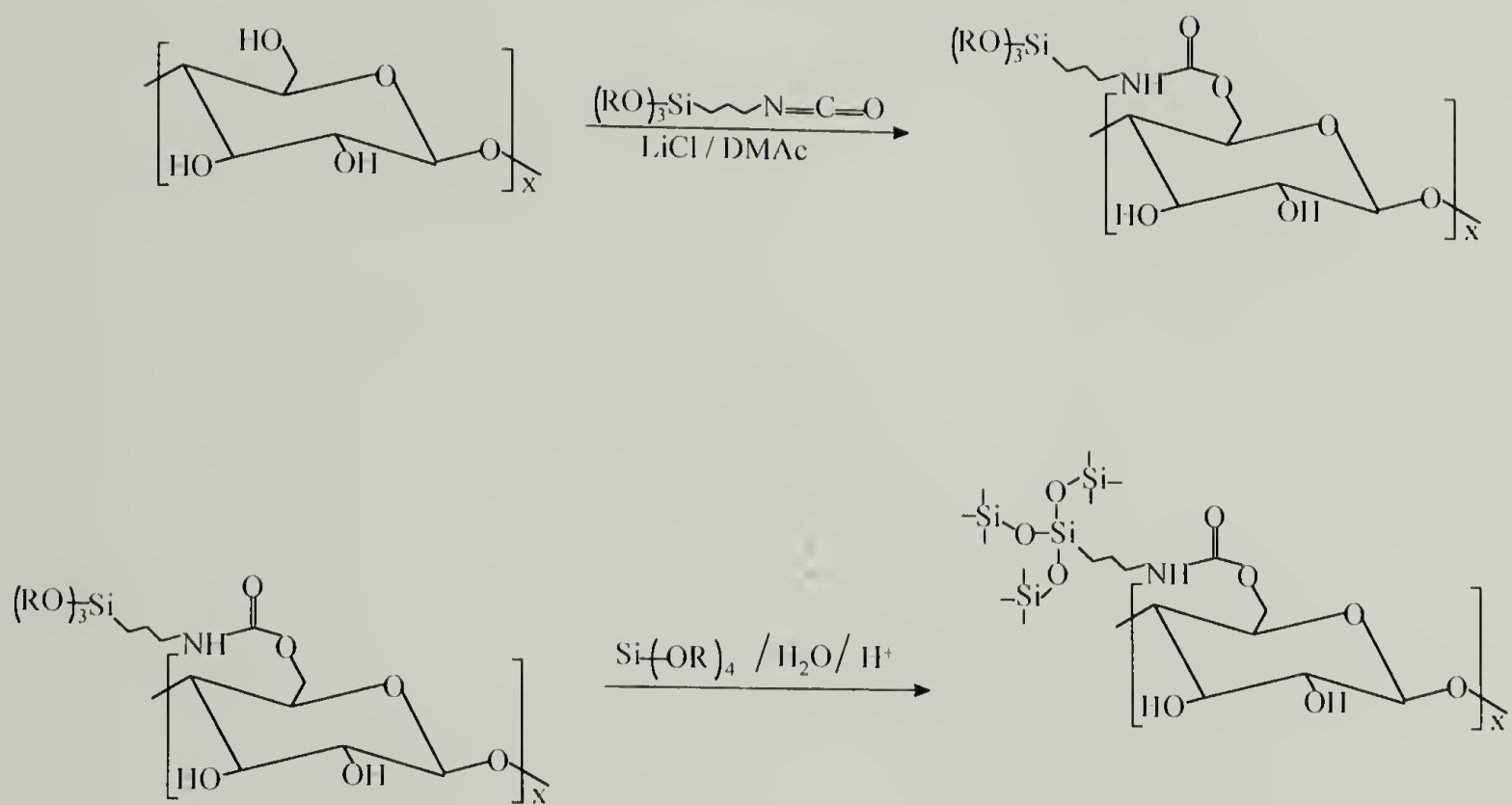
Scheme 2.3. Mechanism of ozonization of disilanes proposed by Spialter and Austin.

In this chapter the case in which embedded, preformed organic polymers possessing covalent bonds to the inorganic network will be discussed. In general terms, the sol-gel process involves the hydrolysis and condensation of an inorganic alkoxide in the presence of a co-solvent to form a three-dimensional SiO_2 network. In the case of the synthesis of a CERAMER, a reactive organic polymer or oligomer is incorporated in the partially hydrolyzed inorganic network. The first of these materials reported by Wilkes [19-21] used silanol-terminated polydimethylsiloxane (PDMS) as the polymeric modifier, tetraethylorthosilicate (TEOS) as the inorganic component and acid catalysts. On the other hand, McGrath [22] used tetramethylorthosilicate (TMOS) with trimethoxysilyl terminated PDMS in a catalyst-free process. The trimethoxysilyl-functionalized PDMS was synthesized from vinyl-terminated PDMS via hydrosilation reaction using a platinum catalyst as described in scheme 2.4. The sol-gel procedure is described in scheme 2.5. The network precursor formed at room temperature in approximately a six hour period using methanol as a co-solvent. The drying was accomplished in three heating stages. The first heating was at 65 °C for 12 hours, the second at 100 °C for 12 hours and the third at 150 °C for the same period of time. Transparent homogeneous materials with low surface polarity and high thermal stability were reported.

In another synthetic method [18], instead of using hydrosilation to incorporate trimethoxysilyl-functionalities into the polymers, a reaction of a polymer that contains amines or alcohols as pendant groups with trialkoxysilyl isocyanates to form urea or urethane linkages is involved. This method is described in scheme 2.6.



Scheme 2.4. Hydrosilation reaction used to incorporate trimethoxysilyl moieties into the polydimethylsiloxane oligomer.



Scheme 2.6. The use of isocyanate reactions to facilitate the incorporation of trialkoxysilyl moieties into a cellulosic polymer.

REFERENCES

1. G. H. Wagner, D. L. Bailey, A. N Pines, M. L. Dunhave and D. B. McIntire. *Ind. Eng. Chem.* **45**, 367 (1953)
2. L. H. Sommer, D. L. Bailey, G. M. Goldberg, C. E. Buck, T. S. Bye, F. .J. Evans, and F. C. Whitmore, *J. An. Chem. Soc.* **76**, 1613 (1954)
3. H. Clasen, *Agnew. Chem.* **70**, 179 (1958)
4. I. Shihara, W. F. Hoskyns, and H. W. Post, *J. Org. Chem.* **26**, 4000 (1961)
5. L. Spialter and J. D. Austin, *J. Am. Chem. Soc.* **87**, 4406 (1965)
6. L. Spialter and J. D. Austin, *Inorg. Chem.* **5**, 1975 (1966)
7. L. Spialter and J. D. Austin, *Adv. Chem. Ser.* **77**, 26 (1968)
8. L. Spialter and W. A. Swansiger, *J. Am. Chem. Soc.* **90**, 2187 (1968)
9. Y, A. Aleksandrov, *Organomet. Chem. Rev., Sect. A* **6**, 209 (1970)
10. Y. A. Aleksandrov and B. I. Tarunin. *Usp. Khim.* **46**, 1721 (1977); *Russ. Chem. Rev. (Engl. Transl.)* **46**, 905 (1977)
11. Y. A. Aleksandrov and N. G. Sheyanov, *Zh. Obshch. Khim.* **39**, 141 (1969); *J. Gen. Chem. USSR (Engl. Transl.)* **39**, 128 (1969)
12. R. J. Quellette and D. L. Marks, *J. Organomet. Chem.* **11**, 407 (1968)
13. L. Spialter, L. Pazdernik, S. Bernstein, W. A. Swansiger, G. R. Buell, and M. E. Freeburger, *Adv. Chem. Ser.* **112**, 65 (1972)
14. L. Spialter, L. Pazdernik, S. Bernstein, W. A. Swansiger, G. R. Buell, and M. E. Freeburger, *J. Am. Chem. Soc.* **93**, 5682 (1971)
15. Y. A. Aleksandrov and B. I. Tarunin, *Dokl. Akad. Nauk SSSR* **212**, 869 (1973); *Dokl. Chem. (Engl. Transl.)* **212**, 789 (1973)
16. J. D. Austin and L. Spialter "Oxidation of Organic Compounds-III" Ed. R. F. Gould, ACS publication, Washington D. C. (1968)

17. P. S. Bailey, "Ozonization in Organic Chemistry", Vol. II, Academic Press, New York, N. Y., 1982, p. 334
18. B. M. Novak, M. Ellsworth, C. Davies, Extended Abstracts, Japan-US Joint Seminar on Inorganic and Organometallic Polymers, p. 160, 1991
19. G. L. Wilkes, B. Orler, and H. H. Huang, Polym. prepr. (Am. Chem. Soc. Div. Polym. Chem.) **26** (2), 300 (1985)
20. H. H. Huang, B. Oreler, and G. L. Wilkes, Polym. Bull. 14 (6), 557 (1985)
21. H. H. Huang, B. Orler, and G. L. Wilkes, Macromolecules **20** (6), 1322 (1987)
22. M. Spinu and J. E. McGrath, Polymer, **2**, 1, 1992

CHAPTER 3

OZONIZATION OF DIMETHYLSILOXANE POLYMERS AND PHENYL CONTAINING COPOLYMERS

3.1 Introduction

In chapter two the interaction of ozone with various silicon compounds was discussed. In addition, the sol-gel process as a method of preparing organic-inorganic hybrids was described. The subject of this chapter is to present the criteria for the selection of the materials used for the ozonization reactions. The experimental conditions and settings are discussed as well. Furthermore, the results of ozone reaction with polydimethylsiloxane polymers, phenyl-containing copolymers and phenyltrimethylsilane are presented and conclusions are drawn.

As was stated before, the purpose of this research is to prepare organic-inorganic hybrids using ozonization chemistry. It was also mentioned that the inorganic network will be formed directly on the polymer backbone. Therefore, for this to be possible, the polymer backbone must be activated to react with the glass forming agent. It was also reported earlier that competitive studies have shown that the SiAr bond is more reactive and it will be oxidized preferentially in the presence of SiCH₃ [1, 2]. There are no

additional reports about reactivity and the mechanism of possible ozone attack on SiCH₃, SiAr or SiOSi groups, excluding the report about the preferential ozonization of SiAr group over the SiCH₃. The ozone interaction with these groups is important because they appear in the materials used to form the organic-inorganic hybrids. It was decided, therefore, as a first step to study a possible ozone interaction with SiCH₃, SiAr and SiOSi moieties.

3.2 Experimental

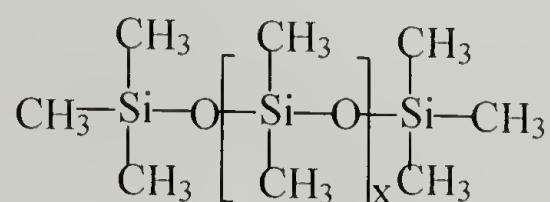
3.2.1 Materials

Conventional silicone fluids, for example, PDMS, have unique properties because they are not products of petroleum or organic chemistry. The basic characteristics of the silicones are:

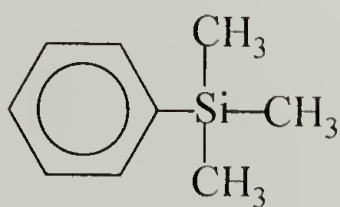
- | | |
|--|----------------------|
| * Wide Service Temperature Range | * Low Flammability |
| * Low Viscosity Change vs. Temperature | * Thermal Stability |
| * High Compressibility | * Chemical Inertness |
| * Low Surface Tension | * Shear Stability |
| * Dielectric Stability | * Low Toxicity |

These features have facilitated the adoption of silicones in many applications. In order to study the ozone reaction with the silicon-carbon bond the following materials were selected:

Polydimethylsiloxane trimethylsiloxyl terminated (liquids): $M_w=(770), (93,700)$ and $(250,000)$

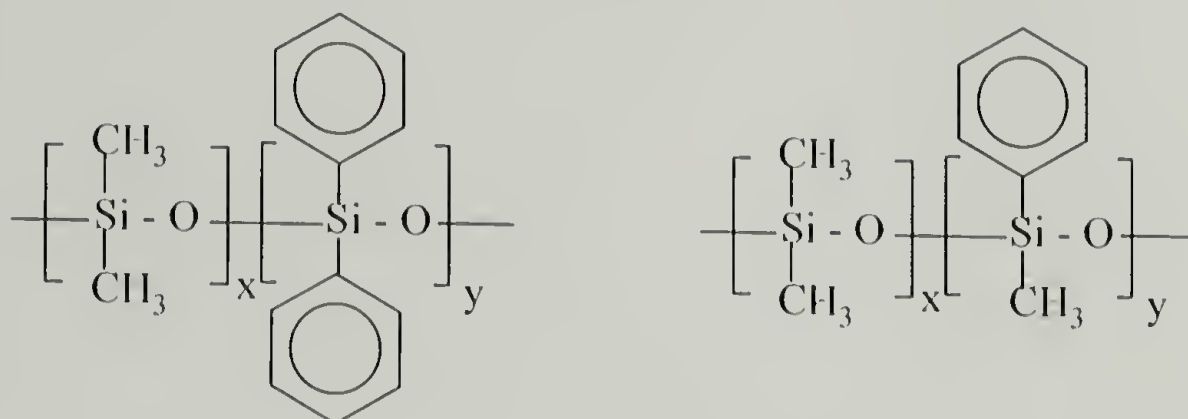


Phenyltrimethylsilane: $M_w=150.3$, $T_b=170^\circ\text{C}$, $d=0.87\text{ g/cm}^{-3}$, $n_d=1.49$



Polydimethyl-diphenylsiloxane, polydimethyl-methylphenylsiloxane copolymers: there were several commercially available copolymers with different amounts of methyl and phenyl content. The phenyl concentration in the copolymers used for the ozonization

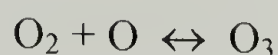
reactions vary from 5 up to 75%. The copolymer studied more extensively however, is the (79-82 %) polydimethyl (18-21 %)-diphenylsiloxane.



The polydimethylsiloxanes were purchased from Polysciences Inc. All the other silicon copolymers were purchased from Huls America Inc. All the samples were offered in good purity and no further purification was pursued. All the chemicals used for thin layer chromatography (glyoxal, 2-4 dinitrophenylhydrazine, benzaldehyde, oxalic, glyoxylic, malonic, maleic, succinic, adipic, benzoic, p-hydroxybenzoic acid, and the various solvents) were purchased from Aldrich and they were used as received unless otherwise indicated.

3.2.2 Experimental setting

For the formation of ozone, the presence of atomic, excited or free radicals containing oxygen (O) is required. The fundamental reaction that leads to ozone formation is:



This is a highly exothermic reaction leading mostly to the formation of ozone. On the other hand the equilibrium of the endothermic reaction



can be shifted to the right by providing a significant amount of energy. There are several methods for ozone generation. Photochemical dissociation of oxygen and subsequent ozone formation can be induced with ultraviolet light. Electrolysis of compounds containing oxygen is another method for ozone production. Ozone generation with electric discharge, however, is the method with the widest application. In this work, ozone was generated by corona discharge (illuminating high voltage discharge) using a Welsbach laboratory ozonator, model T-408. The Welsbach ozonator consists of two metal electrodes separated by a dielectric (electric insulator made of glass) and a discharge gap [3, 4]. A high voltage alternating current is applied to the active electrode while feed gas (clean, dry air or oxygen) passes through the discharge gap, Fig 3.1. The incoming gas is instantly ionized as the molecules collide with the electrons traveling back and forth across the discharge gap at a rate 60 times per second.

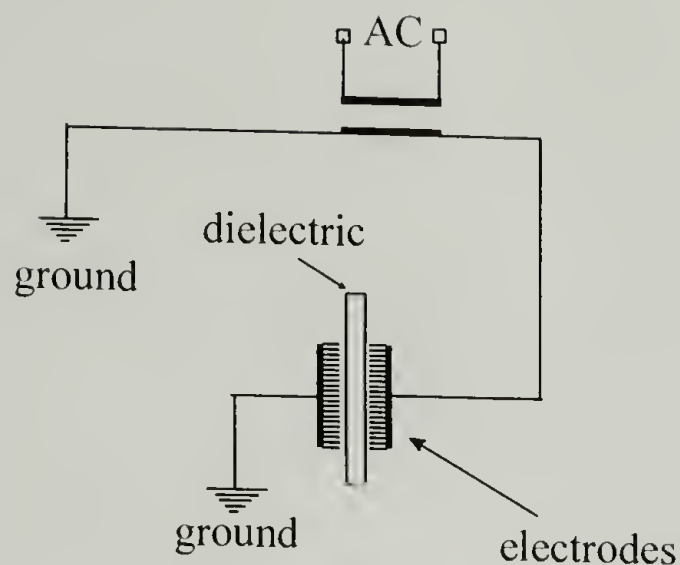


Figure 3.1. Schematic diagram of the ozone generator.

The glass dielectric serves as an electric current insulator to prevent arcing between the electrodes. The result is a silent evenly diffused discharge of energy called a corona discharge. The corona appears purple when the gas stream is air and white if it is oxygen. For the ozonization experiments the Welsbach T-408 ozonator was operated at 115 volts and pressure 8 psig. The flow rate varied from 0.3 to 2 lit/min. Under these conditions, depending on the flow rate [3, 5], 4-6 % ozone concentration is produced. The feed gas was pre-purified dry oxygen. All the connections between the ozonator and reactors were either glass or tygon made tubing (as short as possible).

The general experimental setting for every (unless otherwise stated) ozonization is described in fig. 3.2. Oxygen is allowed to pass through a dry ice / acetone trap and an

absorbent filled with type 4A molecular sieves. Thereafter, the dry oxygen passed through the electrodes where ozone was generated in concentrations up to 6 %. The output ozone-oxygen mixture was allowed to go through a set of two parallel connected reactors. These two reactors were connected to a trap containing saturated solution of potassium iodide, KI. Ozone reacts with KI according to the reaction:



The excess of ozone in the reactors, after the completion of the reaction, was removed by passing a stream of nitrogen for 15-20 minutes. Because of the increase of temperature during ozone formation, the ozonator is cooled down with the circulation of water.

3.2.3 Analytical techniques and methods

Infrared spectra were obtained under nitrogen by using a Nicolet IR/44 Fourier transform infrared spectrometer. For the liquid samples NaCl plates were used and for the solids, KBr pellets.

For the X-ray photoelectron spectroscopy analysis (XPS) the instrument used was a Perkin Elmer-Physical Electronics 5100 spectrometer with MgK α excitation (400 W).

The reported binding energies are not corrected for variable charging.

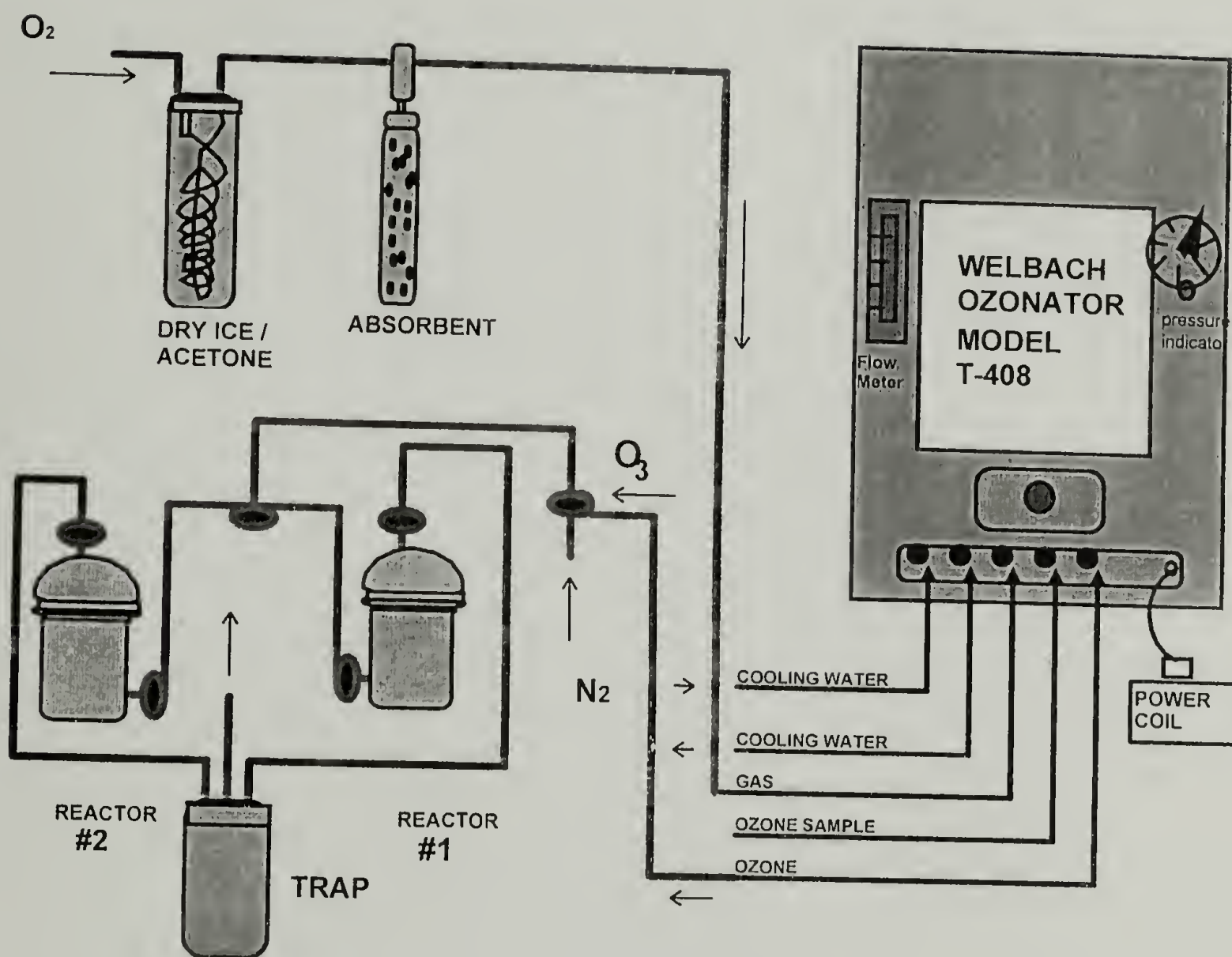


Figure 3.2. Schematic representation of the experimental setting. All the connections are either glass or tygon tubing. The ozonator is cooled with tap water.

The pH measurements were obtained using a standard pH-meter. A standard Fisher calomel reference electrode filled with saturated potassium chloride solution was used. The indicator electrode was a standard Fisher glass electrode.

The plates (10 cm x 20 cm) used for thin layer chromatography (TLC) in the case of identification of carboxylic acids were made by silica G / Kieselguhr layers (from Merck). The impregnating solvent was 60 % acetic acid. The developing solvent was a mixture of benzene / 80 % acetic acid (5:1). The chromogenic reagent was 0.2 % bromocresol green. For the identification of carbonyl-containing compounds, the TLC plates (5 cm x 20 cm) were made by silica G (Fisher) and they were preactivated at 120 °C for 24 hr. The developing solvent was benzene / ethyl acetate (20:1). A chromogenic reagent was not used because the spots were visible.

Size exclusion chromatography data was obtained using a GPC constructed from a Ramin Rabbit Pump, Polymer Laboratories PLgel columns and a (IBM LC 9563) UV detector. The eluting solvent was dry tetrahydrofuran (distilled from sodium / benzophenone).

Thermogravimetric analysis data was obtained using a TA Instruments Thermogravimetric Analyzer. For the determination of the activation energies the materials were heated under nitrogen and three different heating rates were employed (5, 10 and 20 °C / min).

Silicon nuclear magnetic resonance spectra, ^{29}Si NMR, were obtained using a Bruker NC 80 spectrometer. For this solid state ^{29}Si NMR experiments a single pulse, cross polarization technique was used.

The melting points were recorded using an Electrothermal Engineering melting point apparatus.

3.2.4 Ozonization of polydimethylsiloxanes

The ozonization setting is shown in fig. 3.2. The dry oxygen stream was directed through the ozonator. The experimental parameters were set to control ozone concentration at $\sim 6\%$ [3, 5]. The reaction temperature was controlled from $0-5^\circ\text{C}$ using ethylene glycol / water (40:60) as a coolant. The ozone-oxygen mixture was introduced in the reactors through a splitter at a rate of 120 lit/hour. A small amount (4-6 g) of each of the polydimethylsiloxane samples (770, 93.7K, 250K) was placed in a small beaker and they were charged in the reactors, fig. 3.3. Ozone was bubbled through the mixture for 2-24 hours. After the reaction was ceased, the reactors were flushed with nitrogen for about 15 minutes to remove the excess of ozone. Thereafter, the samples were removed and stored in small vials. Analysis was accomplished using FT-IR and XPS spectroscopy. (ntbk-S1, p.5-17, p.21-22, 29, ntbk-S2, p.30-34)

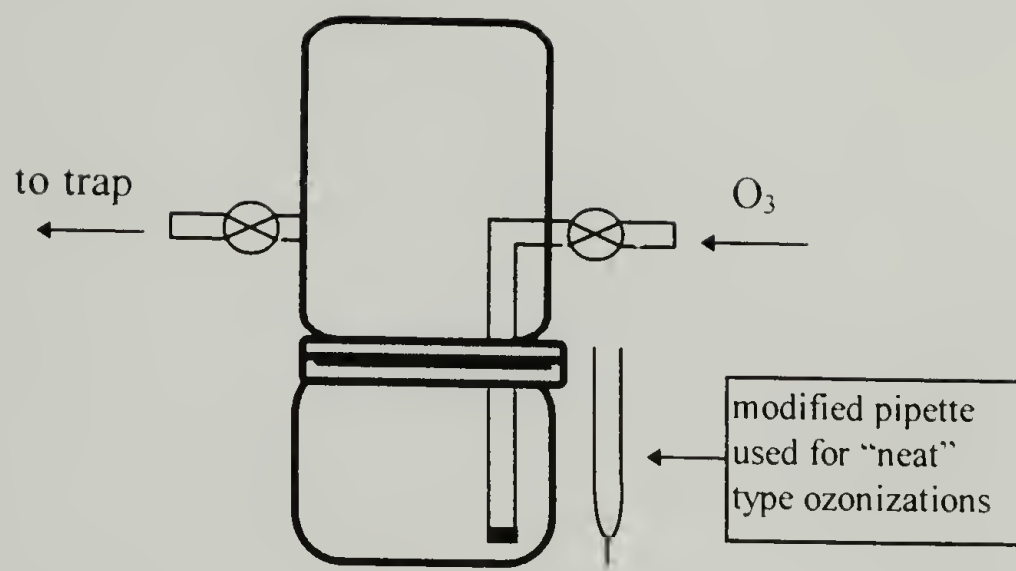


Figure 3.3. Reactor used for the bubbling type ozonizations

3.2.5 Ozonization of phenyl containing siloxanes

Several siloxanes with various phenyl concentration were available. It was decided, however, to use the (80%) dimethyl-(20%)-diphenylsiloxane (PSX 80) as the primary substrate for the ozonization reactions. Three different ozonization techniques were employed: Solid state, Solution, and Neat ozonization:

Solid state ozonization: In this type of ozonizations the reactor has been modified slightly to accommodate the reaction requirements, fig 3.4. This is an example of a “mild” type ozonization. This is a term used to emphasize the limited (surface) ozone-siloxane contact. In a typical ozonization experiment of this type, the silicone oil was allowed to form a thin layer (few millimeters) at the bottom of the reactor and thereafter an open ended glass cylinder (1-6 cm diameter) was placed inside in a manner described in fig. 3.4. Ozone was allowed to pass through the reactor over the surface of the silicone oil for enough time (~ 5 hr) to form a thin solid film inside the glass cylinder. When the film was formed the ozone flow was stopped and the reactor was flushed with nitrogen to remove the residual ozone. The reactor was then opened, the glass cylinder surrounding the formed film was inverted and immersed again in the silicon oil, so that the ozonized surface of the film would rest on unreacted silicone oil(this side would be protected from further ozonization). The ozonization continued until the inverse side solidified (~5 hr). When the film solidified the flow of ozone was stopped and nitrogen flushed through the reactors for 15-20 minutes. The films formed were separated from the glass cylinder and washed with water and then with methylene chloride to remove any by-products and unreactive siloxane. (ntbk-S1, p.40-44, 65-68, 83-91, ntbk-S2, p.7-12, 42)

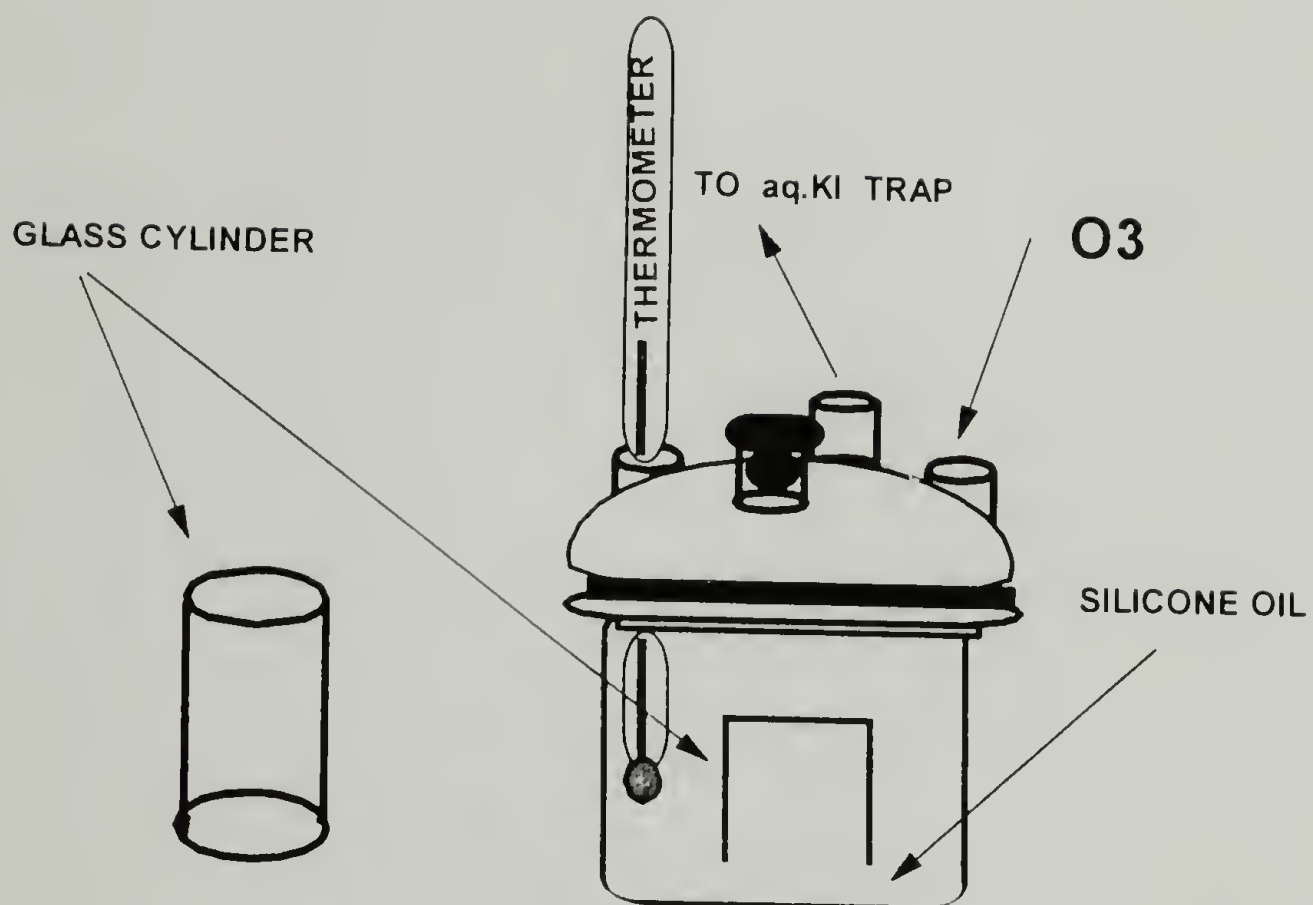


Figure 3.4. The modified reactor for the "solid state" ozonization.

Solution ozonization: The solvent chosen for the solution ozonization reactions in this work was carbon tetrachloride. The solvent was purified by distillation (from phosphorous pentoxide, P_2O_5) and ozonization (30 minutes). Immediately after ozone saturation the color of the solvent turned from transparent to aqueous-blue and coloration persisted until the ozone flow was stopped. The reactor setting is described in fig. 3.2. The ozonator parameters were kept the same as before (115 V and 8 psig). The flow rate, however, was lowered to less than 30 lit/hr to limit solvent evaporation. The reaction temperature was controlled at 0-5 °C. In a typical experiment 10-15 ml of 20 % (v/v) solution of siloxane was placed in a beaker and the beaker was set in the reactor, fig. 3.3. Ozone (~4 %) was bubbled in the solution for 2-6 hr. Ozone dispersion in the solution during the ozonization was accomplished with the help of a glass tube with a fritted glass tip which was dipped in the solution. (ntbk-S1, p.55-61, ntbk-S2, 49-54)

Neat ozonization: In this type of reaction the siloxane was ozonized in the absence of any solvent. The experimental setting and parameters remained the same as for the previous ozonizations. The gas flow was set to 120 lit/hr. In the ozonization of this type neat silicone oil (~200 ml) was placed in the reactor, fig 3.3, and ozone (~6 %) was bubbled through the solution (vigorous ozonization) for up to 43 hours. Portions (~20 ml) of the reacted siloxane were taken out at various time intervals (6, 13, 16, 20, 28, 33, 43 hours). The samples were placed in a mixture (1:1) diethyl ether / water and stored in erlenmeyer flasks for analysis. Dispersion of ozone in this system was impractical to carry out with the fritted glass (high viscosity liquids) and dispersion was achieved by forcing ozone through a Pasteur disposable pipette with a modified (smaller) opening to allow better

dispersion, fig 3.3. After 43 hr the flow of ozone was stopped and nitrogen was bubbled in the liquid for 20 minutes to remove the excess ozone. Ozonization of the (80%) dimethyl-(20%)-diphenylsiloxane (PSX 80) caused the formation of two phases. The minor phase consisted of a low density sponge-like solid and the major was a yellow-orange liquid. At the end of the reaction (43 hr) the sol and gel phases were separated for analysis. The sol phase (~50 ml) was mixed with ~200 ml diethyl ether and about 200 ml water and was stored in a beaker. The aqueous fractions of the sol phase and of all the other ozonized samples were isolated and the water was evaporated. Water evaporation yielded a yellow-orange precipitate.

The gel phase was placed in a beaker and left to swell in methylene chloride for one week. Thereafter, the solid was separated by filtration, washed with water and acetone. The isolated solid (~3 g) was set in vacuum oven at 80 °C for 48 hr. The dry sample was stored for analysis. (ntbk-S2, p.5-6, 62-78, ntbk-S3, p. 7-8)

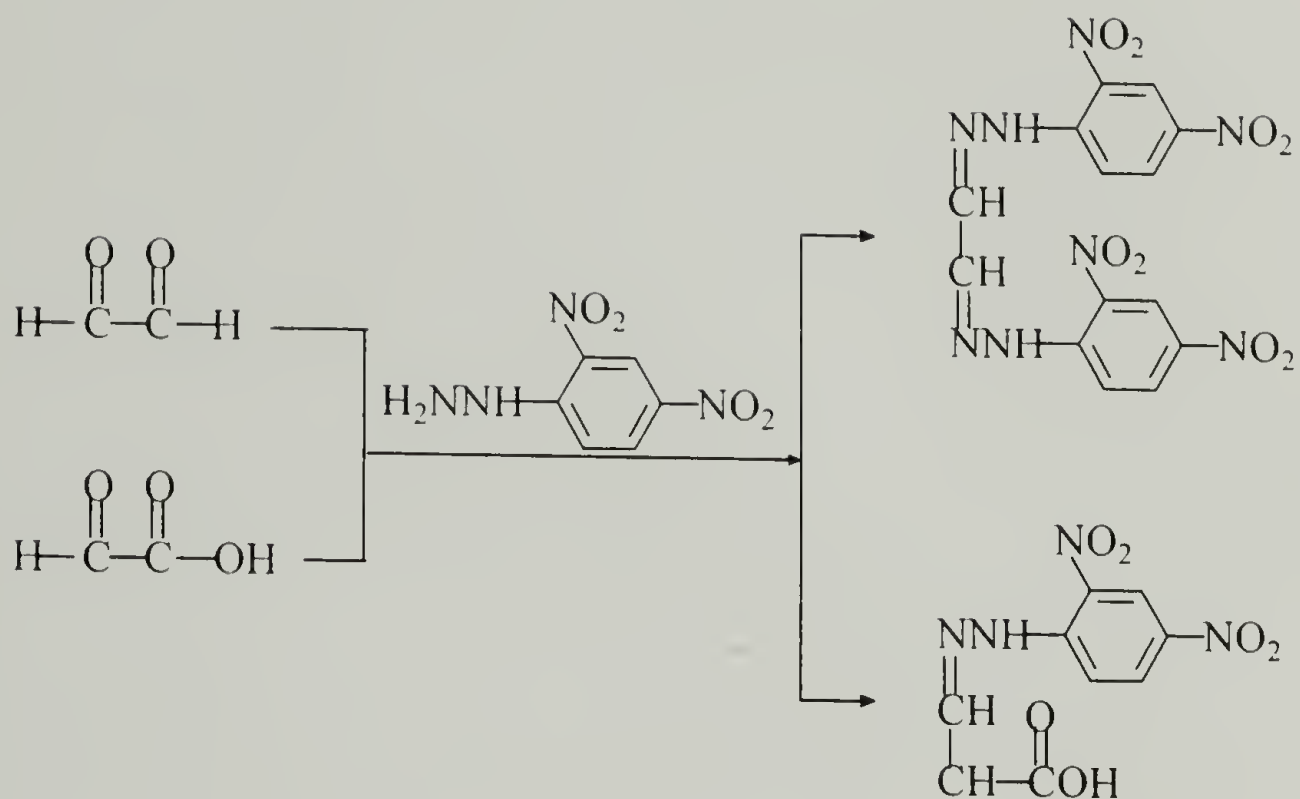
3.2.6 Thin layer chromatography of the isolated solid by-product formed during the ozonization of (80%) dimethyl-(20%)-diphenylsiloxane (PSX 80).

Thin layer chromatography (TLC) was used to identify the likely components of the crude solid. The by-product was suspected to be a mixture of carboxylic acids and possibly other carbonyl compounds [23-26]. Separation of the dibasic acids proved to be more difficult than was expected and a special procedure had to be developed. For the

carboxylic acid identification the TLC plates (Silica G / Kieselguhr layers) were impregnated with 60% acetic acid. The impregnating solvent was poured into a chromatographic tank to equilibrate for about 1 hr. The unknown mixture (0.1% solution in acetone) and a series of standard acids were spotted and the spotted plate was introduced into the impregnating tank for elution for 1 hr. The plate was then sprayed with the chromogenic reagent and introduced in the developing tank. The obtained results are reported in table 3.3 on p. 59. (ntbk-S2, 85-95)

3.2.7 Synthesis of the 2,4-dinitrophenylhydrazone derivatives

In order to identify the possible carbonyl containing by-products, by thin layer chromatography, it was necessary to synthesize the 2,4-dinitrophenylhydrazone derivatives [27]. A solution of 2,4-dinitrophenylhydrazine was prepared with the follow procedure. To about 0.4 g. of 2,4-dinitrophenylhydrazine was added 2 ml concentrated hydrochloric acid. Water (3 ml) was added dropwise with stirring and after the dissolution was complete 10 ml of 95% ethanol was added. The freshly prepared 2,4-dinitrophenylhydrazine solution was added to 20 ml of solution (2% in ethanol) of the carbonyl mixture and the standards used for comparison (glyoxal, benzaldehyde, glyoxylic acid). Crystallization of the 2,4-dinitrophenylhydrazones occurred almost immediately. The 2,4-dinitrophenylhydrazone formed from glyoxal is orange and melts at 328 °C. The glyoxylic acid derivative shows no melting (sublimes at 175 °C). The reactions are illustrated in scheme 3.1. (ntbk-S2, p.81, ntbk-S3, p. 15-18)



Scheme 3.1. The reaction of glyoxal and glyoxylic acid with 2,4-dinitrophenylhydrazines. The 2,4-dinitrophenylhydrazone formed from glyoxal is orange and melts at 328 °C. The glyoxylic acid derivative shows no melting (sublimes at 175 °C).

3.2.8 Thin layer chromatography of the carbonyl-containing by-products formed during the ozonization of (80%) dimethyl-(20%)-diphenylsiloxane (PSX 80).

Thin layer chromatography of the 2,4-dinitrophenylhydrazone derivatives created no major problems. The silica G plates (5x20 cm) were preactivated at 120 °C for 24 hr. in a vacuum oven. The TLC plates were taken out of the oven before their use, they were spotted with the unknown mixture and the standard samples and they were placed in the chromatographic tank. The developing solvent benzene / ethyl acetate (20:1) was placed in the tank one hour earlier for equilibration. Chromogenic reagent was not used because the spots were visible and their separation was followed by the naked eye. The results obtained are reported in table 3.3 on p.59. (ntbk-S3, p.20-22)

3.2.9 Ozonization of phenyltrimethylsilane

Bubbling ozonization: A small amount (~5 ml) of the silane was placed in a screw type glass vial and was set in the reactor described in fig. 3.3. The ozonator parameters were set to allow a ~4% ozone concentration (115V, 8 psig). Ozone was bubbled through the fritted glass in the silane liquid at a rate of 20 lit/hr. The reaction was stopped after three hours and the reactor was flushed with nitrogen for 15 minutes to remove the excess of unreacted ozone. The reacted liquid developed a yellow color and a dark precipitate. A portion of the ozonized silane was immediately analyzed with FT-IR. The remaining portion was mixed with water and the dark precipitate dissolved in the aqueous phase

which became yellow-brownish. The colored aqueous solution was discarded. (ntbk-S3, p. 24-27)

Mild ozonization: Phenyltrimethylsilane (~10 ml) was placed in the reactor depicted again in figure 3.3. In this case, however, the fritted glass tube did not enter into the vial and ozone was allowed simply to pass over the liquid. The reaction, due to the poor solubility of ozone in the silane was limited primarily to the surface of the liquid. The ozonator parameters were set again at 115 V and 8 psig, and the flow was set to 20 lit/hr. The silane was allowed to react up to 20 hr. Small portions were taken out for FT-IR analysis at various time intervals (1/2, 7 and 20 hr.). The silane liquid remained colorless throughout the reaction and no precipitate developed. (ntbk-S3, p.29-30, p. 32-35)

3.3 Results and discussion

3.3.1 Polydimethylsiloxanes

It was mentioned in the previous chapter that one of the most resistant silicon bonds for ozonization cleavage is the Si-CH₃ [6]. Various molecular weight polydimethylsiloxanes (PDMS) were used to examine the reactivity Si-CH₃ under the conditions which are used to synthesize the hybrid materials. Polydimethylsiloxane (PDMS) liquids proved to be ozone resistant and no reaction was observed up to 24 hours. Two representative FT-IR spectra for the 770 PDMS are depicted in fig. 3.5. Both the ozonized and the non-ozonized samples show identical spectra. The asymmetric and

symmetric stretching bands of $\text{SiH}_2\text{C-H}$ appear at 2963 cm^{-1} and 2905 cm^{-1} and the deformation mode at 1413 cm^{-1} . The intense band at 1261 cm^{-1} is due to the symmetrical deformation of Si-CH_3 . This is accompanied by other absorptions around $800\text{-}900\text{ cm}^{-1}$; $\text{Si-(CH}_3)_2$ absorbs at 805 cm^{-1} ; $\text{Si-(CH}_3)_3$ at 843 cm^{-1} and 754 cm^{-1} . The siloxane absorption, Si-O-Si , appears at 1093 cm^{-1} and 1030 cm^{-1} the symmetric stretch is observed at 689 cm^{-1} and 644 cm^{-1} .

In an attempt to quantify the results, the spectra were analyzed and the peaks were normalized to the Si-O-Si peak. The intensities of the normalized bands remain independent of the ozonization time. The results obtained are reported in table 3.1.

Samples for X-ray photoelectron spectroscopy (XPS) were prepared by spin-coating polydimethylsiloxanes on stainless steel substrates. In order to remove any dissolved gases, the thin films were degassed (vacuum, 100°C) overnight before they were analyzed. The atomic concentrations were obtained at 15° and 75° take-off angles and are reported on table 3.2. The results from the XPS analysis show that the relative atomic concentrations of Si, C, and O remain invariant with the ozonization time which verifies that no reaction takes place.

The results obtained from the ozone interaction with polydimethylsiloxane (PDMS) seem to be in agreement with other studies. Others have also observed, under different experimental conditions, that PDMS is resistant to ozone attack [6-8]. Barry and Beck [8], however, have reported that above 50°C solid PDMS has shown a degradation which is a function of temperature.

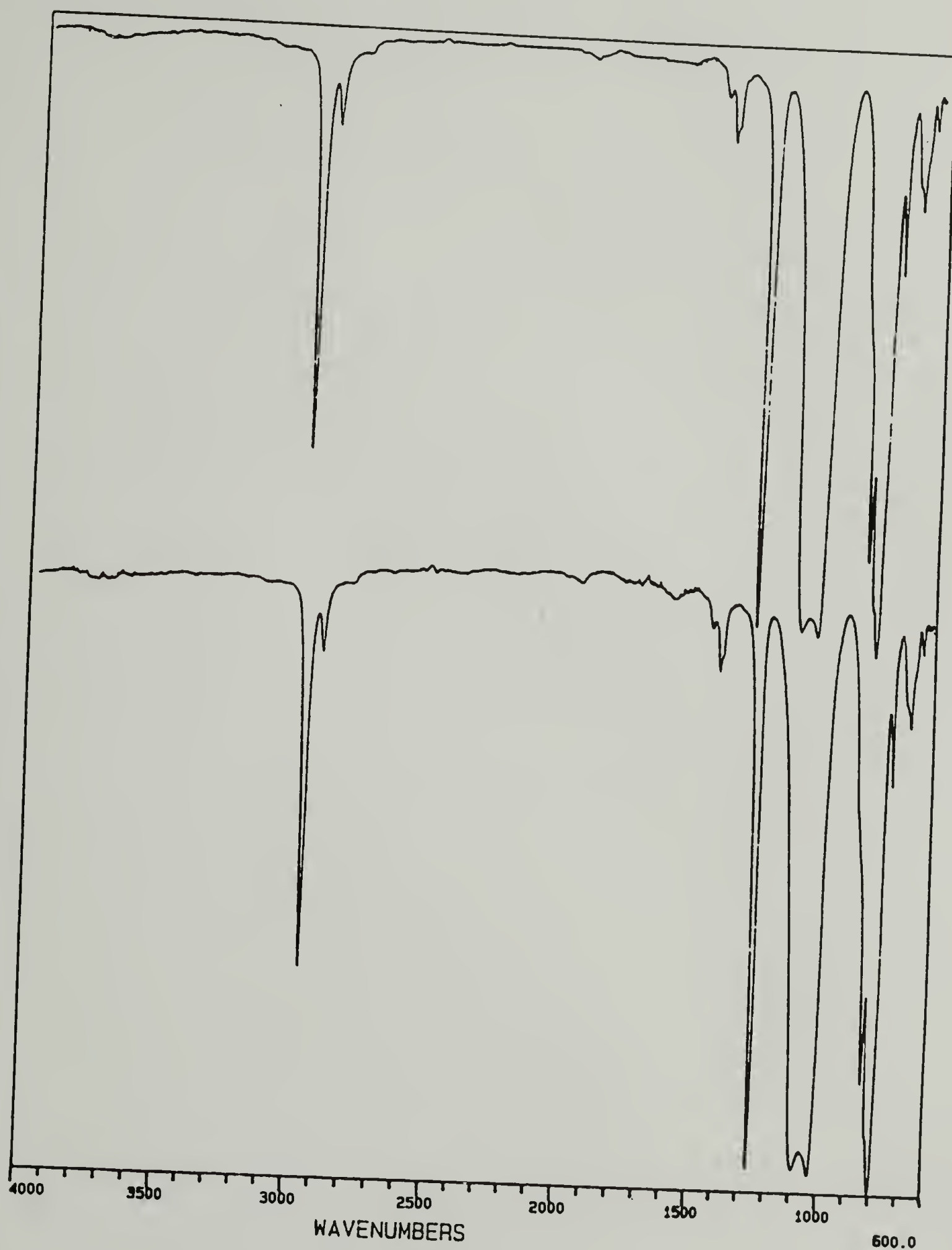


Figure 3.5. Representative FT-IR spectra of a polydimethylsiloxane sample ($M_w=770$). The top is from the pure (non-ozonized) sample and the bottom is taken from the same sample ozonized for 24 hours.

Table 3.1. Relative intensity of characteristic bands of polydimethylsiloxanes normalized to the ν_{as} Si-O-Si (1030 cm^{-1}).

Mw	Absorption bands	Ozonization time (hr)			
		0	2	14	24
770	ν_{as} SiCH ₂ -H (2963 cm^{-1})	0.73	0.73	0.65	0.74
	δ_{s} Si-CH ₃ (1261 cm^{-1})	1.0	1.0	1.0	1.0
	δ_{s} Si-(CH ₃) ₂ (805 cm^{-1})	1.0	1.1	1.1	1.0
93.7K	ν_{as} SiCH ₂ -H (2963 cm^{-1})	0.70	0.72	0.72	0.78
	δ_{s} Si-CH ₃ (1261 cm^{-1})	1.0	1.0	1.0	.0.9
	δ_{s} Si-(CH ₃) ₂ (805 cm^{-1})	1.0	1.0	1.0	0.9
250K	ν_{as} SiCH ₂ -H (2963 cm^{-1})	0.73	0.75	0.75	0.75
	δ_{s} Si-CH ₃ (1261 cm^{-1})	1.0	1.1	1.0	1.0
	δ_{s} Si-(CH ₃) ₂ (805 cm^{-1})	0.9	0.9	0.9	0.9

Table 3.2. The XPS atomic concentrations of 93.7K and 250K polydimethylsiloxane copolymers in relation to ozonization times. The atomic concentrations were determined for two different XPS take-off angles (15°, 75°).

		Atomic concentration (%)					
		C 1s		Si 2p		O 1s	
Mw	Time (hr)	15°	75°	15°	75°	15°	75°
93k	0	53.4	52.9	21.5	21.2	25.1	26.0
	2	54.4	53.5	21.1	20.9	24.5	25.6
	24	-	54.0	-	21.6	-	24.4
250k	0	53.1	53.0	19.9	20.1	27.0	26.9
	2	-	52.9	-	21.6	-	25.5
	24	54.8	54.5	20.9	20.3	24.4	25.2

3.3.2 (80 %) dimethyl-(20 %)-diphenylsiloxane (PSX 80)

In the previous section it was observed that the SiCH_3 moiety is resistant to ozone attack. This was the first step in examining the reactivity of siloxanes toward ozone. The next step was to study the ozone interaction with the Si-Ar moiety. This was significant because, as was stated earlier, both SiCH_3 and SiAr groups are components of the materials used later to form the desired organic-inorganic hybrids. The Si-Ar is especially important because it appears in our glass forming agent (phenylsilane).

Three different methods were examined for the ozonization of PSX. The solid state method was useful in producing self supporting films. The films were formed on the surface of the silicone oil. This was an indication of selective surface oxidation. The preferred surface oxidation was presumably a result of the low ozone solubility and slow diffusion in the silicone oil. This in turn could be a result of difference in polarity of ozone molecule in comparison to polysiloxane. In spite of the success in producing films, this method was not further pursued to study the reaction of SiAr due to the fact that the results were not reproducible from sample to sample.

The solution ozonization is a widely used method for ozone reactions with most organic compounds [9, 10]. This method was utilized in order to examine the possibility of increasing ozone solubility and to control the viscosity of the reaction media. Many different solvents have been reportedly used in the solution ozonization. They are classified as participating and non-participating solvents. The participating solvents react with the intermediates and they become part of the reaction [11, 17]. Some examples of

participating solvents are: alcohols [18, 19], organic acids [20, 21] and water [22]. One of the highest ozone solubilities in these type of solvents is observed in glacial acetic acid [17].

On the other hand the non-participating are the solvents that do not react with zwitterion intermediate [11]. Examples of inert solvents are: alkanes [12, 13], methylene chloride [14], chloroform [15] and carbon tetrachloride [16]. Additional reports have also indicated that ozone solubility in carbon tetrachloride is very high [17].

It was for this reason that carbon tetrachloride was chosen as the solvent of choice in this work. Because of the long reaction times and high gas flow required for this type of ozonization, however, uncontrollable solvent evaporation was observed even at very low temperatures, and therefore, this method proved to be inconvenient and was not further examined.

The neat ozonization used for all the subsequent ozonizations as the method of choice. In this method ozone was bubbled through the siloxane liquid in the absence of any solvent. During the vigorous ozonization of PSX 80 two phases (a solid and a liquid) gradually developed. The solid phase developed on the surface of the liquid (spongy, low density) and was the minor component of the mixture. The solid concentration was increasing (up to 5% of the total weight) at the expense of the liquid phase as the time of ozonization progressed. The liquid phase (viscous oil) shown a continuous color change (from colorless to intense yellow-orange) depending on the ozonization time. As was stated before, the liquid phases were mixed with diethyl ether and water.

The aqueous fractions of all the ozonized samples were isolated and the water was evaporated. Water evaporation yielded a yellow-orange precipitate. The acidic concentration in the different isolated solids, determined by using a pH-meter, showed an increase with the time of ozonization, fig. 3.6. In addition, end point potentiometric titration of the 43 hr isolated solid (after water evaporation), with 0.1 N sodium hydroxide gave pH=4.1. Furthermore, an FT-IR spectrum of this crude by-product is depicted in fig. 3.7. A strong carbonyl band appears at 1732 cm^{-1} . Melting point determinations of the yellow isolated solid showed a continuous melting range from about $50\text{ }^{\circ}\text{C}$ to $190\text{ }^{\circ}\text{C}$. This was a clear indication of a mixture.

Thin layer chromatography (TLC) was used to identify the likely components of the crude solid. The by-product was suspected to be a mixture of carboxylic acids and carbonyl compounds [23-26]. The R_f values obtained from TLC experiments for the identification of the acids, table 3.3, indicate the presence of oxalic acid ($R_f=0$) and a possible presence of glyoxylic acid ($R_f=3.8$). On the other hand, TLC experiments for the identification of the 2,4-dinitrophenylhydrazone derivatives indicate the presence of glyoxylic acid ($R_f=0$) and glyoxal ($R_f=33$).

The identified oxalic acid was removed from the mixture by vacuum sublimation (80 mtorr , $78\text{ }^{\circ}\text{C}$) for 30 minutes. The recovered oxalic acid was about 60 % of the total solid and recrystallization from glacial acetic acid produced white granular flake type crystals. An FT-IR spectrum of the purified oxalic acid is illustrated in fig. 3.8.

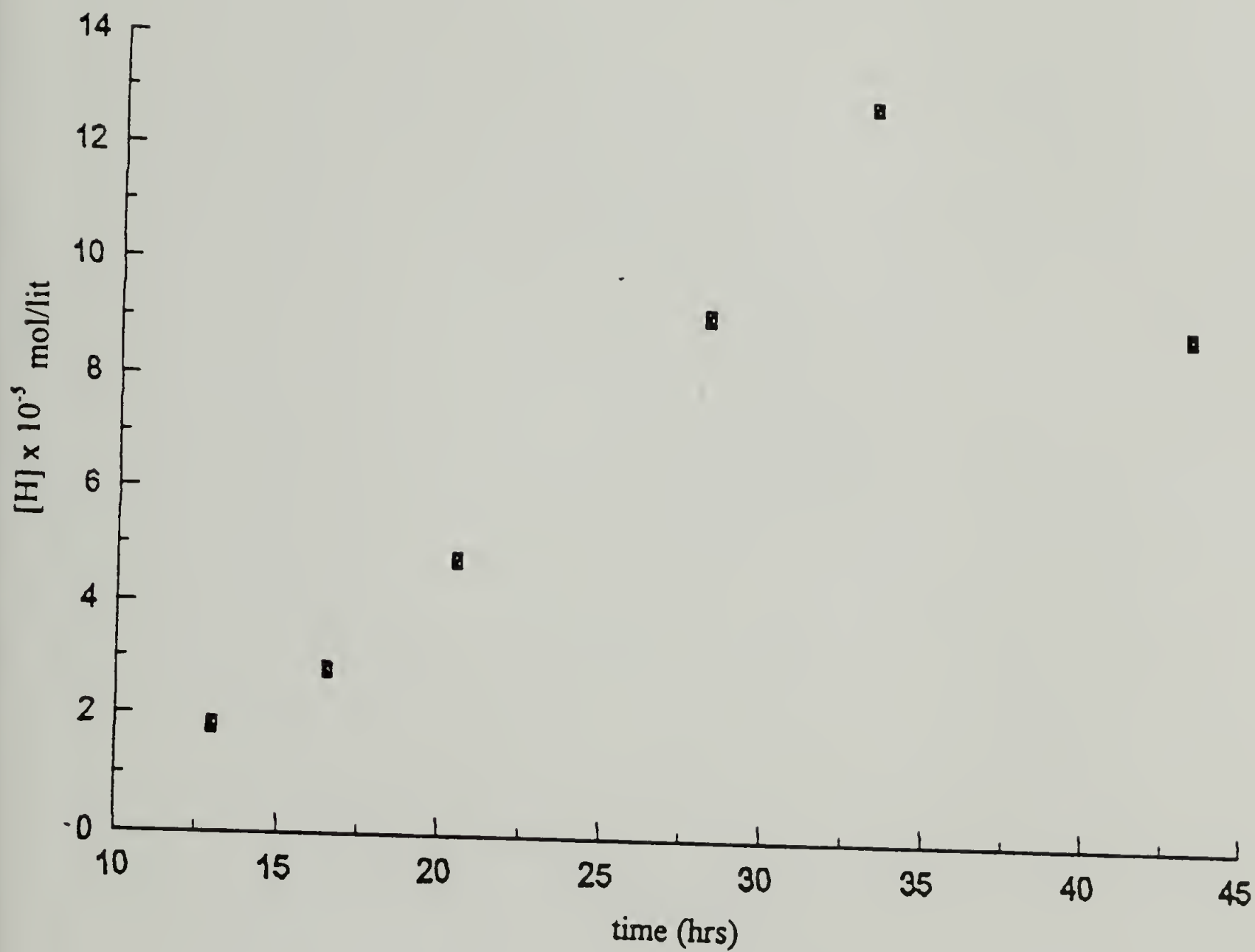


Figure 3.6. Acidic concentration as a function of ozonization time. The ozonized material is the (80 %) dimethyl-20 %-diphenylsiloxane.

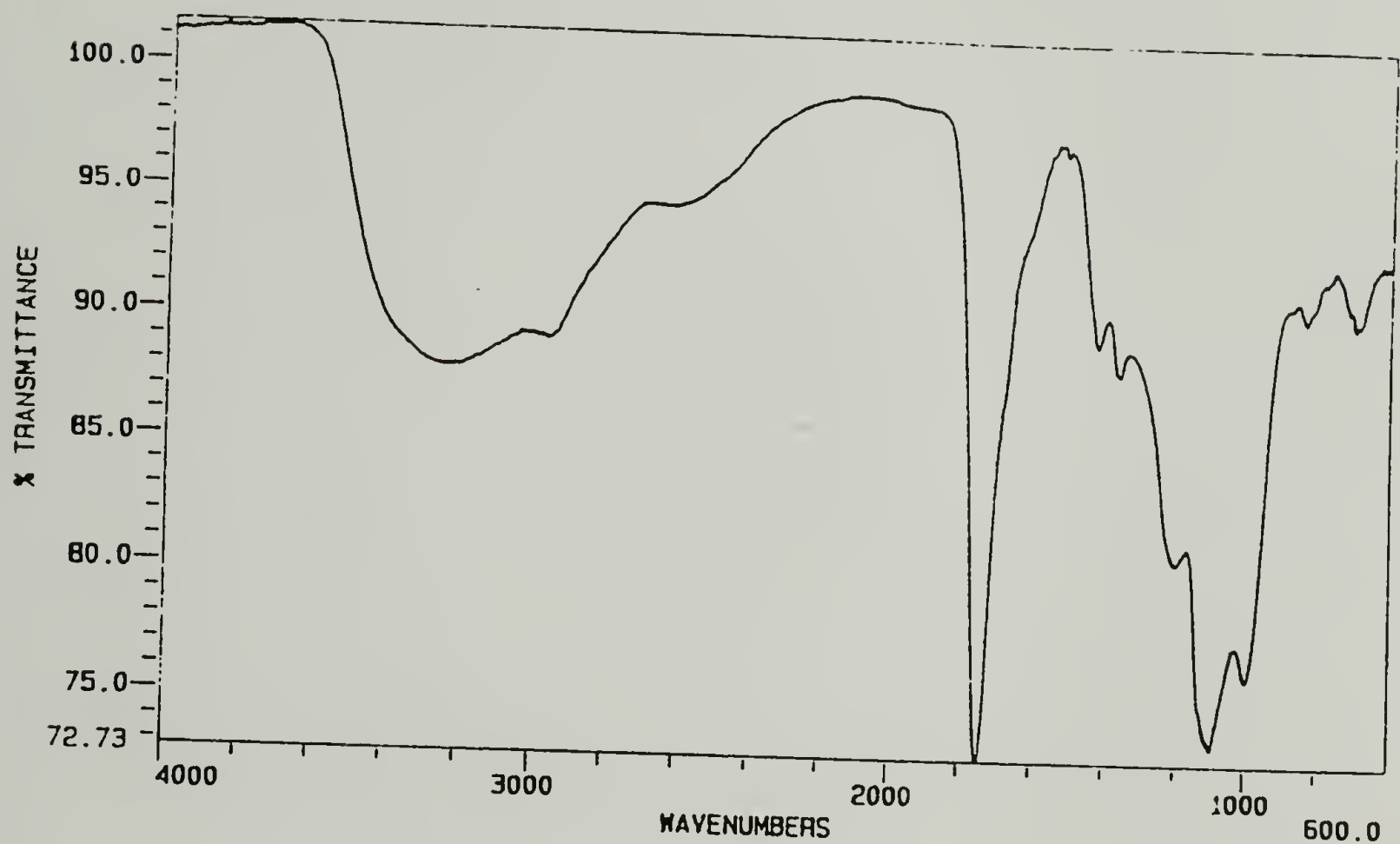


Figure 3.7. FT-IR spectra of the crude isolated by-products from the 43 hr ozonization of the (80%) dimethyl-(20%)-diphenylsiloxane (PSX 80) sample

Table 3.3. Thin layer chromatography of a series of standard compounds suspected in the unknown acidic mixtures produced from ozonization reactions.

Acids ($R_f \times 100$)		Acids ($R_f \times 100$)		Aldehydes ($R_f \times 100$)	
oxalic	0	succinic	35	glyoxal	33
glyoxylic	3.8	adipic	60	benzaldehyde	70
malonic	5.4	benzoic	87	glyoxylic acid	0
maleic	3.3	p-hydroxybenzoic	43		
UNKOWN		0, 3.5		UNKNOWN	
				0, 32	

The spectrum at the top was obtained from a pure commercial oxalic acid; the characteristic carbonyl absorption band appears at 1732 cm^{-1} . Upon heating, no melting was observed and the solid sublimed at $157\text{ }^{\circ}\text{C}$.

After the aqueous portion of the sol phase was analyzed, the organic portion was examined. Ether evaporation showed that the residual liquid siloxane had not been ozonized. In addition, data obtained from size exclusion chromatography of the liquid siloxanes is reported in table 3.4. This data shows that the molecular weight and molecular weight distribution are not affected by the ozonization time. This verifies that the Si-O-Si moiety is more resistant to ozone attack than the Si-Ar.

The solid (gel) phase was analyzed using FT-IR spectroscopy, chemical analysis, ^{29}Si NMR, and thermal analysis. The gel was insoluble to all known solvents for siloxanes (THF, ethers, chlorinated hydrocarbons, MEK, etc.). The infrared spectra shown in fig. 3.9 indicate that the reaction has advanced significantly after 43 hr ozonization.

Zeisel's alkoxy method was employed to examine the possibility of existence of Si-OR, Si-COOR and Si-(COOR)₂. This test is based on the fact that functional groups containing methyl, ethyl, propyl or isopropyl radicals attached to oxygen are cleaved by the hydriodic acid with the formation of volatile alkyl halides:

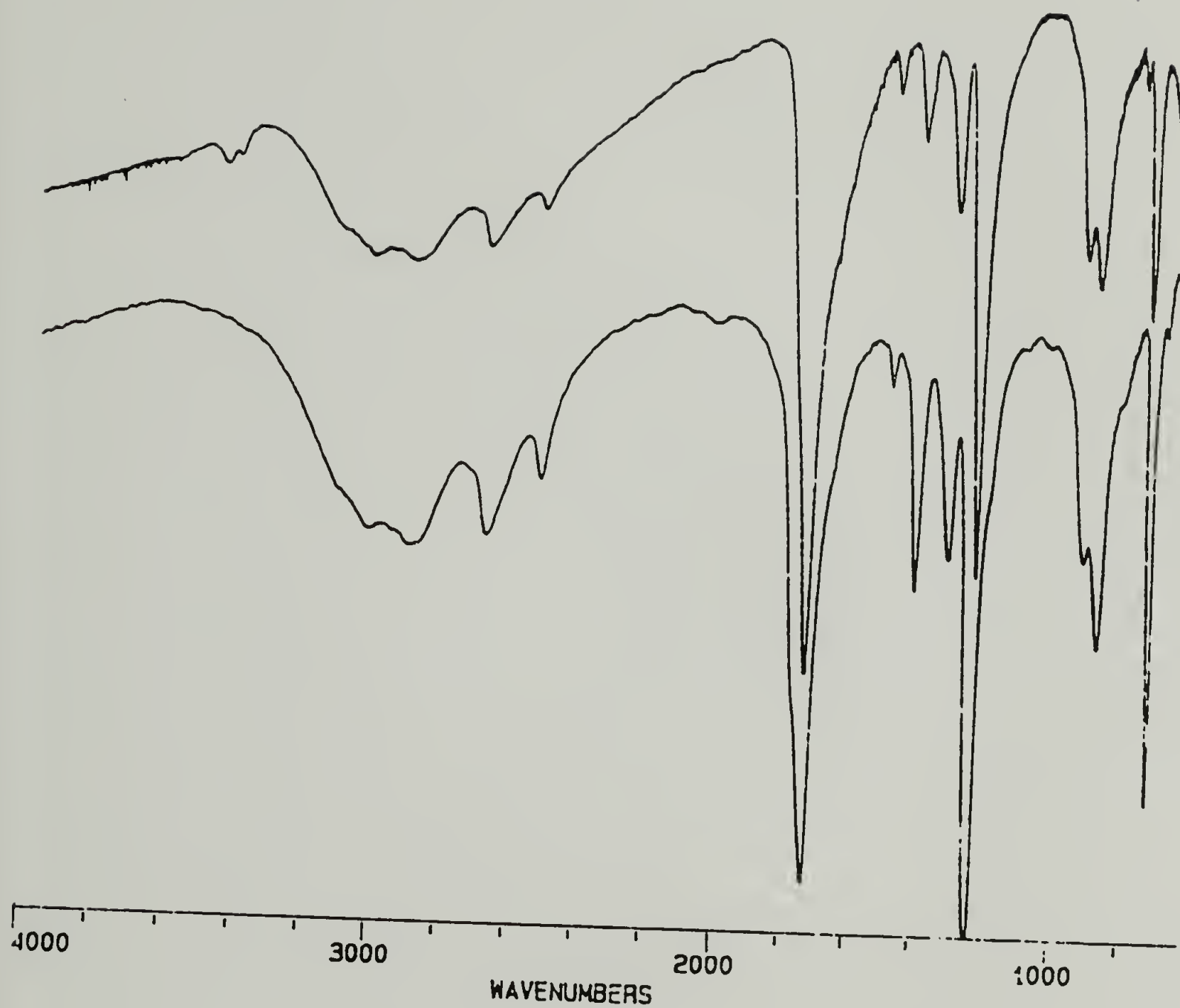


Figure 3.8. FT-IR spectra obtained from a standard sample of oxalic acid (top) and from the purified by-product isolated after the ozonization of (80%) dimethyl-(20%)-diphenyl siloxane (PSX 80) sample.

Table 3.4. Size Exclusion Chromatographic data for the (80%) dimethyl-(20%)-diphenylsiloxane ozonized from 13 to 43 hr.

ozonization time (hr)	Mn	Mw	PDI=Mw/Mn
0	1052	1906	1.8
13	1028	1810	1.8
16	1035	2732	2.6
20	1048	1832	1.7
28	991	1797	1.8
33	982	1705	1.7
43	1161	2866	2.4

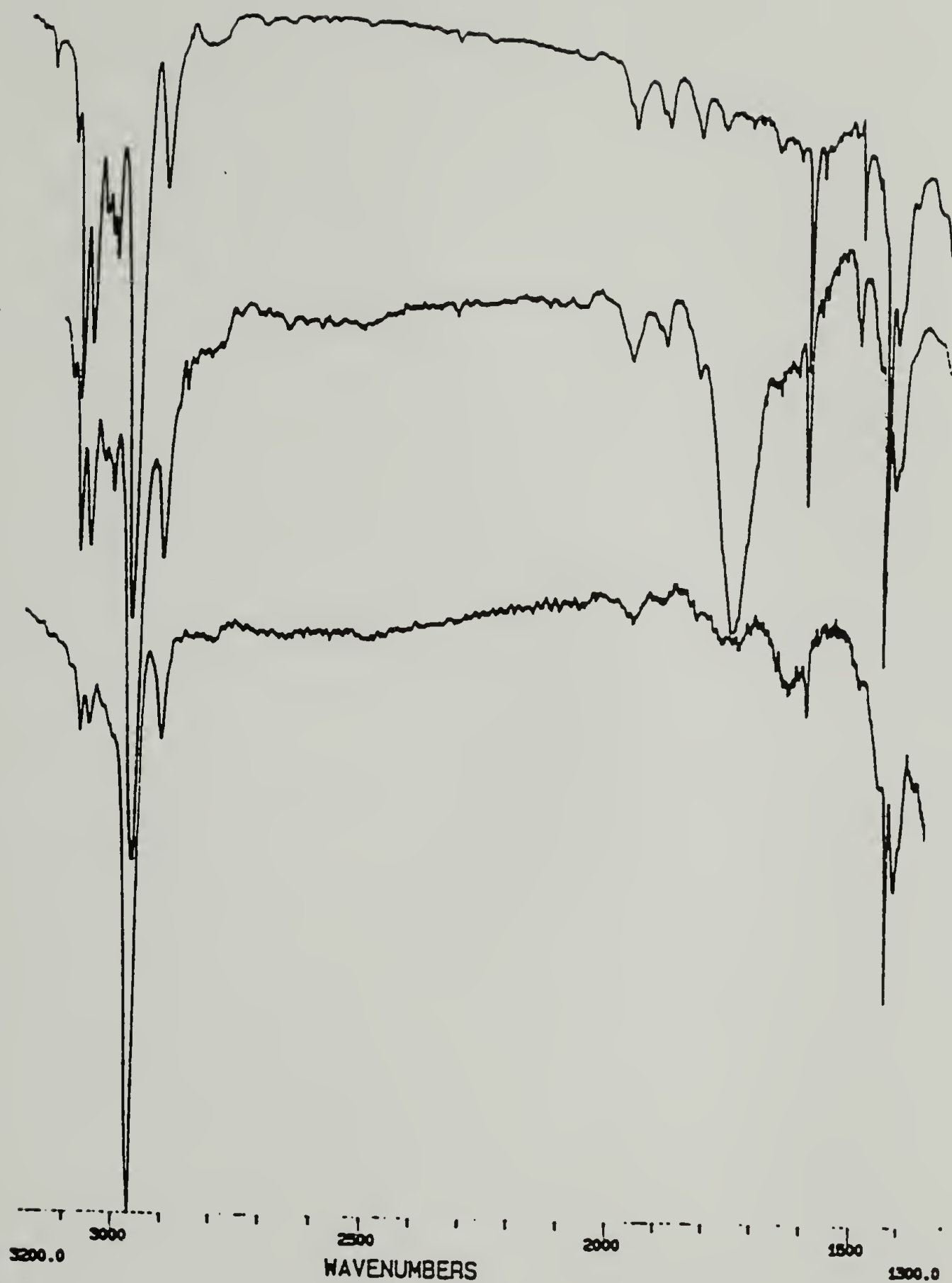


Figure 3.9. FT-IR spectra of the (80%) dimethyl-(20%)-diphenylsiloxane (PSX 80) at different ozonization times. The spectra shown at the top was taken from an non-ozonized PSX 80. The 6 hours ozonization spectra is shown in the middle and the 43 hours on the bottom.



This test gave negative results which indicated the absence of these groups in the crosslinked copolymer. Details about the experimental procedure are described elsewhere [28, 29]. (ntbk-S2, p.69-70)

The representative solid state ^{29}Si NMR spectrum shown in fig. 3.10 indicates the formation of trifunctional (-72 ppm) and tetrafunctional silicon (-82 ppm, -87 ppm) which is a result of the crosslinking due to ozone oxidation. The peak at -23 ppm is due to the $\text{Si}(\text{CH}_3)_2$. ^{29}Si NMR shows the absence of any SiO_2Ph_2 peak which would appear around 43-49 ppm [29.a].

Thermogravimetric analysis (TGA) was employed to examine the thermal degradation and the thermal stability of the 43 hr. ozonized copolymer. The thermograms depicted in fig. 3.11 imply the existence of different degradation mechanisms for the pure copolymer and the ozonized material. In addition, the crosslinked copolymer itself shows two degradation mechanisms. The main degradation begins at 330 °C up to 600 °C (heating rate 10 °C/min under nitrogen) and the residual mass left after the final siloxane degradation was 27 %. Thermogravimetric analysis was useful also for determining the kinetic parameters of the main degradation such as, energy of activation, [30, 31, 32].

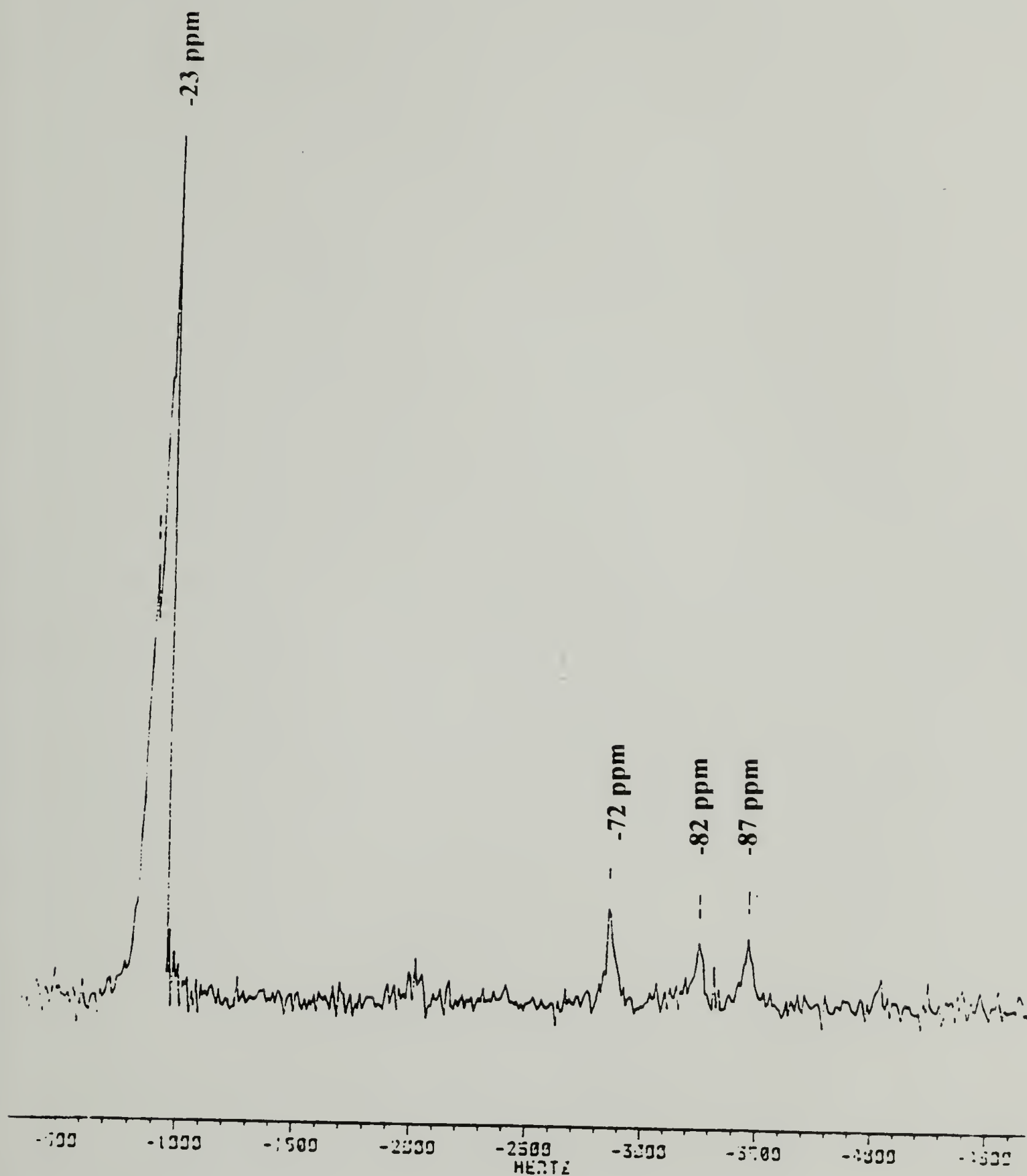


Figure 3.10. Solid state ^{29}Si NMR of the isolated (80%) dimethyl-(20%)-diphenyl siloxane (PSX 80) ozonized for 43 hrs. The peak at -23 ppm is due to unreacted $-\text{Si}(\text{CH}_3)_2$ while the peaks at -72 ppm, -82 ppm, and -87 ppm are due to trifunctional and tetrafunctional silicon.

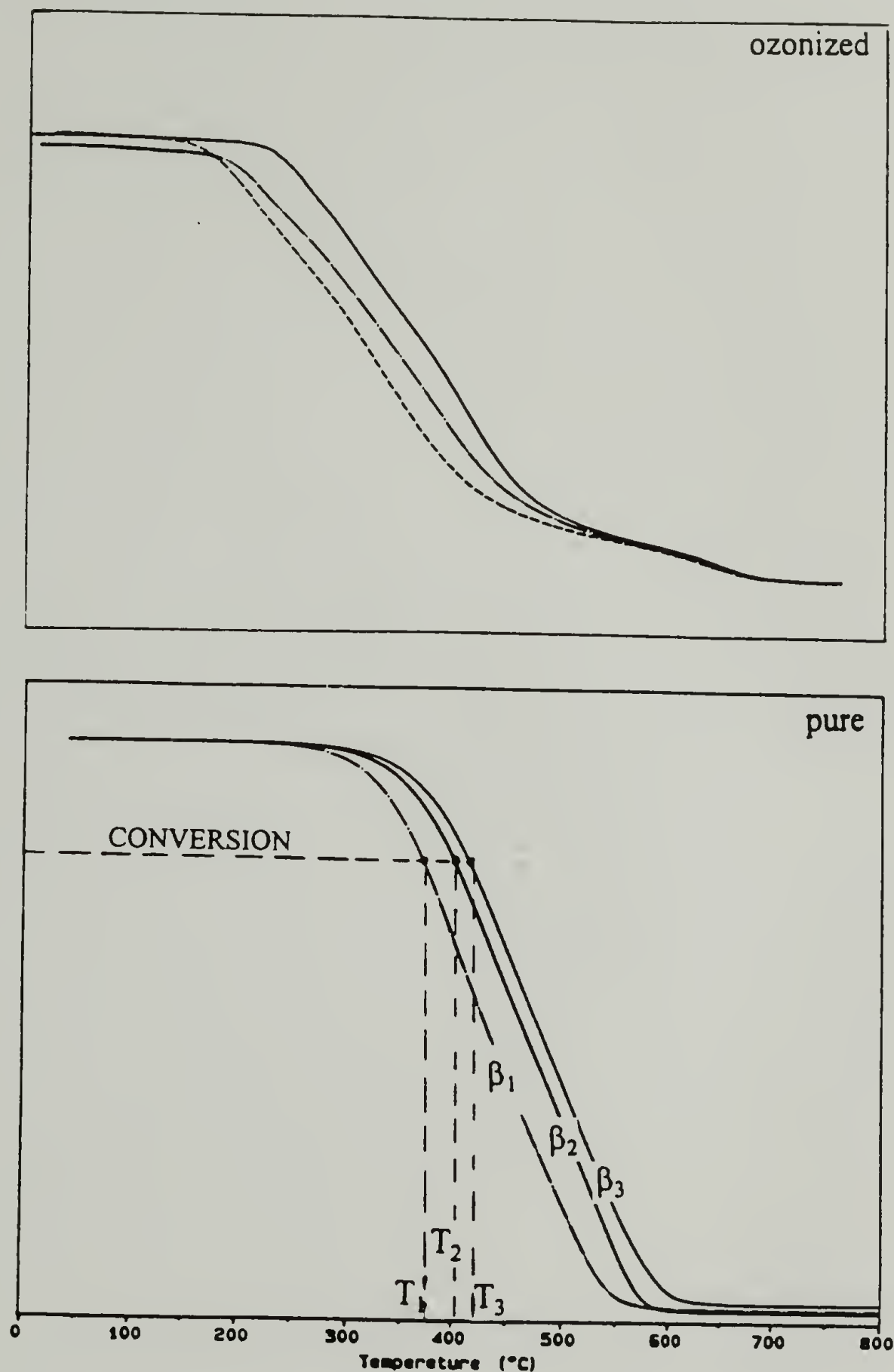


Figure 3.11. Thermograms obtained from the thermal degradation of pure and ozonized copolymer. The heating rates are: $\beta_1=5^\circ\text{C}$, $\beta_2=10^\circ\text{C}$ and $\beta_3=20^\circ\text{C}$. The isoconversion temperatures are T_1 , T_2 , and T_3 . The activation energy can be calculated from the plot of $\log\beta$ vs. $\log 1/T$, while the average value can be obtained from the various isoconversion plots.

In order to calculate the activation energy, the method suggested by Flynn and Wall [32] was utilized. The basic equation is

$$\partial \log \beta / \partial (1 / T) \cong (0.457 / R) \times E$$

β = is the heating rate

T = temperature ($^{\circ}$ K)

R = 1.987 cal./mol* $^{\circ}$ K

E = activation energy (cal./mol)

The temperatures (T_1 - T_3) are determined from the thermograms of weight loss vs. temperature at three different heating rates (5, 10 and 20 $^{\circ}$ C), fig 3.11. The activation energy was calculated from the slope of a plot of the $\log \beta$ vs. $\log 1/T$. The procedure is repeated for several different weight conversions, fig 3.11, and the average activation energy is reported. The average activation energy calculated for the pure copolymer is 30 Kcal/mol and for the ozonized material is 38 Kcal/mol. This method is described in more detail in chapter four of this thesis.

3.3.3 Phenyltrimethylsilane

It was mentioned earlier that the ozone attack on the phenyl containing siloxanes produces carboxylic acids and carbonyl containing by-products. In addition, it was

mentioned that ozonization of the copolymers resulted in crosslinked products, as well. Figure 3.12 illustrates the ozonization of (80%) dimethyl-(20%)-diphenylsiloxane (PSX 80). The results obtained lead to the conclusion that ozone attack on PSX 80 could follow two possible paths. The first path is illustrated in fig. 3.13. The nucleophilic attack of ozone takes place on silicon atom, and a "super" peroxide produced which decomposes to a hydroperoxide before the formation of the final product. On the other hand a second possible path follows a nucleophilic ozone attack on the aromatic ring which causes in the beginning a ring cleavage and then breakage of the SiAr bond to form SiOSi, fig. 3.14. It was not clear, however, which mechanism prevailed. In an effort to better clarify this point, phenyltrimethylsilane was oxidized under two different ozonization conditions (bubbling and mild). A scheme of a plausible ozonization attack on phenyltrimethylsilane is illustrated in fig. 3.15. In this case again ozonization follows two possible paths, either by attacking the Si atom, or by attacking the aromatic ring.

The FT-IR spectrum for the three hours bubbling ozonization is illustrated in fig. 3.16. The spectrum of the unreacted silane is depicted for comparison. The appearance of the carbonyl peak at 1745 cm^{-1} and the development of SiOSi (disiloxane) band at 1056 cm^{-1} is an indication for both SiAr bond and aromatic ring cleavage. Mild type ozonization, however produces different products. There was no observable SiOSi band at 1057 cm^{-1} for ozonizations up to 20 hours, even though the carbonyl peak at 1715 cm^{-1} developed rapidly (first 30 minutes) and broadened with increased intensity as the reaction time increases, Fig. 3.17

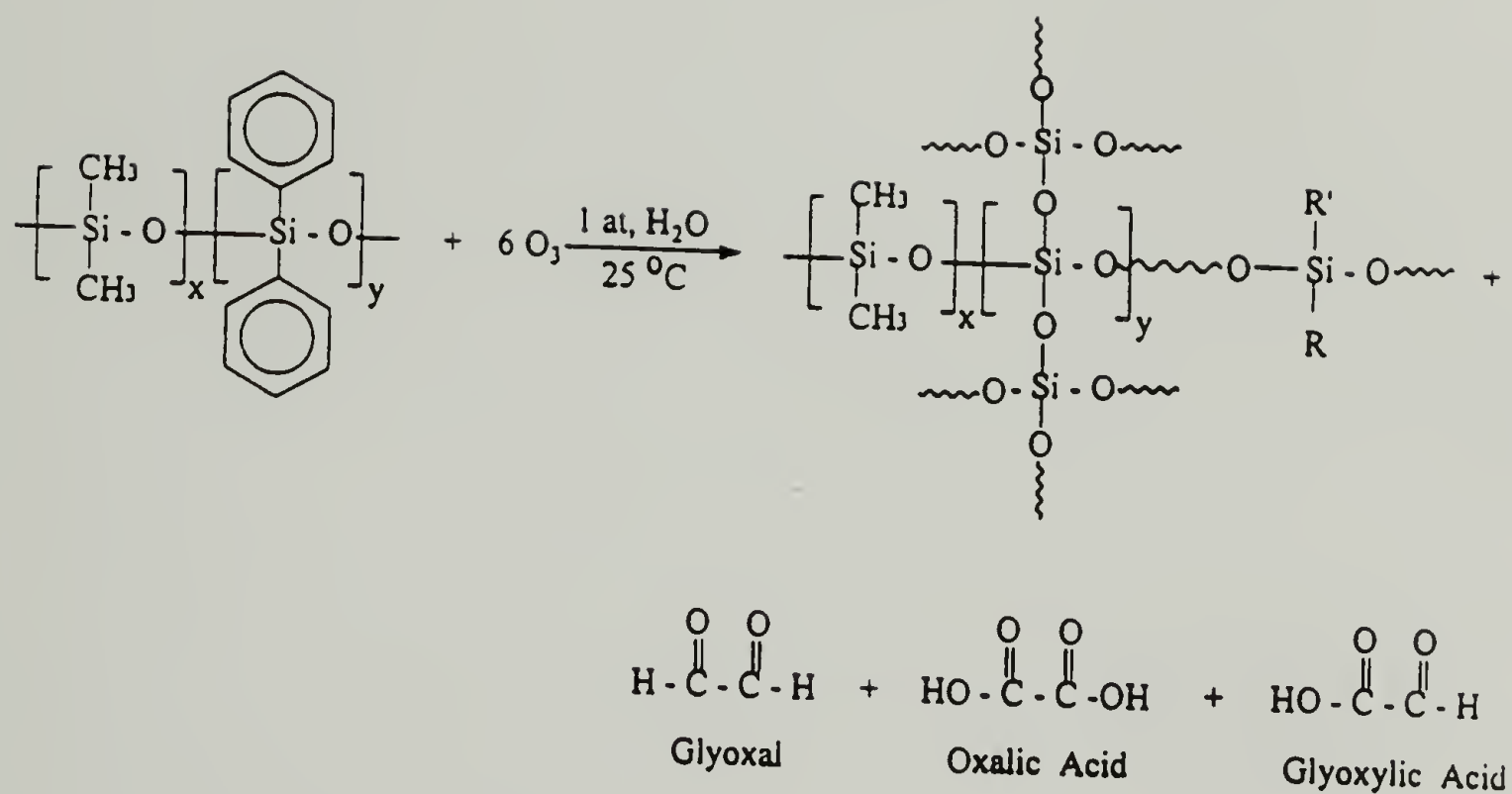


Figure 3.12. Ozonization of the (80%) dimethyl-(20%)-diphenylsiloxane (PSX 80). The isolated by-products are glyoxal, oxalic acid and glyoxylic acid.

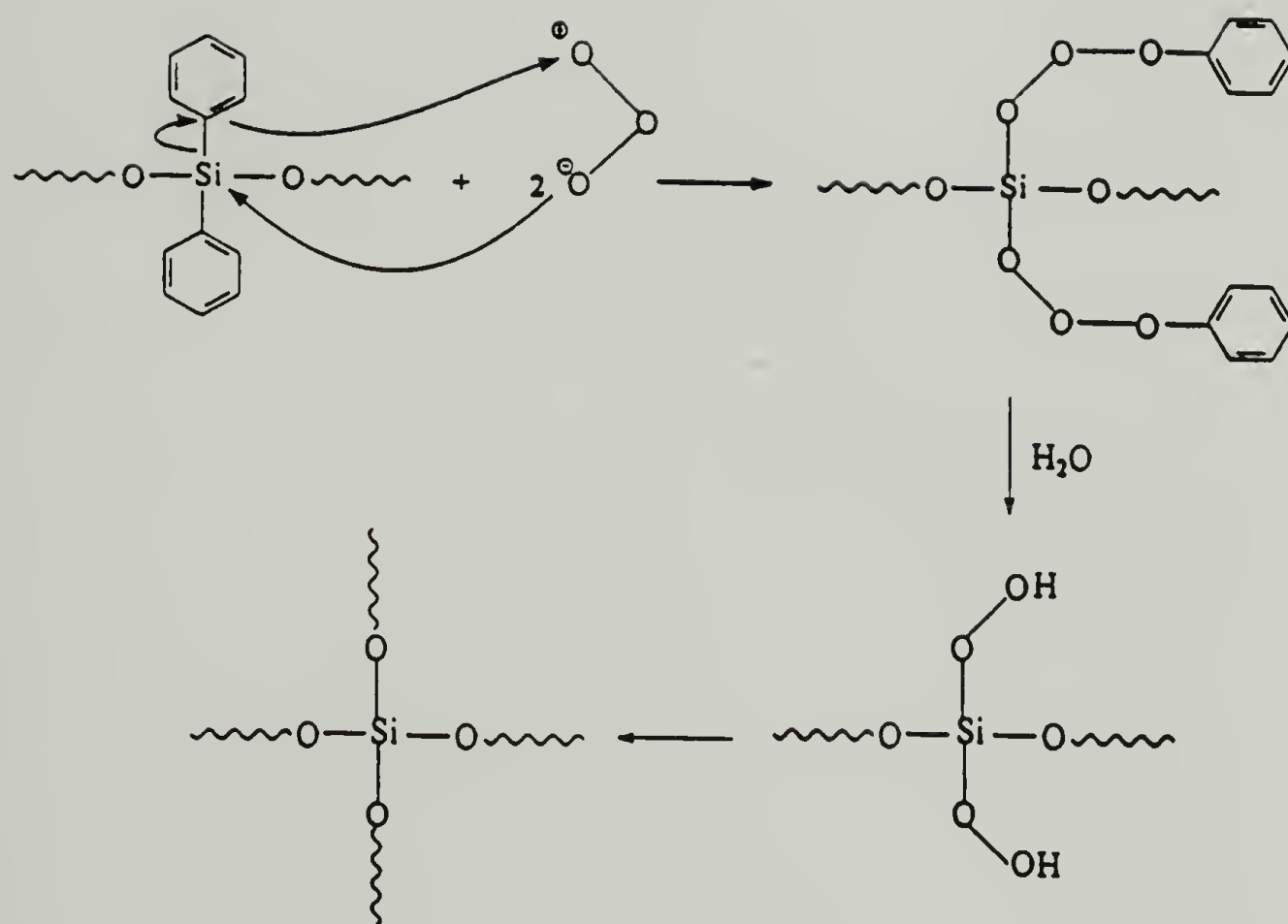


Figure 3.13. A plausible mechanism of the ozonization of the (80%) dimethyl-(20%)-diphenylsiloxane (PSX 80). First, a nucleophilic ozone attack on silicon produces a superdiperoxide which decomposes to form a peroxide. Peroxide decomposition leads to the final products.

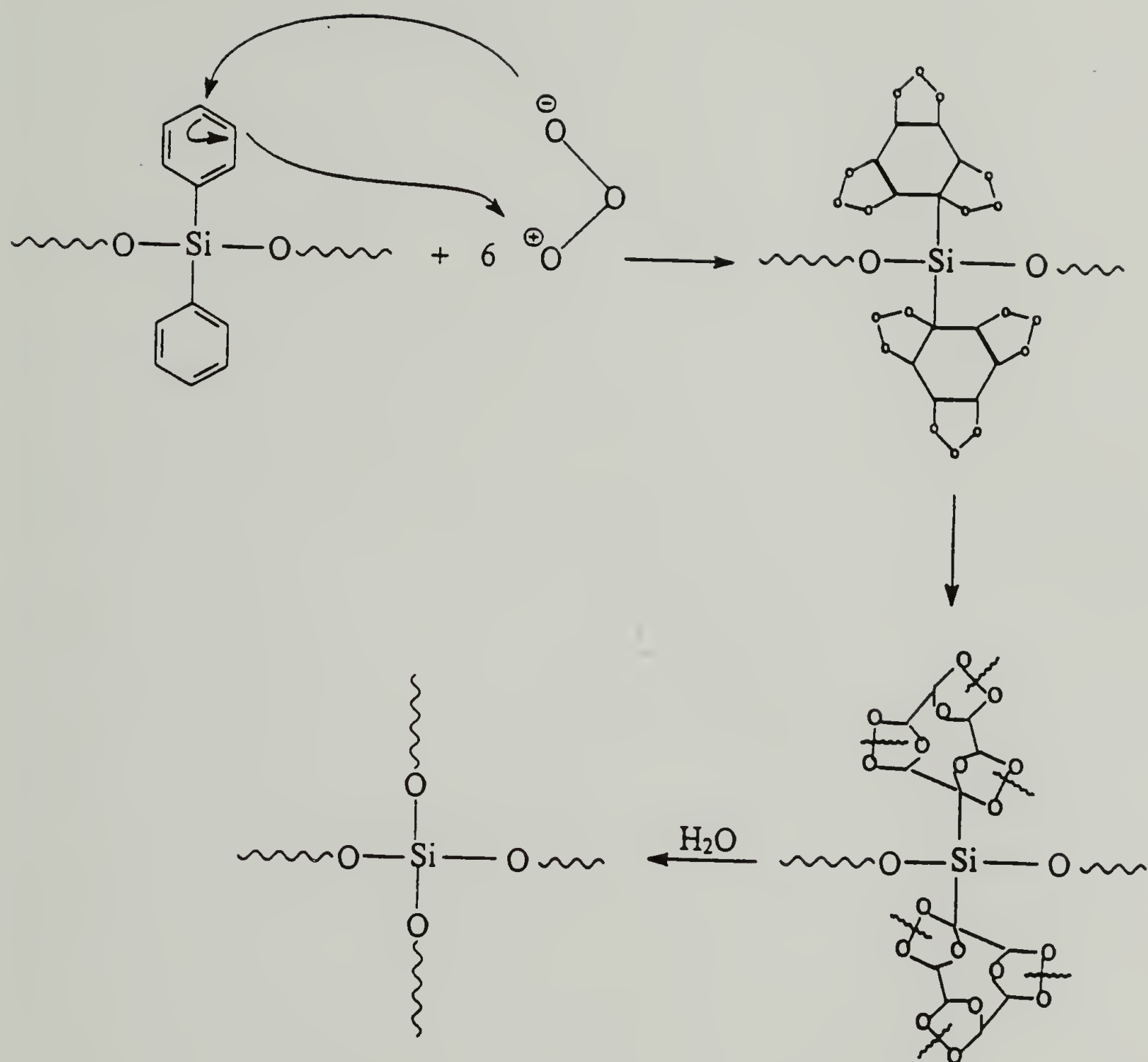


Figure 3.14. A plausible mechanism of the ozonization of the (80%) dimethyl-(20%)-diphenylsiloxane (PSX 80). First, a nucleophilic ozone attack on phenyl ring produces an unstable molozonide which rearranges to form a more stable ozonide. Ozonide decomposition leads to the formation of the desired products.

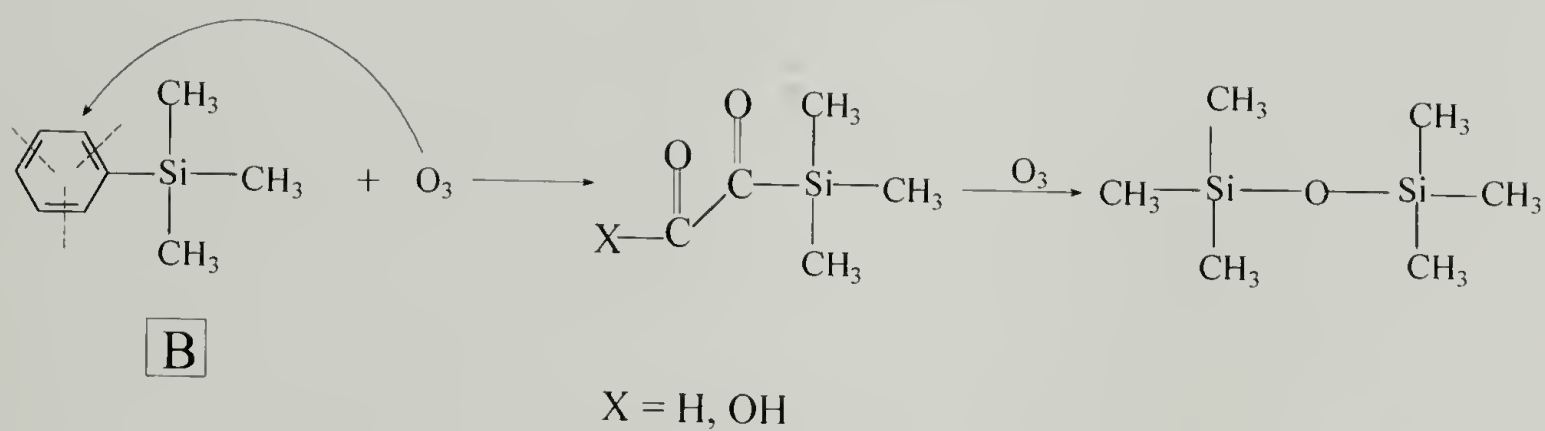
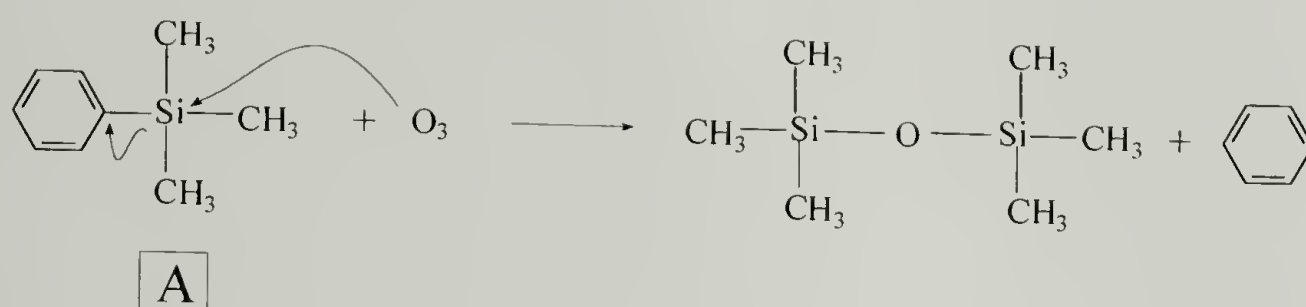


Figure 3.15. Two possible paths for the ozone attack on phenyltrimethylsilane

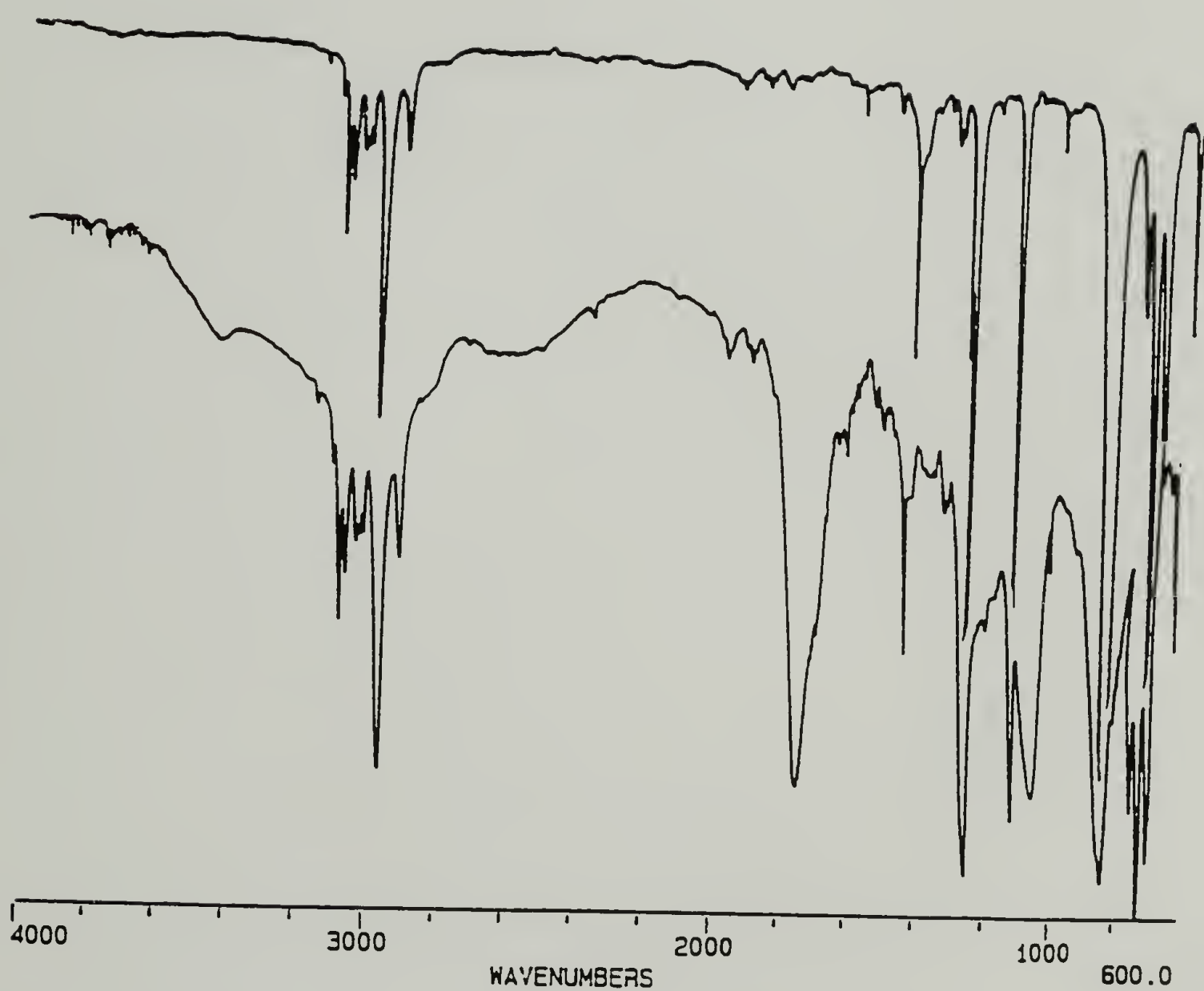


Figure 3.16. FT-IR spectra of the “bubbling” type ozonization (3 hours) of the phenyl trimethylsilane (PTMS). The top spectrum is taken from a non-reacted PTMS sample.

of the carbonyl peak at 1745 cm^{-1} and the development of SiOSi (disiloxane) band at 1056 cm^{-1} is an indication for both SiAr bond and aromatic ring cleavage. Mild type ozonization, however produces different products. There was no observable SiOSi band at 1057 cm^{-1} for ozonizations up to 20 hours, even though the carbonyl peak at 1715 cm^{-1} developed rapidly (first 30 minutes) and broadened with increased intensity as the reaction time increases, Fig. 3.17

The combination of the isolation of glyoxal, glyoxylic acid, and oxalic acid as the only by-products from the ozonization of (80%) dimethyl-(20%)-diphenylsiloxane and the results obtained from the mild and bubbling type ozonizations indicate that ozonization of the SiAr group proceeds in two steps. Ozone attack first the aromatic ring which breaks and creates a functional site at α position to Si atom. This consequently increases the polarity of the Si-C bond (destabilized) and then facilitates a polar ozone insertion, fig. 3.18.

3.4 Conclusions

The appropriate experimental setting and ozonization reactors were designed to facilitate the ozonizations of polydimethylsiloxanes (PDMS), (80%) dimethyl-(20%)-diphenylsiloxane (PSX 80), and phenyltrimethylsilane (PTMS). PDMS was selected for

ozonization in order to examine the reactivity of the SiCH_3 toward ozone. This was important because SiCH_3 group is a component of the functional siloxanes which are used for the synthesis of the organic-inorganic hybrids. PDMS proved to be resistant to ozone attack up to 24 hours. Therefore, ozone does not attack the Si-CH_3 bond under the conditions studied.

Ozone reaction with SiAr was studied due to the fact that this moiety appears in the glass forming agent in the hybrid network (phenylsilane). Experimental data indicate that SiAr oxidizes in a two step process, the SiAr produces a crosslinked network and a number of by-products (glyoxal, glyoxylic acid, and oxalic acid).

PTMS was ozonized in order to examine the mechanism of SiAr ozonization. Data from the ozonization of PTMS in combination with the isolated products from the ozonization of PSX 80 suggested that ozone attacks first at the aromatic ring and then the polarized Si-CO .

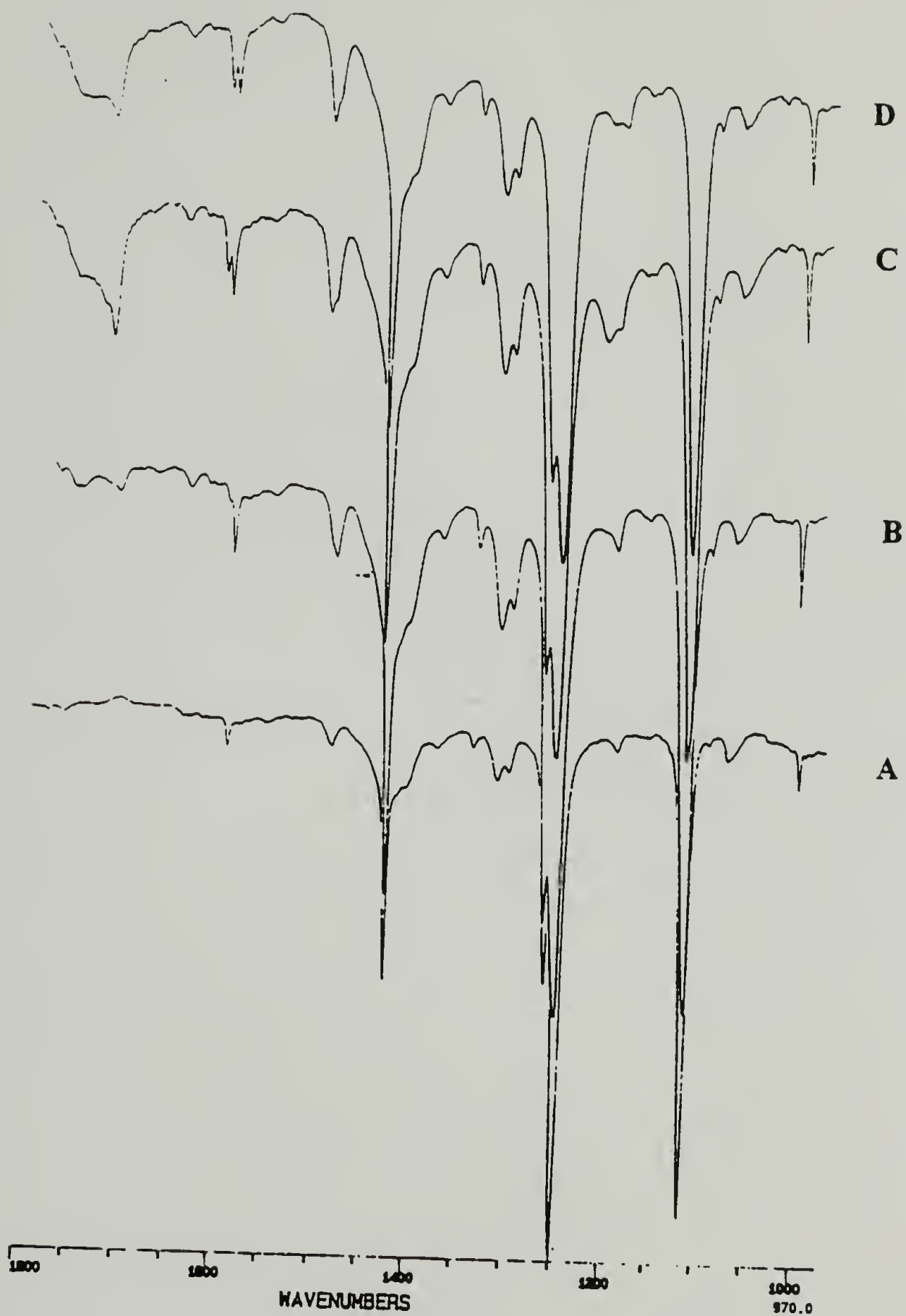
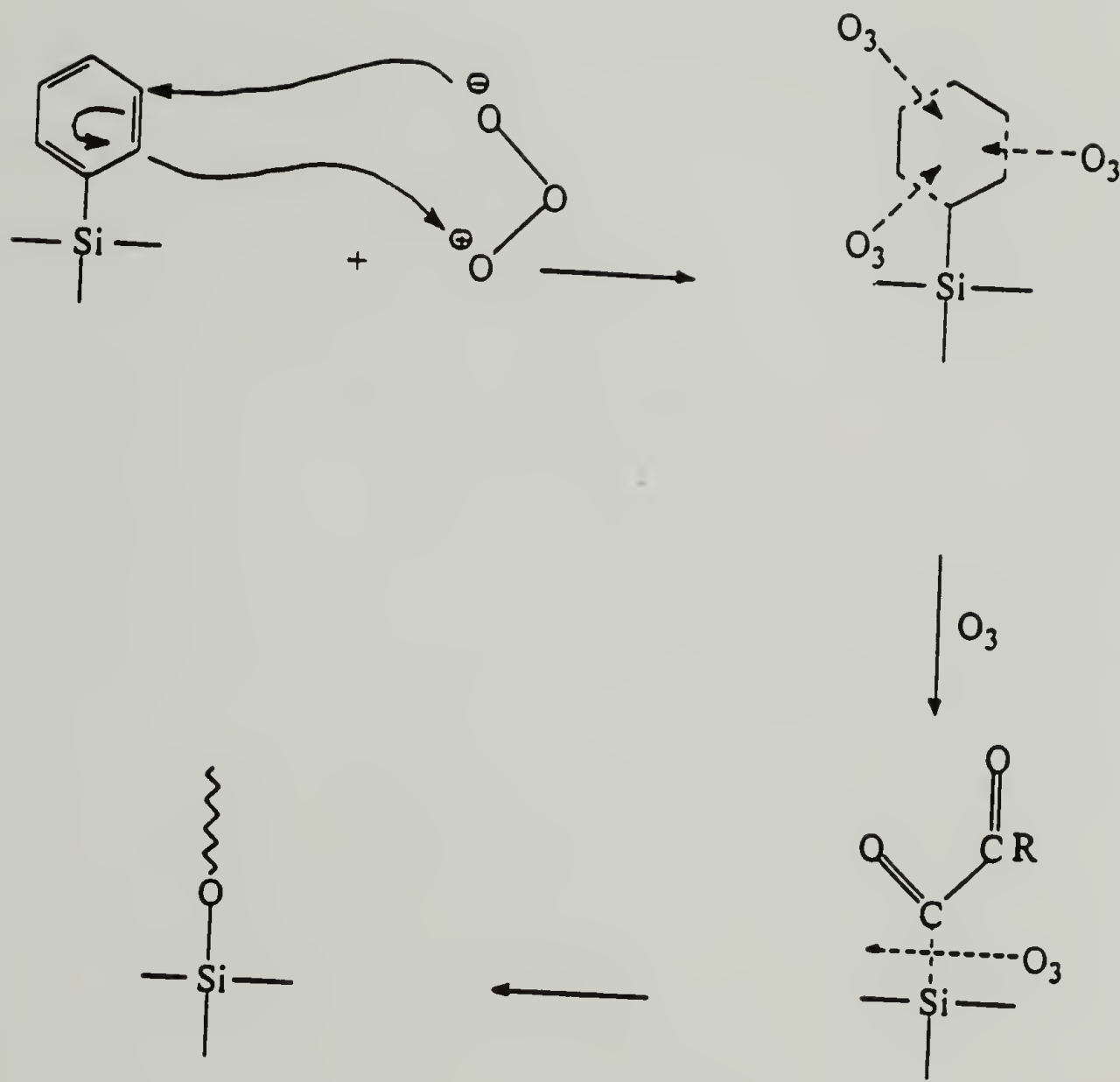


Figure 3.17. FT-IR spectra of the “mild” type ozonization of phenyltrimethylsilane. The recorded ozonization times are, A: 0 h, B: 1/2 h, C: 7 h, D: 20 h.



$\text{R} = \text{H}, \text{OH}$

Figure 3.18. Proposed mechanism of the ozonization of a phenyltrimethylsilane.

REFERENCES

1. Spialter, L., and J. D. Austin, *Inorg. Chem.* **5**, 1975 (1966)
2. Barry, A. J., and H. N. Beck in "Inorganic Polymers", F. G. A. Stone and W. A. G. Graham, Ed., Academic Press Inc., New York, N. Y., 1962, p. 221, 236, 256, and 296.
3. "The Instruction Manual, Welsbach Laboratory Ozonator Model T-408", Welsbach Ozone Systems Corporation.
4. Horvath, M., L. Bilitzky and J. Huttner; "Ozone" Elsevier, New York, N. Y., 1985.
5. "Basic Manual of Applications and Laboratory Ozonization Techniques", Welsbach Corporation Ozone Process Division.
6. Bailey, P. S., "Ozonization in Organic Chemistry", Vol. II, Academic Press, New York, N. Y., 1982, p. 331
7. Vriarte, R. J., "Silicones Product Chemistry", GE Silicones, Waterford N. Y.
8. Barry, A. J., and H. N. Beck in "Inorganic Polymers", F. G. A. Stone and W. A. G. Graham, Ed., Academic Press Inc., New York, N. Y., 1962, p. 256.
9. Long, L. J.R., *Chem. Revs.* **27**, 437 (1940).
10. Bailey, P. S., *Chem. Revs.* **58**, 925 (1958).
11. Bailey, P. S., *Chem. Revs.* **58**, 925 (1958) p. 986.
12. Bailey, P. S., Garcia-Sharp J. F., *J. Org. Chem.* **22**, 1008 (1957).
13. Criegee, R., Kerckow A., Zinke H., *Chem. Ber.* **88**, 1878 (1955).
14. Barton, R. D. H., P. De Mayo, and M. Shafiq, *J. Chem. Soc.* 929, 1957.
15. Sixma, J. L. F., E. Detilleux, *Rec. Trav. Chim.* **72**, 173 (1953).
16. Marvel, S. C., V. Nichols, *J. Org. Chem.* **6**, 296 (1941)
17. "Basic Manual of Applications and Laboratory Ozonization Techniques", Welsbach Corporation ozone process Division, p.5.

18. Bailey, P. S., J. Am. Chem. Soc. **78**, 3811 (1956)
19. Du Pont de Nemours, E. I., and Company, British patent 713, 344 (August 11, 1954).
20. Bailey, P. S., Chem. Ber. **88**, 795 (1955).
21. Wilzbach, E. K., R. F. Mayo, and R. Van Meter, J. Am. Chem. Soc. **70**, 4069 (1948).
22. Nakamori, R., J. Pharm. Soc. Japan **76**, 275 (1956).
23. Levine, A. A., and A. G. Cole, J. Am. Chem. Soc. **54**, 338 (1932).
24. Wibaut, J. P., and P. W. Haaijman, Nature (London) **144**, 290 (1939).
25. Haaijman, P. W., and J. P. Wibaut, Rec. Trav. Chim. Pay-Bas **60**, 842 (1941).
26. Wibaut, J. P., Bull. Soc. Chim. Fr. 996 (1950).
27. Shriner, R. L., R. C. Fuson, D. Y. Curtin, "The Systematic Identification of Organic Compounds; A Laboratory Manual," 5th ed., John Wiley & Sons, Inc., New York, N. Y., 1964, p.126.
28. Shriner, R. L., R. C. Fuson, D. Y. Curtin, (The Systematic Identification of Organic Compounds; A Laboratory Manual," 5th ed., John Wiley & Sons, Inc., New York, N. Y., 1964, p. 130.
29. Cheronis, N. D., J. B. Entrikin, "Identification of Organic Compounds," interscience Publishers, 1962.
- 29.a Taylor, R. B., B. Parbhoo, and D. M. Fillmore, in "The Analytical chemistry of Silicones," ed., A. L. Smith, John Wiley & Sons, Inc., 1991 ch. 12.
30. Coats, A. W., and J. P. Redfern, Analyst, **88**, 910 (1963).
- 31 Flynn, J. H., L. A. Wall, J. Research of the National Bureau of Standards,-A. Physics and Chemistry Vol. 70A, No 6, 1966.
32. Flynn, J. H., L. A. Wall, Polym. Letters, Vol. **4**, p. 323 (1966).
33. Petrovic, Z. S., Z. Zavargo, J. H. Flynn, and W. J. MacKnight, J. Appl. Pol. Sci. Vol. **51**, 1994.

CHAPTER 4

OZONIZATION OF HYDRIDE FUNCTIONALIZED SILOXANES: SYNTHESIS OF ORGANIC-INORGANIC HYBRIDS

4.1 Introduction

Much effort in the modern science of materials is devoted to the design and synthesis of new substances that optimize the advantages and minimize the disadvantages of existing materials. Perhaps the most productive approach is the synthesis of materials that can combine properties of different classes of materials (polymers, ceramics, metals) [1].

Polymers are tough, flexible, easy to fabricate, and lightweight but suffer from the drawback that they are soft and prone to thermo-oxidative decomposition. On the other hand, ceramics are stable at high temperatures, and hard; yet they are heavy, brittle and difficult to fabricate. Thus, a considerable effort has been directed in designing hybrids that can share the advantages of these two different types of material and minimize their disadvantages.

A very efficient way to form hybrid materials, by using polymers and glass forming components, is to combine the components at a molecular level [2]. It was mentioned in chapter two that the sol-gel method is the most common procedure to

develop molecular composites. The general principles of sol-gel chemistry were discussed in chapter two.

In this chapter a new and completely different synthetic method for the organic-inorganic hybrid is described. The new approach described here utilizes ozone chemistry, and unlike the sol-gel technique, where the inorganic precursor is formed prior to the combination with the polymer, the ozonization method allows the formation of the glass component directly on the polymer backbone.

It was reported earlier that ozonization of the SiH group forms SiOSi. The mechanism and reactivity of SiH toward ozone has been extensively studied [4-9]. In addition, in chapter three the potential reactivity of other groups of interest (SiCH₃, SiPh, SiOSi) was discussed. The SiCH₃ and SiOSi groups proved to be ozone resistant, while the SiPh moiety was oxidized by ozone, in a two step reaction, to form the SiOSi moiety. These results to some extent determined which materials would be appropriate for hybridization.

The polymers used in this work are hydride containing siloxanes. Hydrosiloxane polymers are readily available [3] in a variety of hydride concentrations (0.1-50 %). In this work the hydride substitution in siloxanes is 1.5, 15, 25 and 50 %. The three lower hydride content silicones are dimethyl/methyl/hydro-copolymers while the 50 % content is methylhydrosiloxane polymer. The glass forming agent is phenylsilane.

Hydrosiloxanes are oxidized in the presence of several different concentrations of phenylsilane in order to form the hybrid network. The inorganic content of the materials is controlled by both the concentration of hydride on the polymer backbone and the

amount of phenylsilane in the mixture. Synthesis, characterization and properties of the ozonized materials are reported in this chapter.

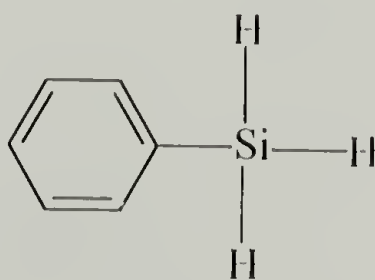
4.2 Experimental

4.2.1 Materials

All the chemicals and solvents were obtained in the highest available purity and they were used as received. Methylene chloride (CH_2Cl_2), phosphorous pentoxide (P_2O_5), phosphorous pentachloride (PCl_5), hydrobromic acid 48 % (HBr), dichlorodimethylsilane (CH_2SiCl_2), and phenyl dichlorophosphate ($\text{C}_6\text{H}_5\text{O}_2\text{PCl}_2$) were purchased from Aldrich; hydrochloric acid (HCl 37 %) from Fisher, phenylsilane (PhSiH_3) and all the functional silicones from Huls America Inc..

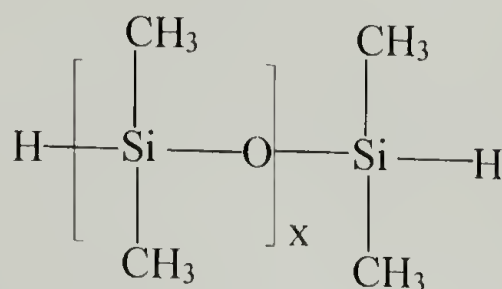
Phenylsilane (PhSiH_3): Phenylsilane is used as the glass forming agent in the hybrid network.

PhSiH_3 : $M_w=108$, $T_b=120^\circ\text{C}$, $d=0.868$



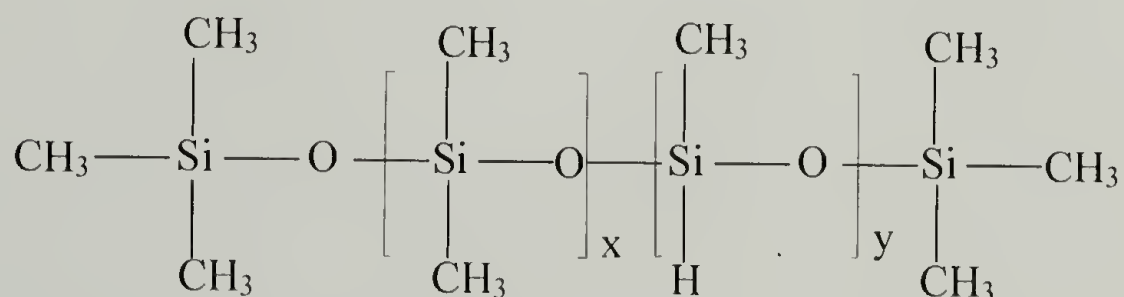
Polydimethylsiloxane hydride-terminated (PDMS-H): The active centers are located at the end of the polymeric chains and therefore, it can react only at the end groups.

PDMS-H: $M_w=400$, $d=0.905$



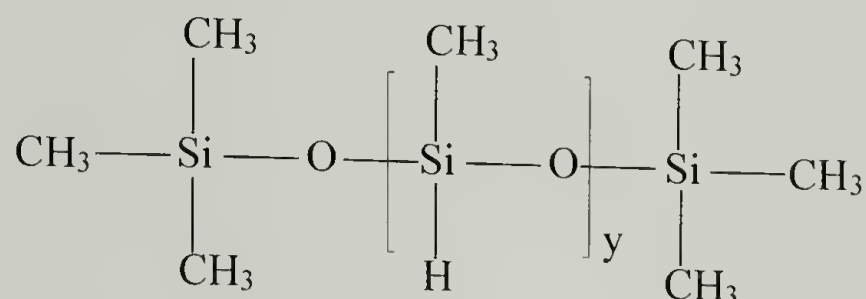
Poly (dimethyl methylhydrosiloxanes), trimethylsilyl terminated (PDMMHS): The PDMMHS copolymers are the network forming material in the hybrid network. Several hydrosiloxanes with different methyl hydro concentration are commercially available. The following are three siloxanes selected for the ozonization reactions in this work.

- a) PDMMHS-3 (3 % methyl hydro): $M_w=13000$, $d=0.97$
- b) PDMMHS-30 (30 % methyl hydro): $M_w=2000$, $d=0.99$
- c) PDMMHS-50 (50 % methyl hydro): $M_w=2000$, $d=0.99$



Polymethylhydrosiloxane trimethylsilyl terminated (PMHS): This siloxane is chosen to provide the highest concentration (per chain) of active centers.

PMHS: $M_w=1500$, $d=0.99$



4.2.2 Analytical techniques and methods

Infrared spectra were obtained under nitrogen by using a Nicolet IR/44 Fourier transform infrared spectrometer. NaCl plates were used for the liquid samples and KBr pellets for the solids.

Size exclusion chromatography data was obtained using a Waters refractive index detector. The eluting solvent was chloroform (A.C.S. HPLC grade). The indicator was toluene. Samples were prepared by making solutions ($\sim 10\text{mg/ml}$) of siloxanes in chloroform.

Thermogravimetric analysis data was obtained using a TA Instruments Thermogravimetric Analyzer, model 2950. The materials ($\sim 10\text{ mg}$ samples) were heated to 800°C either under nitrogen or air at 10°C/min . For the determination of the activation energies the materials were heated under nitrogen and four different heating rates were employed ($1, 5, 10$ and 20°C / min.).

Silicon nuclear magnetic resonance spectra, ^{29}Si NMR, were obtained using a Bruker NC 80. For these solid state ^{29}Si NMR experiments, magic angle, single pulse, cross polarization techniques were used.

^1H NMR spectra were obtained using a Bruker AC 200 spectrometer operating at 200 MHz. Samples were prepared by making 10 % solutions in deuterated chloroform containing 0.03 % tetramethylsilane.

Scanning electron micrographs (SEM) were recorded on a JEOL-35CF. Accelerating voltages of 20 kV were used at various magnifications. The samples were mounted on aluminum cylinders using a conductive adhesive and sputter-coated with a few angstroms of gold.

Differential scanning calorimetry (DSC) data was obtained using a TA Instruments calorimeter. The samples (~10 mg) were placed in non-hermetic aluminum pans and were cooled to $-150\text{ }^{\circ}\text{C}$ using liquid nitrogen. The heating rate was $10\text{ }^{\circ}\text{C}/\text{min}$ (to $30\text{ }^{\circ}\text{C}$).

Nitrogen adsorption experiments were done using a B.E.T apparatus. The adsorption experiments were used for surface area calculations of the powders produced. The surface area is reported in m^2/g . The apparatus was calibrated with helium gas. The experimental setting and the procedure is described in the experimental section.

4.2.3 Ozonization of phenylsilane

The experimental setting for this reaction is described in chapter three (fig. 3.2). In addition, the appropriate reactor is illustrated in fig. 4.1. The reactor was modified

slightly in order to increase the residence of phenylsilane in the reaction mixture. The experimental settings were kept constant as before (115 V, 8 psig). The flow however was set as low as possible (6-12 lit/hr) because the phenylsilane showed a strong tendency to escape from the reactor. The reaction temperature was controlled around 0 °C using an immersion cooler (cryocool) and ethylene glycol / water (40:60) as a coolant liquid. The need for temperature control arises because the reaction is exothermic (temperature increases up to 50-60 °C). In a typical experiment a small amount (2-5 ml) of phenyltrimethylsilane was placed in the reactor and the reactor was immersed in the cooling media. Stirring of the coolant ensured homogeneous temperature. The produced ozone-oxygen mixture (~6 % O₃) was introduced in the reactors through a splitter. A thin white cloud formed in the reactor within the first two minutes of the reaction and was becoming thicker gradually as the reaction progressed. A small sample was taken out of the reactor within the first 15 minutes for analysis. The reaction was stopped after three hours, to avoid significant losses of phenylsilane. After the reaction was terminated the reactor was flushed with nitrogen (slow flow for 10 min) to remove the excess ozone. Ozonization of phenylsilane resulted in two phases (yellow liquid and white solid powder). The powder was filtered off, washed with methylene chloride and dried in a vacuum oven at ~100 °C. The yellow liquid was discarded. (ntbk-S3, p. 40-43, p. 50-55, p. 67).

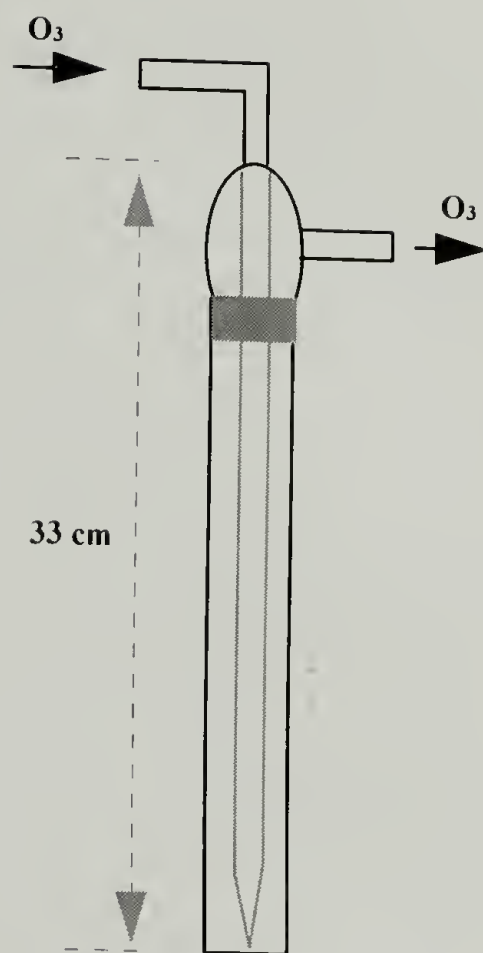


Figure 4.1. Modified reactor for the ozonizations of phenylsilane and hydrosiloxanes and their mixtures.

4.2.4 Ozonization of polydimethylsiloxane hydride-terminated (PDMS-H)

The reaction setting, parameters, and the reactor was described in the previous section. In a typical experiment ~5 ml of PDMS-H placed in the reactor and the gas (~6 % O₃) bubbled through the liquid for 2 hours at a rate of 1 lit/min. After the reaction ceased the ozone flow was stopped and the reactor was flushed with nitrogen for 15 minutes. The colorless liquid which was substantially more viscous was taken out of the reactor and stored for analysis. (ntbk-S3, p. 60-63, p. 71).

4.2.5 Ozonization of polydimethylsiloxane hydride-terminated (PDMS-H)/phenylsilane (PhSiH₃)

The reactor, experimental parameters and setting remained the same as before. Several mixtures of PDMS-H/ PhSiH₃ were prepared by mixing the siloxane with various amounts of the silane. The concentration of silane in the mixture varied from 3 to 41 %, table 4.1. In a typical experiment 5 ml of a prepared mixture was placed in the reactor and ozone gas bubbled through. The reaction times and gas flows are reported in table 4.1. After the reaction was terminated, the mixture was taken out of the reactor, washed with methylene chloride to remove the unreacted organic soluble portion and thereafter with water to remove the water soluble by-products. The materials were dried in vacuum oven at 100 °C and stored for analysis. (ntbk-S3, p. 70-72, p. 75-85)

Table 4.1. Ozonization conditions of polydimethylsiloxane hydride-terminated (PDMS-H) and mixtures of PDMS-H with PhSiH₃ (phenylsilane).

Sample	PhSiH ₃ (% w/w)	Reaction time (hr)	Gas flow (lit/min)
PDMS-H	0	2	1
PDMS-H ₃	3	4	0.5
PDMS-H ₁₂	12	5	0.3
PDMS-H ₂₅	25	6	0.3
PDMS-H ₄₁	41	6	0.3

4.2.6 Condensation of the PDMS-H/ PhSiH₃ mixtures

The ozonized materials exhibited a time dependent instability. At first when mixtures were taken out of the reactor their physical appearance varied from gel-like to gum-like. Gradually, within a week period they exhibited a significant hardening which was presumably due to the slow silanol condensation [10-13]. In an effort to speed up the condensation process different potential catalysts were examined.

The general procedure for the condensation of the ozonized materials was as follow; After the ozonization mixture was taken out of the reactor it was weighed and then mixed under stirring with a small amount of the potential catalyst (~2 % w/w). The results are reported in table 4.2. The only exception in the general procedure was the case of the hydrochloric acid which was mixed with PDMS-H/PhSiH₃ before the ozonization and consequently becoming a part of the reaction. (ntbk-S3, p.75-85, p.92, p.95)

Table 4.2. Tested potential catalysts (dehydrating agents) for the silanol (-SiOH) condensation. All catalysts used in 2% concentration.

Catalyst (dehydrating agent)	Results and observations
P_2O_5	solid immiscible in the reaction mixture at ambient but miscible at elevated temperatures ; forms stable silicone films (after 4-5 days)
PCl_5	solid immiscible in the reaction mixture at ambient but miscible under light heating; it forms a clear stable film with visible bubbles (1-2 days)
$(CH_3)_2SiCl_2$	produces soft gum material
HCl	used as part of the reaction mixture; forms two liquid phases and a solid precipitant (slows down the reaction)
HBr	produces a mixture of liquids and solids, slow reaction, not satisfactory results
$C_6H_5O_2PCl_2$	very effective catalyst; fast condensation at room temperature; miscible with the ozonized mixture

4.2.7 Ozonization of mixtures of poly(dimethyl methylhydrosiloxanes), trimethylsilyl-terminated (PDMMHS) copolymers, and methylhydrosiloxane (PMHS) trimethylsilyl-terminated polymer with various amounts of phenylsilane (PhSiH₃)

The experimental settings and parameters for these sets of reactions remained the same as before. The modified reactor is illustrated in fig. 4.1. The general procedure developed for all the ozonizations of hydrosiloxanes/phenylsilane mixtures is described in fig. 4.2. A small amount (~5 ml) of a mixture was placed in the reactor and ozone was bubbled through for 8 hours at a rate of ~18 lit/hr. After the reaction was terminated the reactor was flushed with nitrogen for 15-20 minutes to remove the excess ozone. The gel products were taken out of the reactor, weighed and mixed under stirring with a dilute solution of phenyl dichlorophosphate in methylene chloride. The mixture was allowed to condense for 48 hours. The products were extracted first with water to remove the water soluble by-products and then with methylene chloride to remove any unreacted material. The products exhibited high hydrophobicity and the water extractions were not very efficient. In order to make the procedure more efficient an additional extraction followed with a 50:50 mixture of methylene chloride/water. The ozonized products showed a tendency to stay in the interface of the two phases. After the extraction the products were isolated by vacuum filtration and they were dried under vacuum at 100 °C. (ntbk-S3, p. 97-98, ntbk-S4, p. 5-75)

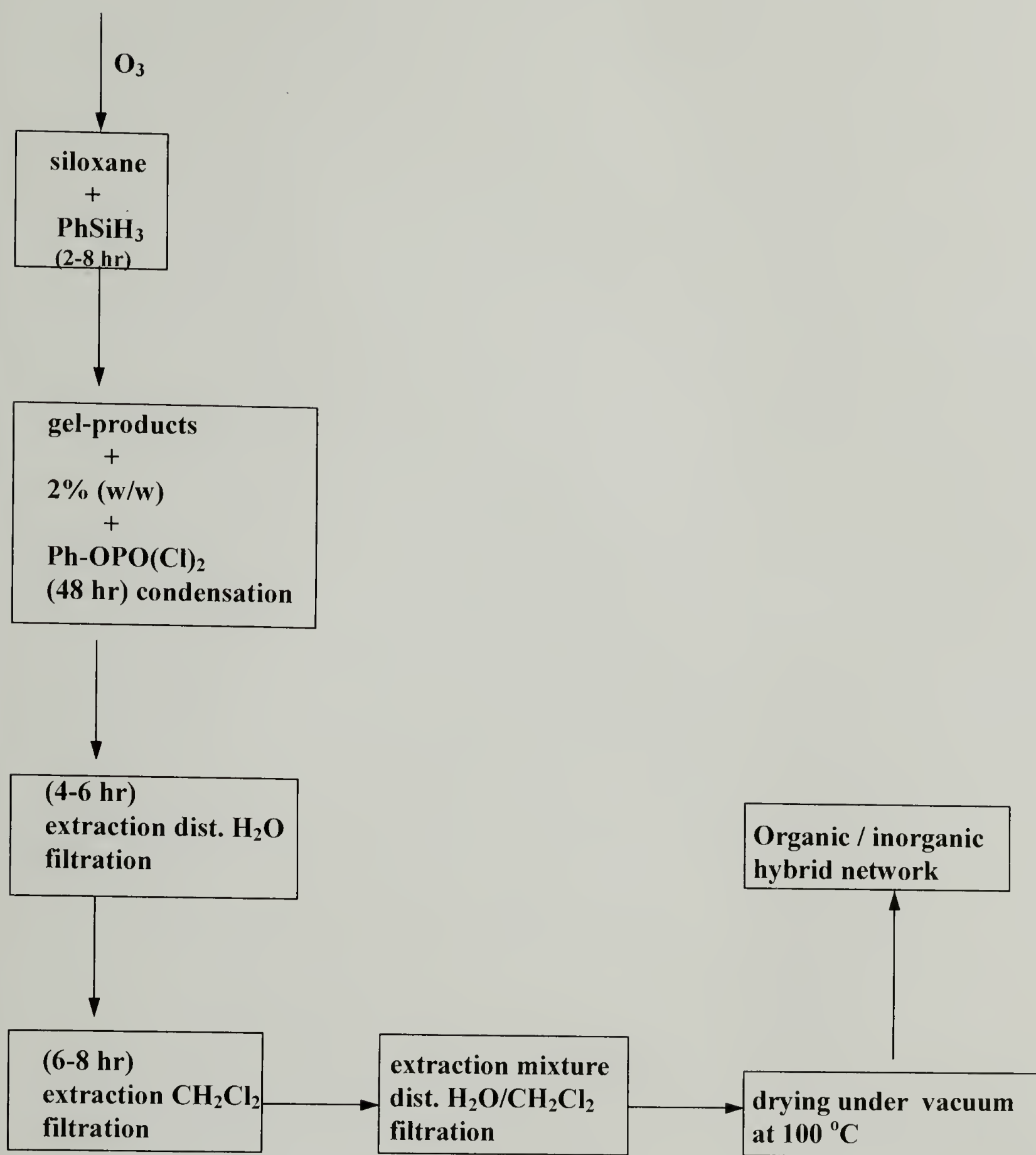


Figure 4.2. General procedure for the ozonization/condensation of the various hydrosiloxanes.

4.2.8 Nitrogen adsorption (B.E.T experiments) for surface area calculations

The experimental setting is described in fig. 4.3. The B.E.T apparatus includes a diffusion and mechanical pump for a high vacuums and a small experimental volume including sample volume plus dead volume. The apparatus has the ability to change volume while maintaining constant mass by means of a number of bulbs of known volume which can be filled with mercury. The system is calibrated at constant temperature with helium (He) below its vapor pressure. This inert gas is assumed not to adsorb on the surface of the sample [13.a]. With a change in volume vs. pressure, a total volume can be calculated, the so called dead volume (the total volume other than that taken up by the sample). With volume known, the B.E.T equation is used to find the surface area in m^2/g .

Sample preparation: Three different samples were prepared. One sample for surface area calculations of silica gel powder (0.2515 g), one for polymethylhydrosiloxane mixed with 41 % phenylsilane (0.3008 g), and one for (50 %) dimethyl-(50 %)-methylhydrosiloxane mixed with 41 % phenylsilane (0.2335g). The samples were placed in a sample holder connected to the B.E.T apparatus, fig.4.3, and were heated overnight under vacuum at 150 °C. (ntbk-S4, p.81)

Experimental procedure: The room atmospheric pressure is measured with a manometer, and then the sample holder, connected to the apparatus with the sample inside is immersed in the liquid nitrogen trap and the sample valve is opened (No. 7), Fig.4.3. The system is evacuated using the diffusion pump. With the valve above the sample (No. 6) closed, helium is released in the system while maintaining a pressure lower than the atmospheric. The valve No. 8 opens to atmosphere and this causes the mercury level to

increase. The pressure readings between the five bulbs are recorded as the mercury level increases. Five data points are collected from this set of measurements. The same procedure is repeated with the sample holder open to helium and another set of five data points are collected. After the calibration with helium is completed the system is evacuated again. Valves six and seven are closed again and nitrogen is released in the system. The same procedure described for the helium calibration is used again. The last set of data is collected with the sample holder open. The results are reported in tables 4.3.a, 4.3.b and 4.3.c. (ntbk-S4, 83-88)

4.2.9 Qualitative picture of the surface polarity differences between a hybrid powder (PMHS⁴¹) and an inorganic powder (silica gel)

In order to demonstrate the difference in surface properties between PMHS⁴¹ and silica gel, the following experiment was designed [14]: The two powders were pressed down on a flat surface (fig. 4.21) and a drop of water colored with potassium permanganate was placed on the surface of each powder. Water, as was expected, spread on the surface of silica gel (hydrophilic surface). The hybrid powder, however, proved to be extremely hydrophobic and no wetting was observed even after an extended period of time. (ntbk-S4, p. 70, p.78)

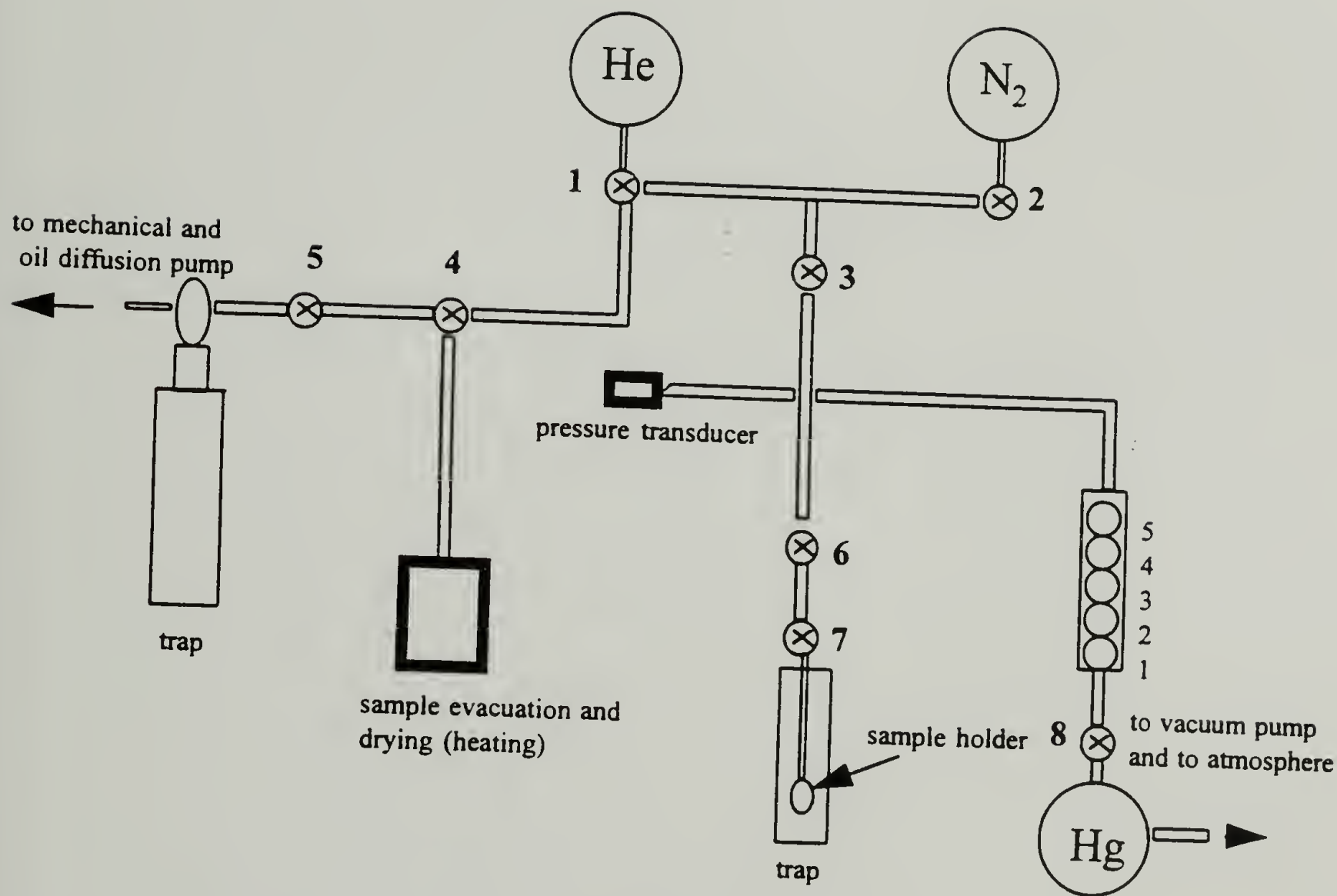


Figure 4.3. Experimental setting for nitrogen adsorption (BET method), in order to determine the surface area of the hybrid powders.

4.2.10 Determination of activation energy from thermogravimetric analysis for the organic-inorganic hybrids

The determination of kinetic parameters such as energy of activation directly from weight loss vs. temperature data at several heating rates, is possible by using thermogravimetry [15-18], fig 4.28. The thermogravimetric rate is given by eq. (1)

$$dC/dT = (A/\beta) \times f(C) \times e^{-E/RT} \quad (1)$$

C (weight loss at T_i divided by the total weight loss) = W_i/W_t

β = heating rate (1, 5, 10, 20 °C)

A = Arrhenious pre-exponential factor

E = activation energy

R = gas constant

$f(C)$ = function of the degree of weight loss

Assuming that A, $f(C)$, and E are independent of T and A, E are independent of C [15], then after integrating the eq. (1) and expressing the results in a logarithmic form the eq. (2) is obtained

$$\log F(C) = \log (AE/R) - \log \beta + \log h(E/RT) \quad (2)$$

for $E/RT \geq 20$ then

$$\log h(E/RT_i) \cong -2.315 - 0.457 \times E/RT_i \quad [19] \quad (3)$$

$$\log F(C) \cong \log (AE/R) - \log \beta + -2.315 - 0.457 \times E/RT \quad (4)$$

For C= constant and differentiating eq. (4) becomes

$$d \log \beta / d \log (1/T) \cong 0.457 \times E/R \quad (5)$$

A plot of $\log \beta$ vs. $1/T$ gives a slope equal to $0.457 E/R$ (fig 4.29). The activation energy is calculated from eq. (6)

$$E = \text{slope} \times R/0.457 \quad (6)$$

The materials were heated under nitrogen. The activation energies were not re-evaluated for correction [15]. The results are reported on tables 4.6-4.8.

4.3 Results and discussion: Analysis

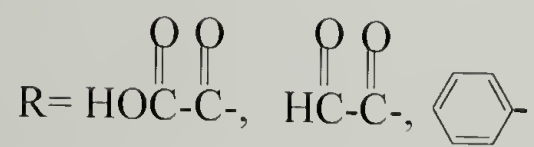
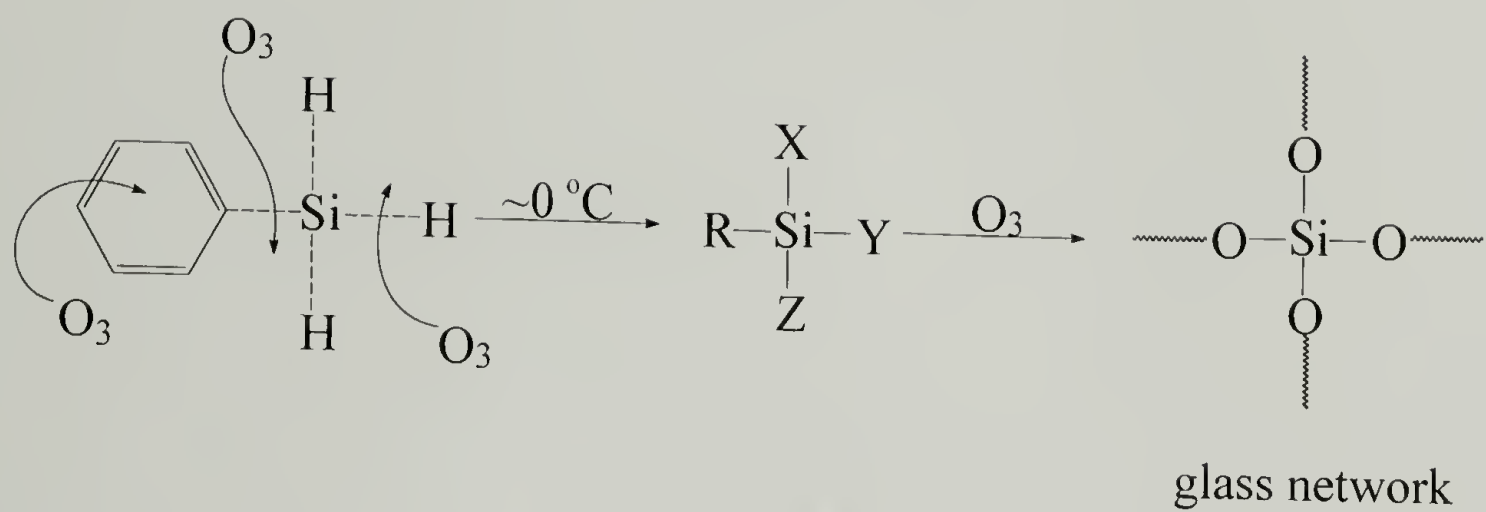
4.3.1 Phenylsilane

It was reported in chapter three that ozonization of a SiPh group is accomplished in two steps and results in the formation of a siloxane moiety. It was also discussed in chapter two that ozone oxidation of SiH results in the formation of siloxane. It was conceivable therefore, that ozonization of phenylsilane (PhSiH_3) would form a tetrafunctional silicon (SiO_2), scheme 4.1. Indeed ozonization of PhSiH_3 was fast, exothermic and a white SiO_2 cloud begun forming within the first few minutes of the reaction. The ozonization reaction was monitored with infrared spectroscopy. The spectra displayed in fig. 4.4 illustrate the results of the 15 and 180 minutes oxidation. The characteristic absorption bands due to SiH stretching (2175 cm^{-1}) and SiPh stretching $2900\text{-}3100 \text{ cm}^{-1}$ are reduced considerably after 180 minutes ozonization. In addition, the initial formation of a sharp SiOSi peak at 1120 cm^{-1} is an indication of the formation of similar low molecular weight species (i.e. disiloxanes, trisiloxanes); however, more

extensive ozonization, causes SiOSi band broadening which is an indication of the formation of more complex species (trifunctional and tetrafunctional silicon) [20]. Solid state ^{29}Si NMR, fig. 4.5, confirms the IR results. The characteristic peak of the tetrafunctional silicon (SiO_2) appears at -102 ppm, while a very broad peak at -86 ppm is due to complex trifunctional species. A thermogram, obtained under air, of the ozonized PhSiH_3 is depicted in fig. 4.6. The thermal stability exhibited by this material is characteristic for that of SiO_2 , even though it is clear that there is some residual organic content. Longer reaction times however, were avoided because of extensive loss of PhSiH_3 .

4.3.2 Polydimethylsiloxane hydride-terminated (PDMS-H)

The first ozonized hydrosiloxane was PDMS-H. The reaction was monitored again with FT-IR spectroscopy. The spectra displayed in fig. 4.7 indicate that the reaction is complete after 2 hours as indicated by the absence of SiH band at 2128 cm^{-1} . Data from size exclusion chromatography was obtained using chloroform as a solvent and toluene as an indicator. The employment of chloroform, instead of tetrahydrofuran (THF) as a solvent, was necessary because PDMS-H and THF have similar refractive indices and detection was impossible. Size exclusion chromatography showed an increase in molecular weight from 400 for the virgin PDMS-H to 3,000 for the ozonized. Some residual low molecular weight was observed as well, which could be due to either monohydride or non-hydride terminated siloxane, fig. 4.8.



X, Y, Z = H-, HO-, SiO-

Scheme 4.1. Ozonization of phenylsilane

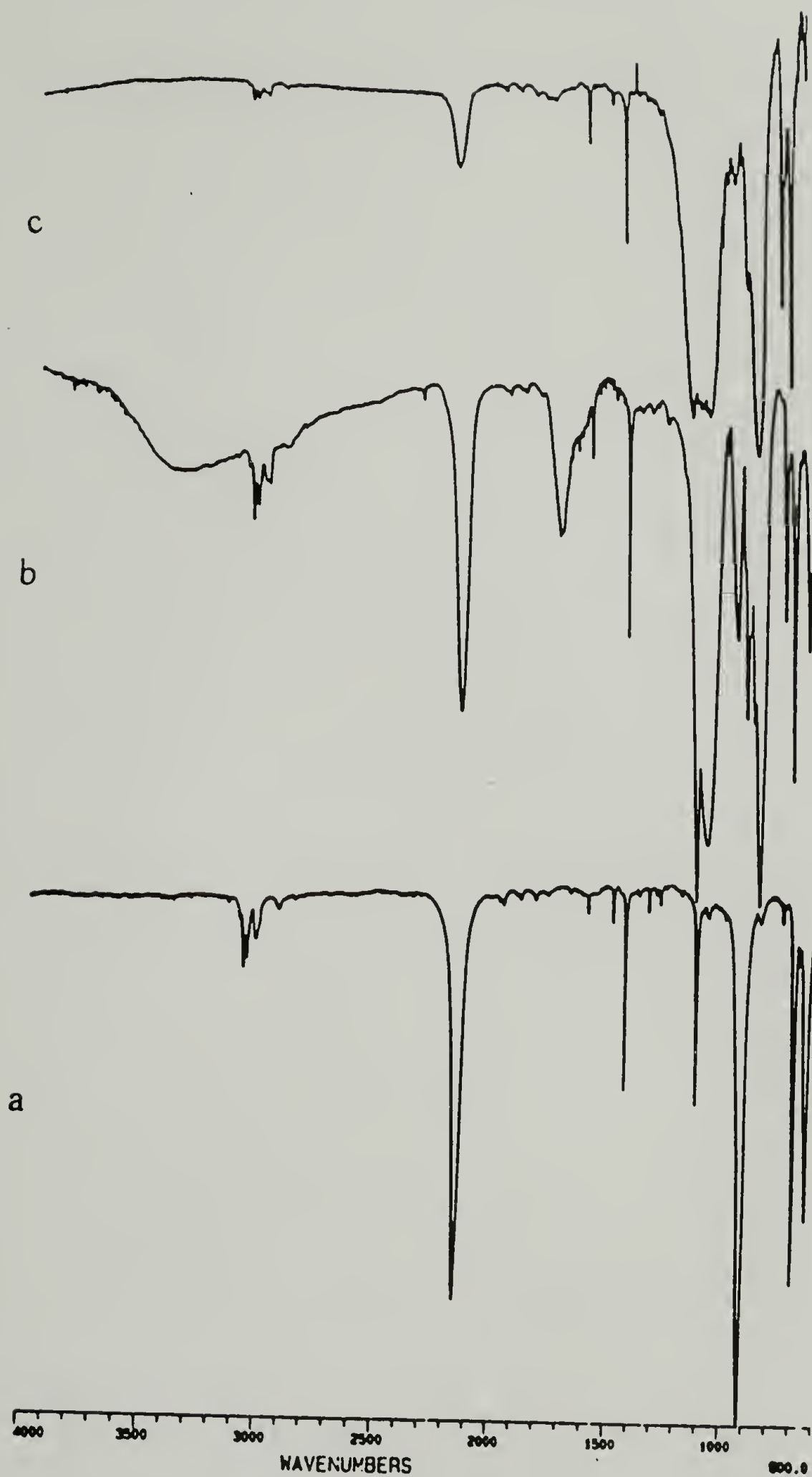


Figure 4.4. FT-IR spectra of phenylsilane (PhSiH_3); a: non-ozonized, b: 15 minutes ozonized, c: 180 minutes ozonized.

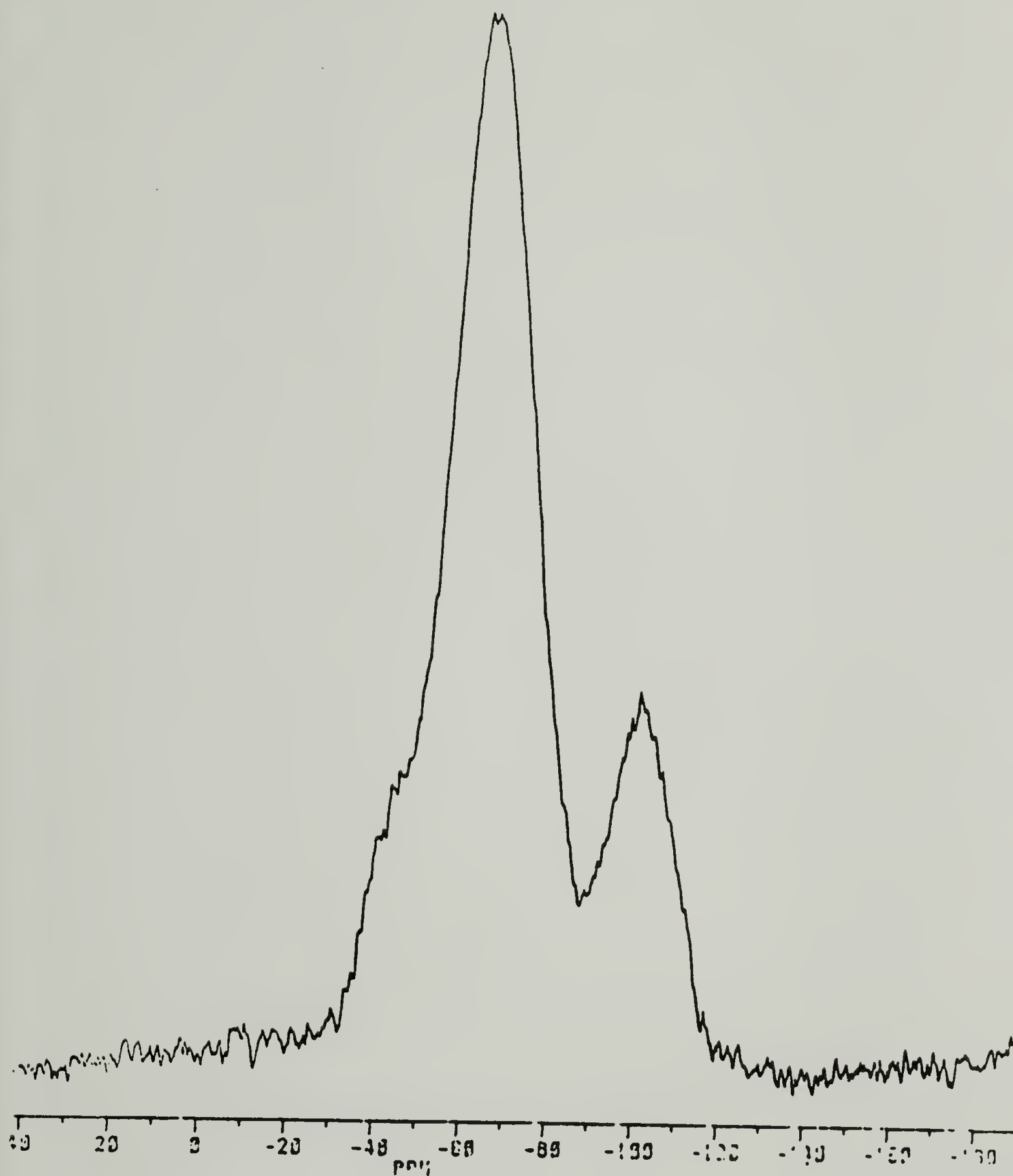


Figure 4.5. Solid state ^{29}Si NMR spectrum obtained from the phenylsilane (PhSiH_3) ozonized for 3 hours. The SiO_2 peak appears at -102 ppm. The peak at -86 ppm is due to the partial PhSiH_3 oxidation.

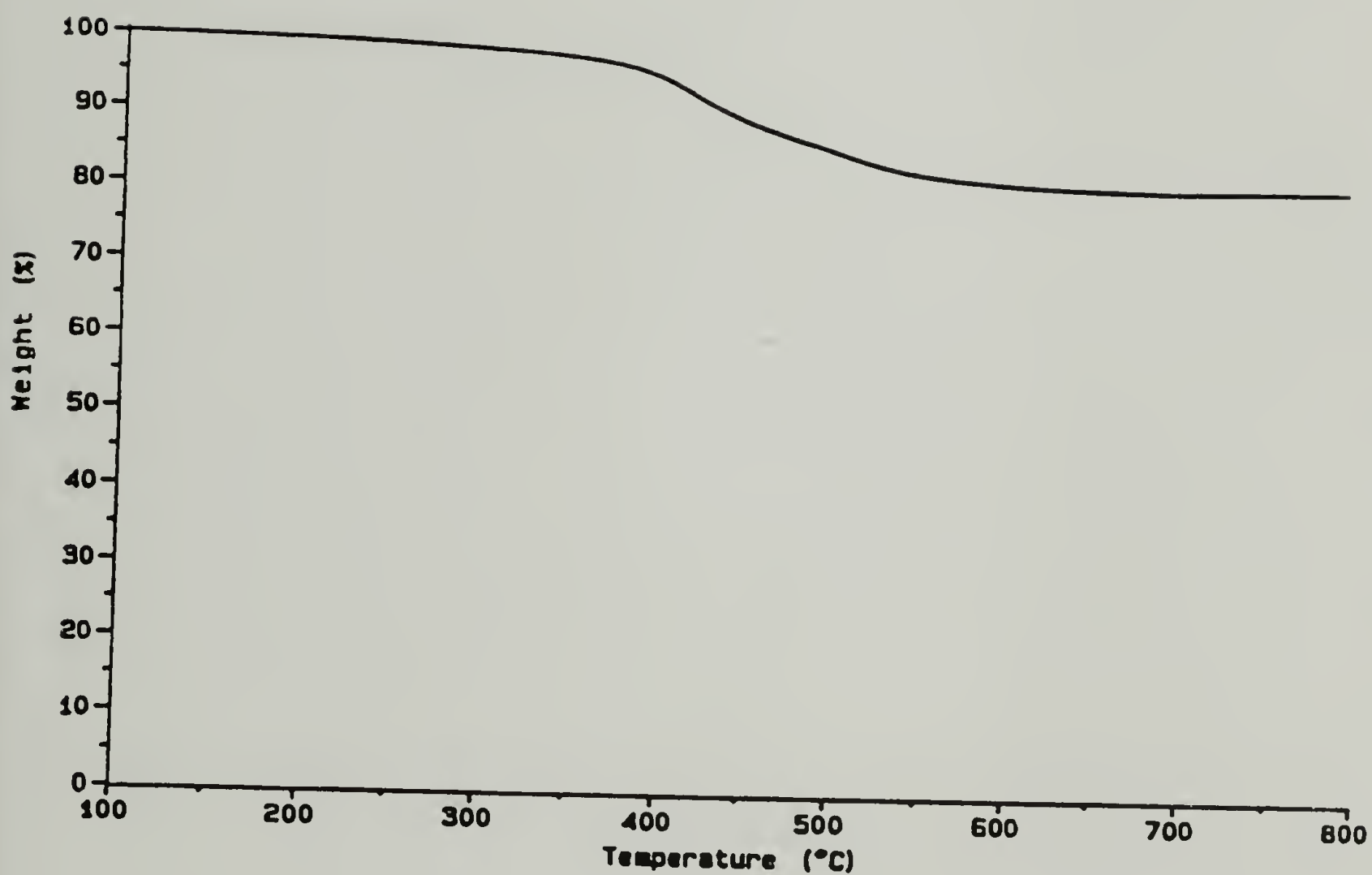


Figure 4.6. TGA thermogram of the ozone oxidized (3 hours) phenylsilane. The heating rate is 10 °C/min under air.

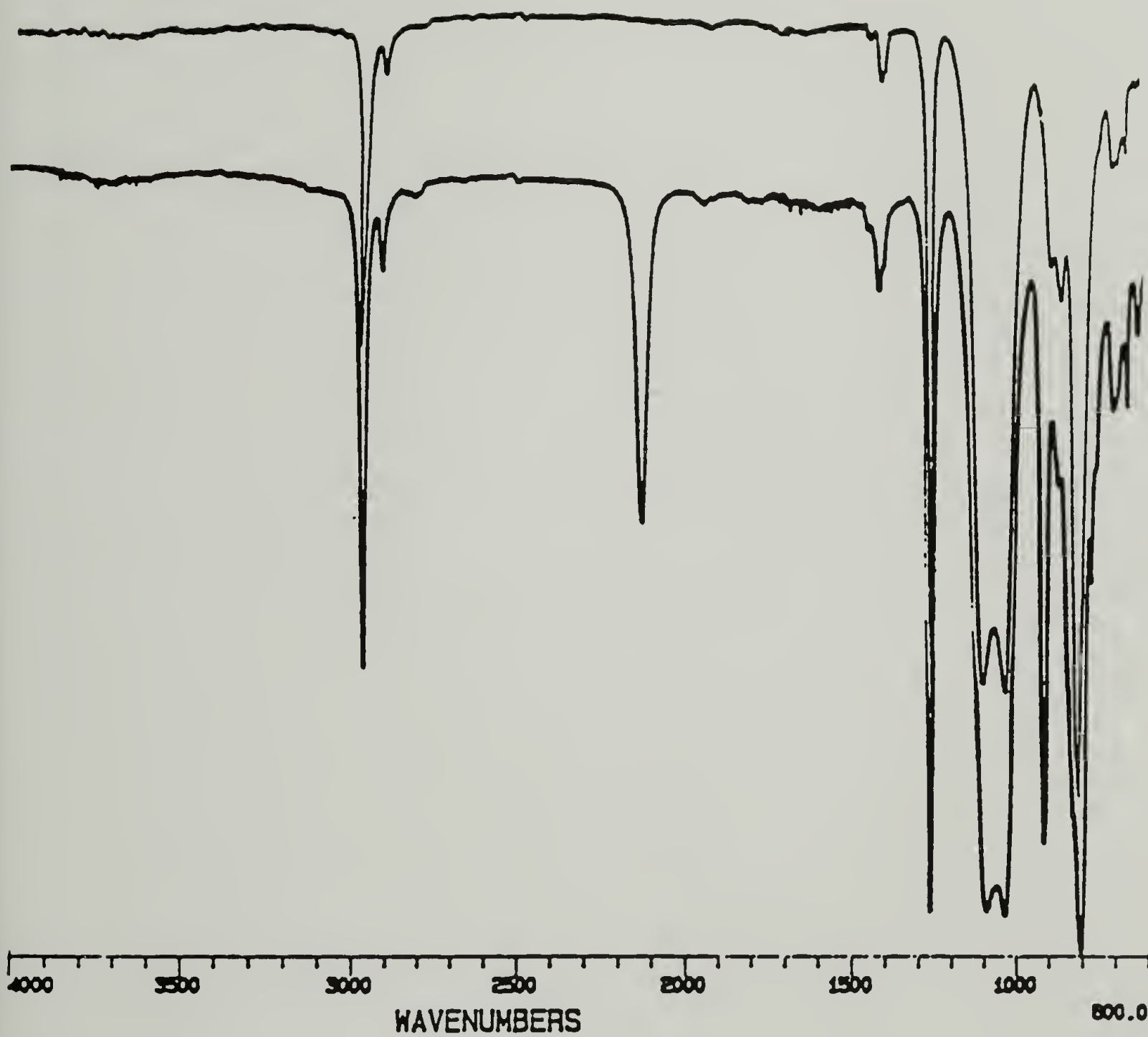


Figure 4.7. FT-IR spectra of unreacted (bottom) and reacted (top) PDMS-H. The Si-H absorption bands appear at 2128 cm^{-1} (stretching) and at 913 cm^{-1} (bending).

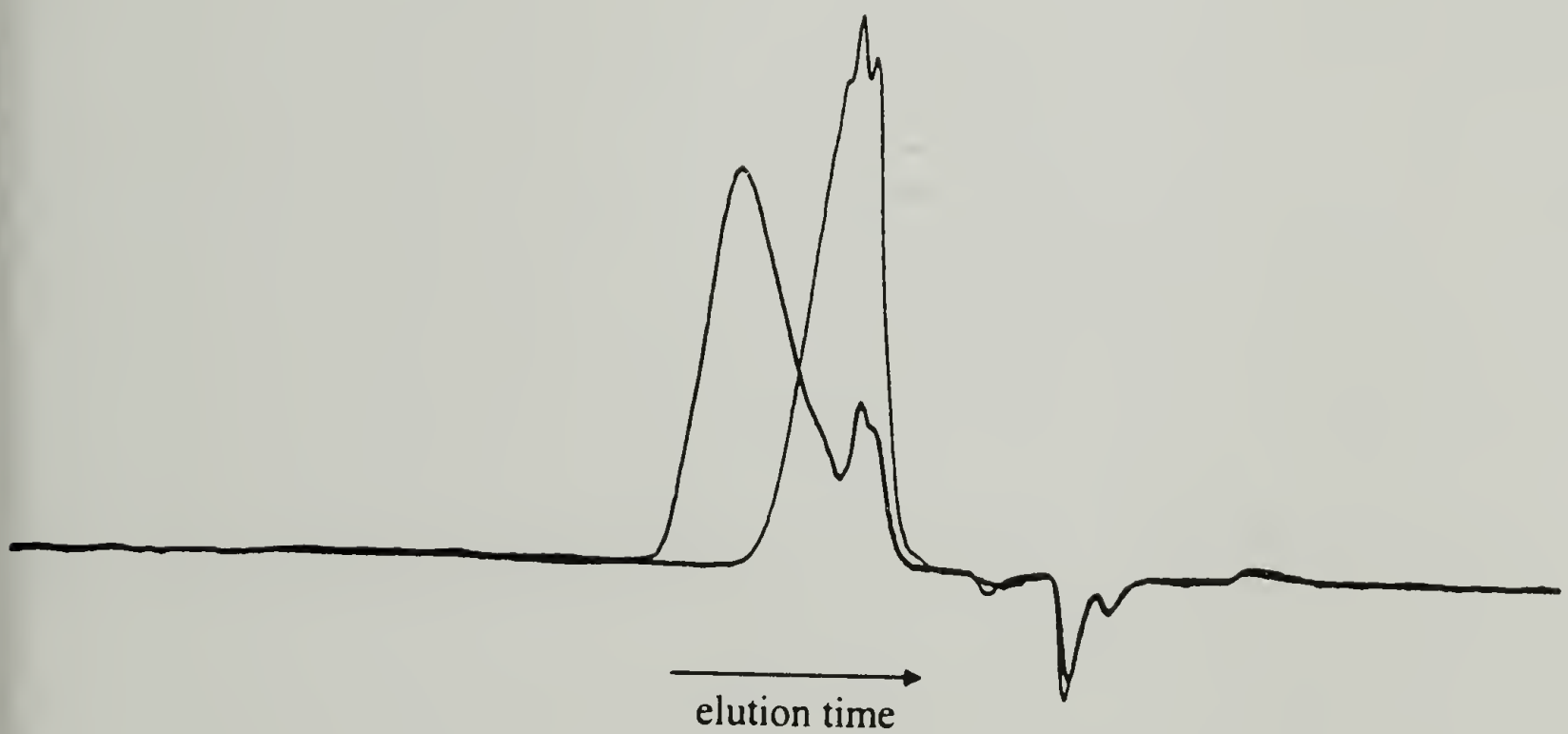


Figure 4.8. Size exclusion chromatography of the ozonized PDMS-H (10% in chloroform). Ozonization time was 2 hrs. The molecular weight increases from 400 (non-ozonized siloxane) to 3,000 for the ozonized.

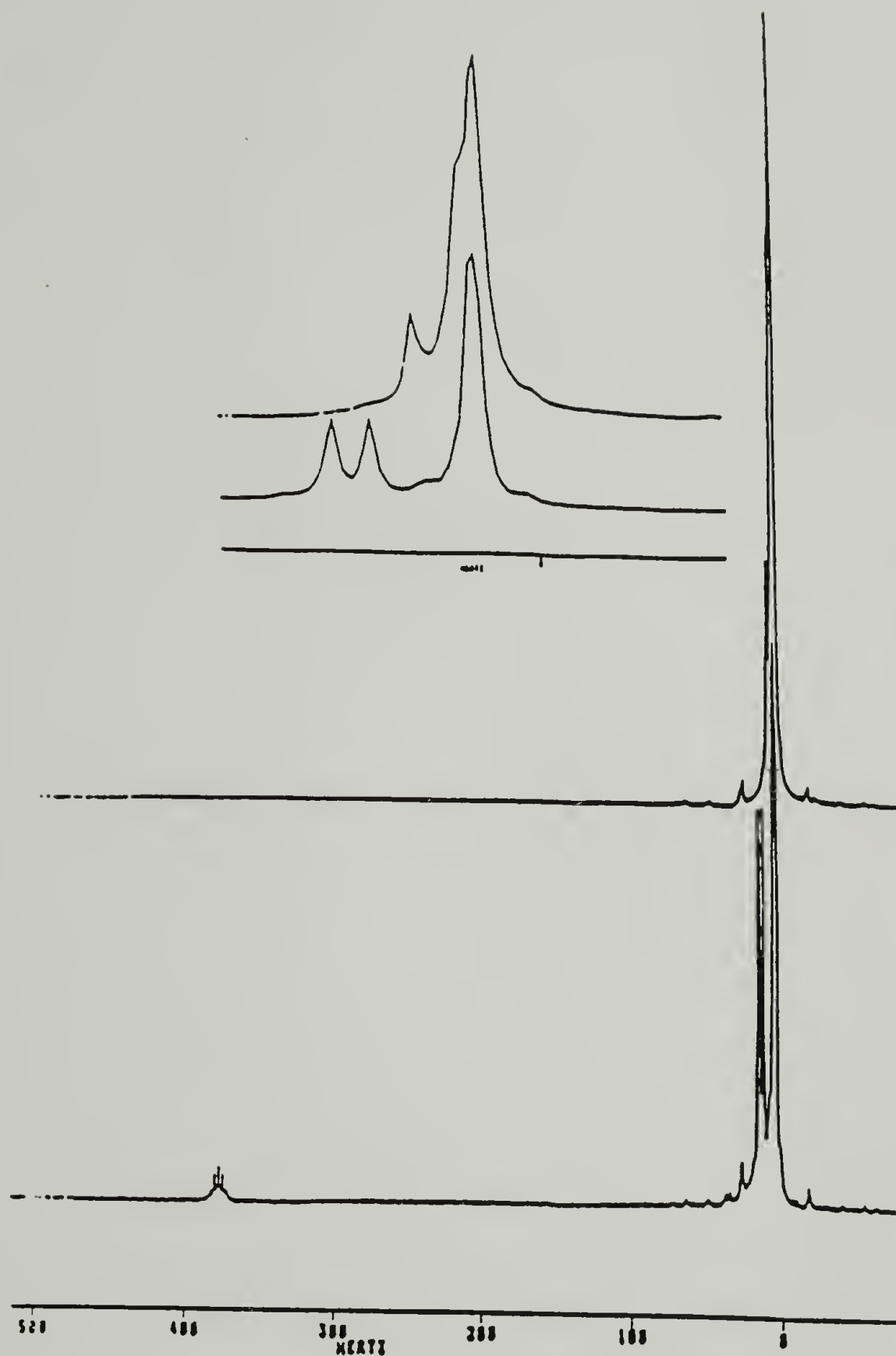


Figure 4.9. ^1H NMR spectra (20% concentration in CDCl_3 containing 0.03 % tetramethylsilane) of the ozonized (top) and non-ozonized (bottom) polydimethylsiloxane hydride-terminated (PDMS-H). The Si-H peak appears at 4.69 ppm and the doublet due to the $-\text{Si}(\text{CH}_3)_2$ at 0.19 and 0.16 ppm.

This conclusion was corroborated by ^1H NMR. The $(\text{CH}_3)_2\text{OSi-H}$ peak [21] splitted by the neighboring protons appear at 4.69 ppm. In addition, the peak due to $\text{OSiH}-(\text{CH}_3)_2$ is splitted to a doublet (0.16 and 0.19 ppm) because of the proton attached to silicon. Both peaks are absent in the spectrum taken from the ozonized sample, fig. 4.9.

4.3.3 Polydimethylsiloxane hydride-terminated (PDMS-H)/phenylsilane (PhSiH_3)

Ozonization of mixtures of PDMS-H/ PhSiH_3 formed the first set hybrid materials. A representative FT-IR spectra of the highest PhSiH_3 concentration (41 %) is shown in fig. 4.10. The absence again of the SiH peak at 2158 cm^{-1} is an indication of the completion of the reaction. The solid state ^{29}Si NMR spectrum in fig. 4.11 shows an intense peak at -23 ppm which is due to SiCH_3 . The peaks due to SiO_2 and other tetrafunctional species appear at -102 ppm and -111 ppm [21]. A schematic representation of the reaction is depicted in scheme 4.2.

Even though the ozonizations did not present any particular difficulties, slow condensation of silanols [10-13] to the final products was observed. The use of a catalyst (phenyl dichlorophosphate, table 4.2) accelerated the stability of the products (48 hr).

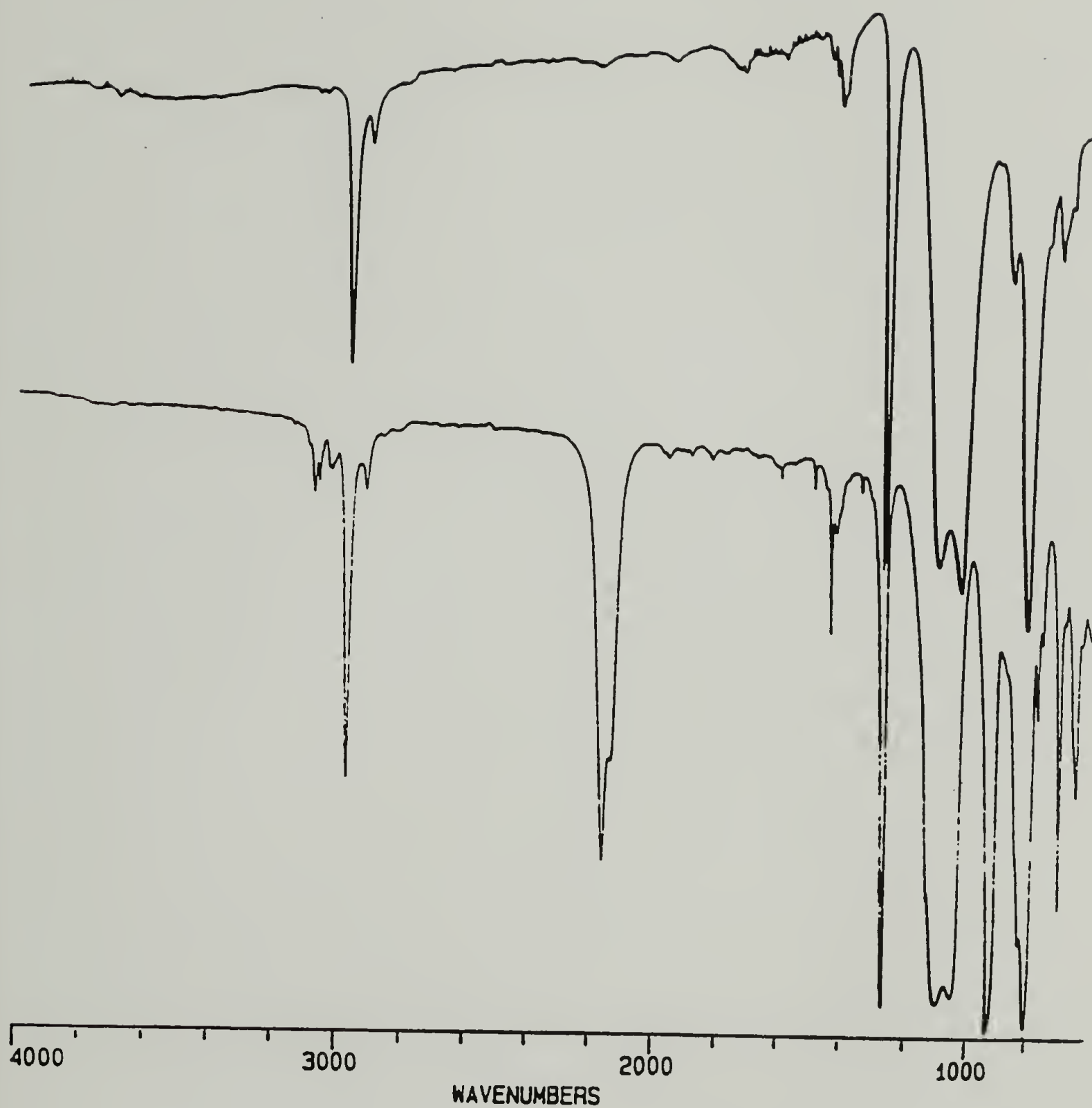


Figure 4.10. Representative FT-IR spectra of the ozonized (top) and non-ozonized (bottom) hydride-terminated polydimethylsiloxane mixed with 41 % phenylsilane (PDMS-H⁴¹).

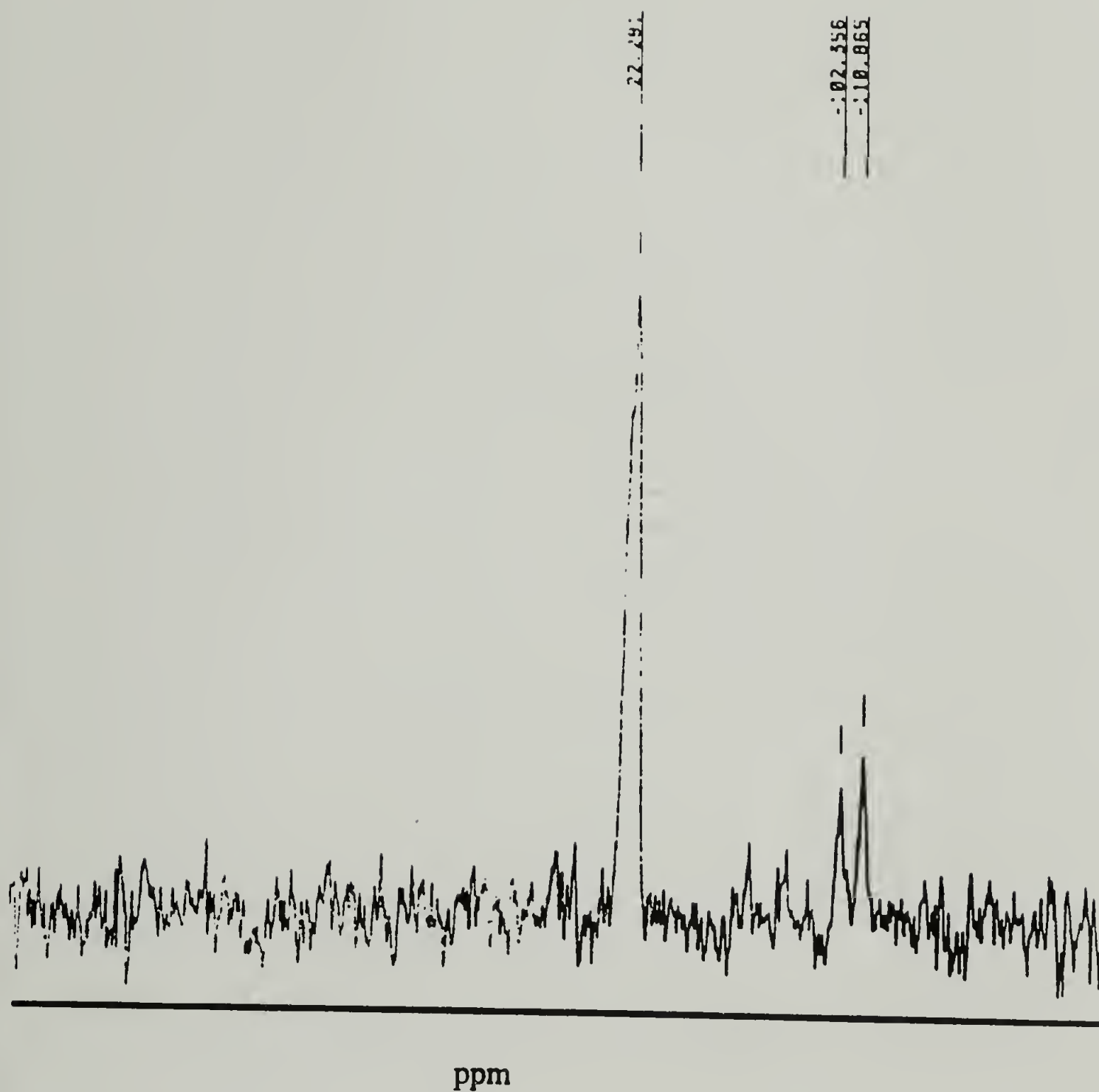
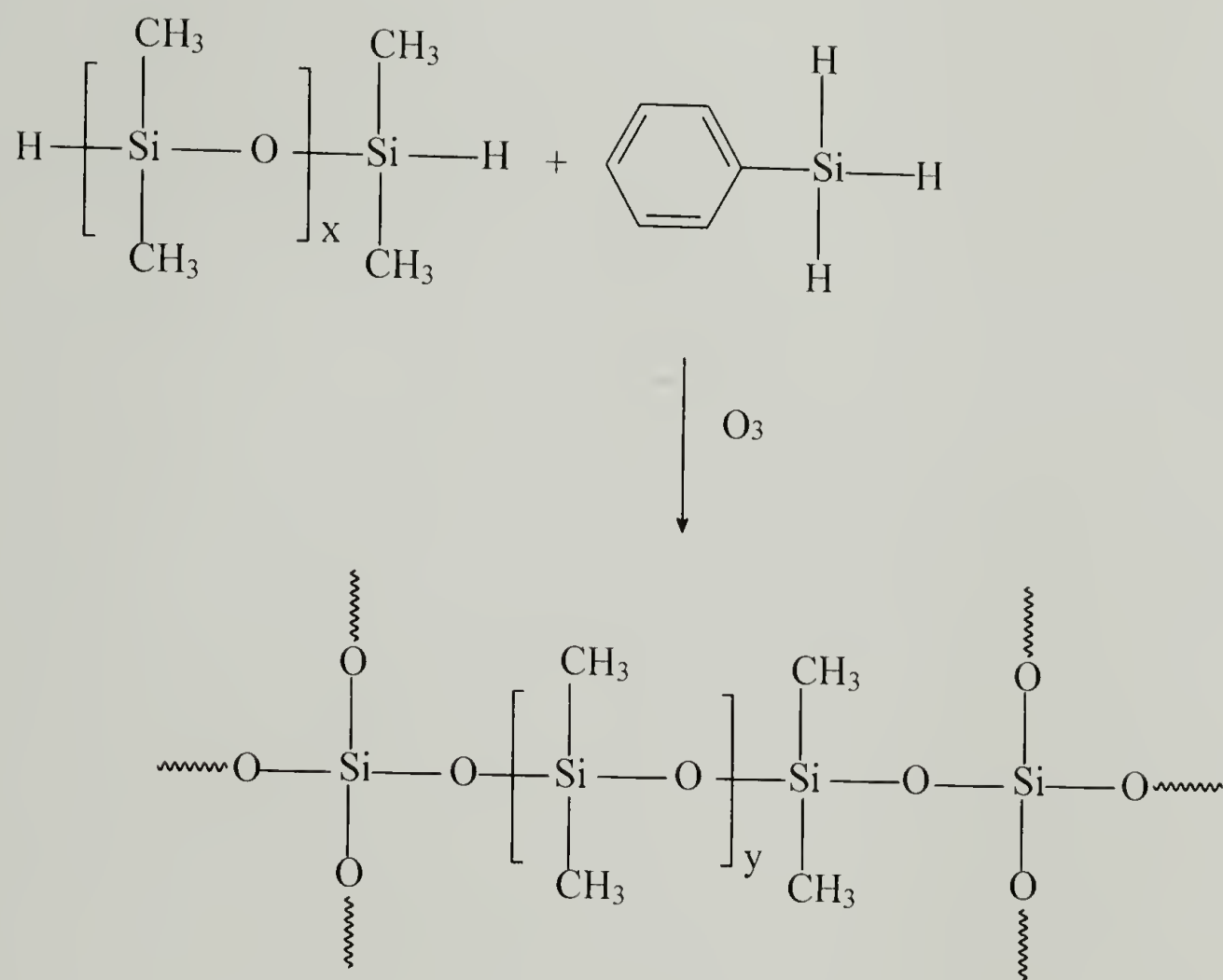


Figure 4.11. Solid state ^{29}Si NMR spectrum taken from the PDMS- H^{41} sample. The peak at -23 ppm is due to the $\text{Si}(\text{CH}_3)_2$ the SiO_2 peak appear at -111 ppm. The peak at -102 ppm is possibly due to some unreacted phenyl residue.

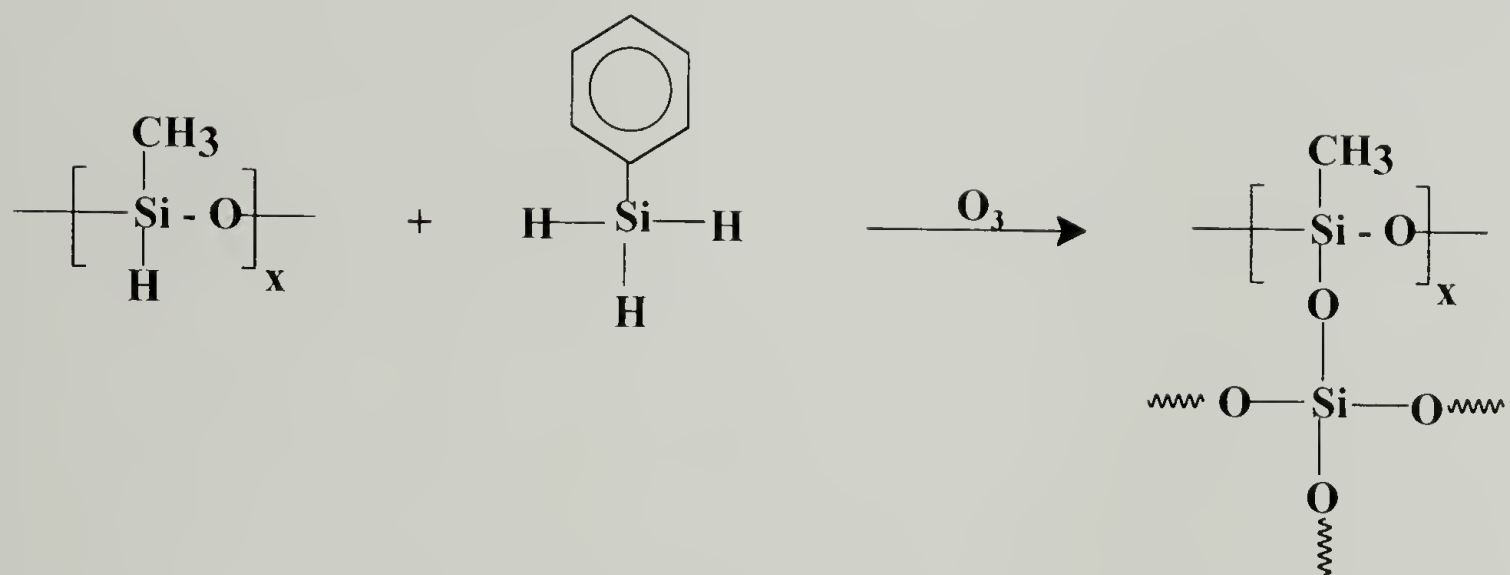
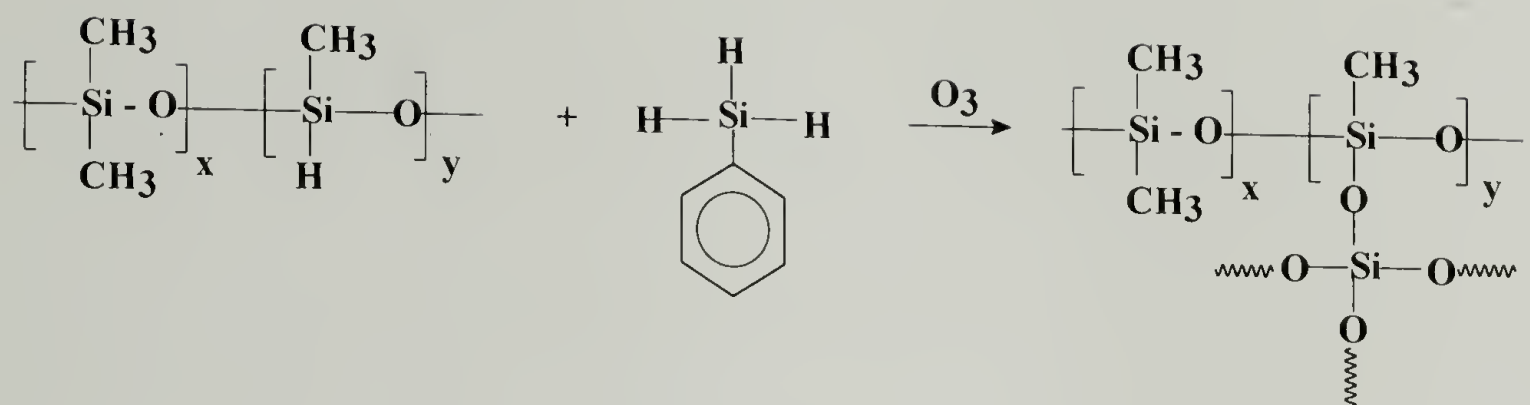
4.3.4 Poly(dimethyl methylhydrosiloxanes), trimethylsilyl-terminated (PDMMHS) copolymers, methylhydrosiloxane (PMHS) trimethylsilyl-terminated polymer mixed with various amounts of phenylsilane (PhSiH₃)

The ozonization of the previous set of mixtures resulted in the development of a general experimental procedure used for all ozonizations for the synthesis of the hybrid materials, fig. 4.2. A schematic representation of the ozonization reaction of hydrosiloxanes mixed with phenylsilane is depicted in scheme 4.3. The reactions were followed by FT-IR spectroscopy. Representative spectra are depicted in figures 4.12 and 4.13. The band of SiH around the 2158 cm⁻¹ does not disappear completely for the samples with very high concentration of SiH centers. Solid state ²⁹Si NMR spectroscopy was used when it was necessary and possible. Representative spectra are presented in figures 4.14 - 4.16. The formation of tetrafunctional trifunctional silicon is evident. Due to the complexity of the reactions no attempts were made to quantify the results and only a qualitative picture is given [21].

Attempts to oxidize further the high SiH concentration isolated powders were unsuccessful. Surprisingly, when ozone was introduced in a reactor containing a small amount of hybrid powder within a very short time the reactor was in flames and the reaction was terminated immediately.



Scheme 4.2. Ozonization of a polydimethylsiloxane hydride-terminated (PDMS-H) mixed with phenylsilane (PhSiH₃). The concentration of PhSiH₃ varies from 3 to 41 %.



Scheme 4.3. Ozonization of poly(dimethyl methylhydrosiloxane) copolymers (PDMMHS) and polymethylhydrosiloxane polymer (PMHS).

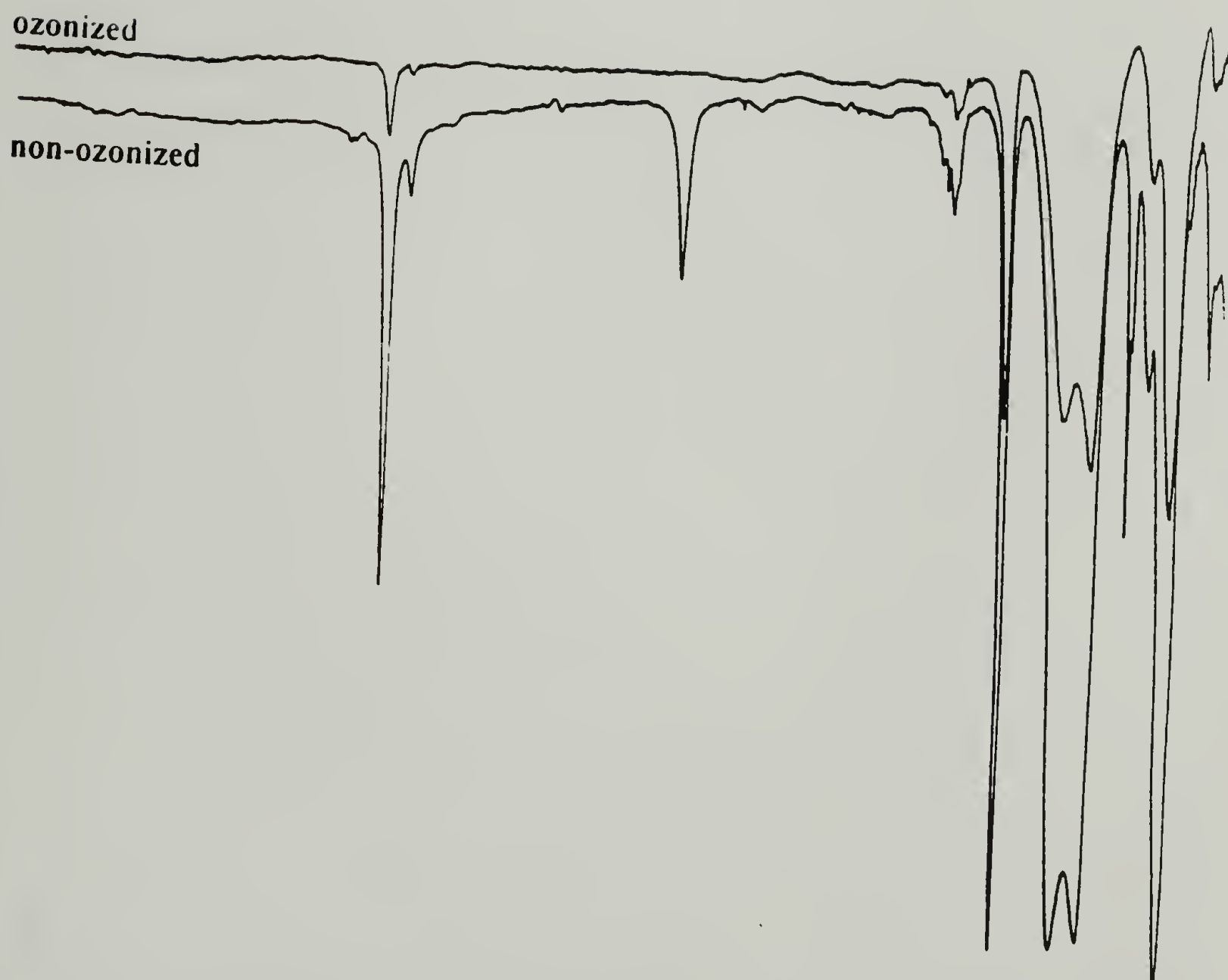


Figure 4.12. FT-IR spectra of the 3% methylhydrosiloxane copolymer (PDMMHS³-3).

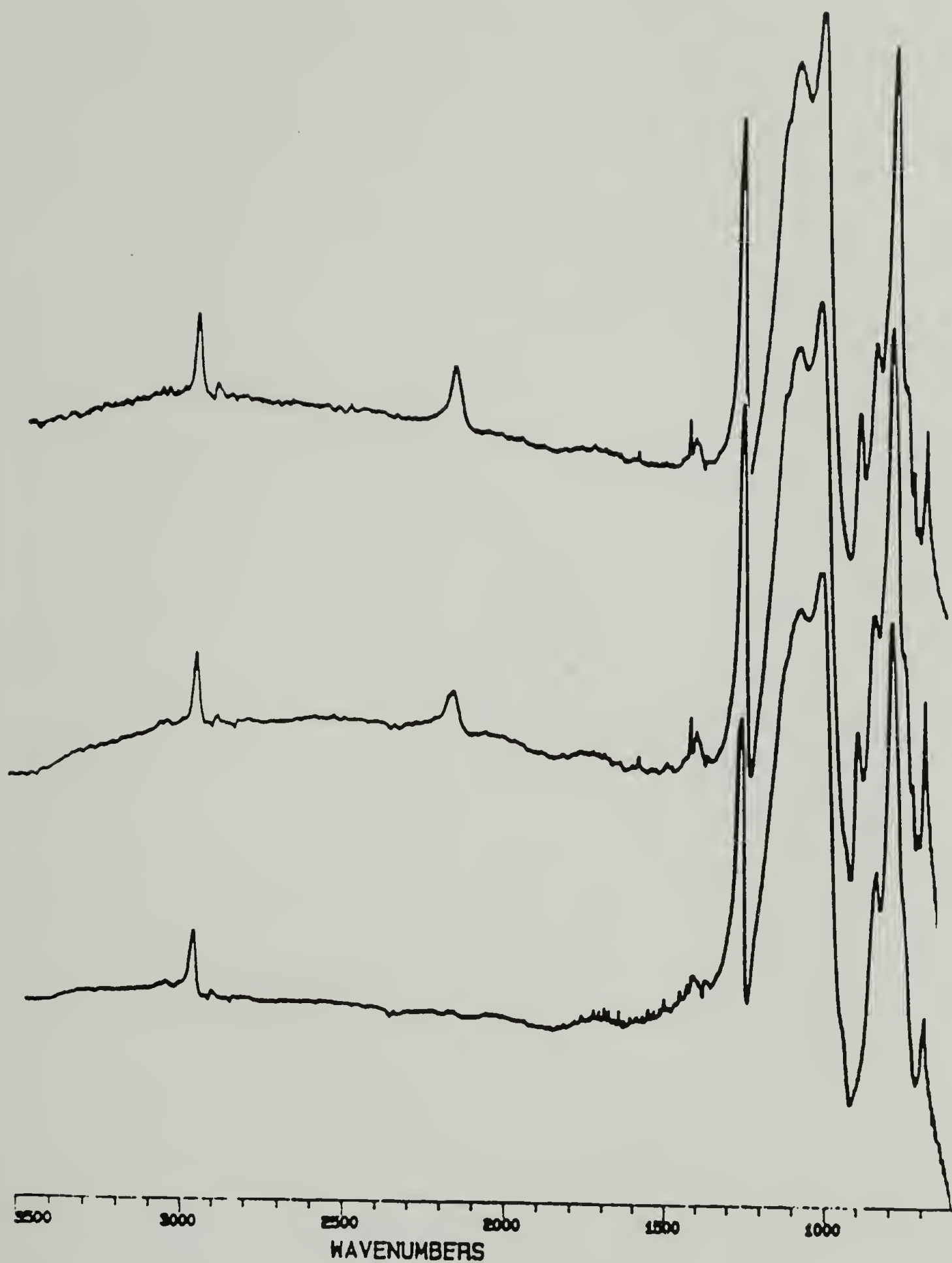


Figure 4.13. Representative FT-IR spectra of three different ozonized hydrosilicones.

The top spectrum is taken from the PMHS⁴¹; the one in the middle is due to PDMMHS⁴¹-50 and the PDMMHS⁴¹-30 spectrum is depicted on the bottom.

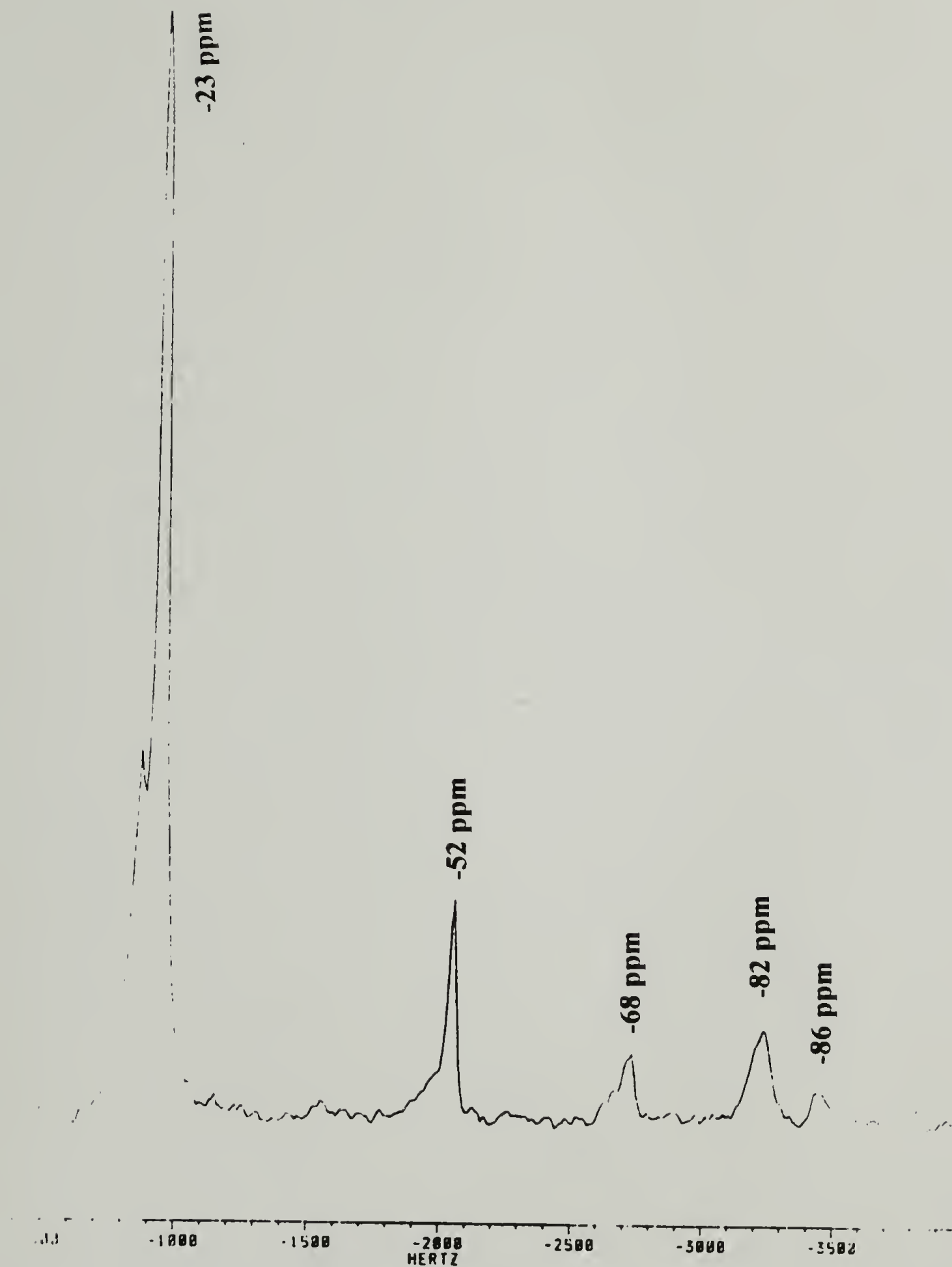


Figure 4.14. Solid state ^{29}Si NMR spectrum of the PDMMHS¹²-3 sample. The peak at -23 ppm is due to difunctional silicon, $(\text{CH}_3)_2\text{SiO}_2$; the -52 ppm, -68 ppm, -82 ppm and -86 ppm peaks are due to the trifunctional part (RSiO_3).

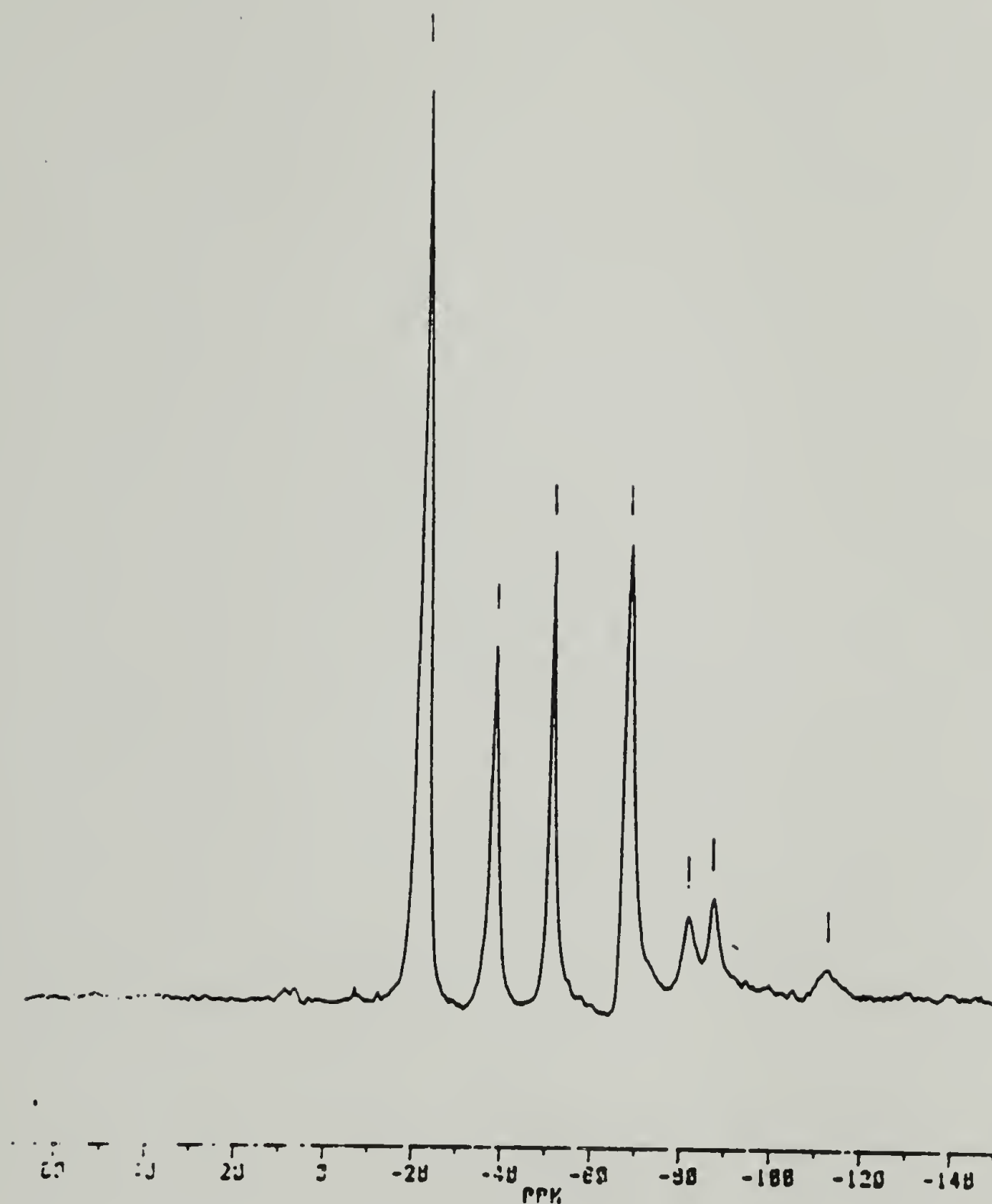


Figure 4.15. Solid state ^{29}Si NMR spectrum of the PDMMHS²⁵-30 sample. The peak at -23 ppm is due to difunctional silicon, $(\text{CH}_3)_2\text{SiO}_2$; the -40 ppm, -70 ppm, -82 ppm and -88 ppm peaks are due to the trifunctional part (RSiO_3). The peak of the SiO_2 appears at -113 ppm.

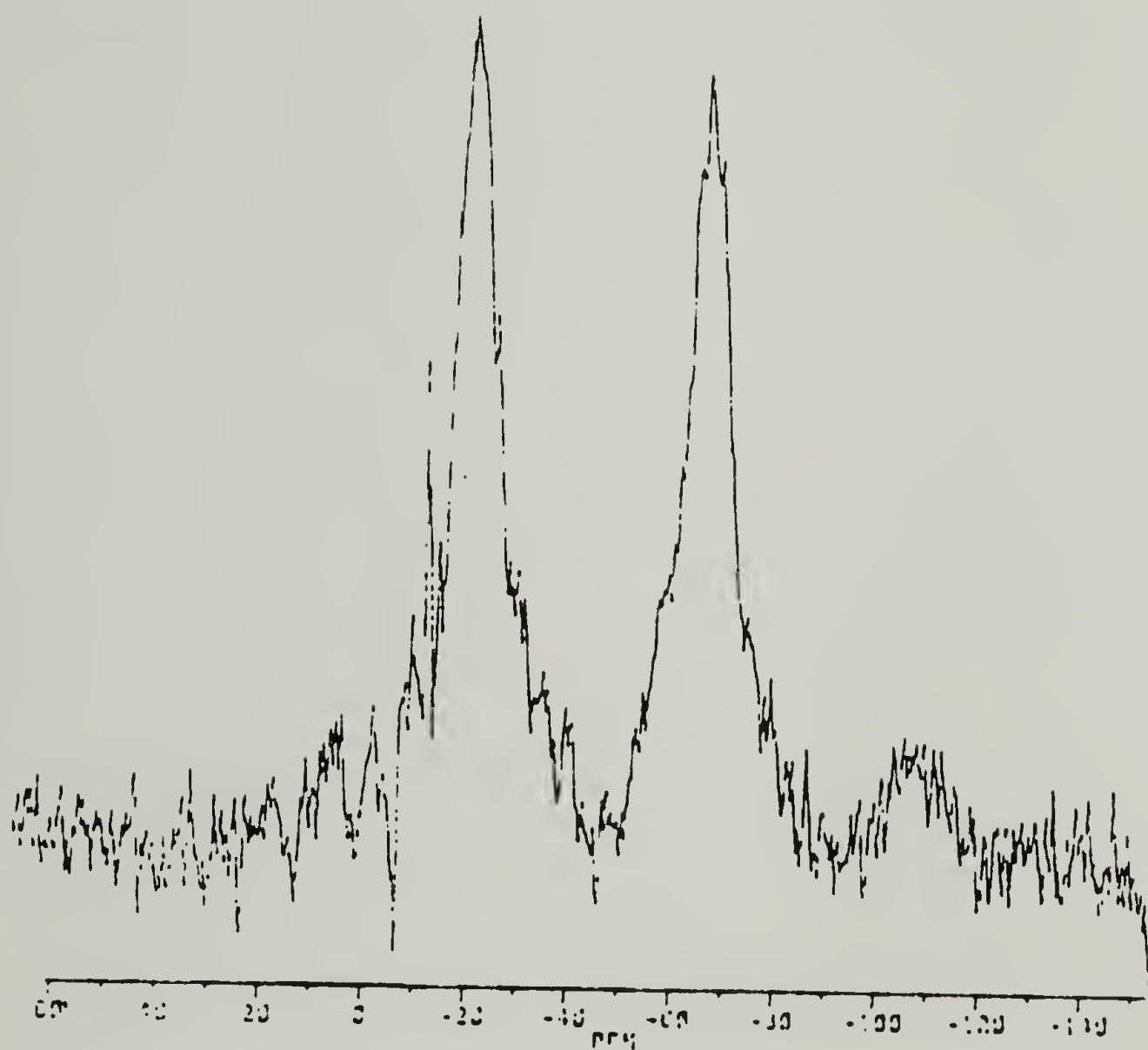


Figure 4.16. Solid state ^{29}Si NMR spectrum of the PMHS¹² sample. The peak at -23 ppm is due to difunctional silicon $(\text{CH}_3)_2\text{SiO}_2$; the -67 ppm due to RSiO_3 ; and the peak at -108 ppm is due to SiO_2 .

4.4 Results and discussion: Properties

A summary of the products obtained from the ozone reactions with hydride functionalized siloxanes and their mixtures with different amounts of phenylsilane, is reported on table 4.3. The amount of inorganic content of the materials was controlled by either the hydride concentration on the polymer backbone, or the concentration of phenylsilane in the mixture. The low inorganic content materials appear on the upper left corner of the table 4.3. High inorganic concentration materials are on the low right corner. Ozonization reactions produced materials with a wide variety of properties. The products were obtained either as liquids (PDMS-H⁰), gels (gums), films or powders. The gel type materials were obtained in the cases of low hydride, low phenylsilane concentration while high concentrations produced films and powders.

Scanning electron microscopy reveals some morphological characteristics of and differences in the produced materials. The micrograph displayed in fig. 4.17 is obtained from PDMMHS³-3. The ductile fracture of the surface of this very soft rubber is evident. The higher PhSiH₃ content in the hybrid depicted in fig. 4.18 makes the material behave as a hard rubber. The fractured surface of the film PMHS⁴¹ displayed in the micrograph in fig. 4.19 is essentially featureless which is an evidence of fracture of a brittle material.

Inorganic (silica gel) and hybrid powders, fig. 4.20, displayed some substantial differences. Nitrogen adsorption calculations (B.E.T experiments) revealed large differences in the surface areas (tables 4.4-4.6). The surface area of silica gel is found to be 285 m²/g, while the hybrid powders have a very small surface area, ~2.9 m²/g.

Table 4.3. Summary of the ozonized hydrosilicones; PDMS-H: polydimethylsiloxane hydride-terminated, PDMMHS: poly(dimethyl methylhydrosiloxane) copolymers, PMHS: polymethylhydrosiloxane. The superscript indicates the weight concentration of the glass forming agent (PhSiH_3). The number at the end of each siloxane copolymer name indicates the molar concentration of methylhydro groups.

PDMS-H ⁰	PDMMHS ⁰ -3	PDMMHS ⁰ -30	PDMMHS ⁰ -50	PMHS ⁰
PDMS-H ³	PDMMHS ³ -3	PDMMHS ³ -30	PDMMHS ³ -50	PMHS ³
PDMS-H ¹²	PDMMHS ¹² -3	PDMMHS ¹² -30	PDMMHS ¹² -50	PMHS ¹²
PDMS-H ²⁵	PDMMHS ²⁵ -3	PDMMHS ²⁵ -30	PDMMHS ²⁵ -50	PMHS ²⁵
PDMS-H ⁴¹	PDMMHS ⁴¹ -3	PDMMHS ⁴¹ -30	PDMMHS ⁴¹ -50	PMHS ⁴¹

Surface polarity is another property where the inorganic and hybrid powders differ.

Hybrid powder (PMHS⁴¹) proved to be extremely hydrophobic, as opposed to the silica gel surface which was readily wet by water (fig. 4.21).

The PhSiH₃ concentration affected the glass transition temperature (T_g) of the ozonized materials as displayed in fig. 4.22 and reported in table 4.7. Even though there is a definite increase in glass transition, the differences are not as dramatic as one might expect. On the other hand, PhSiH₃ concentration has a dramatic effect on the weight loss of the hybrids (fig. 4.23). TGA thermograms in fig. 4.24 demonstrate that the residual mass left after pyrolysis under nitrogen is a function of PhSiH₃ concentration. There is, however, a more complex response when thermolysis is carried out under air, as fig. 4.25 depicts.

Decomposition temperature and thermal stability of the hybrids is also greatly affected by the PhSiH₃ concentration. The decomposition temperatures for the hybrid materials are reported in table 4.8. There is a noticeable difference in the effect of the PhSiH₃ concentration, when the hybrid is heated under air and under nitrogen. Fig. 4.26 is a plot of the T_d of the PDMMHS-30 vs. PhSiH₃ concentration. When the heating is under nitrogen the decomposition temperature is independent of phenylsilane concentration. This is because the pyrolysis is incomplete due to lack of oxygen. On the other hand, under air there is enough oxygen to complete the pyrolysis and the T_d increases from 290 °C to 376 °C. The same trend is observed for the PMHS, however there is a difference. This polymer contains a large hydride concentration and the decomposition under nitrogen represents the low decomposition limit, fig. 4.27.

The effect of phenylsilane and hydride concentration on the thermal stability of the hybrid materials was evaluated by using again thermogravimetric data, fig. 4.28. The results are reported in fig. 4.29 and tables 4.6-4.8. The data obtained indicate that an increase in concentration of hydride active centers in the polymer backbone results in a decrease in the thermal stability of the hydrosiloxanes from ~ 60 Kcal/mol to ~ 9 Kcal/mol. It is also evident from the results that incorporation of phenylsilane increases only the thermal stability of the hybrids with high hydride concentration. For example, the activation energy for the PDMMHS-30 increases from 18 Kcal/mol to ~ 55 Kcal/mol (avg.), table 4.10. For the PDMMHS-50 the activation energy increases from 9 Kcal/mol to ~ 40 Kcal/mol (avg.), table 4.11. There is not a definite conclusion for the thermal stability of the PDMMHS-3.

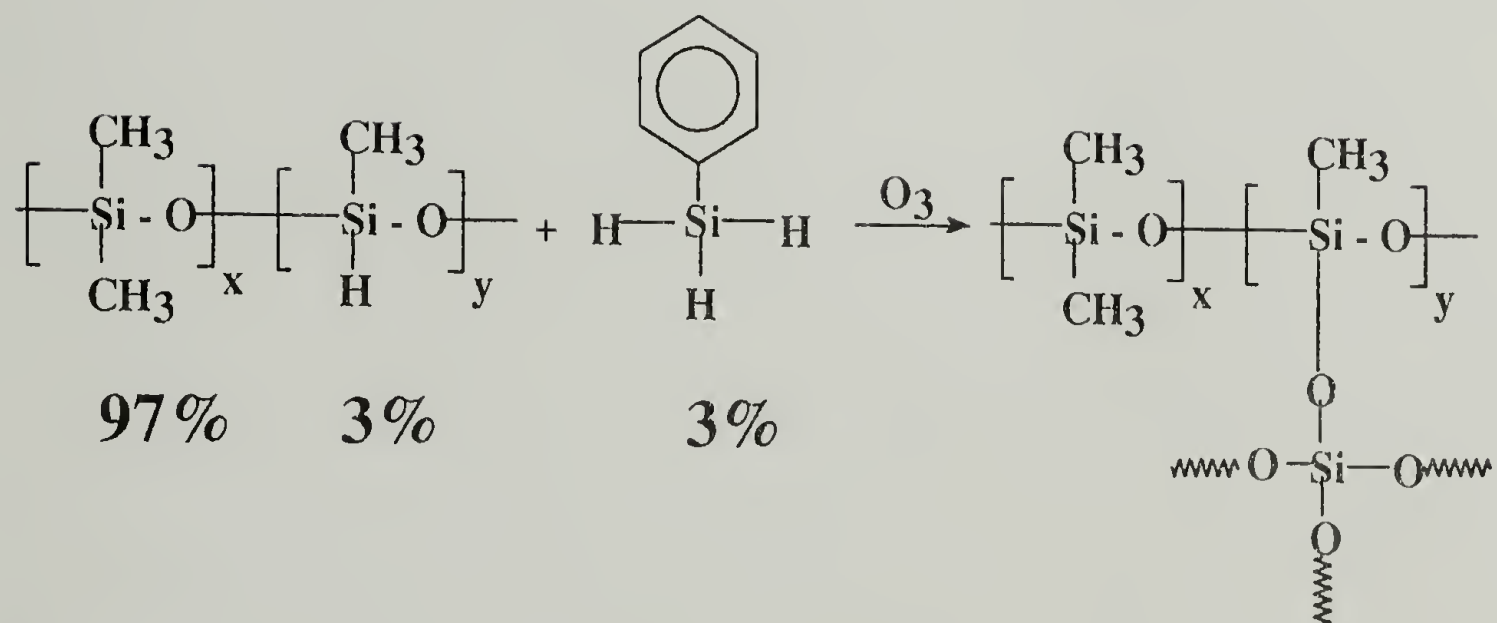
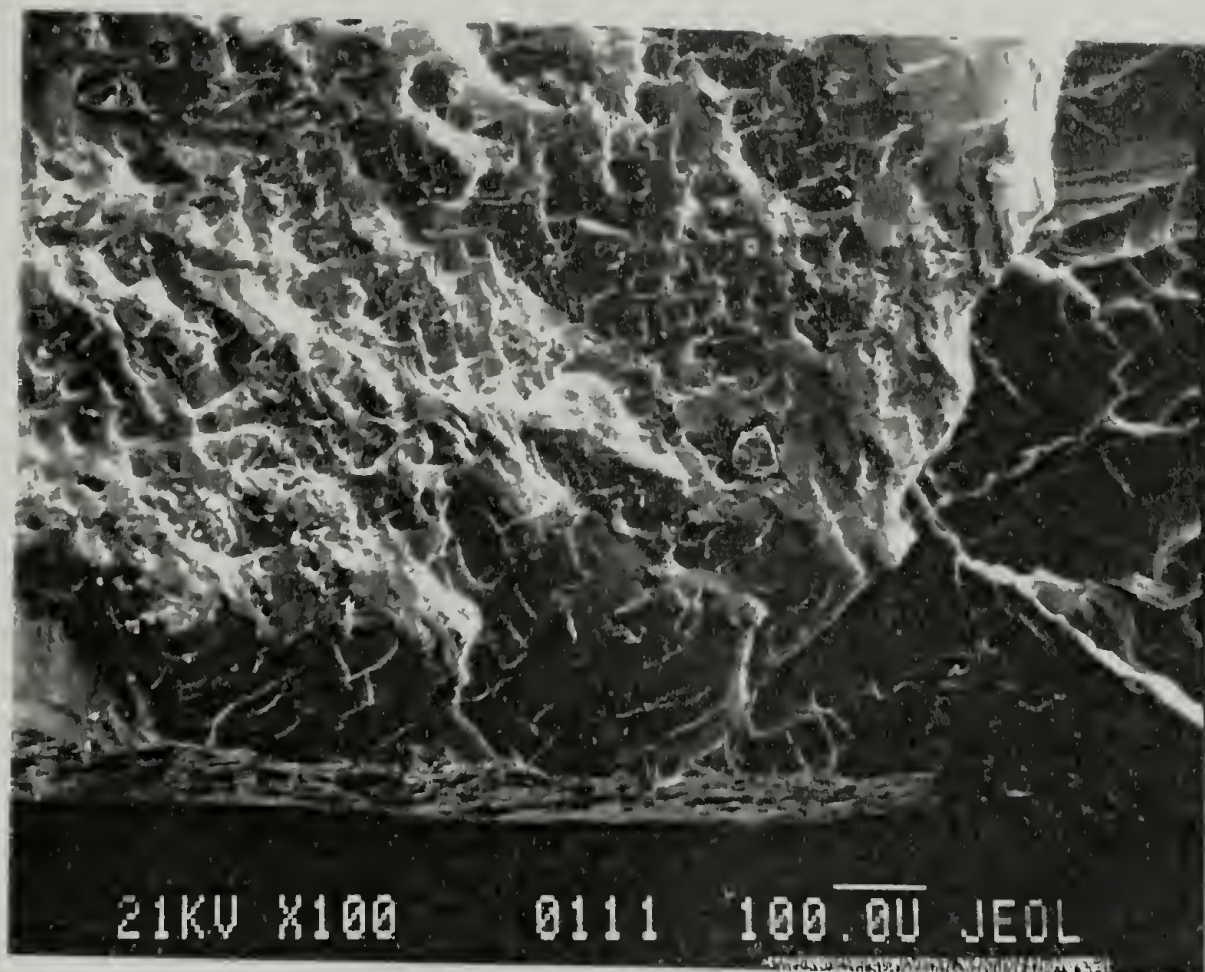


Figure 4.17. Scanning electron micrograph obtained from a PDMMHS¹-3 film. The ductile fracture indicates the rubbery nature of the polymer film.

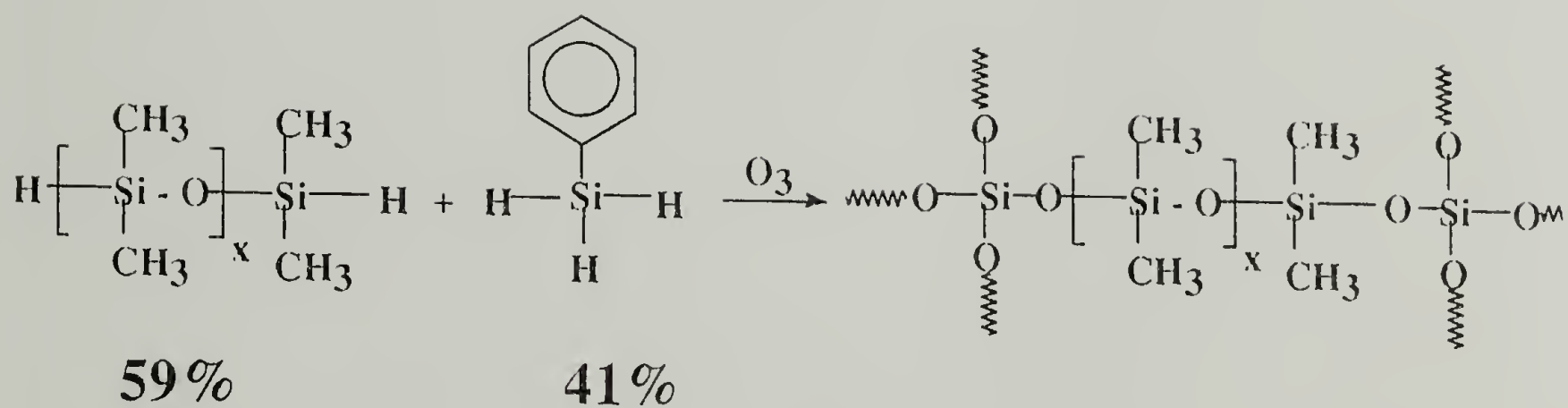


Figure 4.18. Scanning electron micrograph obtained from a PDMS⁴¹ film. The polymer film behaves as a hard rubber.

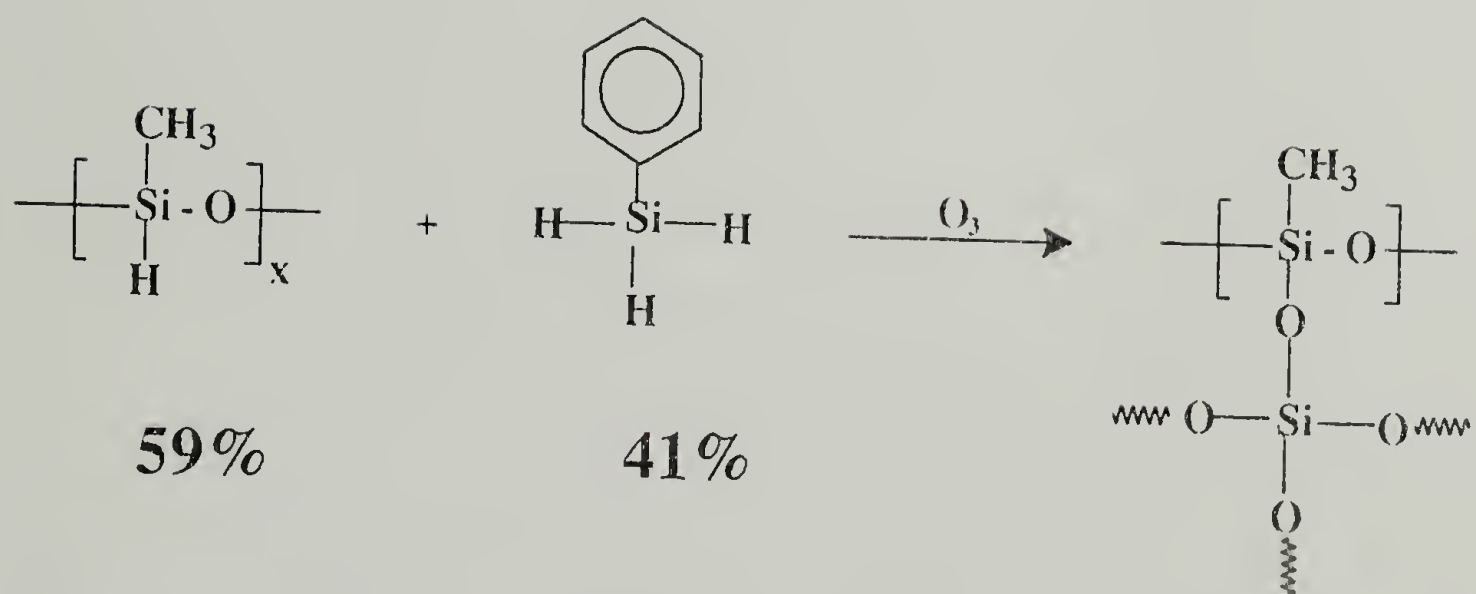


Figure 4.19. Scanning electron micrograph obtained from a PMHS⁴¹ film. The brittle and almost featureless fracture is an indication of the high inorganic content.



Figure 4.20. Scanning electron micrographs obtained from silica gel (top) and the hybrid PMHS⁴¹ powder (bottom).

Table 4.4. Nitrogen adsorption results (silica gel) for surface area calculations (B.E.T experiments). The pressure is reported in torr. The atmospheric pressure was 753.6 and the vacuum pressure 0.05. The sample weight was 0.2515 g. The calculated surface area is 285.3 m²/g.

Bulb position	Pressure for He/	Pressure for He/	Pressure for N ₂ /	Pressure for N ₂ /
	without sample	with sample	without sample	with sample
1	45.7	41.5	100.9	53.3
2	69.7	60.3	153.95	74
3	117.2	92.9	259.15	106.4
4	243.6	157.7	538.8	162.45
5	408.3	213.7	901.4	203.45

Table 4.5. Nitrogen adsorption results (dimethyl methylhydrosiloxane mixed with 41% phenylsilane) for surface area calculations (B.E.T experiments). The pressure is reported in torr. The atmospheric pressure was 757.5 and the vacuum pressure 0.2. The sample weight was 0.2335 g. The calculated surface area is 2.8 m²/g.

Bulb position	Pressure for He/	Pressure for He/	Pressure for N ₂ /	Pressure for N ₂ /
	without sample	with sample	without sample	with sample
1	45.7	41.6	79.1	72.1
2	69.6	60.5	120.6	104.9
3	116.8	93.3	202.9	161.9
4	242.6	159.4	422.55	275.7
5	406.6	217.2	709.3	373.6

Table 4.6. Nitrogen adsorption results (polymethyhydrosiloxane mixed with 41% phenylsilane) for surface area calculations (B.E.T experiments). The pressure is reported in torr. The atmospheric pressure was 759 and the vacuum pressure 0.0. The sample weight was 0.301 g. The calculated surface area is 2.9 m²/g.

Bulb position	Pressure for He/	Pressure for He/	Pressure for N ₂ /	Pressure for N ₂ /
	without sample	with sample	without sample	with sample
1	45.75	41.4	91	82.1
2	69.7	60.0	138.8	119.0
3	117.2	92.1	233.6	182.3
4	243.65	155.4	485.5	306.2
5	407.6	209.6	812.7	411.5

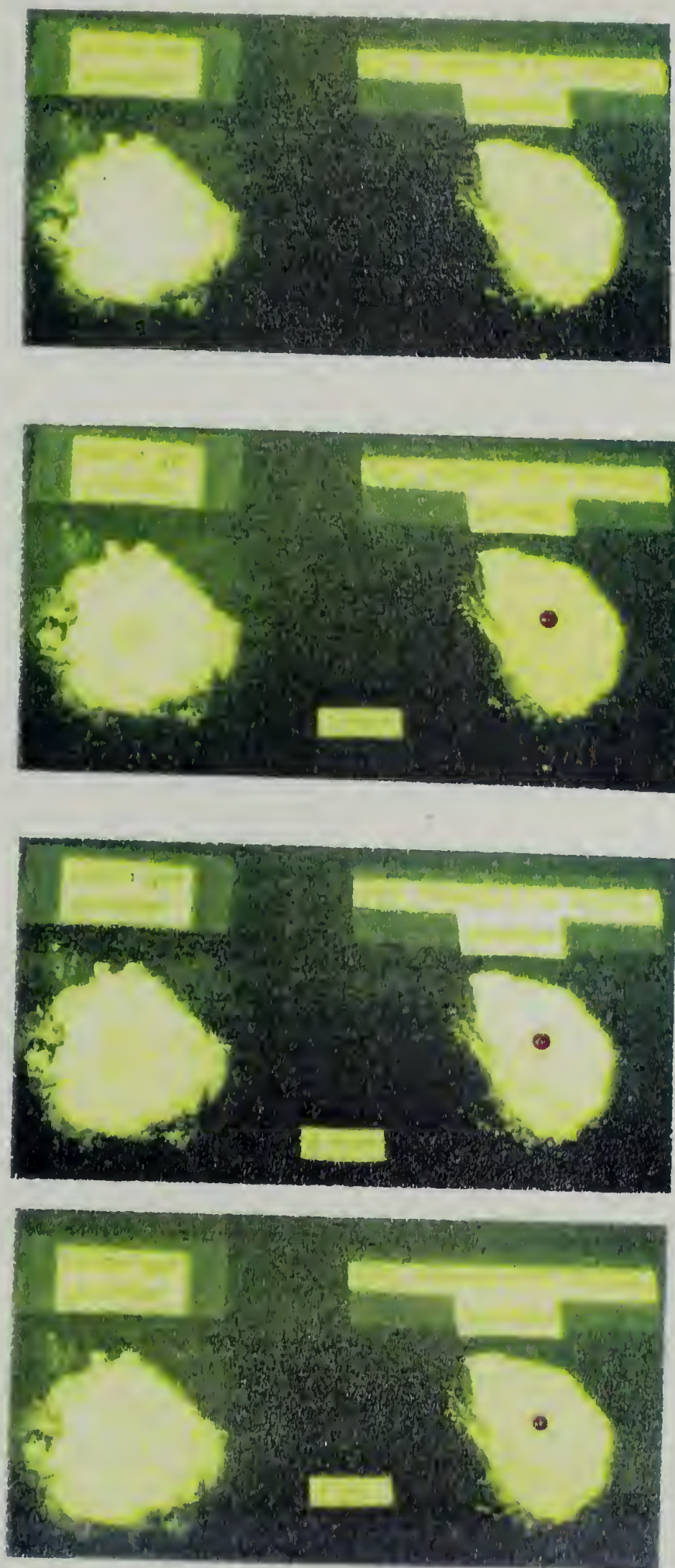


Figure 4.21. Qualitative test for the surface polarity of the hybrid powder. A drop of water colored with potassium permanganate is placed on the surface of a silica gel and the PMHS⁴¹ hybrid powder. The wetting of the surface is observed with time.

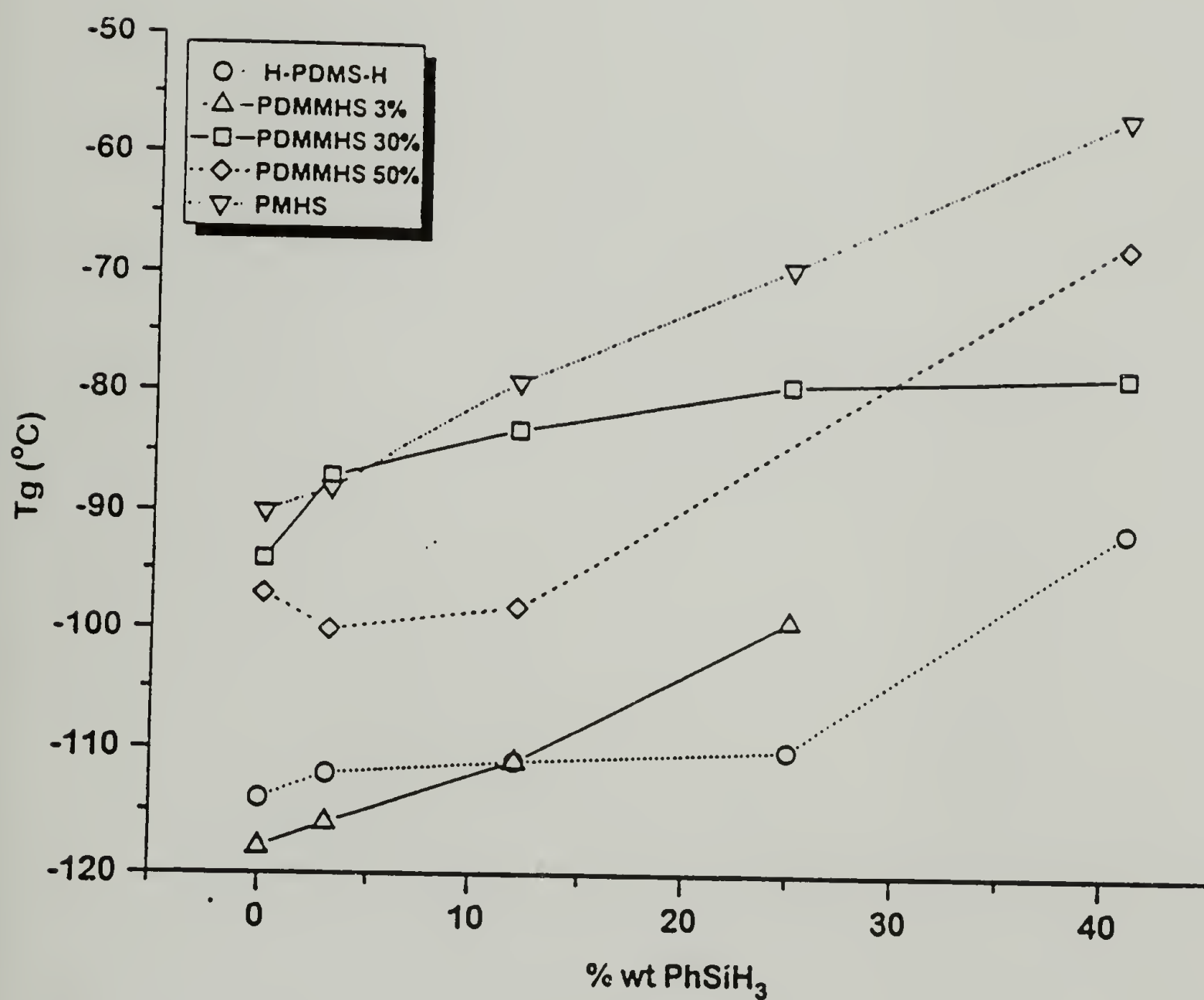


Figure 4.22. The effect of the phenylsilane on the glass transition temperature of the various siloxanes. The heating rate was 10 °C/min under N₂.

Table 4.7. The effect of the glass forming agent (PhSiH₃) on the Tg of the ozonized siloxanes.

PhSiH ₃	PDMS-H	PDMMHS-3	PDMMHS-30	PDMMHS-50	PMHS
0	-114	-118	-94	-97	-90
3	-112	-116	-87	-100	-88
12	-111	-111	-83	-98	-79
25	-110	-99	-79	-	-69
41	-91	-	-78	-67	-56

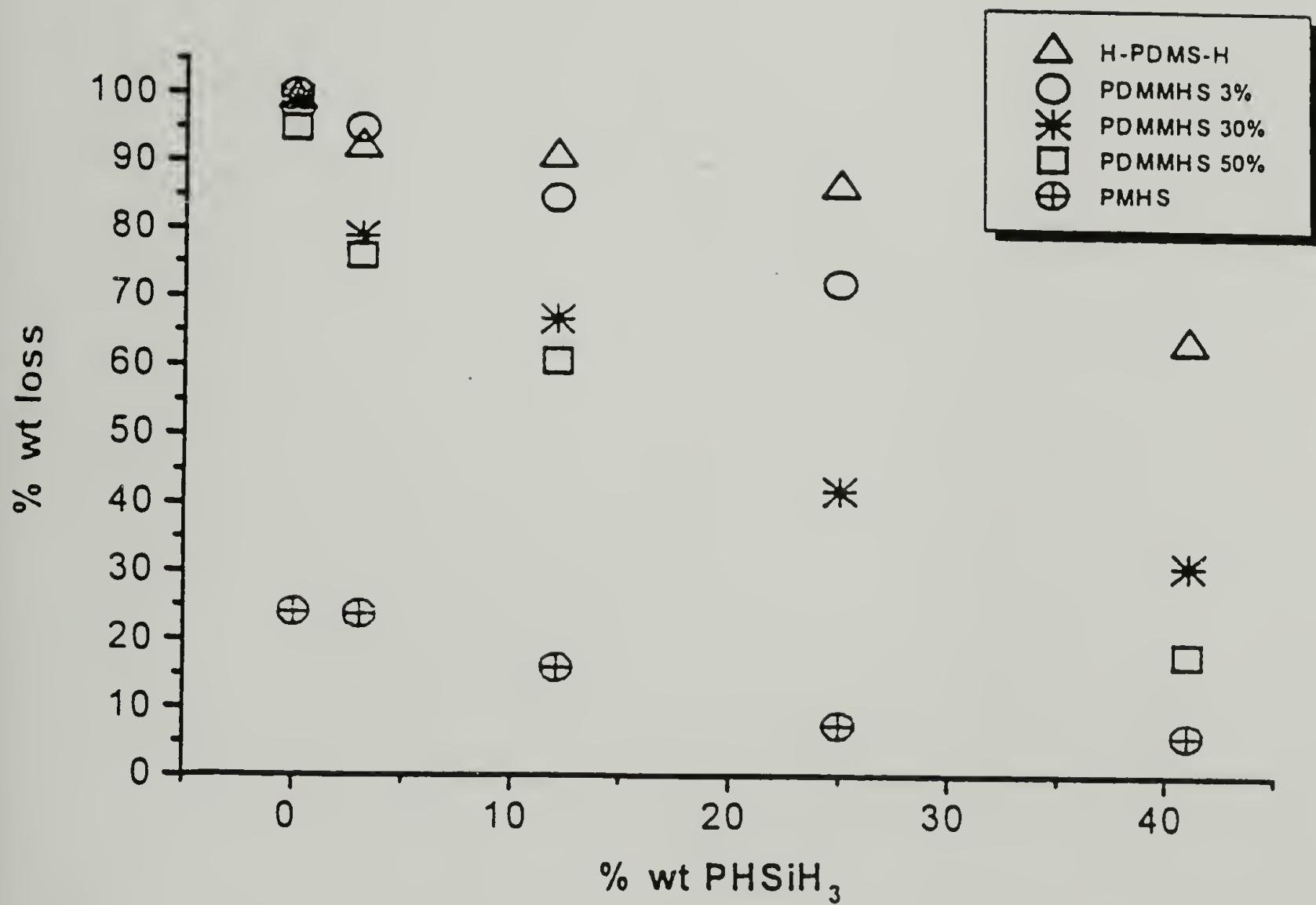


Figure 4.23. The effect of the glass modifier (PhSiH₃) on the weight loss of the hybrid networks heated under N₂ at 10 °C/min.

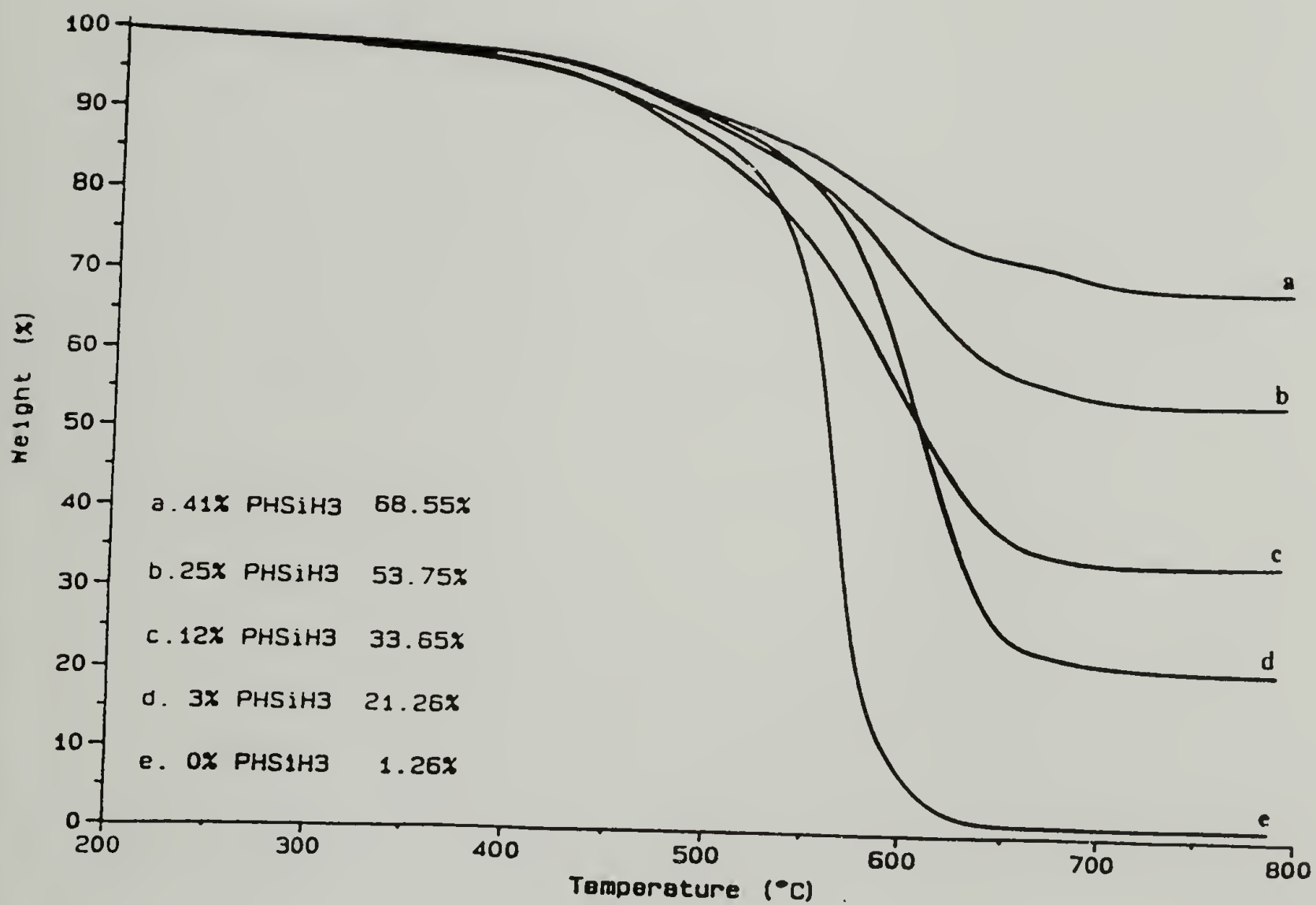


Figure 4.24. Thermogravimetric analysis of the PDMMHS-30/PhSiH₃ hybrids. The heating rate was 10 °C/min under N₂.

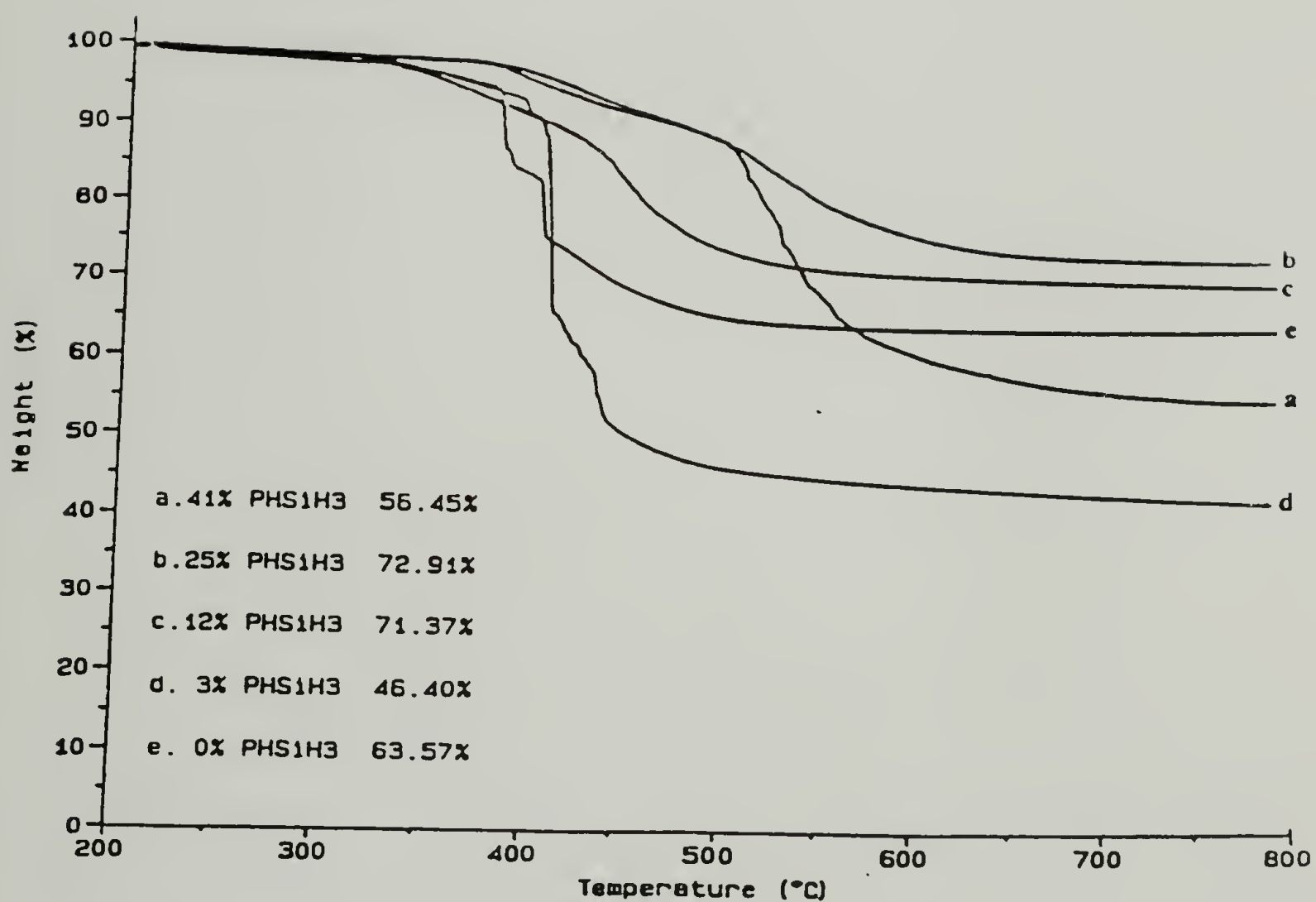


Figure 4.25. Thermogravimetric analysis of the PDMMHS-30/PhSiH₃ hybrids. The heating rate was 10 °C/min under air.

Table 4.8. The effect of the glass modifier (PhSiH₃) on the decomposition temperatures of the hybrid networks. The materials were heated under nitrogen and air at 10 °C/min.

PhSiH ₃ [% wt.]	PDMS-H		PDMMHS-3		PDMMHS-30		PDMMHS-50		PMHS	
	N ₂	Air	N ₂	Air	N ₂	Air	N ₂	Air	N ₂	Air
0*	50	50	300	300	-	-	-	-	-	-
0	270	330	400	370	375	290	255	295	360	355
3	450	370	450	390	375	300	255	330	360	370
12	450	400	450	360	378	320	250	360	370	430
25	450	390	450	380	375	350	-	-	370	455
41	450	380	-	-	375	376	255	360	370	485

* non-ozonized samples

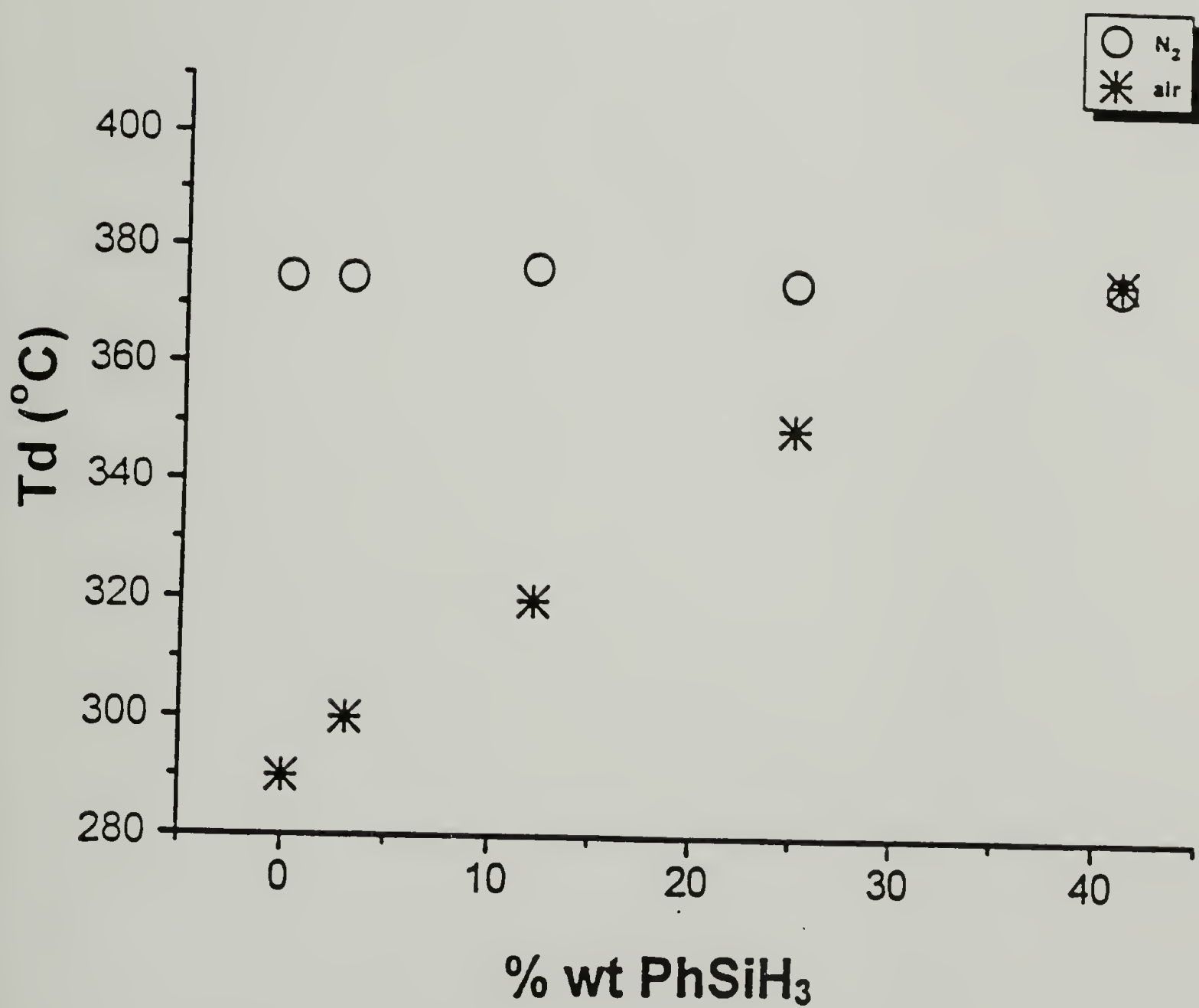


Figure 4.26. The effect of the glass modifier (PhSiH_3) on the decomposition temperature, T_d , of the PDMMHS-30 hybrid networks heated under N_2 and air at $10^\circ\text{C}/\text{min}$.

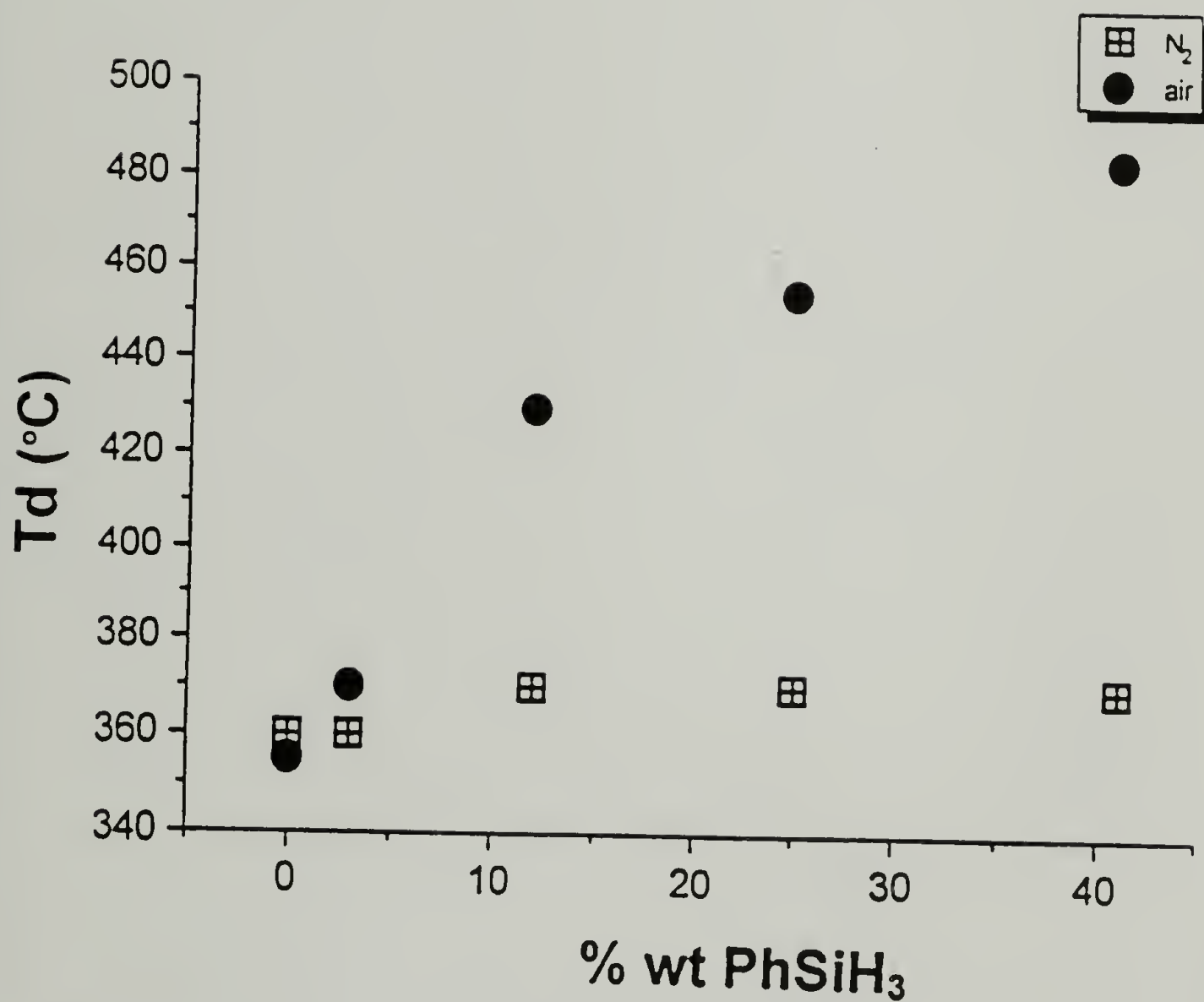


Figure 4.27. The effect of the glass modifier (PhSiH_3) on the decomposition temperature, T_d , of the PMHS hybrid networks heated under N_2 and air at $10\text{ }^{\circ}\text{C}/\text{min}$.

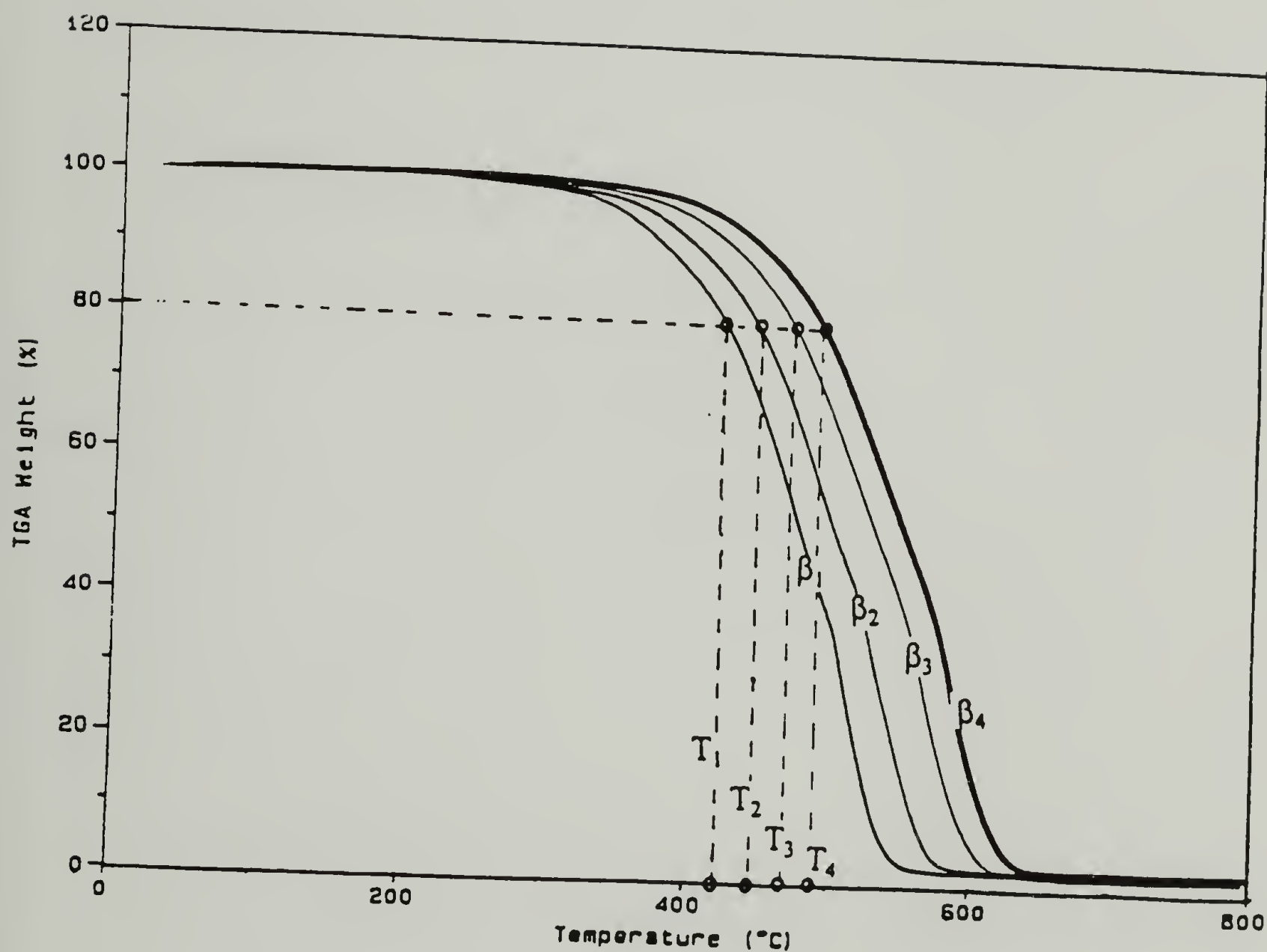


Figure 4.28. Example of isoconversional analysis of TGA thermograms in order to study the kinetics of the thermal degradation. The heating rates are, β_1 : 1°C/min, β_2 : 5°C/min, β_3 : 10°C/min, β_4 : 20°C/min. For a given conversion, four different temperatures are determined (T_1 , T_2 , T_3 , T_4) and the activation energy can be calculated from a plot of $\log \beta$ vs. $1/T$.

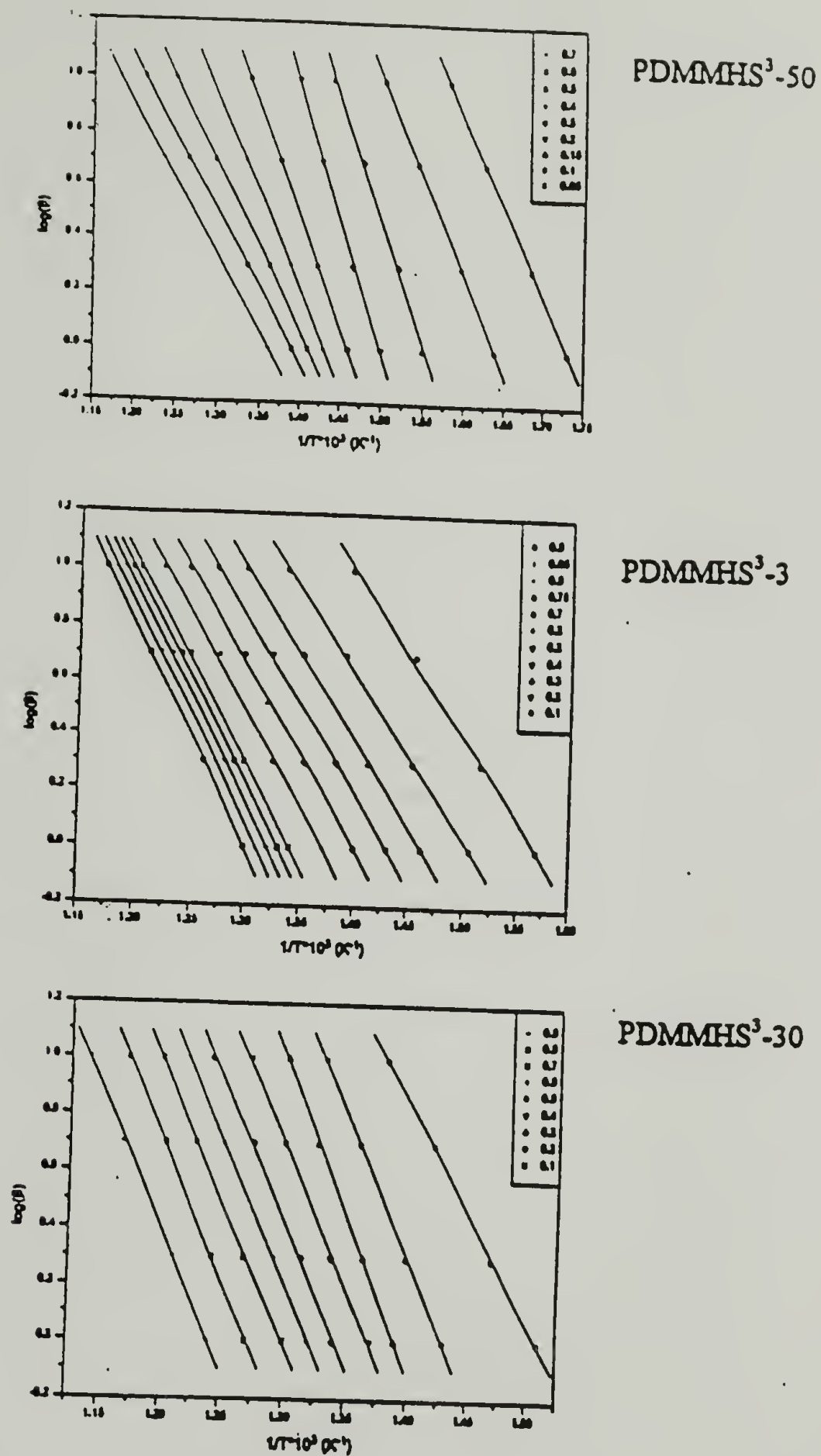


Figure 4.29. Plots of $\log\beta$ (heating rate) vs. $1/T$ for various conversions (0.1-0.9) during the thermal degradation of the PDMMHS³-3, PDMMHS³-30, PDMMHS³-50. The activation energy is calculated from the slopes and is averaged over the chosen conversions.

Table 4.9. Calculated activation energies for the 3% methylhydro group-containing siloxane copolymers.

Conv.	PDMMHS-3	PDMMHS ³ -3	PDMMHS ¹² -3	PDMMHS ²⁵ -3	PDMMHS ⁴¹ -3
C	Ea (kcal/mol)	Ea (kcal/mol)	Ea (kcal/mol)	Ea (kcal/mol)	Ea (kcal/mol)
0.10	36.9	25.5	39.3	26.0	45.9
0.15	42.2		43.7	31.6	
0.20	45.8	25.8	46.3	32.6	49.4
0.25			50.7	34.5	
0.30	55.8	26.7	55.5	35.9	49.7
0.40	82.1	27.5	65.3	37.5	46.9
0.50	75.0	28.6	70.0	39.1	43.2
0.60	64.0	30.0	75.0	40.0	37.8
0.70	75.0	32.0	73.1	41.7	36.3
0.75		32.7			
0.80	64.0	33.5	67.8	42.9	33.8
0.85		33.9			
0.90	59.6	34.7			33.5
0.95	51.1				
AVG.	59.2	30.1	58.7	36.2	41.8

Table 4.10. Calculated activation energies for the 30% methylhydro group-containing siloxane copolymers.

Conv.	PDMMHS- 30	PDMMHS- 30	PDMMHS ¹² - 30	PDMMHS ²⁵ - 30	PDMMHS ⁴¹ - 30
C	Ea (kcal/mol)	Ea (kcal/mol)	Ea (kcal/mol)	Ea (kcal/mol)	Ea (kcal/mol)
0.10	23.6		68.9	33.6	64.8
0.15	16.8				
0.20	14.4	50.7	74.0	43.6	64.9
0.30	14.4	51.1	65.0	47.9	63.4
0.35	15.1				
0.40	16.2	52.4	59.6	43.6	59.5
0.50	22.2	49.1	61.2	43.5	55.4
0.60		58.5	55.7	43.3	52.7
0.65	20.8				
0.70	20.1	70.5	54.2	42.7	48.0
0.75	18.32				
0.80	16.9	103.4	49.2	43.4	38.2
0.90			31.8	43.0	
AVG.	18.1	62.3	57.7	42.7	55.9

Table 4.11. Calculated activation energies for the 50% methylhydro group-containing siloxane copolymers.

Conv.	PDMMHS-50	PDMMHS ³ -50	PDMMHS ¹² -50	PDMMHS ⁴¹ -50
C	Ea (kcal/mol)	Ea (kcal/mol)	Ea (kcal/mol)	Ea (kcal/mol)
0.05		29.2		
0.10	14.2	32.2	28.2	36.9
0.15		39.6	29.8	
0.20	11.6	42.4	35.2	51.3
0.30	10.4	35.4	37.0	54.4
0.40	9.7	31.2	33.3	49.4
0.50	9.6	27.1	28.9	44.7
0.60	10.9	24.6	27.9	38.5
0.70	7.5	24.4		37.7
0.80	5.2			
0.90	4.5			
AVG.	9.3	31.8	31.5	44.7

4.5 Conclusions and future work

A new system for the synthesis of organic-inorganic hybrids was developed, by applying ozone and silicon chemistry. The relative amount of organic-inorganic content was controlled by the amount of the glass forming agent added and by the concentration of hydride functional groups on the polymer backbone. In this new system the glass forming agent was phenylsilane which upon ozonization produced thermally stable powders with high inorganic content. The tendency of phenylsilane to escape from the reactor during ozonization was a major problem. The polymers employed for the network formation were hydride-functionalized siloxanes.

Ozonization of the composite mixtures (phenylsilane/siloxane polymer) was accomplished within eight hours in a procedure designed to accommodate all ozonization reactions. This procedure included the use of phenyldichlorophosphate as a catalyst to speed up the condensation process.

Ozonization reactions produced hybrid materials with a variety of properties. The effect of inorganic content on the hybrid properties was established. The hybrids exhibit high thermal stability, high hydrophobicity and very low surface areas. The complexity of the system makes a very precise characterization of these materials a very difficult task. There are many avenues that could be explored in the future to further investigate and optimize the ozonization method as a useful synthetic procedure for hybridization. Future investigation might include quantitative determination of the component in the system, detailed structural determinations and detailed kinetic studies. In this case, however, due to the complexity of the reactions (multifunctional materials with variable

concentrations of functional centers undergoing more than one type of reaction which are accomplished in more than one step) the future work should be concentrated in the simplest and easier-to-ozonize material (PDMS-H). In addition, a different glass forming agent could be utilized (Ph_2SiH_2 , Ph_3SiH) to avoid losses during ozonizations. This should require longer reaction times, however, a precise component determination and a wider flexibility of the reaction conditions (flow rates, reaction times etc.) would be possible. In future work it would be interesting to investigate the case where the main component of the hybrid is the glass forming agent and the variable component would be a low molecular weight siloxane polymer. Interesting changes in the surface behavior of the hybrids could occur (i.e. inversion of surface polarity, abrupt increase of the surface area, porous materials etc.). The low surface area should give a more effective interface blending between hybrids and pure polymers, therefore, these materials could be introduced as fillers for rubbers.

It should also be pointed out that many other types of composite materials could be synthesized. Instead of using siloxanes or silanes other inorganic or organometallic compounds could be used which have shown remarkable activity toward ozone [22, 23].

REFERENCES

1. Allock, H. R., "Chemical Processing of Advanced Materials," Eds. L. L. Hench and J. K. West, John Wiley and Sons Inc., New York, N. Y. 1992, p. 699.
2. Schmidt, H. K., "Better Ceramics Through Chemistry IV." B. J. J. Zelunski, C. J. Brinker, D. E. Clark D. R. Ulrich, MRS, Pittsburgh, PA, 1990 p. 961.
3. Anderson, R., G. L. Larson and G. Smith, "Silicon Compounds: Register and Review," 5th ed., Huls American Inc., Piscataway N. J. 1991.
4. Spialter, L., Leroy Pazdernik, S. Bernstein W. A. Swansiger, Glen R. Buell, and M. E. Freeburger, J. Am. Chem. Soc. 93, 22 (1971).
5. Aleksandrov, Y. A., and B. I. Tarunin, Russian Chem. Rev. (English Translation) 46, 1721 (1977).
6. Austin, J. D., and L. Spialter, "Oxidation of Organic Compounds" Vol. 3. Advances in Chemistry Series 77, Am. Chem. Soc. Washington, D. C. (1968).
7. Spialter, L., J. D. Austin, J. Am Chem Soc. 87, 19 (1965).
8. Aleksandrov, Y. A., and B. I. Tarunin, Doklady Akademii Nauk SSSR, Vol. 212, No. 4 p. 869 (1973).
9. Spialter, L., W. A. Swansiger, J. Am. Chem. Soc. 90, 8 (1968).
10. Sprung, M. M., C. A. Burkhard, U. S. Pat. 2, 448, 556 (1948).
11. Sprung, M. M., U. S. Pat. 2, 472, 629 (1949).
12. McGregor, R. R., E. L. Warrick U. S. Pat. 2, 459, 389 (1949).
13. Rochow, E. G., U. S. Pat. 2, 371, 068 (1945).
14. Spinu, M., J. E. McGrath, J. Inorganic and Organometallic Polymers 2, 1 (1992).
15. Flynn, J. H., L. A. Wall, Polym Letters, Vol. 4, p. 323 (1966).
16. Petrovic, Z. S., Z. Zavargo, J. H. Flynn, and W. J. Macknight, J. Appl. Pol. Sci. Vol. 51, 1994.
17. Anderson, D. A., E. S. Freeman, J. Pol. Sci. 54, 253 (1961).

18. Freeman, E. S., and B. Carroll, *J. Phys. Chem.* 62, 394 (1958).
19. Doyle, C. D., *J. Appl. Polymer Sci.*, 6, 639 (1962).
20. Lipp, E. D., A. L. Smith, "The Analytical Chemistry of Silicones," Ed. A. L. Smith, John Wiley & Sons, Inc., (1991) ch. 11.
21. Taylor, R. B., B. Parbho and D. M. Fillmore, "The Analytical Chemistry of Silicones," Ed. A. L. Smith, John Wiley & Sons, Inc., (1991) ch. 12.
22. Aleksandrov, Y. A., *Organometal. Chem. Rev.* 6 209 (1970).
23. Bailey, P. S., "Ozonization in Organic Chemistry," Vol. II, Academic Press, New York, N. Y., 1982.

CHAPTER 5

POLYMETHYLHYDROSILOXANE: WET STRENGTHENING COATING FOR PAPER

5.1 Introduction

Nearly all synthetic polymers have been used or have been suggested for use in coating applications. The utility of a particular polymer as a coating depends on many factors which can be both technical and economic. Since the early sixties considerable research effort has been directed to the development of polymeric coatings for paper to improve the wet strength retention, tensile properties, opacity, and brightness and to impart a smooth and receptive surface for printing [1, 2].

Chemical modification of cellulosic fibers has been used as method to produce papers with special properties. The major modifications fall into the following categories: esterification, etherification, oxidation, crosslinking and graft copolymerization. All the modifications, except graft copolymerization, involve the utilization of small molecules [3]. Graft copolymerization is of great importance in paper production as a means of modifying the surface properties of paper. The long polymer chains hinder the free access of liquids or vapors to the inner core of cellulose and the properties, especially on the surface, are those of the polymer rather than those of the cellulose. The effects of grafting can be seen on specific properties of paper (dry and wet

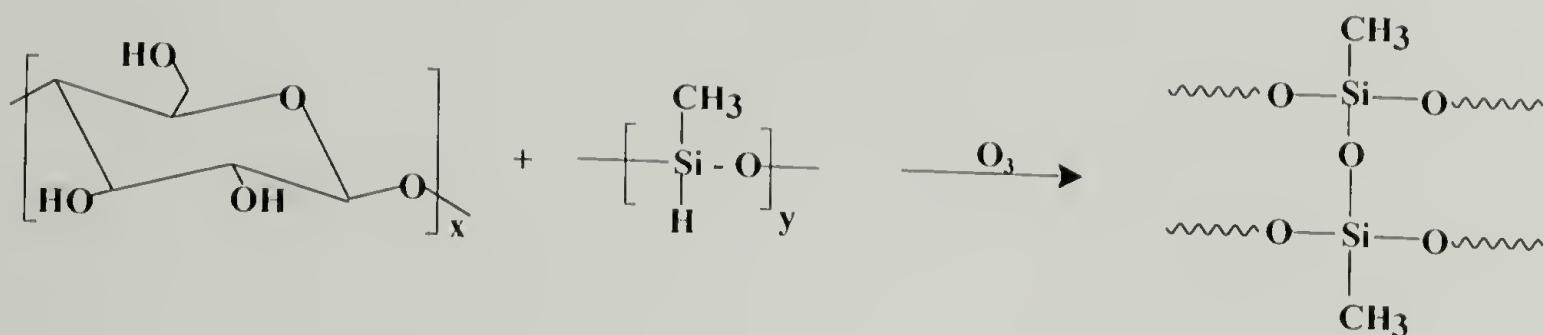
strength, stiffness and elastic modulus, water sorption, thermal and electrical properties, resistance to deterioration, etc.) [5-11].

It was mentioned above that many polymers have found application as paper coatings (polyethylene, polyvinylidene chloride, polyvinyl alcohol, styrene-butadiene copolymers, acrylic latexes etc.). Silicon compounds, both in monomer and polymer form, have also been used for this purpose due to their unique properties [12-18].

Silicon tetrachloride and aryl- or alkylchlorosilanes react easily with the cellulosic hydroxyls in the presence of pyridine to form organosilylcellulose [18]. However, the Si-OR formed bond is easily hydrolyzed by atmospheric moisture, even at room temperature. Hydrolysis of the silicon-modified cellulose regenerates the initial material [18].

Various functionalized siloxane polymers have been used as paper coatings with better success. The siloxanes reported to be used as paper coatings are terminated with: vinyl [17], amine and hydroxyl [14] functional groups. In addition, it has been reported that the use of siloxanes as coatings on paper completely change its surface properties. For example, the effects could be seen, among others, in adhesion properties (diminished), in printing quality (prevent bleeding), in abrasion resistance and in water repellency.

It was described in chapter four that methylhydrosiloxanes can easily be crosslinked by ozonization to form a semi-organic network. In addition, if phenylsilane is used as a glass forming agent then an organic-inorganic hybrid can be generated. In this chapter the possibility of applying this system to the preparation of high performance coatings for paper is examined.



Scheme 5.1. Ozonization of polymethylhydrosiloxane coated cellulose.

The objective of the research is to modify the surface characteristics, examine the thermal behavior and increase the wet and dry mechanical properties of paper. The completion of the ozonization reactions was followed with ATR-IR. The surface characteristics were examined with dynamic contact angle and X-ray photoelectron spectroscopy (XPS). Morphological information concerning the nature of the coating was provided by scanning electron microscopy (SEM). The thermal behavior of the coated paper was studied by thermogravimetric analysis (TGA) and thermomechanical analysis (TMA). The wet and dry mechanical properties were determined using an Instron tensile tester.

5.2 Experimental

5.2.1 General

The paper substrate used was Whatman #1 filter paper purchased from Fisher Scientific. The Whatman #1 filter paper was chosen, first because it is claimed to be pure cellulose fibers, and second because this type of paper is inherently very weak and particularly so when it is wet. The salts used to control the humidity, potassium carbonate and potassium acetate were also obtained from Fisher. Anhydrous methylene chloride (Aldrich) was used as received. Polymethylhydrosiloxane trimethylsilyl-terminated Mw=1500 (Huls America Inc.) was employed to form the silicon coating and was used as received. Attenuated total reflectance infrared spectra (ATR-IR) were obtained under dry air using a Nicolet IR/44 FTIR spectrometer and a thallus bromide iodide (KRS-5) internal reflection element with an entrance angle of 45°.

X-ray photoelectron spectra (XPS) were taken on a Perkin Elmer-Physical Electronics 5100 spectrometer using Mg K α excitation (400 W). The spectra were recorded at two different take-off angles (15°, 75°). The reported binding energies were not corrected for charging.

Scanning electron micrographs (SEM) were recorded on a JEOL-35CF. Accelerating voltages of 20 kV were used at various magnifications. The samples were mounted on aluminum cylinders using a conductive adhesive and sputter-coated with a few Angstroms of gold.

Dynamic advancing and receding contact angle (θ_A/θ_R) measurements were made using a Rame'-Hart telescopic goniometer and a Gilmont syringe with a 25-gauge flat

tipped needle. The contact angles were measured using distilled water as the probe fluid. The values reported are an average of at least five measurements taken at different locations on the sample.

Thermogravimetric analysis data was obtained using a TA Instruments, Inc. model 2950. The sample holders were platinum pans. The samples were heated from ambient temperature to 800 °C at 10 °C/min. under a nitrogen flow.

Thermomechanical analysis (TMA) was performed on a TA Instruments, Inc. model 2940 analyzer. The TMA was set up for thin films. The sample strips (5 mm x 25 mm) were subjected to two cycles of thermal treatment (1st heating-cooling, 2nd heating-cooling) under nitrogen at a ramp rate of 10 °C/min. The dimensional changes were determined and the coefficient of thermal expansion was calculated solely from the second heating.

The tensile properties were obtained using table-top type Instron tester model 5564. The dimensions of the tested samples were approximately (5 mm x 0.15mm x 50 mm). The samples for wet-strength determinations were dipped in a beaker filled with distilled water and left soaking overnight. The reported mechanical properties are values averaged from three specimens cut from the same sample.

5.2.2 Sample preparation

Preconditioning and conditioning of the paper samples [20]: Small test samples (0.1x10 cm) were cut in different directions from the paper sheets (58x68 cm) in order to determine the machine direction. Machine direction was the direction with the highest

orientation (highest modulus). When the machine direction was determined about 30 sample strips (5x200 mm) were cut in this direction to prepare for preconditioning [20]. The salt used for precondition was CH_3COOK . A supersaturated solution of the salt was placed in a gas absorption vessel, fig. 5.1 and a nitrogen stream was bubbled through [19]. After the relative humidity (RH) had reached equilibrium ($\sim 22\%$) the samples were allowed to remain at low humidity for 24 hr. Then the flow of nitrogen through this vessel was stopped and the gas was forced to pass through the second vessel containing the conditioning salt solution (K_2CO_3). The samples were allowed to stay in the controlled atmosphere for an additional 24 hr, after the relative humidity had approached equilibrium $\sim 43\%$ [19]. The experimental temperature was $\sim 25^\circ\text{C}$. The relative humidity was monitored with a Taylor Humidiguide hygrometer/thermometer. The equilibrium values reported for relative humidity are the ones obtained from the literature [19]. The hygrometer was used only to determine the equilibrium time and not to read the RH [19].

Impregnation of the samples with polymethylhydrosiloxane (PMHS): Silicone impregnated samples were prepared by dipping the paper strips in different concentration solutions of PMHS in dry methylene chloride. The sample were allowed to stay in the solution for 2-3 hr for impregnation. After the impregnation was completed, the samples were removed and were placed in the reactor similar to the one shown in Fig. 5.1. A stream of nitrogen was allowed to pass through the reactor for 1-2 hr to speed up the solvent evaporation. The samples were weighed and were placed back in the reactor. The different concentrations and the weight gained after impregnation and solvent

Table 5.1. PMHS solutions prepared for impregnation of the paper samples and the weight gained after impregnation and solvent evaporation.

PMHS solution concentration (%)	Weight gained (%)
0.15	0.2, 0.4, 0.9
0.5	1, 1.3, 1.7
2	5, 5.7, 7
9	16.2, 16.7
100	48.1

evaporation are reported on table 5.1. The dry impregnated samples were ready for the ozonization reactions.

5.2.3 Ozonization of the cellulose paper strips impregnated with PMHS

The impregnated sample strips along with two control non-impregnated strips were placed in a reactor container, similar to the one described in fig. 5.1, for the ozonization reactions.

The experimental setting for the ozonization reactions has been described in chapter two.

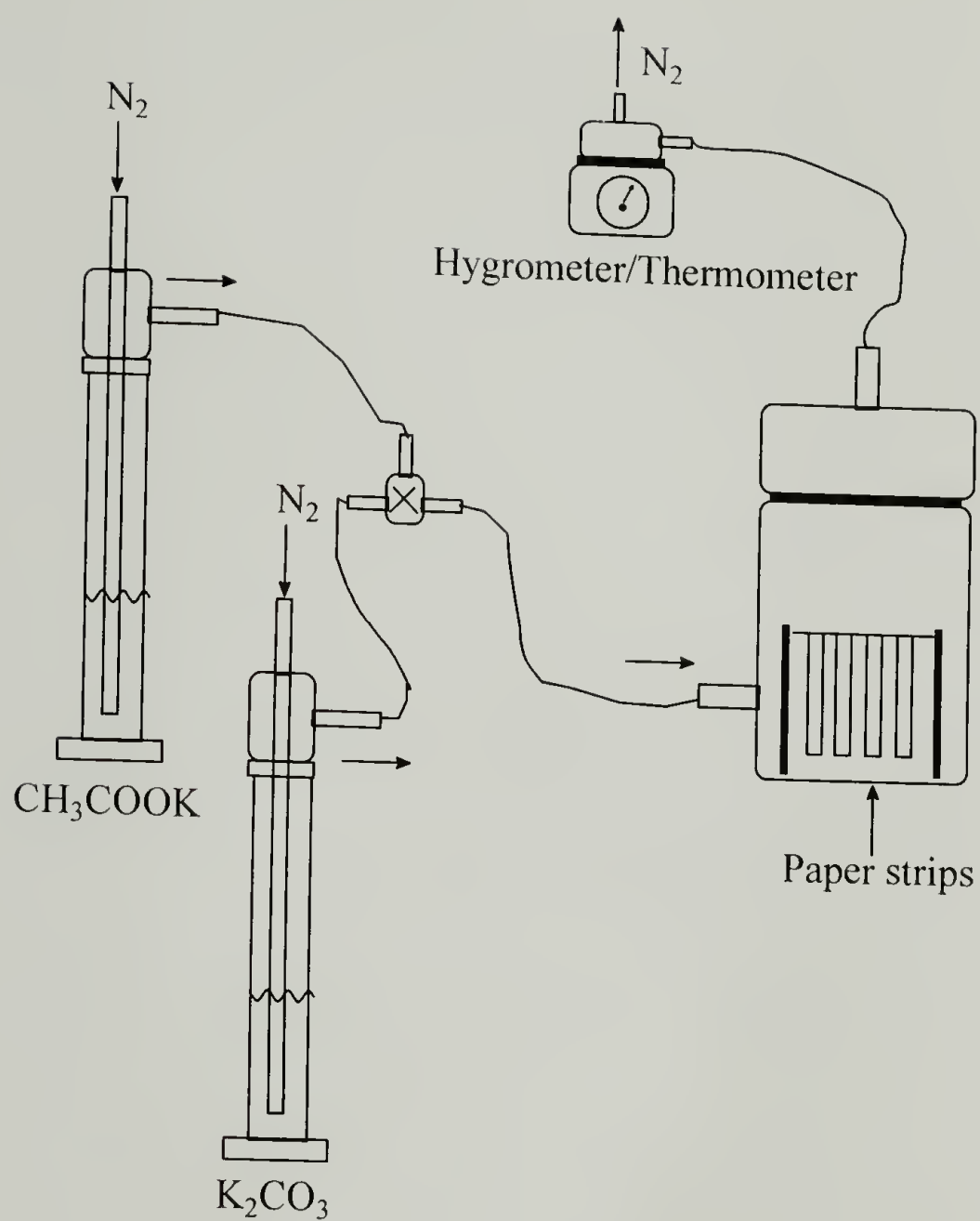


Figure 5.1. Experimental setting for humidity control. The CH₃COOK is the pre-conditioning salt ($22 \pm 1\%$ RH) and the K₂CO₃ is the conditioning salt ($43 \pm 0\%$ RH).

Temperature range 25 ± 3 °C.

The ozonator parameters for voltage and pressure were set at 115 V, and 8 psig accordingly. The reactor was immersed in a bath (40:60 ethylene glycol /H₂O) and the temperature controlled around 0 °C, using a cold finger cooling unit. A stream of gas (~4% ozone/oxygen mixture) was allowed to pass through the reactor for 3 1/2 hr. After the reaction was complete, the ozone flow was terminated and the reactor was flushed with nitrogen (~15 min.). The ozonized samples were washed with dry methylene chloride to remove any unreacted PMHS and then, after solvent evaporation, they were placed in individual vials and were stored in a desiccator for analysis. (ntbk-S5, p. 37-61)

5.3 Results and discussion

The products of the ozonization reactions were analyzed with ATR-IR spectroscopy, contact angle, SEM, TGA, and TMA. The infrared spectra of the control (non-impregnated) sample before and after ozonization were found to be identical (fig.5.2). The absence of the development of any carbonyl bands indicated that no appreciable ozonization of cellulose occurred under the current working conditions [21-24]. In contrast, the spectra depicted in fig. 5.3 shows the virtual disappearance of the Si-H absorption band at 2168 cm⁻¹, indicating that extensive ozonization takes place. Contact angle measurements showed a dramatic difference on the surface polarity of the plain paper and the ozonized samples. The results reported in table 5.2 illustrate that even a small amount (0.2%) of PMHS can completely alter the surface properties of the paper sample. The large hysteresis observed between the advancing and receding angles

Table 5.2. Dynamic contact angle (θ_A , θ_R) dependence on PMHS content of the cellulose paper samples.

PMHS (% w/w)	Advancing (θ_A)	Receding (θ_R)
0	0	0
0.2	108	78
1.3	115	48
5.7	114	46
16.2	113	47
48.1	92	80

is due to the rough paper surface. Rough surfaces have a tendency to enhance the hysteresis effect.

The surface roughness could also explain the lower contact angle and lower hysteresis observed for the 48.1 % impregnated sample. The surface of this sample is completely different from the other samples as can be seen in fig. 5.7. However, it is not clear why the 0.2% sample shows an unusually high receding contact angle.

Additionally, several drops of distilled water colored (purple) with potassium permanganate were placed on the surface of a control as well as the 1 % coated sample, fig. 5.4, in an effort to give a visual picture of the results obtained from contact angle experiments.

Scanning electron microscopy (SEM) and thermogravimetric analysis were employed in order to examine the surface topography and to confirm the formation and continuity of the silicone coating. The micrographs depicted in fig 5.5 illustrate the surface of the plain cellulose paper in two different magnifications. The micrographs in fig. 5.6 attempt to show the similarity in the topography of a control with an ozonized coated sample (16.7 % PMHS). It can be seen that the porosity of the paper is maintained even for this highly coated sample (porous and hydrophobic). It was mentioned before that the contact angle and the hysteresis effect of the 48.1 % sample were lower than the other coated papers. The micrographs in fig. 5.7 shows the surface characteristics of the 48.1 % and the 16.2 % samples. The 48.1% is highly coated and the silicone has formed a continuous coating on the surface (sandwich-like) that effectively makes the surface smoother, lowers the contact angle and makes the hysteresis phenomenon less pronounced. The porosity is completely lost for this sample.

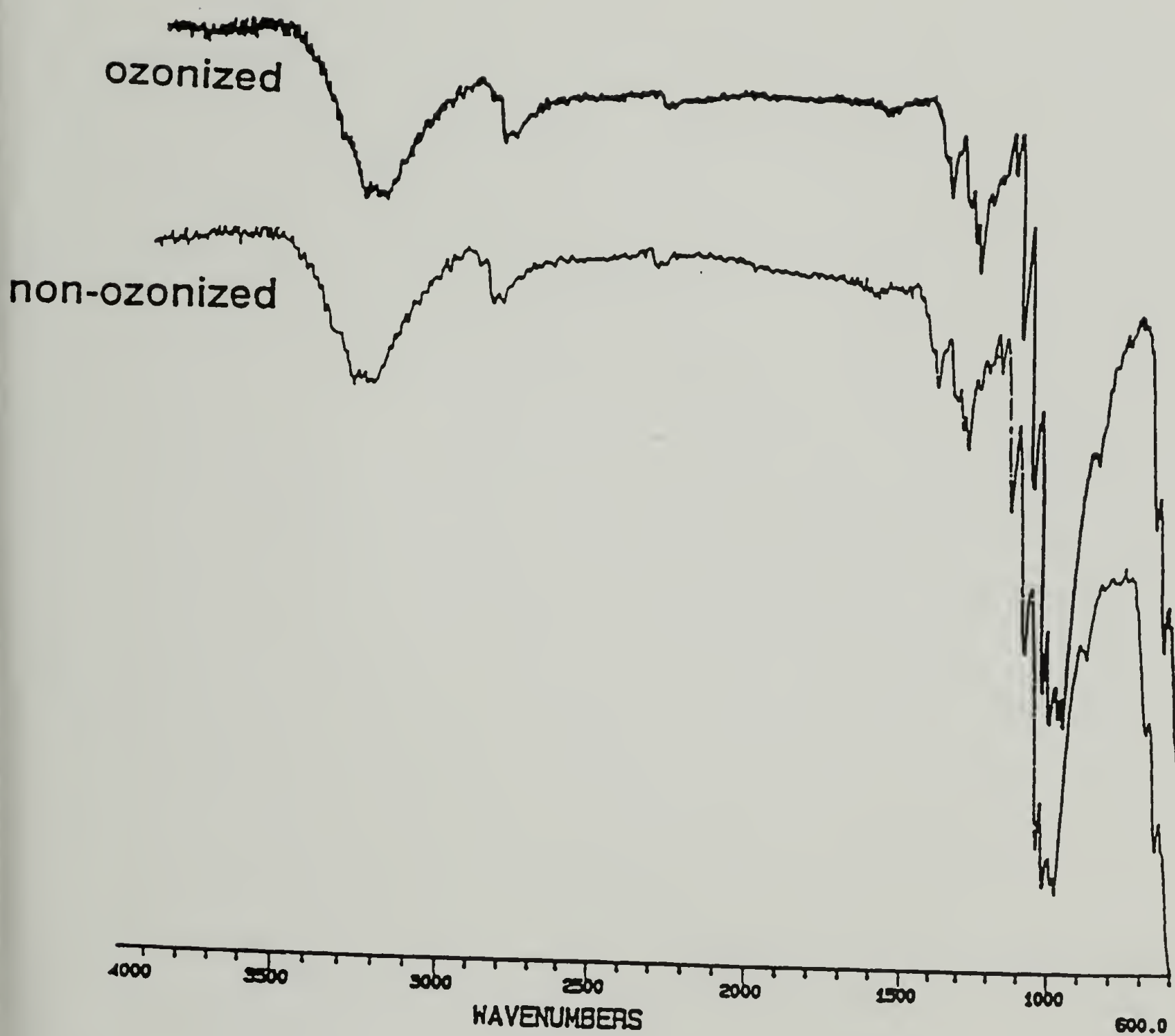


Figure 5.2. ATR-IR spectra of the control (non-impregnated) paper strip. The absence of carbonyl absorption bands indicates that no appreciable ozonization takes place.

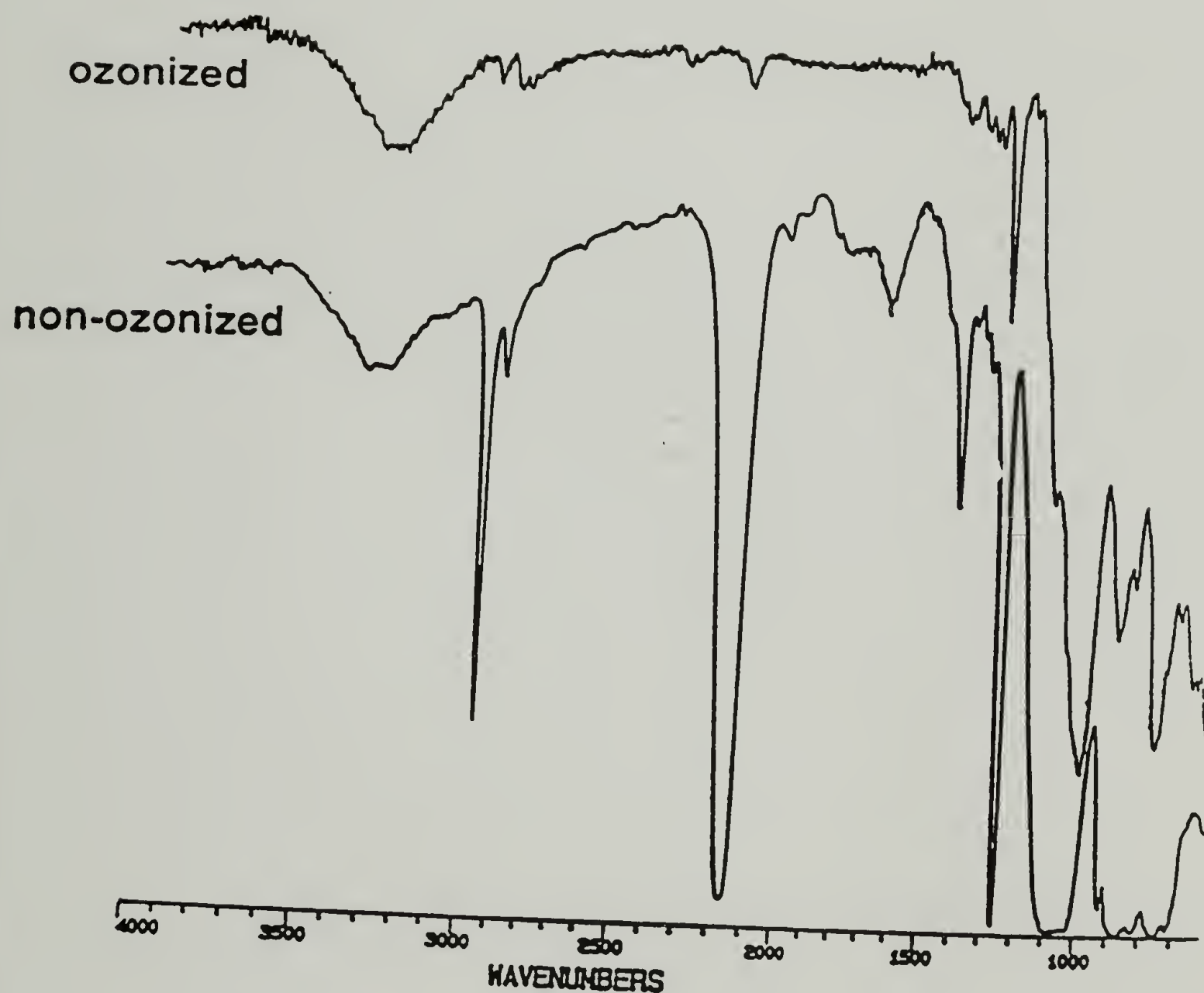


Figure 5.3. The ATR-IR spectra of the 48.1% polymethylhydrosiloxane-impregnated paper sample, before and after ozonization. There is a significant reduction of the characteristic absorption band at 2168 cm^{-1} due to Si-H. There is also a notable reduction of the absorption bands at 2969 cm^{-1} , 1428 cm^{-1} and 1271 cm^{-1} due to $\text{SiHCH}_2\text{-H}$.

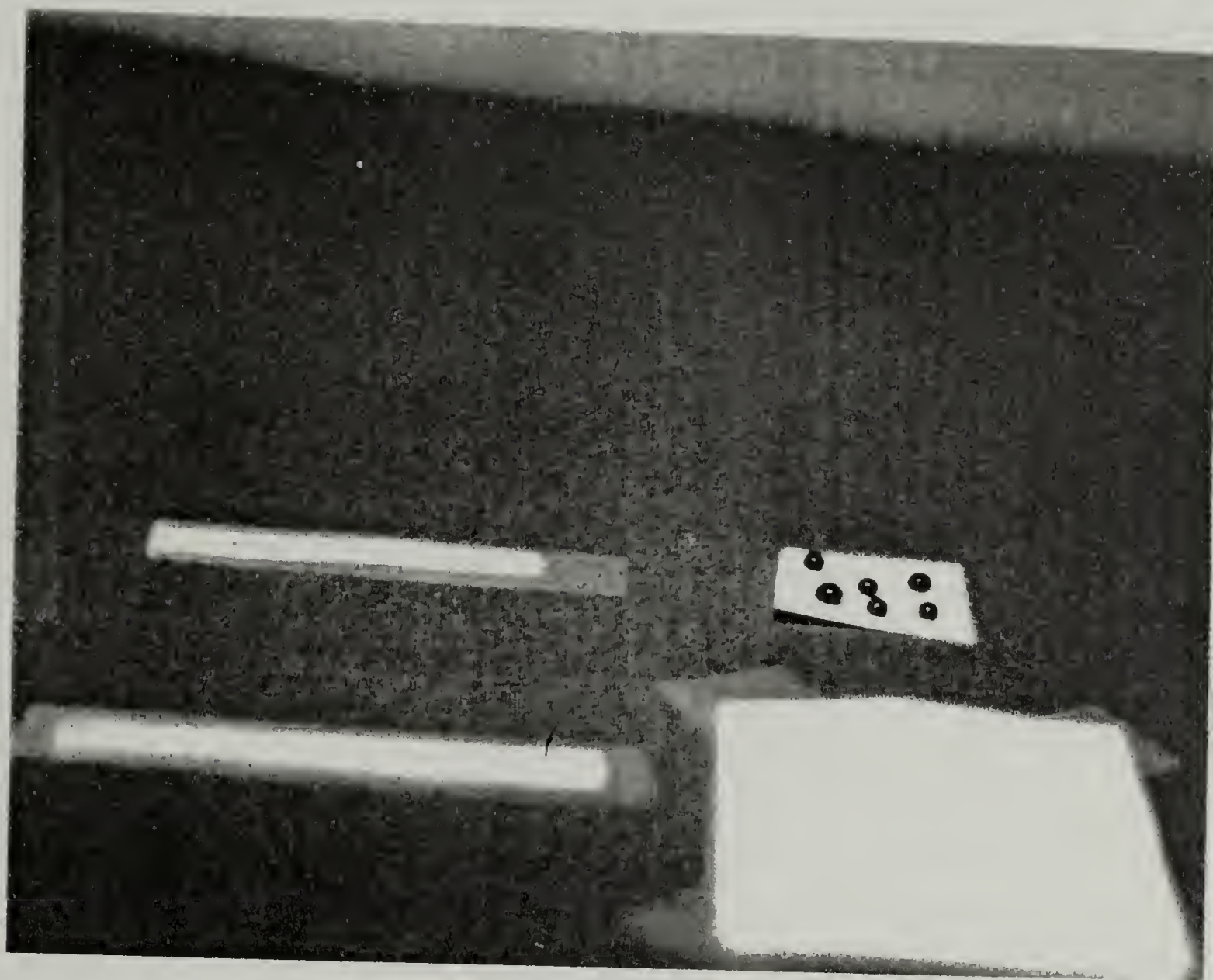


Figure 5.4. Several drops of water colored with potassium permanganate are placed on the surface of two pieces of paper in order to demonstrate the results obtained from contact angle experiments. The hydrophobic paper is coated with 1% polymethylhydrosiloxane (PMHS).



Figure 5.5. Scanning electron micrographs (SEM) at two different magnifications of pure cellulose paper (control) samples.

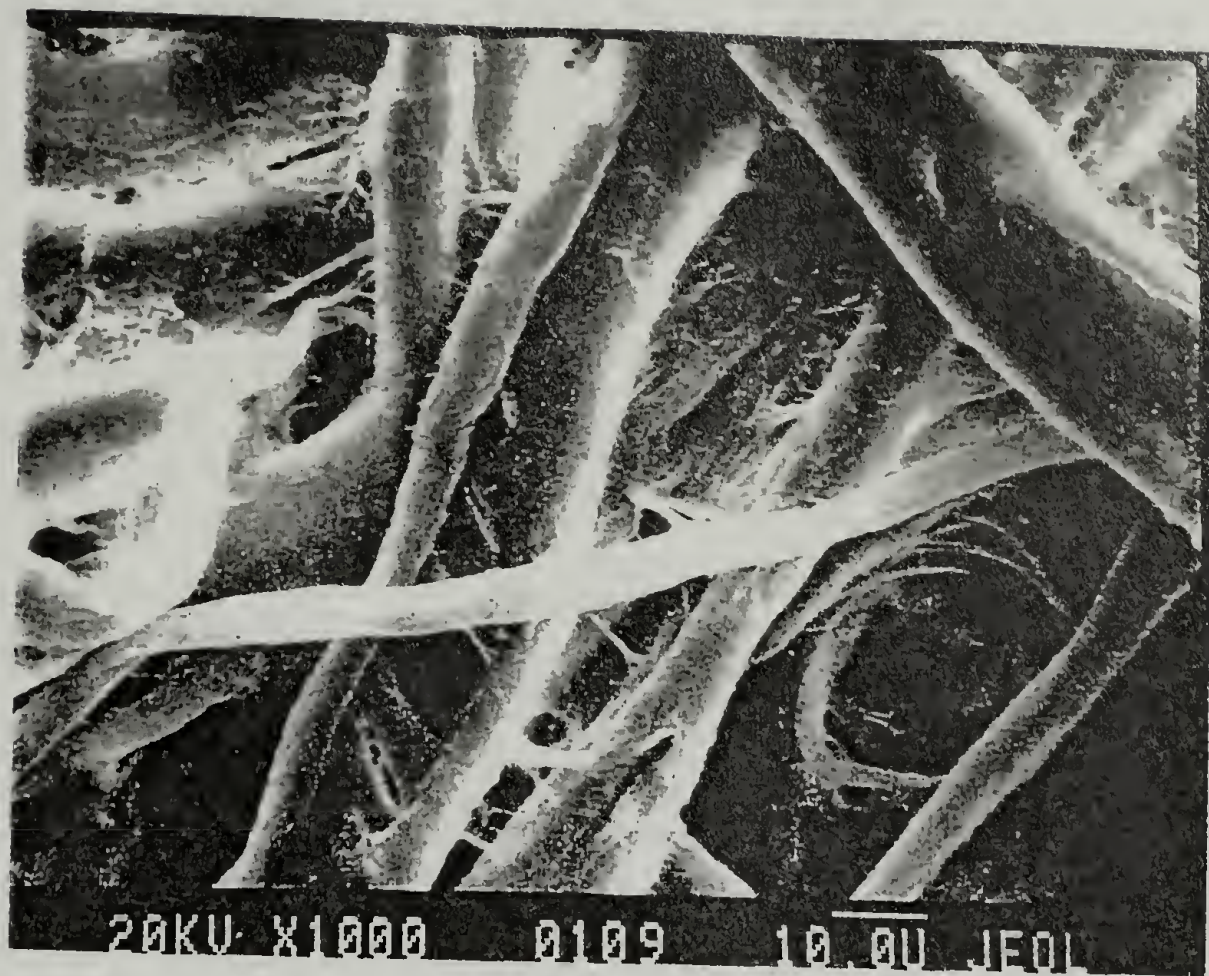


Figure 5.6. Scanning electron micrographs (SEM) of paper samples. The top micrograph is obtained from a control sample while the bottom is taken from the 16.2% PMHS coated paper. It is noticeable, from the bottom micrograph, that the coating does not eliminate the porosity of the filter paper.

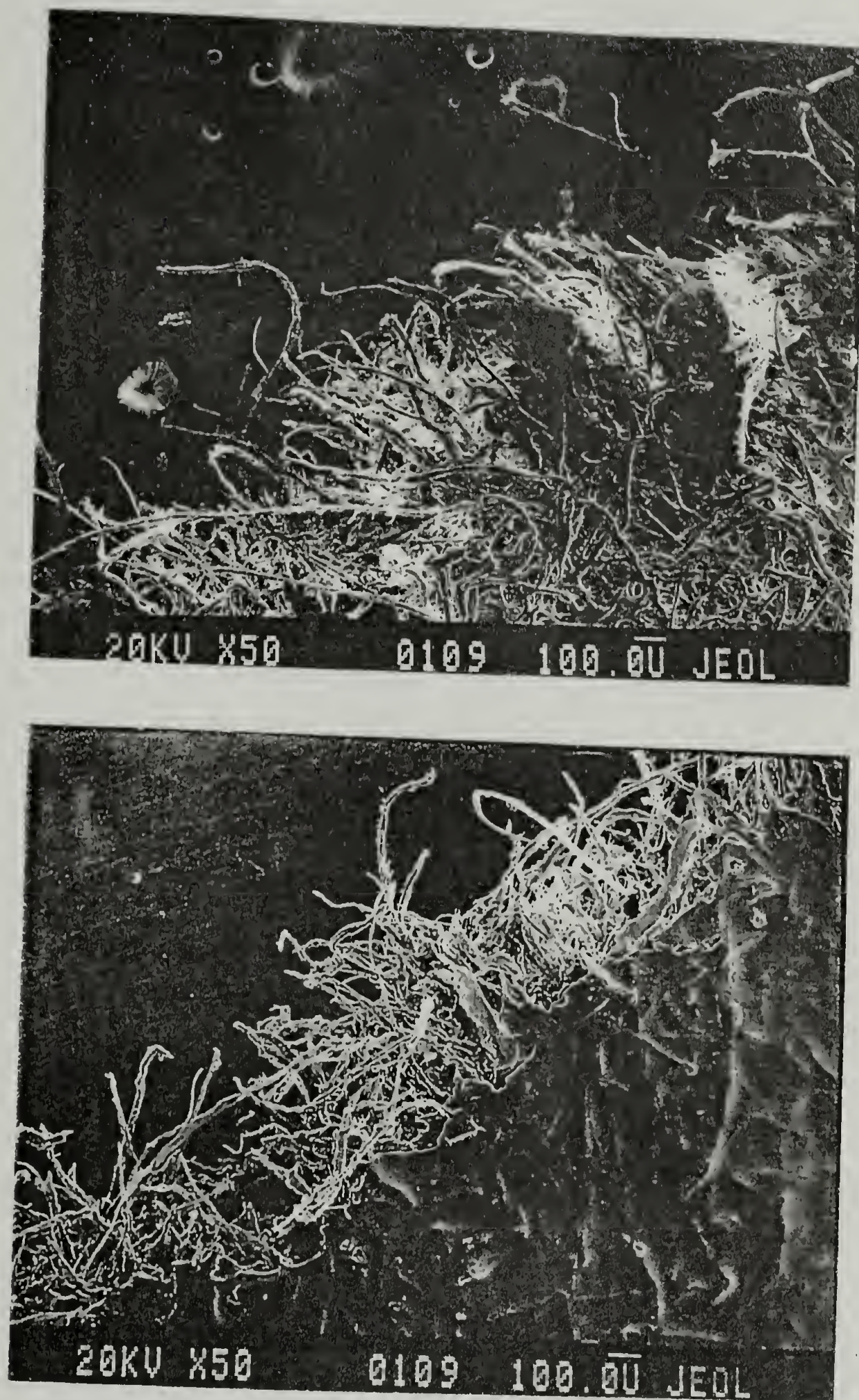


Figure 5.7. Scanning electron micrographs (SEM) of two PMHS coated paper samples. The top micrograph shows the porous surface of the 16.2% coated paper. In contrast, PMHS in the 48.1% sample has formed a continuous coating (sandwich) which completely destroy the surface porosity.

In order to verify the existence of a continuous coating, as opposed to a non-continuous, island-like coating, both TGA and SEM were employed. Different samples (0, 1, 7, 16.7, and 48.1 %) were heated to 800 °C under nitrogen at 10 °C/min. (fig.5.9). In addition, the control sample was heated under air for comparison purposes. Even though the thermal stability does not seem to change as a function of the coating concentration, the residual mass increases as the PMHS concentration increases (table 5.3 and fig. 5.9). The plain cellulose paper (control) leaves a 9% residue when heated under nitrogen (fig. 5.9) and 0% when heated under air (fig. 5.8). This is an indication of an incomplete pyrolysis when the sample is heated under nitrogen.

The residue (black color) left when the samples were heated under nitrogen is obviously either due to substrate (control sample) or due to both substrate and coating (coated samples). The Scanning electron micrographs depicted in fig. 5.10 show the degraded substrate (control sample). The “ghosts” of the cellulose fibers are depicted in two different magnifications. The micrographs in fig. 5.11 show the degraded 16.7 % sample. These micrographs revealed two important findings: First, no regions of coating-formed islands were observed and second, a number of fibers that have burst open are visible. These observations indicate that PMHS creates a homogeneous coating around the individual fibers. The fact that burst fibers were found can be attributed to the continuity of the coating. If the PMHS indeed forms coating cylinders around the cellulose fibers, then the large amount of gasses formed during the cellulose degradation caused the coating to burst as the gasses force their way out through the walls of cylinder forming coating.

In addition, it is shown in fig. 5.8 that no residue was left when the substrate was heated under air. In order to verify the observations made during incomplete pyrolysis, the 16.7 % sample was heated under air to 800 °C. In this case the substrate was completely vaporized and all the solid (white color) residue was due to the coating. The micrograph shown in the bottom of fig. 5.12 shows the “footprints” of the completely pyrolyzed cellulose fibers. The top micrograph is taken from an unreacted non-heated control sample and is shown only for comparison.

After it was confirmed that PMHS can form a coating, questions about the thickness (thick or thin coating) and thickness control had to be answered. In order to answer these type of questions X-ray photoelectron spectroscopy (XPS) was employed. Representative low resolution XPS spectra of a control and a coated sample are shown in fig.5.13. The spectrum of the 0.2% coated sample shows the appearance of the two silicone peaks (Si_{2p} at 103 eV and Si_{2s} at 153 eV). The peak at ~300 eV is due to carbon (C_{1s}), the peak due to oxygen (O_{1s}) appears at 534 eV and the high binding energy peaks (around 740 and 760 eV) are Auger lines. The carbon (C_{1s}) peak around 300 eV shows high sensitivity to the surrounding electronic environment. The more electronegative the element bonded to carbon, the higher the binding energy of the carbon (C_{1s}) peak. Therefore, it was expected that the peak due to carbon bonded to Si would appear at lower binding energy than the carbon bonded to oxygen. In addition, the highest binding energy carbon (C_{1s}) peak was expected to be due to carbon bonded to two oxygen atoms.

Table 5.3. Relationship of coating concentration with residue left after degradation of paper samples under nitrogen. R_{mS} is the (%) residue found from the different coated samples. R_{mC} is the (%) residue due to control non ozonized sample. The residual masses were estimated at a temperature of 780 °C.

Sample [%] PMHS	Residual mass (% w/w)	$\Delta Rm=R_{mS}-R_{mC}$
0 (non-ozonized)	9.1	0
0 (ozonized)	9.0	0.1
1	9.8	0.7
7	14.1	5
16.7	23.6	14.5
48.1	42.0	32.9

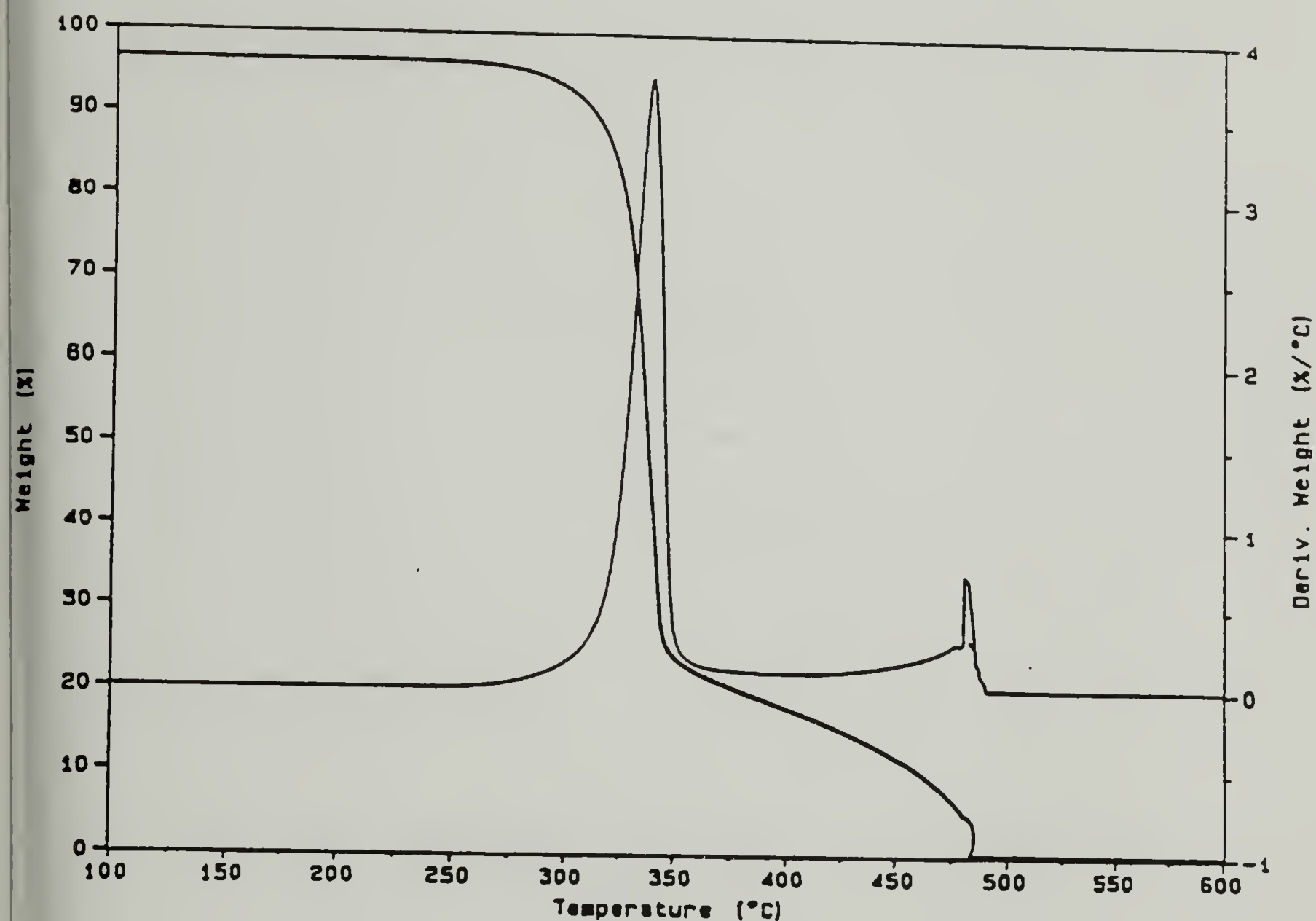


Figure 5.8. A TGA thermogram of a control (non-coated) sample. The sample was heated under air to 800 °C at a rate of 10 °C/ min. The first degradation started at 266 °C and the second at 358 °C. There is no residue left at the end of the second degradation (490 °C).

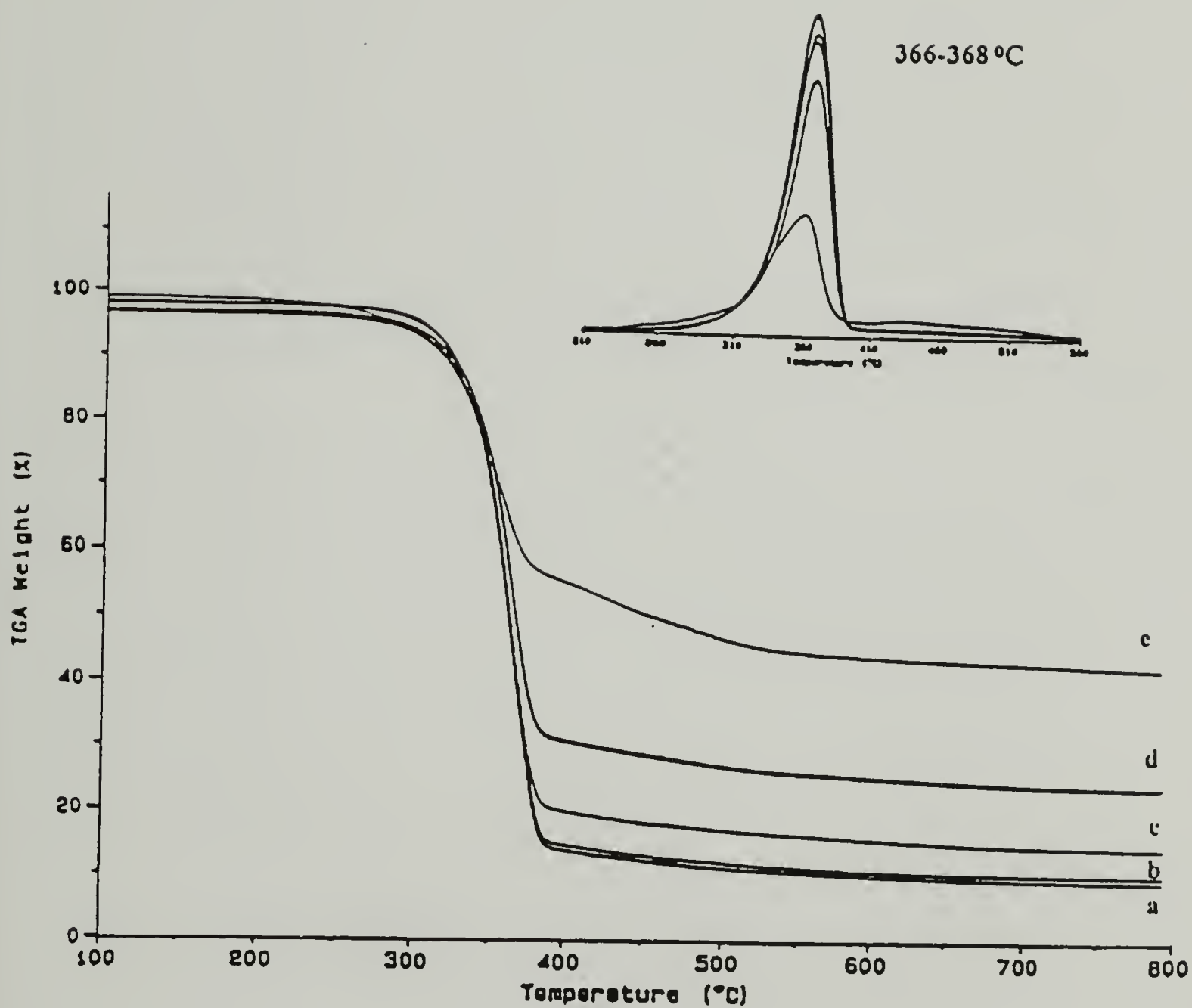


Figure 5.9. A series of TGA thermograms of several samples heated under N_2 at $10^\circ C/min$; a: is the control non-ozonized sample , b: the 1%, c: the 7%, d: the 16.7%, e: the 48.1% PMHS-coated sample. The differential thermogram at the top indicates that coating does not affect the thermal stability of the substrate.

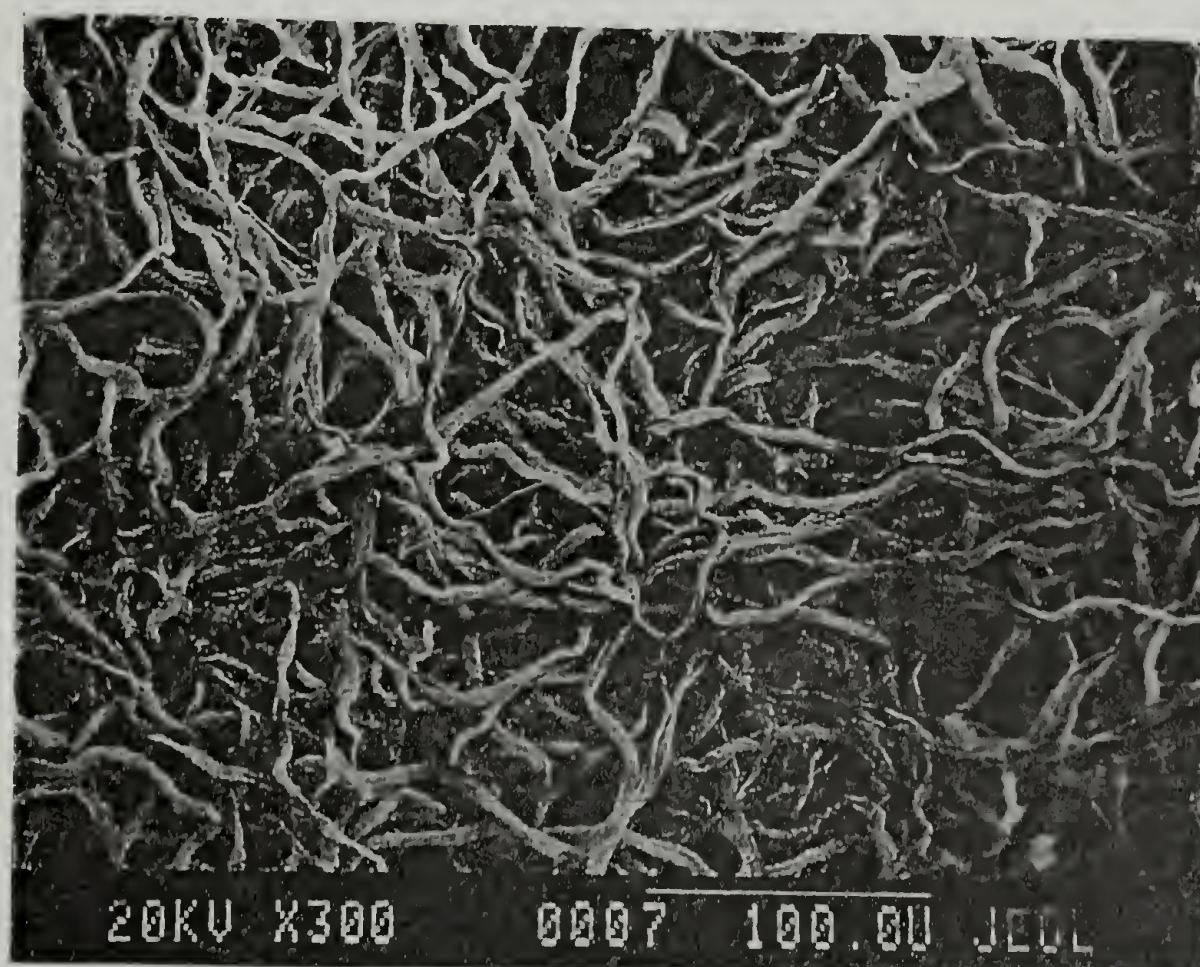


Figure 5.10. Scanning electron micrographs (SEM) at two different magnifications of a control (non-coated) sample heated under N_2 to $800\text{ }^{\circ}\text{C}$ at $10\text{ }^{\circ}\text{C}/\text{min}$. The residue left in a fiber form is a result of incomplete pyrolysis.

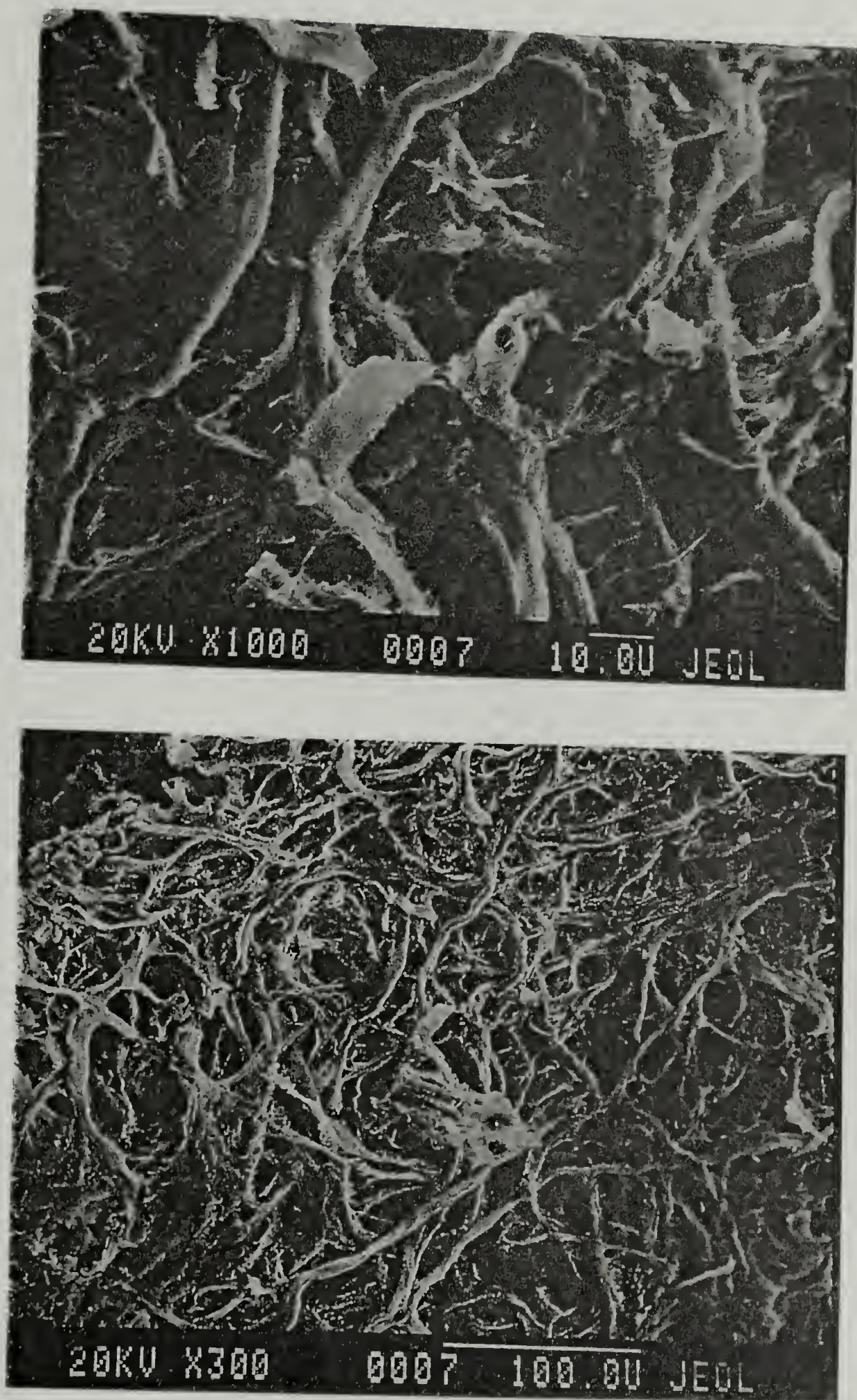


Figure 5.11. Scanning electron micrographs (SEM) at two different magnifications of the 16.7% PMHS-coated sample heated under N₂ at 10 °C/min.

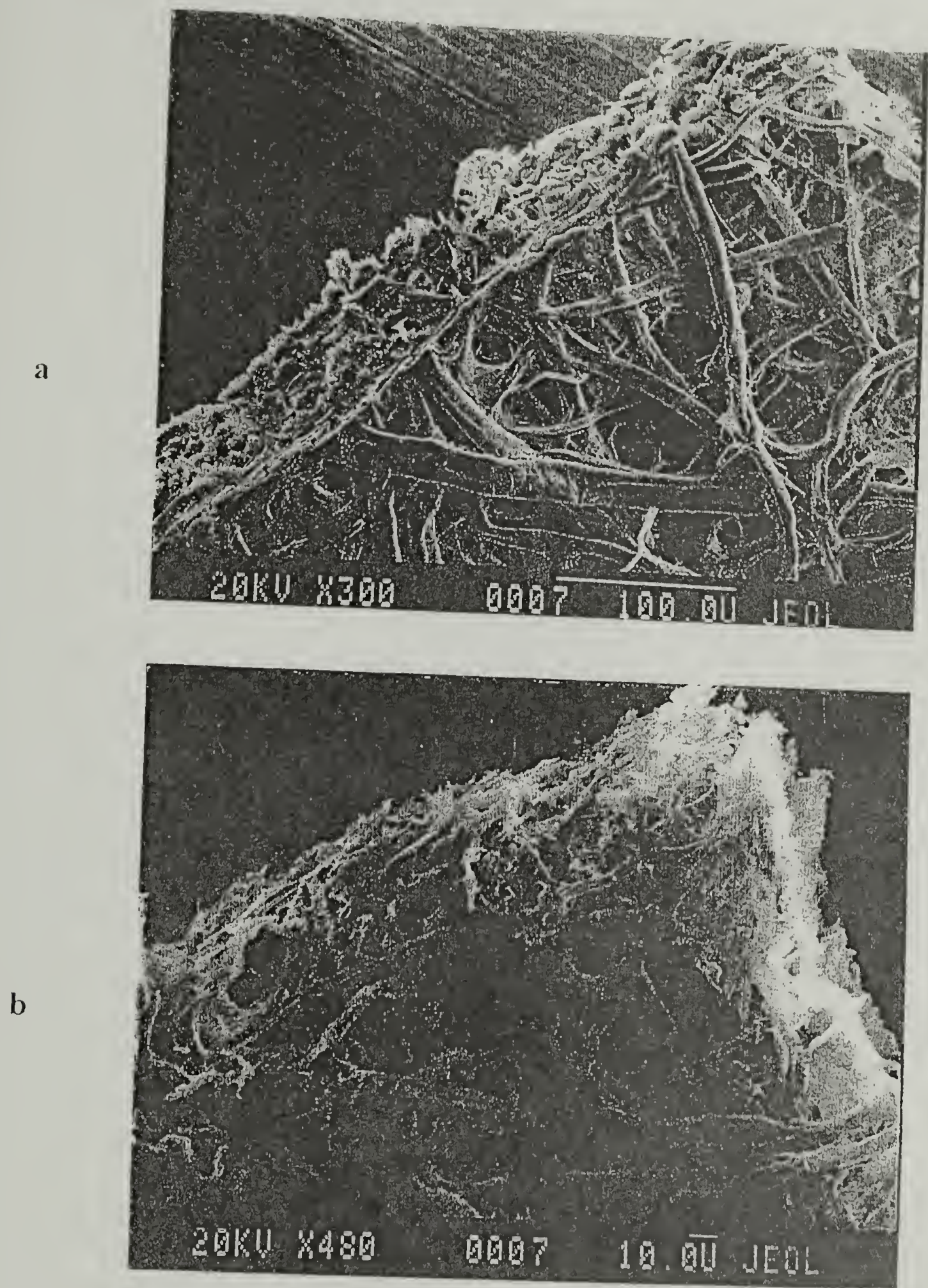


Figure 5.12. Scanning electron micrographs (SEM) of two different paper samples, a: non-heated control sample, 16.7% coated sample heated under air to 800 °C at 10 °C/min. The residue is due only to the coating and appears as the footprints of the pyrolyzed cellulose fibers.

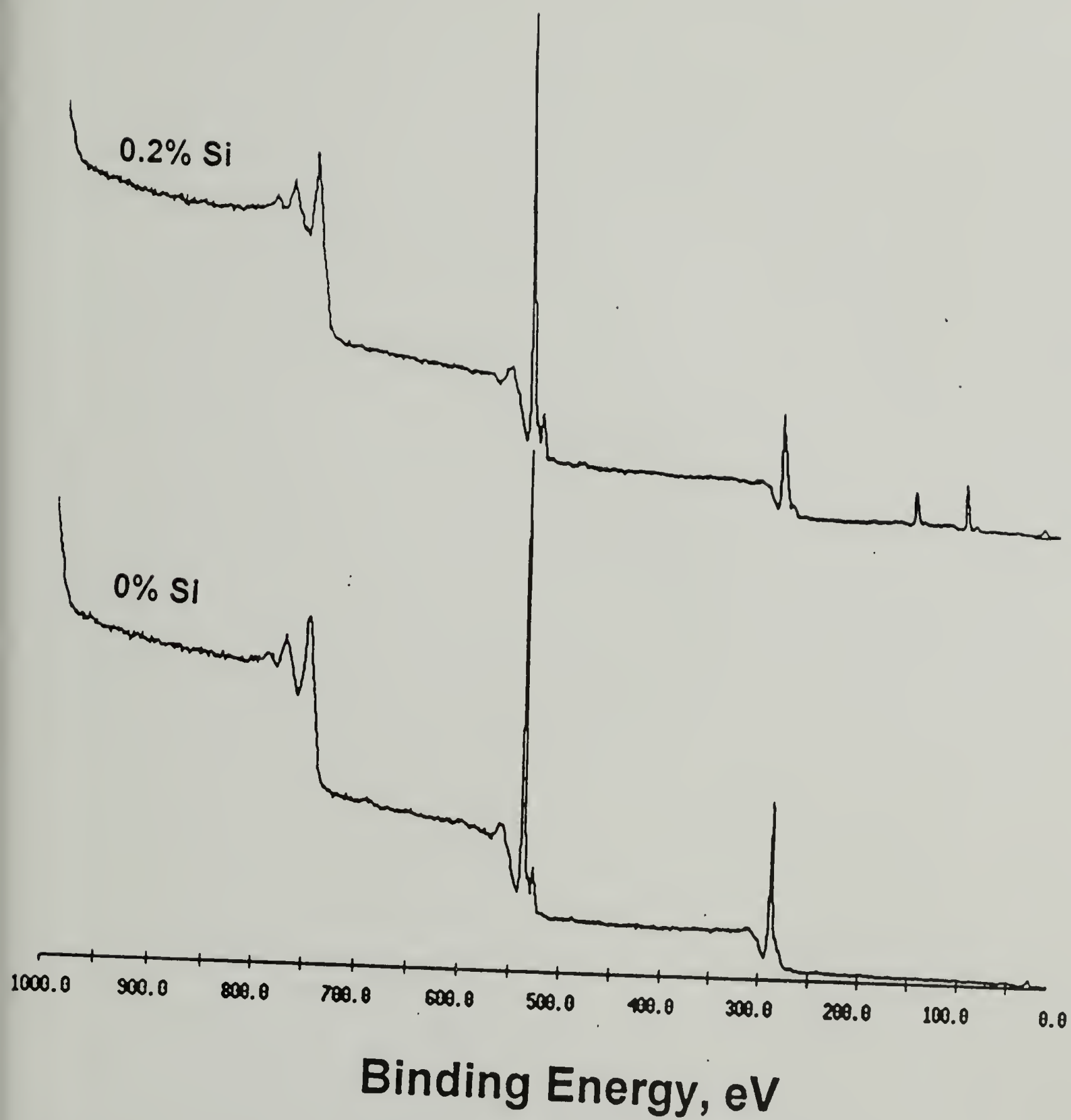


Figure 5.13. Low resolution X-ray photoelectron (XPS) spectra obtained from a control (top) and the 0.2 % PMHS coated sample.

Figures 5.14 and 5.15 depict a series of high resolution XPS spectra of different paper samples taken at 75°. The control sample shows one broad carbon (C_{1s}) peak at 289 eV due to C-O and O-C-O. The coated samples, on the other hand, show an additional carbon (C_{1s}) peak at 286 eV due to C-Si. This peak increases as the concentration of the coating increases. When the coating concentration reaches 7 % the peaks due to substrate at 289 eV disappear. This means that over this coating concentration the substrate stops being detectable by XPS. Deconvoluted high resolution XPS spectra are shown in fig. 5.16. XPS data presented here suggest that it is possible to form thin silicone coatings for paper. In addition, the thickness can be controlled by increasing the coating concentration.

Thermomechanical (TMA) data showed that the silicone coating does have some effect on the dimensional stability of the paper samples, however, this effect does not seem to be large (compare table 5.4 with table 5.5). The dimensional stability of the different samples was determined from the linear coefficient of thermal expansion (LCTE). The LCTEs were calculated from the following equation:

$$\alpha = \frac{\Delta L \times K}{\Delta T \times L}$$

α = coefficient of thermal expansion ($\mu\text{m}/\text{m} \cdot ^\circ\text{C}$)

L = sample length (m)

ΔL = change in sample length (μm)

ΔT = temperature change ($^\circ\text{C}$)

K = cell constant

Therefore, LCTE is calculated from the slope of a plot of dimensional change vs. temperature. A representative TMA plot is shown in fig. 5.17. The LCTE is calculated from the second heating cycle. The LCTE values obtained are reported on table 5.4 and they are plotted against PMHS (%), fig. 5.18. It was mentioned earlier that paper samples were cut in different directions in order to determine the machine direction. The tensile properties obtained from three different directions (including the machine direction) are reported on table 5.6. The direction with the highest modulus and strength ($E = 1.8 \text{ GPa}$, $\sigma = 17 \text{ MPa}$) was determined to be the machine direction [25, 26].

Table 5.4. Increase of linear coefficient of thermal expansion (LCTE) as a function of coating concentration for paper samples.

PMHS (%)	LCTE, α ($\mu\text{m}/\text{m} \cdot ^\circ\text{C}$)
0	6.2
0.2	6.2
1.7	6.6
5.7	9.8
16.2	10.2
48.1	13.3

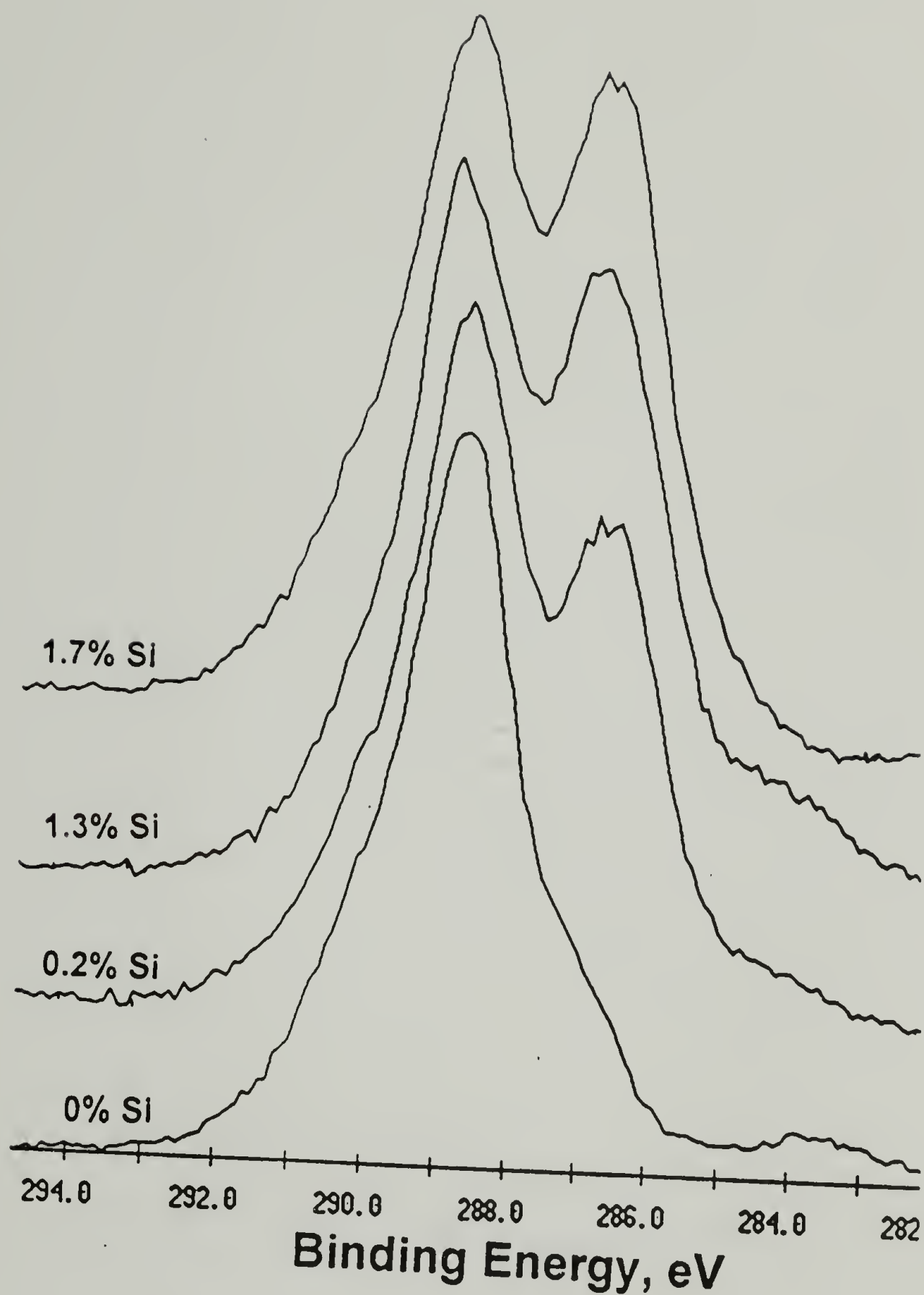


Figure 5.14. High resolution X-ray photoelectron spectra (XPS) obtained from a series of samples. The high binding energy carbon (C_{1s}) peak at 289 eV is due to substrate C-O and O-C-O. The lower binding energy carbon (C_{1s}) peak at 286 eV is due to coating (Si-C). The intensity of the Si-C peak increases as the concentration of the coating increases.

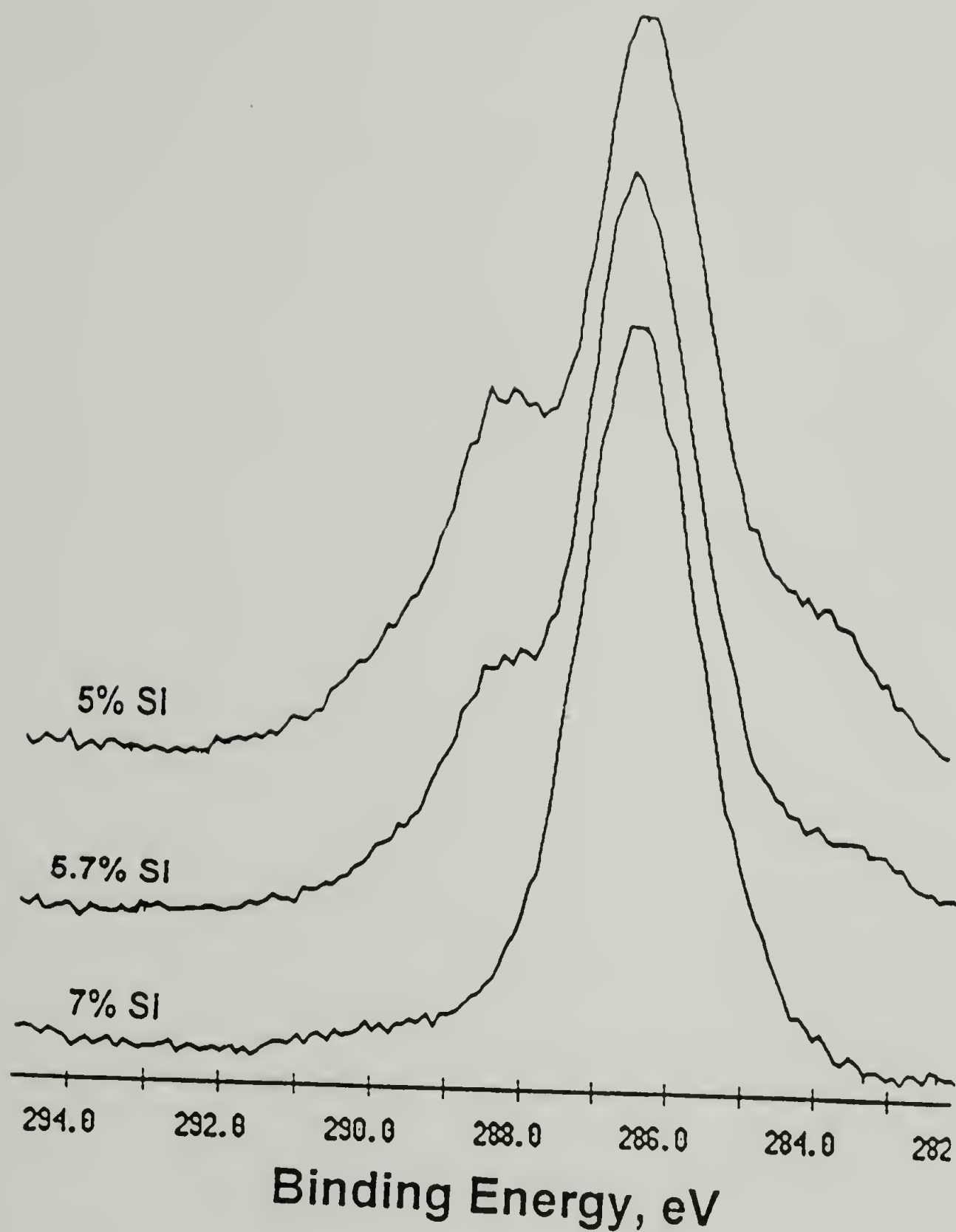


Figure 5.15. High resolution X-ray photoelectron spectra (XPS) obtained from a series of highly coated samples. The high binding energy carbon (C_{1s}) peak at 289 eV due to substrate vanishes above 5.7% PMHS. Only the carbon peak (C_{1s}) at 286 eV (Si-C) due to coating is detected.

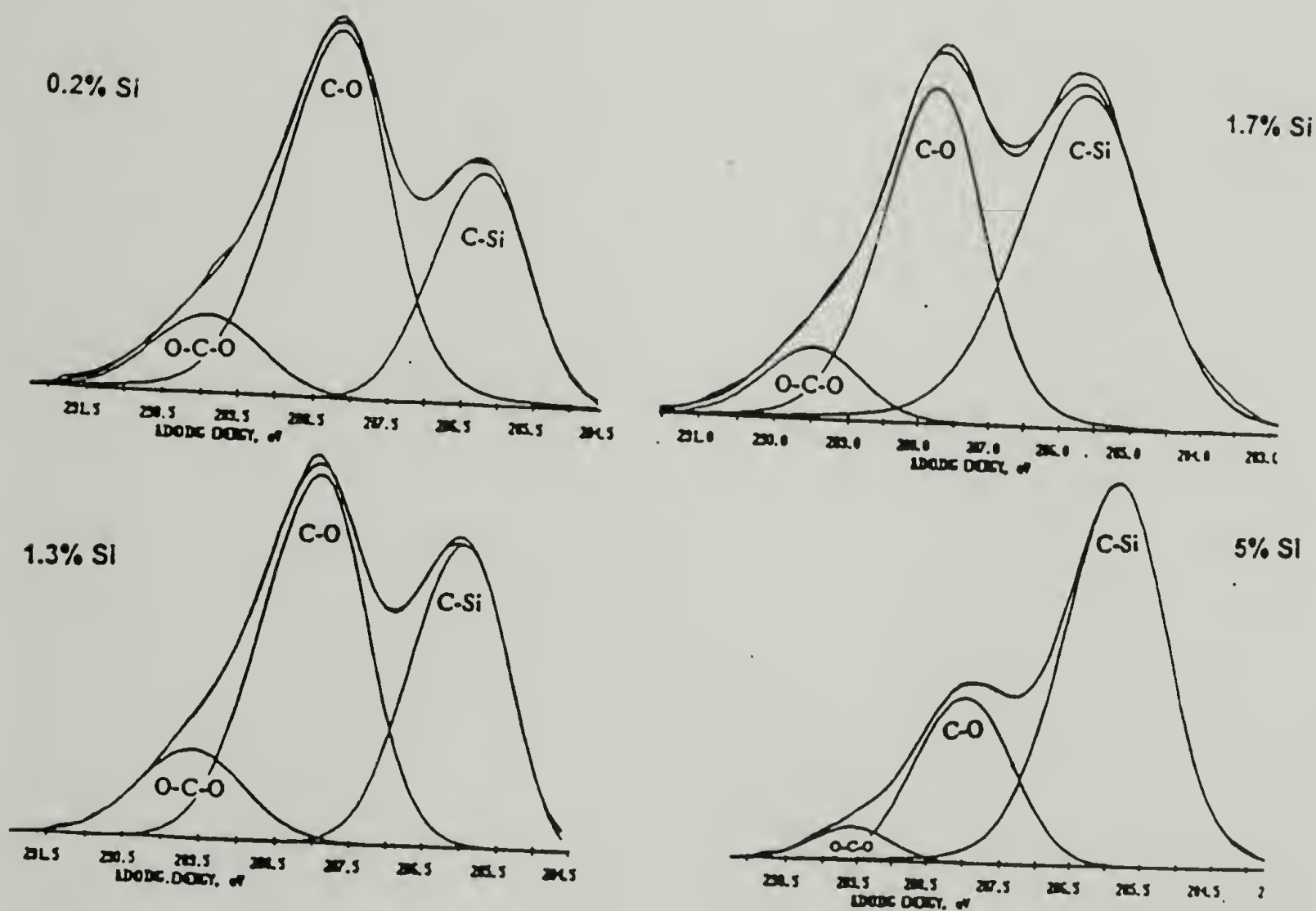


Figure 5.16. Deconvoluted high resolution X-ray photoelectron spectra (XPS) obtained from a series of coated samples.

Table 5.5. Linear coefficient of thermal expansion (LCTE) for selected polymers.

Polymer	LCTE, α ($\mu\text{m}/\text{m}^{\circ}\text{C}$)
polyethylene	100-130
polypropylene	105-145
PVC	70 ($< T_g$), 170 ($> T_g$)
PMMA	60-80 ($< T_g$)
nylon 66	70-100
polyimide	30
PET	16

A large difference between dry and wet properties were observed for the control (non coated) samples. The wet modulus and ultimate strength, in the machine direction, showed ~96 % reduction of the dry values.

It has been reported in the literature [27] that normal or untreated papers have a wet strength which is usually less than 10 % of the dry strength. The wet strength of paper which has been treated to enhance this property usually falls in the range of 20 - 40% of the dry strength. It has been stated that papers which show a wet strength greater than 15% of the dry strength may properly be considered to be wet-strength paper [28].

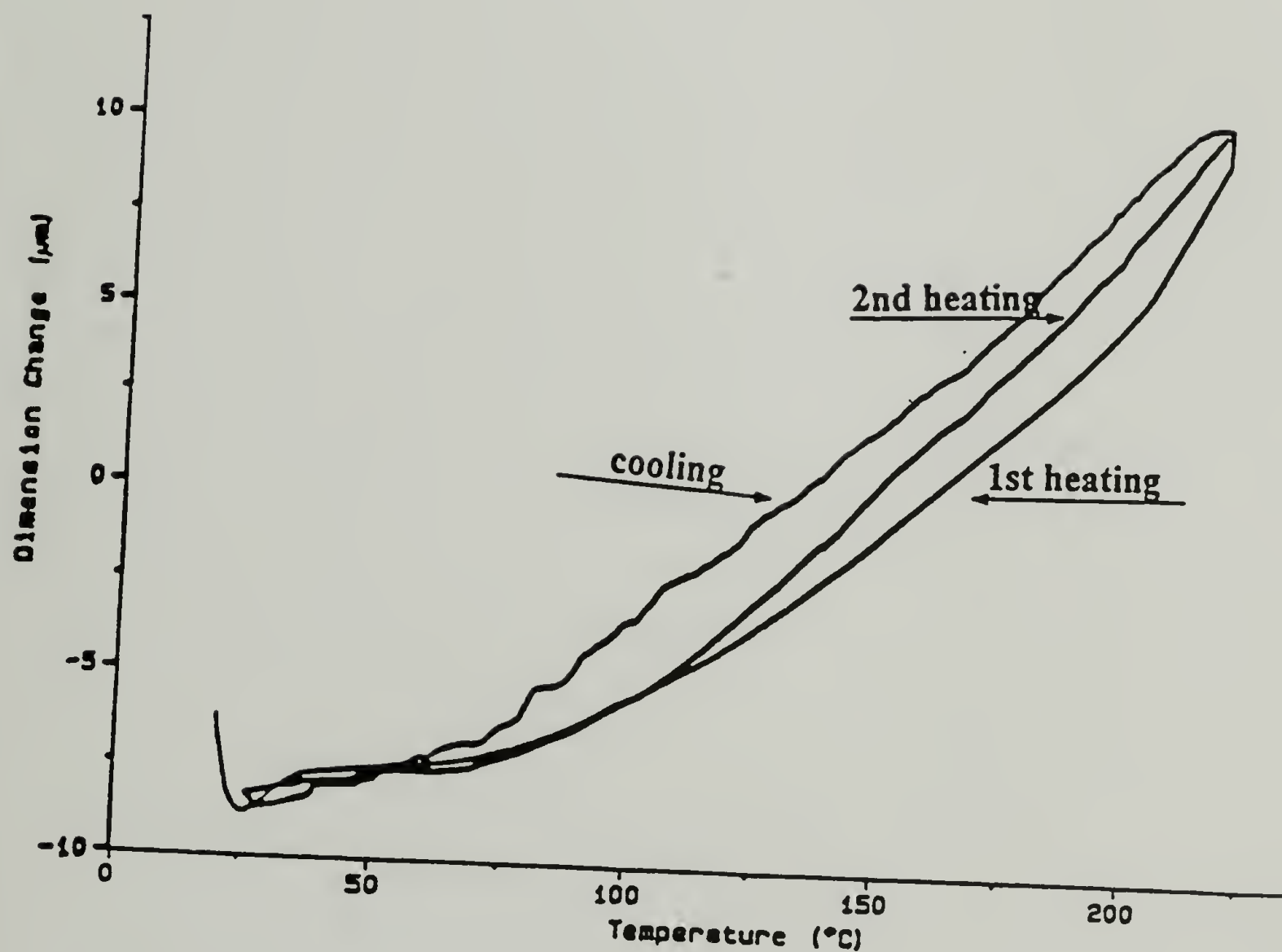


Figure 5.17. Typical thermomechanical analysis plot of dimensional change vs. temperature. The linear coefficient of thermal expansion (LCTE) can be calculated from the slope of the second heating.

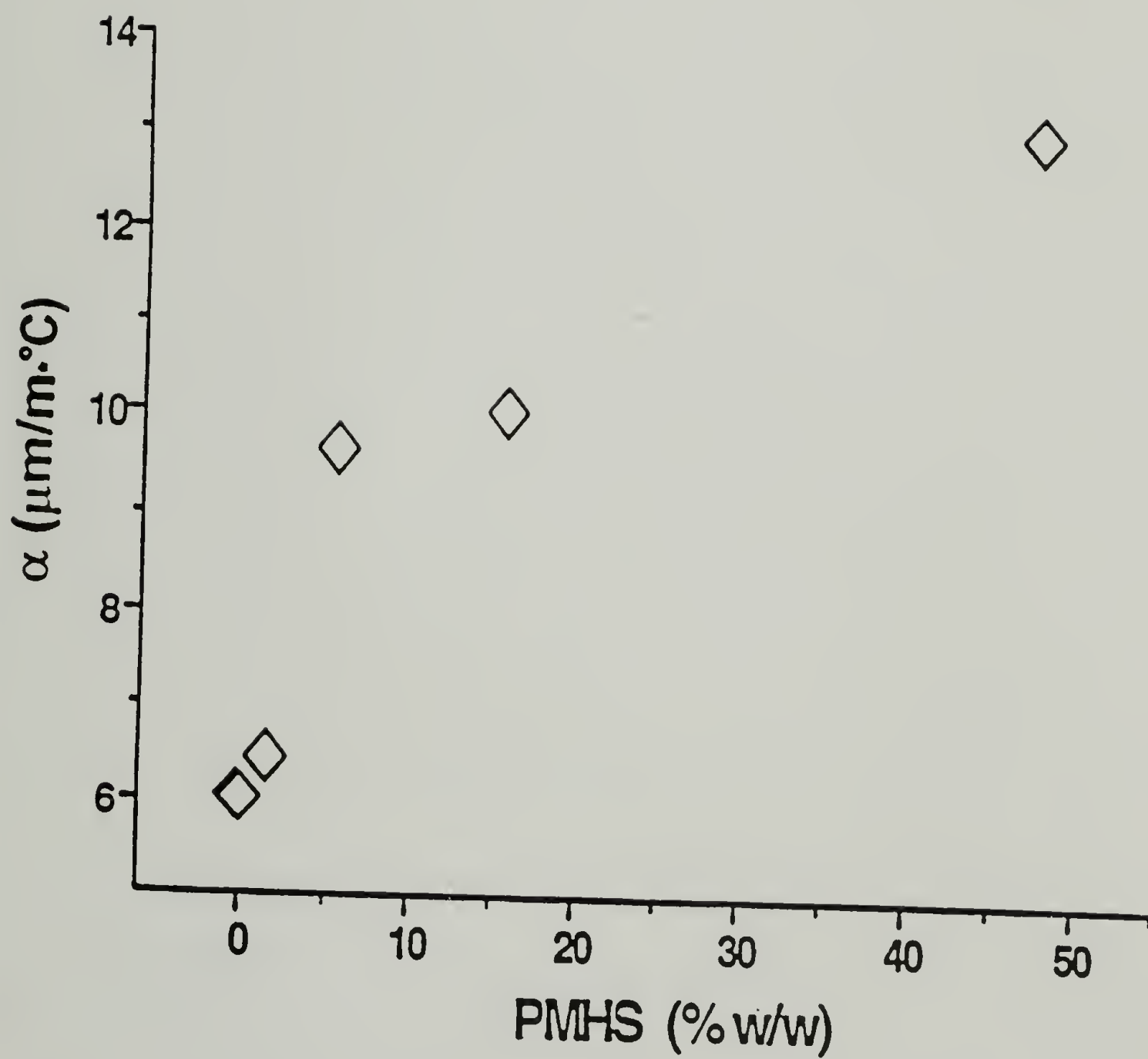


Figure 5.18. Plot of linear coefficient of thermal expansion (LCTE) as a function of PMHS (%) concentration.

Table 5.6. Dry and wet tensile properties of non-coated samples (control) cut in three different (including the two principal) directions.

Sample direction, (angle)	Modulus [GPa]	Ultimate stress		Maximum. strain	
	dry, (wet)	[MPa]	dry, (wet)	[%]	dry, (wet)
0° (machine)	1.8, (0.09)	17, (0.7)		3.4, (3.9)	
45°	1.4	11		3.6	
90°	1.3, (0.4)	11, (0.4)		5.1, (4.7)	

The results obtained from testing the paper coated with silicone are reported on table 5.7. The effect of the coating on the wet properties of paper is immediately realized even for the minimum coating concentration. The 0.4 % sample has wet-strength 4.1 MPa and wet modulus 0.4 GPa. This is the 28 % of the dry strength (14.5 MPa) and 23 % of the dry modulus (1.7 GPa). The significant improvement of the wet strength and modulus continuous up to 44 % and 50 % of the dry properties for the 16.7 % sample. The properties of the 48.1 % sample were not determined due to the fact that it presented completely different surface characteristics.

Table 5.7. The dry and wet tensile properties of papers coated with different concentration of PMHS polymer.

Sample, (%) PMHS	Modulus E [GPa]		Ultimate stress σ [MPa]		[%] Strain to load at break		Retention of the dry properties	
	Dry	Wet	Dry	Wet	Dry	Wet	E [%]	σ [%]
0	1.8	0.09	17	0.7	3.4	3.9	5	4
0.4	1.7	0.4	14.5	4.1	3.8	3.0	28	23
1.3	1.9	.5	14.8	4.6	3.4	3.6	26	31
5.7	2.1	.7	18.5	6.1	2.9	4.1	33	33
16.7	2.2	1.1	26.6	11.5	3.1	5.2	50	43

5.4 Conclusions

In an effort to produce papers with special properties, filter paper strips were impregnated with polymethylhydrosiloxane (PMHS) solution of various concentrations (0.2-48.1 %). The impregnated samples were allowed to react for sufficient time (3 1/2 hr) for extensive ozonization to take place. The control (non-coated) samples showed no ozonization induced changes by ATR-IR.

Contact angle data showed that even a small amount of coating (0.2 %) was able to dramatically alter the surface polarity of the filter paper. New hydrophobic surfaces

were created and scanning electron microscopy revealed that these surfaces were remained porous. The only exception was the 48.1 % sample; because of the high silicone concentration, a continuous film was formed on the surface. Evidence was found from scanning electron microscopy (SEM) and thermogravimetric analysis (TGA) that a cylindrical coating around the fibers was formed instead of small island regions.

X-ray photoelectron spectroscopy (XPS) data showed that thin coating could result if low coating concentrations were used and that thickness could be controlled by changing the coating concentration.

TGA data indicated that PMHS coating did not affect the thermal stability of the substrate paper. Thermomechanical (TMA) data showed that coating had only a small effect on the linear thermal expansion coefficient (from 6.2 ppm for the plain paper to 13.3 ppm for the 48.1 %). The most dramatic effect of the oxidized silicone coating was realized from the mechanical data obtained. The wet strength increased from 4 % for the plain paper up to 43 % for the 48.1 % sample. The wet modulus followed the same trend (from 5 % up to 50 %). These properties can classify this coated paper as a very high wet strength paper.

REFERENCES

1. Johnson, K., "Paper Coatings Based on Polymers," Noyes Data Corporation Park Ridge, N. J. 1971.
2. Rogers, C. E., "Surfaces and Coatings Related to Paper and Wood," Eds: R. H. Marchessault, C. Skaar, Syracuse University Press 1967 p. 463.
3. Ward, K. Jr., "Chemical Modification of Papermaking Fibers," Marcel Dekker, Inc., New York N. Y., 1973.
4. Ward, K. Jr., "Chemical Modification of Papermaking Fibers," Marcel Dekker, Inc., New York N. Y., 1973 p. 5.
5. Shcwab, E., V. Stannett, D. H. Rakowitz, and J. N. Magrane, Tappi, 45, 390 (1962).
6. Daniel, J. H. Jr., S. T. Moore, and N. R. Sergio, Tappi, 45, 53 (1962).
7. Zosim, Z. L., N. I. Levi, S. S. Gusev, and I. N. Ermolenko, Bumazh. Prom, no. 12 p. 11, 1966.
8. Lynch, L. W., Tappi, 46, 480 (1963).
9. Conte, J. S., and R. W. Faessinger (to Scott Paper Co.), U. S. Pat. 3, 505, 257 (1970).
10. Kulagina, T. G., M. A. Askarov, and S. D. Savranskaya, Uzbek. Khim. Zh. 10, 34 (1966).
11. Richards, G. N., and E. F. T. White, J. Polym. Sci., C-4, 1251.
12. Wilkins, C. W., U. S. Pat. 3, 162, 543, 1964.
13. Johnson, K., "Paper Coatings Based on Polymers," Noyes Data Corporation Park Ridge, N. J. 1971 p. 236.
14. Atkinson, H. C., and R. M. Gibbon U. S. Patent 3, 565, 838 (Imperial Chemical Industries Ltd.), England, 1971.
15. Leavitt, H. J., U. S. Pat. 3, 004, 871 (GE Co.), 1961.
16. Quaal, G. J., U. S. Pat. 3, 419, 423 (Dow Corning), 1968.

17. Curry, J. W., U. S. Pat. 3, 538, 049 (Texas Instruments), 1970.
18. Shcuyten, H. A., J. F. Jurgens, Paper presented in Southwestern Regional Meeting, Houston Texas, 1947.
19. Virts, J. K., PhD Dissertation, Polymer Science & Engineering, University of Massachusettes, Amherst MA 1995 p. 42.
20. "Standard Test Method of Conditioning Paper and Paper Products for Testing," ASTM Designation: D685, American Society for Testing and Materials, Philadelphia, PA (1986).
21. Galimova, L. G., V. D. Komissarov, and E. T. Denisov, Bull. Acad. Sci. USSR, Div. Chem. Sci. (Engl. Tranl.) p. 295 (1973).
22. Razumovskii, S. D., and G. E. Zaaikov, Neftekhimiya 13, 565 (1973).
23. Whiting, M. C., A. J. N. Belt, and J. H. Parish, Adv. Chem Ser. 77, 4 (1968).
24. Pollart, K. A., and R. E. Miller, J. Org. Chem. 27, 2392 (1962).
25. "Standard Test Method for Tensile Breaking Strength of Paper and Paperboard," ASTM Designation: D828, American Society for Testing and Materials, Philadelphia PA (1986).
26. "Wet Tensile Breaking Strength of Paper and Paperboard," TAPPI designation: T456, Technical Association of the Pulp and Paper Industry, Atlanta, Ga (1982).
27. Britt, K. W., J. E. Donahue, R. P. Goodale, I. J. Gruntfest, L. E. Kelley, C. S. Maxwell, and J. P. Weidner, "Wet Strength in Paper and Paperboard," Tappi monograph series-No. 13, Technical Association of the Pulp and Paper Industry, New York N. Y. (1954) ch. 1, p. 4.
28. Britt, K. W., Paper Ind. 26, No. 1 (1944).

PART II

SYNTHESIS, CHARACTERIZATION AND MECHANICAL PROPERTIES OF POLYSTYRENE-POLYETHERIMIDE ABA BLOCK COPOLYMER

CHAPTER 6

INTRODUCTION

6.1 The major routes for obtaining high performance polymers

Nature has been designing and making high performance polymers (organic and ceramic) for millions of years. The base materials are proteins, carbohydrates and a variety of clays. The properties that had to be brought up to exceptionally high levels of performance were: modulus, tensile strength, toughness, elasticity and durability. The construction principles were: for linear systems (fibers) very high molecular weight, flexible (proteins) or rigid (cellulosic) chains. For planar structures (membranes, leaves, skin) the principles were plied and crosslinked layers.

The demanding requirements of modern industry have necessitated the development of new materials for high mechanical performance. It has been long recognized that the theoretical tensile modulus of a polymer chain should approach the modulus of steel. However, it is recognized that the polymer chain assumes folded, entangled and twisted configuration with low load bearing capacity [1-3]. Although the observed strengths and moduli of the commercially available fibers are still lower than the theoretical estimates (table 6.1) it is encouraging to note that with the gradual

Table 6.1. Comparison between the theoretical and actual values of elastic moduli for selected polymers [4,5,8]

Polymer	E_{actual} [GPa]	E_{theor} [GPa]
Polyvinyl alcohol	30	200-250
Polyester (PET)	20	120-150
Nylon-6	6	170-270
Polypropylene	12	35-49
Polyethylene*	220	250-300
Carbon	140-820	~1000
PPTA (kevlar 49)	130	~200

* Single crystal, draw ratio about 250x [2, 10]

elimination of performance-limiting structural defects, the actual tensile parameters of some fibers now approach the theoretical values.

It was realized that the greatest strength arises from the elimination of chain folding in flexible macromolecules and the spinning of rigid chains from liquid crystalline solutions (nematic systems) [6]. The result is a structure which is highly oriented with extended and densely packed chains. In an effort to make high moduli and high strength polymers two main approaches were adopted:

- I. The development of various processing techniques (flexible polymer chains) [8]
- II. The design of different chemical structures (rigid rod-like polymers) [7]

6.1.1 Processing of flexible polymers

Attempts have been made to process polymeric materials in such a way that a permanent deformation of the internal structure may occur. One of the most common methods of changing the structure of a polymer (for strength increase) is by drawing during processing. During drawing, chain orientation parallel to the fiber axis is achieved. The aim of these efforts is to uncoil and extend the polymer backbone in order to achieve high modulus structures. Flexible chains in their relaxed state, without an applied force, can assume many possible conformations and the system is randomly oriented. If, however, a load is applied, the mobility (segmental oscillations and rotations) and the available conformations are restricted. When a force is applied, the distance between the chain ends tends to increase and for extreme loads fully extended chains can be obtained. Furthermore, it is important to realize that the chain is regarded as elastic with very high modulus. It can be proved that [9]

$$\sigma = (NkT/M_0) (l/L) \quad (1)$$

when $l \ll L$ (flexible chains)

σ = stress, N = Avogadro's number, k = Boltzmann's constant, T = absolute temperature,
 l = persistence length, L = contour length

Equation (1) indicates the stress increases as the deformation increases ($l \rightarrow L$), however when the chain approaches full extensibility, the strain decreases and the modulus increases rapidly.

In addition, macroscopically, flexible chains tend to fold during crystallization and consequently, with conventional spinning methods, folded-chain type crystals will be formed. The folded-chain morphology will result during solidification (melt spinning), solvent evaporation (dry spinning) or coagulation (wet spinning) [10]. In order to obtain high modulus structures one has to enhance the fibrous chain-extended content at the expense of the chain folded lamellae. Two principal methods have been identified for chain extension[11]:

- a) Aligning the chains from the random state (solution or melt) and thus enabling them to crystallize in the extended form.
- b) Extending the solid crystalline material, forcing the chains to become fully stretched out.

Method a: Developments in solution and melt extrusion have occurred at almost the same time. First, during the solution extrusion, the polymers form a shish-kebab morphology and it is realized that chain extension is induced by elongation flow and only such flows can lead to ultra-high chain extension of the dissolved macromolecules [12-14]. Flows of this nature are induced with the appropriate jets [15-17] or rollers [17-21]. However, it is also found that “micro shish-kebabs” are present even when the chains have been completely aligned prior to crystallization [22]. The maximum modulus value achieved by this method for polyethylene is about 100 GPa [23].

Moreover, it was realized that oriented extrudates could be obtained from the melt by extruding through a capillary rheometer with a conical die [24-26]. The morphology obtained in this case is two dimensional spherulitic or structural intermediates between parallel platelets (shish-kebabs) and fully twisted ribbons (spherulites) [14]. In the case of melt extrusion, a substantial fraction of the melt remains uncrystallized. Therefore, upon cooling a formation of "macro shish-kebab" structure will occur outside the orifice. Consequently, unless the whole material solidifies under the influence of the flow, low modulus (~ 10 GPa for polyethylene) is obtained [27].

In other developments, polymer extrudates were produced either by crystallizing the polymer melt under combined orientation and pressure effects (hydrostatic extrusion) [28-30] or by solid state co-extrusion and co-extrusion aided by drawing [31, 32]. In hydrostatic extrusion process the pressure is transmitted to the polymer through a pressure transmitting fluid (e.g. ester oil) [33]. Intensive efforts have been devoted to understand several variables affecting these processes (extrusion draw ratio, pressure, molecular weight etc.) [33].

On the other hand, Porter and co-workers [25, 26, 34] have investigated the solid state deformation of semicrystalline polymers. This modification of the extrusion techniques produced transparent fibers with moduli ranging from 30-70 GPa for linear polyethylene. In another development [33], an unprocessable polymer was co-extruded with a processible polymer in a sandwich arrangement. The process is a form of substrate drawing and has been used for the extrusion of films (split billet co-extrusion) and fibers (concentric billet co-extrusion). The split billet co-extrusion approach has been used for the preparation of highly oriented films of polyamides [35], polystyrene [36] and

polyethylene terephthalate [33]. In the concentric billet co-extrusion, ultra-high molecular weight polyethylene was co-extruded within nylon 11 billets. The polyethylene rods exhibited modulus of ~ 15 GPa. [33].

Method b: Extensive research has been directed toward finding ways to transform as-spun structures into chain-extended type crystals via post-drawing techniques, usually in a temperature range close to, but below the melting point. Different investigations have shown that under appropriate draw conditions a wide range of initial products, including those of different molecular weight distribution and those prepared using different crystallization conditions, can be drawn to very high extensions. In addition, early investigators were surprised to discover the ease by which ultra-high draw ratios could yield ultra-high modulus [37]. It was demonstrated, for example, that a sample of polyethylene of sufficiently high draw ratio ($\sim 30\times$) exhibited an ultra-high modulus (70 GPa); this could be readily prepared [37]. It has been observed that the axial elastic modulus of a fibrous material increases as a function of draw ratio, as shown for polyethylene in fig.6.1.

As can be seen, the modulus is a function of the draw ratio for samples of different origin. This indicates that the only criterion for high modulus is the drawability. As long as a sample can be extended by the required amount, no matter how it was achieved, the appropriate modulus is attained [38].

In a more recent development, a combined gel-spinning and subsequent drawing of ultra-high molecular weight polyethylene afforded moduli over 100 GPa [39].

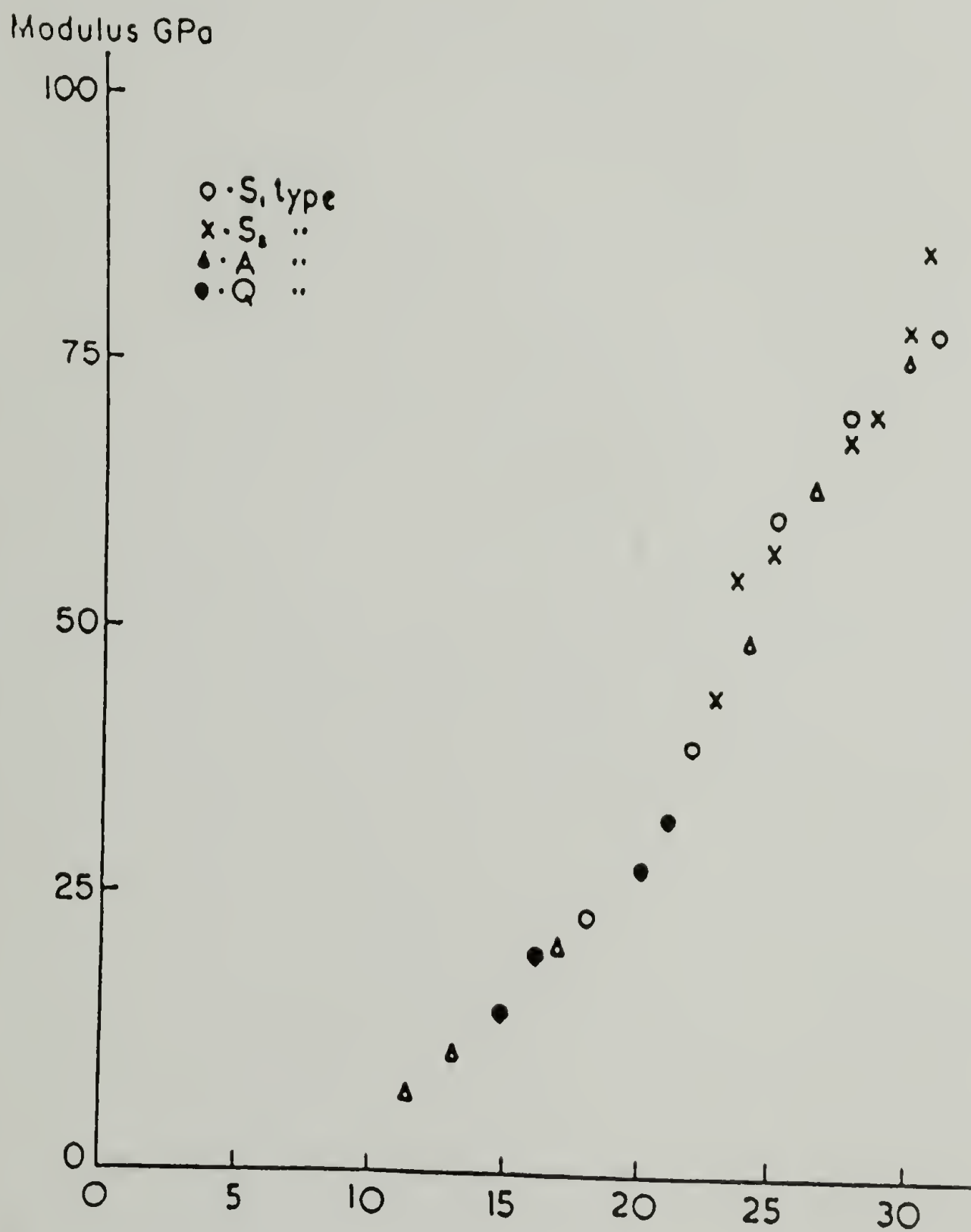


Figure 6.1. Modulus dependence on the draw ratio for drawn polyethylene sheets. The S1, S2, A, and Q are different starting materials [47].

The gel-spinning is said to reduce the chain entanglements (defects) and therefore allow ultra-drawing without breaking the fibers [10]. The tendency of flexible molecules to exhibit a high degree of reversibility of the imposed deformation and the extremely high molecular weight requirements are examples of the limitations of this approach.

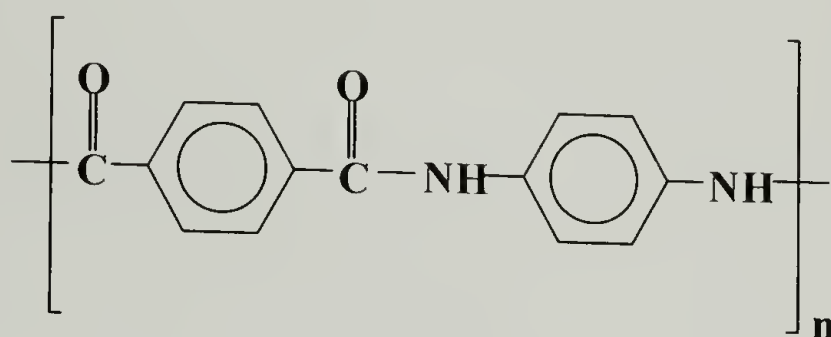
The developed techniques and processes, however good, have been only partly successful as shown in table 6.1. The theoretical moduli and the actual values for the technical yarns indicate a major gap between practical and theoretical limits.

6.1.2 The rigid chains

As was mentioned above, the requirement to obtain high modulus, and high strength structures is the ultimate extension and alignment of the polymer chains. Another approach is the selection of a suitable system capable of forming nematic liquid crystalline phases for subsequent extrusion of highly aligned molecular domains into fibers without the necessity of subsequent conventional drawing. For a polymer to exhibit liquid crystalline character, it is necessary to have a degree of conformational rigidity. This can be achieved by polymerization of rod-like, plate-like monomers (mesogens). Even helical conformation structures can form liquid crystals [40]. The target has been the construction of rigid rod-like polymers containing aromatic rings in the backbone.

Theoretical studies [41, 42] predict that incorporation of rigid or semi-rigid units into the chain backbone will lead to the formation of anisotropic phases in solution or the

melt, depending on the conditions. Examples of really rigid chain molecules are PBT (poly-p-phenylene benzobisthiazole) and PBO (poly-p-phenylene benzobisoxazole) with typical moduli of about 250 GPa [43]. The most well known rigid chain polymers are the aromatic polyamides and in particular kevlar, which is marketed by Du Pont.



A simple picture of poly(p-phenylene terephthalamide) (PPTA), or kevlar, is one of a rigid rod-like molecular chain held together laterally by hydrogen bonds between the carbonyl and amino moieties of the amide groups. It has been estimated that about 36 monomers would be needed to make a single chain fold, so folding is unlikely [44]. The rod-like molecules are well oriented due to the high persistence length of the chains. These materials (called aramids) find use in special applications where high temperature stability and modulus is required and also as liquid crystal polymers in electronic devices.

Unlike the solution processed liquid crystalline materials (lyotropic), many aromatic polyesters can be melt processed (thermotropic). These systems usually exhibit nematic phase in the melt, from which high strength fibers and extrudates can be obtained. The properties of fibers prepared from some of the wholly aromatic liquid

crystalline polyesters (LCPEs) compare well with those of other high strength organic fibers including kevlar [40]. For example, hydroxybenzoic acid (HBA)/polyethylene terephthalate (PET) (60/40) has a density of 1.4 g/cm^3 and a modulus of $\sim 23 \text{ GPa}$ [40] and HBA/HNA (75/25) has a density of 1.4 g/cm^3 and a modulus of $\sim 66 \text{ GPa}$.

Elongation at break, generally, for LCPs are quite small $\sim 3\text{-}4\%$. The as-spun fibers are not drawable and fiber properties can be enhanced in some degree by heat treatment or annealing [45].

The approach described above (rigid structure), however, presents some serious problems. The rigid chemical structure creates many difficulties in fabricating fibers. For example, aramid fibers cannot be melt spun because of their high melting temperature. Instead of melting, they decompose at high temperatures ($\sim 580^\circ\text{C}$); they have to be spun from solution. Because of their poor solubility however, strong acids or hydrogen bonding solvents need to be used. For example, PPTA is spun into extremely high modulus fibers from lyotropic liquid crystalline solution in sulfuric acid. Once dried, the fibers are generally not redrawable [46]. They can be heat treated ($400\text{-}500^\circ\text{C}$) under tension to increase the modulus [7]. The mechanical properties that have been achieved are comparable to glass or steel fibers (strength of $\sim 3 \text{ GPa}$ and modulus of $\sim 130 \text{ GPa}$). PPTA has one of the highest specific tensile strengths of the commercially available materials, and a reasonably high specific modulus even when compared with carbon fibers (figure 6.2). Another problem that the stiff rod-like molecules exhibit is a poor compressive strength. This problem recently has attracted considerable attention and several studies and models for compressive failure prediction have appeared in the literature [48-50].

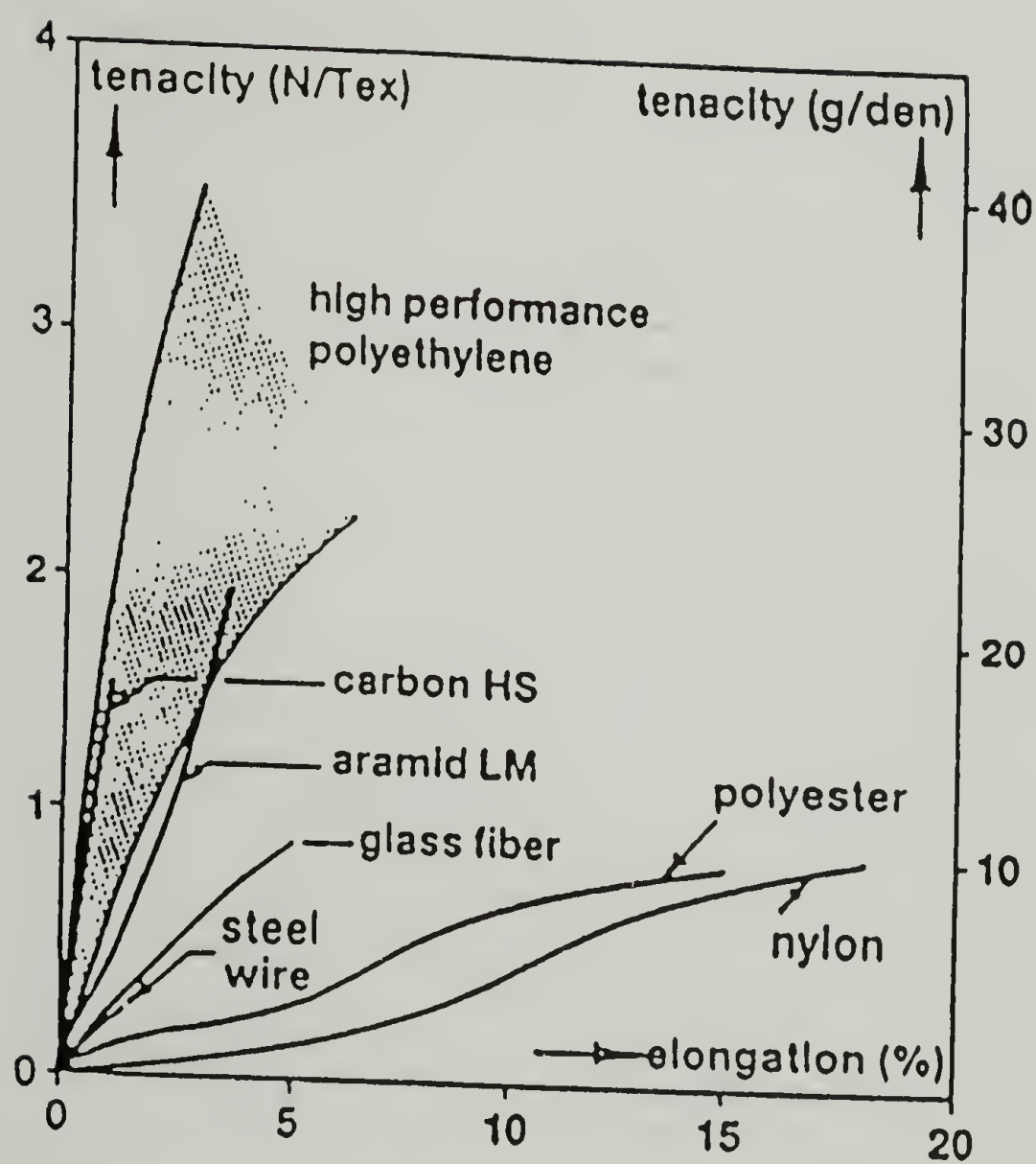


Figure 6.2. Stress-strain behavior of various yarns. Strain rate was $10\% \text{ min}^{-1}$ at 23°C [10].

6.2 Objective

The previous paragraphs described two different approaches used by other researchers to produce materials with high-strength and high modulus. The purpose of the research described in this part of the thesis is to examine the possibility of attaining high-strength, high modulus structures using a completely different route. The approach described here will utilize the unique properties of another class of polymers, that is elastomeric materials (natural rubber, SBS rubber, polyurethanes etc.).

Ordinary solids such as metals, crystals, glasses etc., can be deformed elastically to a very small extent ($\sim 1\%$). If a larger load is applied they either break or deform plastically.

Elastomers, on the other hand, are unique in having the capacity to undergo very large deformations which generally are reversible (elastic). Rubbers and rubber-like materials in their relaxed state are generally isotropic (properties do not depend on direction). However, when a load is applied and the elastomer deforms, some orientation is induced along the direction of the applied force and the material becomes anisotropic (directional properties). This phenomenon is due to the fact that macroscopic strains are related to microscopic orientation, which depends on the alignment of chains or segments of chains or crystalline regions in the polymer.

Most crystalizable elastomers when stretched at high elongation form microfibrils and fracture by splitting along the direction of orientation (fig. 3.5). The phenomenon of crack propagation along the direction of the applied force (splitting) has been observed not only in rubber-like materials that can exhibit fibrillation but in some glasses as well.

For example, when perspex is stretched ($\sim 100\%$) in temperatures above or around its glass transition, T_g , and remains elongated as the temperature drops below T_g , then highly anisotropic material is obtained [51].

Therefore crystallization is not an essential requirement for the development of anisotropy in polymer properties. The important factor is the degree of molecular alignment [52].

The goal of the research described here is to synthesize a block copolymer which can exhibit the unique elastomeric properties, not at ambient temperatures as the conventional elastomers do, but at elevated temperatures. The soft segment in the copolymer will have a glass transition temperature, T_{gs} , above the ambient and the hard will have $T_{gh} > T_{gs}$. Also, $\Delta T (T_{gh} - T_{gs})$ must be large enough to allow the formation of a rubbery region where the copolymer will be able to sustain extensive deformations.

The following chapter will give a description of the properties and the main characteristics of the elastomers. The theory and the related models concerning their mechanical properties will be briefly presented.

In chapter three we will use the conclusions drawn from the previous chapter to examine the mechanical properties and the behavior of selected elastomeric materials at liquid nitrogen temperatures.

Chapter four describes the criteria and principles for the selection of the appropriate materials. Also in this chapter the synthetic method used for the synthesis of the A-B-A block copolymer will be presented. In addition, the methods of analysis (^1H NMR, FT-IR, etc.) and characterization of the synthesized block copolymer will be cited.

In chapter five the thermal and mechanical properties of the synthesized copolymer will be presented, conclusions will be drawn and directions for further research concerning this approach for developing high-strength and high-modulus materials will be proposed.

REFERENCES

1. Bartenev, M. G., and Zuyev, S. Yu., "Strength and Failure of Viscoelastic Materials," Pergamon Press Ltd., Oxford, 1968
2. Powell, C. P., "Engineering with Polymers, " Chapman and Hall Ltd., London, 1983
3. Flory, P. J., J. Am. Chem. Soc. **43**, 447 (1947)
4. Perepelkin, K. E., Angew. Makromol. Chem., **22**, 181 (1972).
5. Sakurada, I., and Kaji, K., J. Polym. Sci. C, **31**, 57 (1970).
6. Mark, H. F., Trans. Farad. Soc., **43**, 447 (1947)
7. Ward, M. I., "Structure and Properties of Oriended Polymers," Halsted Press, New York, 1975
8. Smook, J., "Preparation and Properties of Ultra-High Strength Polyethylene Fibers," Krips Repro Meppel, 1984
9. Hearle, J. W. S., "Polymers and Their Properties V. I: Fundamentals of Structure and Mechanics," Ellis Horwood, New York, N.Y. (1982) ch. 2
10. Lemstra, J., R. Kirschbaum, T. Ohta and H. Yasuda., "Developments in Oriended Polymers-2," ed. Ward, M. I. Elsevier Applied Science Publishers Ltd., New York, 1987 ch. 2
11. Keller, A., "Ultra-high modulus polymers," eds. A. Ciferri and I. M. Ward, Applied Science Publishers Ltd., London, (1979) ch 11, p. 324
12. Keller, A., J., Polymer Sci., Polymer Symposia, **58**, 395, 1977
13. Frank, F. C., Proc. Roy. Soc. Ser. A, **319**, 127, London (1970)
14. Keller, A., and Mackley, M. R., Pure Appl. Chem., **39**, 195, 1974
15. Frank, F. C., Keller, A. and Mackley, M. R., Polymer, **12**, 467, 1971
16. Mackley, M., and R Keller, A., Phil. Trans. Roy. Soc., **278**, 29, London, 1975
17. Mackley, M. R., and Keller, A., Polymer, **14**, 16, 1973

18. Crawley, D. R., Frank, F. C., Mackley, M. R. and Stephenson, R. G., J., *Polymer Sci., Phys. Edn.*, **14**, 1111, 1976
19. Frank, F. C., and Mackley, M. R., *J. Polymer Sci., Phys. Edn.*, **14**, 1121, 1976
20. Pope, D. P., and Keller, A., *Colloid Polymer Sci.*, **255**, 633, 1977
21. Berry, M. V., and Mackley, M. R., *Phil. Trans. Roy. Soc.*, **287**, 1, London, 1977
22. Mackley, M., and R Keller, A., *Phil. Trans. Roy. Soc.*, **278**, 29, London, 1975
23. Keller, A., "Ultra-high modulus polymers" Eds. A. Ciferri and I. M. Ward, *Applied Science Publishers Ltd.*, London, ch 11, pg 333 (1979)
24. Bowman, M., U. S Patent 3,382, 220 (1968)
25. Southern, J. H., R. S. Porter, *J. Macromol. Sci. Phys. B4*, 541 (1970)
26. Southern, J. H., R. S. Porter, *J. Appl. Polym. Sci.* **14**, 2305, (1970)
27. Mackley, M. R., *Polymer Rheology and Plastics Processing*, Eng. Conf. Loughborough (Brit. Soc. Rheology and Plastics and Rubber Inst.), 1975, p. 250
28. Imada, K., and M. Takayanagi, *Int. J. Polym. Mater.*, **2**, 71, (1973); *ibid.* **2**, 89, 1973
29. Imada, K., T. Yamamoto, K. Shigematsu and M. Takayanagi, *J. Mater. Sci.*, **6**, 537, (1971)
30. Maruyama, S., K. Imada and M. Takayanagi, *Int. J. Polym. Mater.*, **2**, 125, (1973); *ibid.* **1**, 211, 1972
31. Mead, W. T., and Porter, R. S., (1976). *J. Polymer Sci.*, **C**, accepted (1977)
32. Mead, W. T., and Porter, R. S., *Flow Induced Crystallization Symposium*, Midland Macromolecular Institute, Michigan, August, 1977
33. Zachariades, A. E., Porter, R. S., "The strength and Stiffness" Marcel Dekker, Inc., New York, N. Y. (1983) ch. 1
34. Southern, J. H., N. E. Weeks and R. S. Porter, *Makromol. chem.* **102**, 19 (1977)
35. Zachariades, A. E., Porter, R. S., *J. Appl. Polym. Sci.* **24**, 1371 (1979)
36. Zachariades, A. E., Sherman, E. S., Porter, R. S., *J. Polym. Sci., J. Appl. Polym. Sci.* **24**, 2137 (1979)

37. Keller, A., "Ultra-high modulus polymers" Eds. A. Ciferri and I. M. Ward, Applied Science Publishers Ltd., London, ch 11, p. 346, (1979).
38. DSM/Stamcarbon, NL 7900990 (1979); 7904990 (1979) / US patent 4,344,908; 4,422,993; 4,436,689.
39. Keller, A., "Ultra-high modulus polymers" Eds. A. Ciferri and I. M. Ward, Applied Science Publishers Ltd., London, ch 11, p. 347 (1979)
40. Blackwell, J., A. Biswas, "Developments in Oriented Polymers-2," ed. Ward, M. I. Elsevier Applied Science Publishers Ltd., New York, 1987 ch. 5
41. Flory, P. J., Proc. Roy. Soc. A 234, 73 (1956)
42. DeMarzio E. A., J. Chem. Phys. 35, 658 (1961)
43. W-Fang Hwang, Proc. Int. Symp. Fibre Sci. Technol. (ISF), Hakone, (1985) p.39
44. Carter, G. B., and Schenk, V. T. J. (1975). In: "Structure and properties of oriented polymers" Ed. I. M. Ward, John Wiley, Applied Science Publishers
45. Dobb, M. G., McIntyre, J. E., J. Polym. Sci., Polym, Symp. 63, 67, (1978)
46. Owen, J. A., "Developments in Oriented Polymers-2", Ed. Ward, M. I. Elsevier Applied Science Publishers Ltd., New York, 1987, ch. 7
47. Barham, P. J., and Keller, A., J. Mater. Sci., 1976, **11**, 27
48. Deteresa, S. J., Porter, R. S., Farris, R. J., J. Mat. Sci. 20 1645 (1985)
49. Deteresa, S. J., Allen, S. R., Farris, R. J., Porter, R. S., J. Mat. Sci. 19 57 (1984)
50. Deteresa, S. J., Porter, R. S., Farris, R. J., J. Mat. Sci. 23 1886 (1988)
51. Curtis, J. W., J. Phys. D., Appl. Phys., **3**, 1413 (1970).
52. Treloar, L. R. G., "Introduction to Polymer Science," Wykeham Publications, London (1970) p. 144

CHAPTER 7

BACKGROUND

7.1 Rubber and rubberlike materials

Rubberlike materials or elastomers, as they are usually called, have long been of extraordinary interest. Their unique nature, their elastic properties and their relationship to molecular structure have attracted the attention of numerous investigators interested in structure-property relationships.

Elastomers exhibit an unusual behavior described as rubberlike elasticity. This behavior is defined by very high deformability and recoverability. In order for a material to exhibit this type of elasticity, three molecular requirements must be satisfied [1].

- a) The material must consist of polymeric chains
- b) The polymeric chains must have a high degree of flexibility and mobility
- c) The chains must be joined into a network or network-like structure

The first requirement is associated with high deformability. Long-polymer molecules are able to alter their spatial arrangement and extend in response to an imposed stress.

Table 7.1. Examples of some elastomeric and non-elastomeric polymers at ambient temperature.

Polymer	T _g (°C)	T _m (°C)	Classification
Natural rubber	-73	28	elastomer
Butyl rubber	-73	5	elastomer
SB ^a copolymer	Low	-	elastomer
Polyethylene	-	125	crystalline
Polystyrene	100	-	Glassy
PVC ^b	87	-	Glassy

^a Styrene-butadiene copolymer

^b Poly(vinyl chloride)

The second characteristic required for this type of elasticity also relates to the high deformability. It asks for flexibility and mobility in order for the different spatial arrangements of the chains to be readily accessible. This implies that extensive crystallization and high rigidity (glassy state) must not exist. The last requirement is necessary in order to prevent chains from sliding past each other and therefore recoverability can be obtained. Some examples of rubberlike materials (at ambient temperatures) and some non elastomeric are given in table 7.1. Notice that all elastomeric materials have glass transition temperature (T_g) lower than the service

temperature. On the other hand, not all elastomers can be processed in the liquid state (crosslinked systems do not dissolve). Therefore, only thermoplastic elastomers will be considered here.

7.2 Phase separation and morphological characteristics for elastomeric block copolymers

The physical behavior of block copolymers is related to solid state morphology. Block copolymers frequently exhibit phase separation which typically gives rise to a dispersed phase consisting of one block type and a continuous matrix consisting of the second block. Usually the dispersed phase consists of hard domains (crystalline or glassy) and the matrix is soft and rubber-like, fig. 7.1.

When the hard domain is crystalline, the phase separation depends on the factors governing crystallization in homopolymers and the basic morphology in block copolymers is the lamellar crystal [2]. Phase separation in amorphous systems is described in literature [3]. Some of the conclusions are:

1. Phase separation of two non-polar segments A and B will occur easier if the difference in their solubility parameters $\delta_A - \delta_B$ is large.
2. For constant copolymer composition and the same number of blocks per molecule, phase separation becomes easier as the molecular weight increases.
3. The phase separation becomes more difficult as the number of blocks per chain increases. For example, separation is easier in an A-B-A system than in an $(A-B)_n$ system.

3. The phase separation becomes more difficult as the number of blocks per chain increases. For example, separation is easier in an A-B-A system than in an $(A-B)_n$ system.

When the segments A and B of a block copolymer phase separate, the minor component will form domains which will be dispersed in the matrix (major component). The sizes of these domains are much smaller than aggregates found in a mixture of incompatible blends and the phase separation in block copolymers is usually called microphase separation. The size depends on the conformational entropy and on the interfacial energy. Block copolymers are capable of forming three basic morphological units: spheres, rods (or cylinders) and lamellae [4]. The geometric shape depends on the molecular weight of the segment forming the domain, as well as on its relative concentration in the copolymer. Figure 7.2 shows the morphology dependence on composition.

7.3 Properties of block copolymers

7.3.1 Glass transition

From the previous discussion it is realized that block copolymers generally have two phase morphology. This type of morphology results in some unique characteristics and properties and is especially beneficial in elastomeric systems.

A single T_g is observed in the case of random copolymers. The observed T_g is usually intermediate between those of the individual homopolymers [6].



Figure 7.1. Morphological model of a physical network formed in poly(styrene-b-butadiene) copolymers. Polystyrene has molecular weight $\sim 10^4$ and polybutadiene $\sim 7 \times 10^4$ [11].

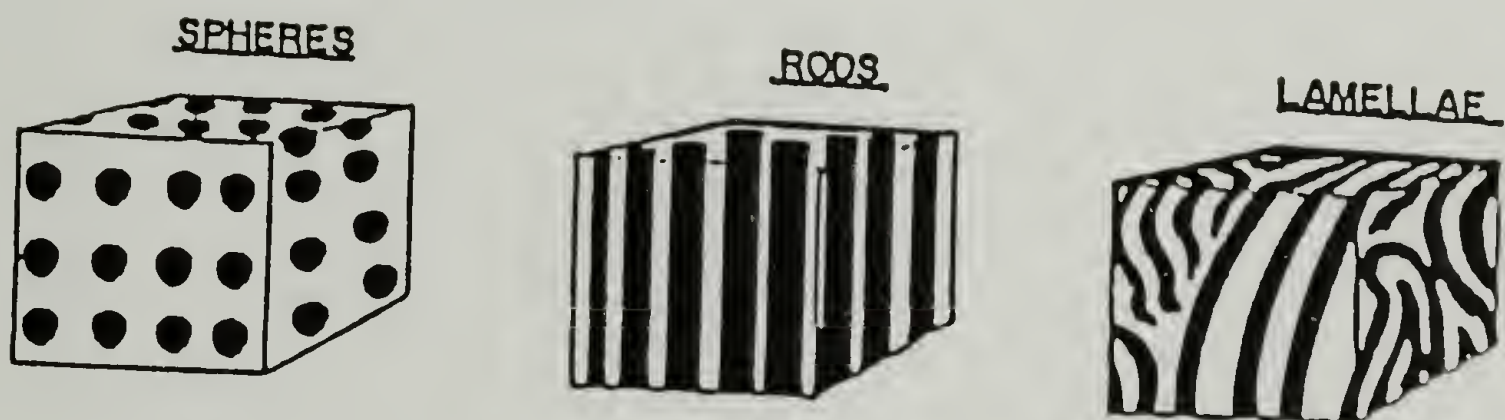


Figure 7.2. Schematic representation of morphological forms in block copolymers [5].

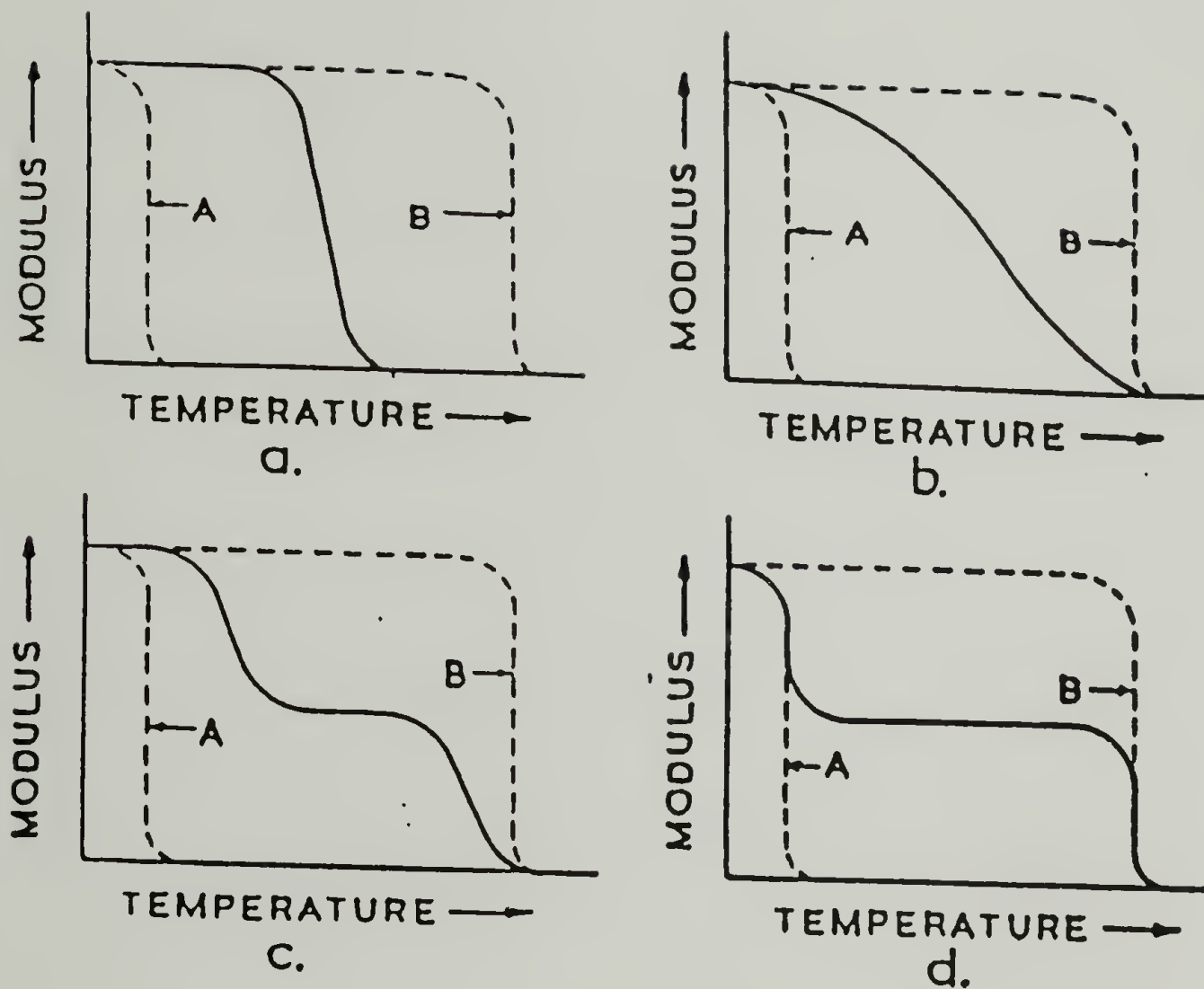


Figure 7.3. Dependence of modulus-temperature curves on block copolymer morphology: (a) A and B units are fully compatible giving one phase system, (b) bundling of units without phase separation, (c) phase separation with diffuse phase boundaries, (d) phase separation with boundaries between phases. Curves A and B correspond to the pure homopolymers (reproduced from Ref. 9).

On the other hand, for block copolymers the number of glass transition temperatures will be determined by the block lengths and interaction between monomer units. For example, a single T_g can be found for ABA type of block copolymers if the blocks are not too dissimilar as in the case of poly(styrene-*b*- α -methyl styrene) where the $T_g=140^\circ\text{C}$ [7]. When the blocks are short and not too different, a single T_g is also observed for the (AB) $_n$ type of block copolymers. The observation of a single glass transition temperature suggests that the block copolymer has a one-phase morphology in which the A and B units are well mixed. When The block copolymer has AB or ABA structure with long blocks, then microphase separation usually occurs and two glass transitions are observed which are close to $T_{g,A}$ and $T_{g,B}$ [8].

7.3.2 Modulus-temperature behavior

The modulus-temperature curves obtained from dynamic mechanical data can be used to characterize the materials, as can be seen from the curves in fig. 7.3. A single T_g is observed for both a random copolymer (fig. 7.3.a) and a single phase block copolymer (fig. 7.3.b). The position of the single T_g is found to be in between $T_{g,A}$ and $T_{g,B}$. The exact position depends on the weight fraction of A and B components. If partial microphase separation occurs, however, the plateau may exist in a very narrow temperature range (fig. 7.3.c) or the modulus might decrease gradually (fig. 7.3.b). Two-phase block copolymers (fig. 7.3.d) exhibit two T_g values. The compositional variations do not affect the position of the T_g significantly.

It is the position of the modulus plateau that is dependent upon the variations of the composition. Therefore, for different compositions the modulus plateau might move up or down.

7.3.3 Stress-strain behavior and mechanical properties

Tensile properties are dependent on the copolymer structure, on the copolymer composition and on the solid state morphology [10]. Block copolymers can be divided therefore, on the base of their service modulus, into either rigid or elastomeric materials.

Rigid materials can consist of either two hard segments or a hard segment and a small fraction of a soft segment. The hard segment is the segment that has T_g above the service temperature, while the soft segment has T_g below the service temperature. Rigid copolymers can offer advantages in mechanical properties such as creep or stress relaxation. Furthermore, the inherent ductility of the segments in a hard-hard block copolymer could be retained due to the fine dispersion and the adhesion of the two phases [11]. In contrast, physical blends of the two homopolymers are often very brittle.

On the other hand, an elastomeric copolymer is the one that contains a small amount of hard segment and the major component is the soft polymer. Elastomers can be thermoset (chemically crosslinked) or thermoplastic (physically crosslinked) copolymers. Thermoplastic elastomers are two phase block copolymers comprised of a soft matrix and hard domains.

Rubbers exhibit elastomeric properties (extendibility, recovery) as exemplified by spandex fibers. The high flexibility is due to the low viscosity of the soft segment. The

soft segment is important because it is the primary factor that determines recovery efficiency, sorption properties, and oxidative and hydrolytic stability. The hard segment serves as the binding media to keep the soft chains from flowing. When a force is applied, the soft chains align in the direction of the applied force. Consequently, when the chains pack closer together, they form crystallites with low T_m (strain induced crystallization) [12, 13]. The crystallization process is generally reversible and upon release of the load the low T_m crystallites melt. At low elongation the force required to deform the material is small and the elongation large; therefore, the modulus is very small, Fig 7.4. However, as the hard domains begin to orient in the direction of the applied force, the soft chains start to pack together, forming low melting crystalline areas that resist further deformation. Crystallization will continue as a function of the force increase until the whole system acts as a hard fiber. If the fiber is allowed to relax, then the soft segment crystallites will melt and the chains will retract.

7.4 Conclusions

It was mentioned earlier that the mechanical properties depend on the morphology among others. The type of morphology obtained with amorphous two phase block copolymers depends on both the segment ratio and on the method of fabrication. The major component will exist as continuous phase while the minor component as dispersed domains. The domains form spherical shapes at low segment concentration

(< 20%). At higher concentrations (20-40%) the domains assume a rod-like shape and at equivalent concentrations they form lamellar or co-continuous phases [14,15], fig 7.2.

The different morphologies have a profound effect on the physical properties and mechanical properties, with the continuous phase being the major influence.

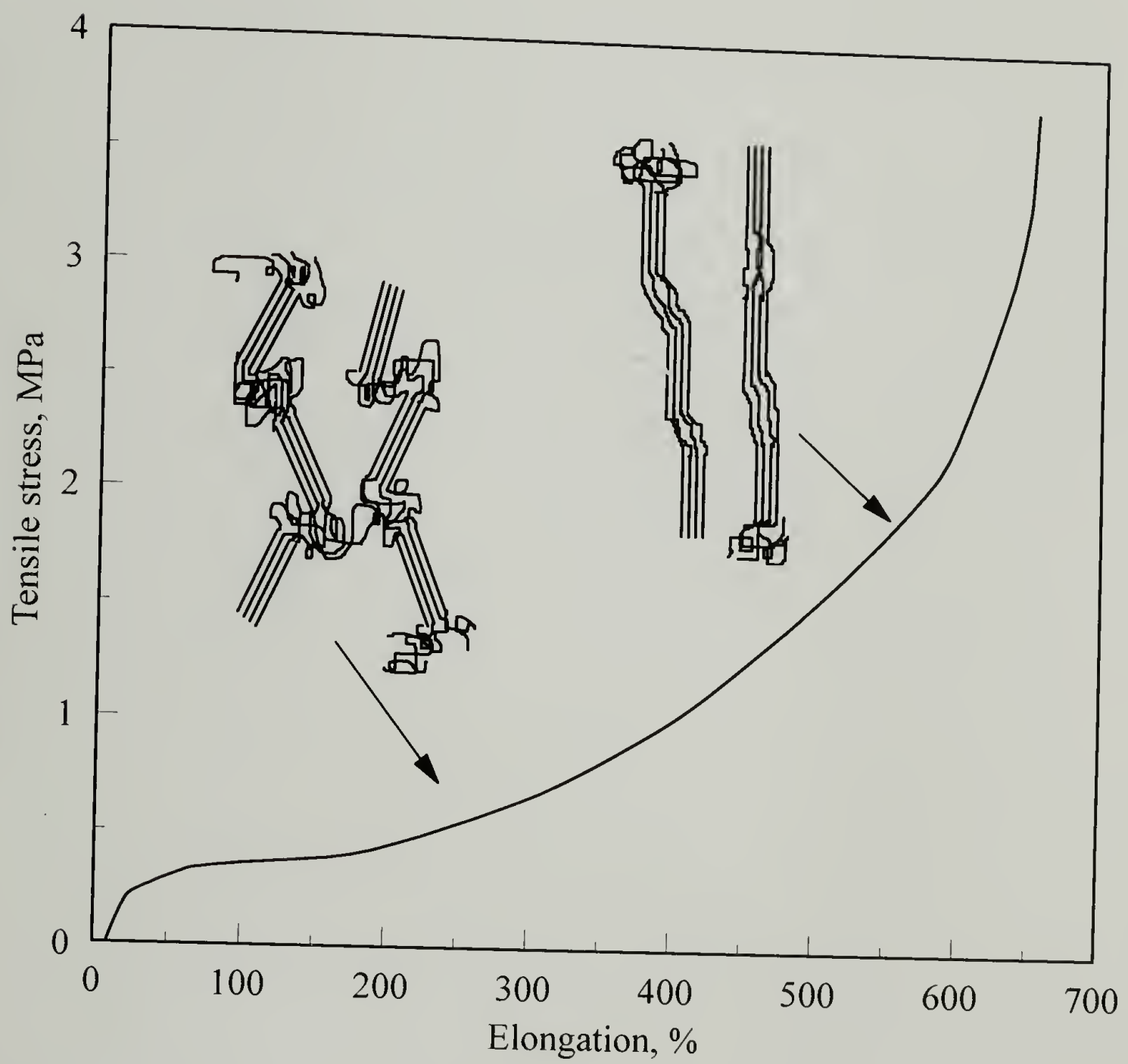


Figure 7.4. A typical stress-strain plot for rubber or rubber-like materials.

The orientation of polymer chains increases with elongation.

REFERENCES

1. Mark, E. J., Erman Burak, "Rubberlike Elasticity a Molecular Primer", Wiley-Interscience, New York, 1988, ch 1, p.4
2. Allport, C. D., and Janes, H. W., eds: "Block Copolymers," Halsted Press, New York, 1973, ch. 8A, p. 365
3. Krause S. J., Polymer Sci., A-2, 7, 249 (1969)
4. Matsuo, M., Sagae, S. and Asai, H., Polymer, 10, 79 (1969)
5. Noshay, A., and J. E. McGrath, eds: "Block Copolymers", Academic Press, New York, 1977, ch. 4, p. 59
6. Miller, M. L., "The structure of Polymers", Reinhold, New York, (1966)
7. Baer, M., J. Polymer Sci., A2, 417, (1964)
8. Fedors, R. F., J. Polymer Sci., C26, 189, (1969)
9. Bonart, R., L. Morbitzer and H. Rinke, Kolloid-Z., 240, 807, (1970)
10. Allport, C. D., and Janes, H. W., eds: "Block Copolymers," Halsted Press, New York, 1973, ch. 8B, p. 420
11. Noshay, A., and J. E. McGrath, eds: "Block Copolymers", Academic Press, New York, 1977, ch. 4, p. 65
12. Aklonis, J. J., and MacKnight, J. W.: "Introduction to Polymer Viscoelasticity", Wiley-Interscience, New York, 1972, ch. 6, p. 134
13. Allport, C. D., and Janes, H. W., eds: "Block Copolymers," Halsted Press, New York, 1973, ch. 8c
14. Bradford, E. B., Amer. Chem. Soc., Polymer Preprints, 11, 392, (1970)
15. Fischer, E., J. Macromol. Sci., A2, 1285, (1968)
16. Matsuo, M., and S. Sagae, Amer. Chem. Soc., Polymer Preprints, 11, 384, (1970)

17. Beecher, J. F., L. Marker, R. D. Bradford and S. L. Aggarwal, J. Polymer Sci., **C26**, 117, (1969)

CHAPTER 8

MECHANICAL PROPERTIES OF ORIENTED ELASTOMERS AT LIQUID NITROGEN TEMPERATURES

8.1 Introduction

In the previous chapter the stress-strain behavior of rubber or rubber-like materials is described. A typical stress-strain curve for rubber is shown in fig. 8.1. The most obvious feature of this plot is that stress is not proportional to deformation; this is a feature encountered in ordinary solids [1,2]. For such materials the law of elasticity, as described by Hooke, that is, in any elastic deformation the stress is proportional to strain, is not satisfied. Hooke's law generally holds only for small deformations ($\sim 1\%$) and rubber obviously does not fall into this category [3]. As can be seen from fig. 8.1, at very high extensions a limiting stress-strain relationship can be observed even for rubber. In this limited region the modulus becomes very large. In this state of high extension, many chains in the material are fully oriented (they have reached maximum extensibility) and the material behaves as a hard rod [4]. In order to examine the mechanical properties of the materials at this stage where the chains are extended and oriented, we would need to keep the rubber deformed even when the load is removed. It is obvious that this is impossible at ambient temperature, but it is possible at very low temperatures where the chains can remain frozen in extended position. Therefore, if the extended material is subjected to stress in a frozen state, high modulus should be observed.

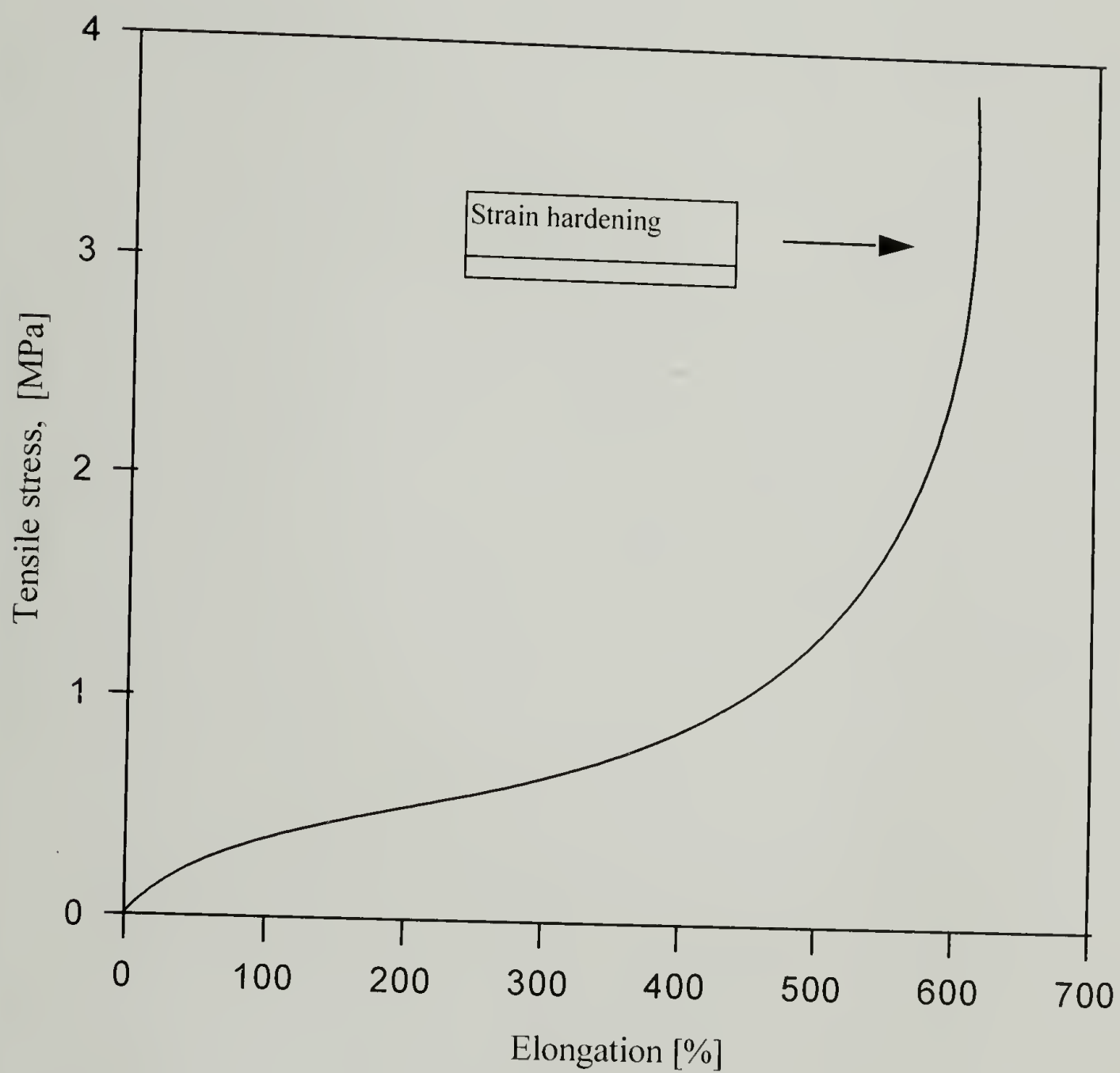


Figure 8.1. A typical stress-strain plot for an elastomeric material at ambient temperatures. A strain hardening can be observed, at very high elongation.

8.2 Experimental

The materials used for these experiments were commercial polyurethane rings used in tape recording systems, natural rubber rings used in dental applications, radiation crosslinked polyethylene used for tubing, and Spandex fibers (T-126) supplied by Du Pont. The mechanical properties were determined using an Instron tensile testing machine operated with a crosshead speed of 20 mm/min. Figure 8.2 shows the tensile test set up modified to perform tests at liquid nitrogen temperatures. The Instron tester was fitted with a plastic container having a small opening valve at the lower end in order to empty and reuse the liquid nitrogen. A ceramic insulator cylinder (3.5 cm diameter and 6.5 cm length) was used to connect the upper grip with the load cell in order to avoid a possible thermal shock of the cell. The temperature, close above the surface of the liquid nitrogen but not inside the container, was measured using a thermocouple connected to a digital meter. The applied force was measured using 10 and 100 lb. load cells (Interface Corp. SM-10 and SM-100). The grip displacement was measured using an LVDT (Linear Variable Differential Transformer) model number 1000 DC-D made by Schaevitz Engineering. Data was acquired using a personal computer with A/D board interface and analyzed using standard software (Microsoft Excel).

The thermal decomposition temperatures were determined using a Thermogravimetric analyzer 2950 from TA Instruments. The thermograms were obtained under air atmosphere with a heating rate of 10 °C/min. The T_g's were determined using a TA Instruments DSC (Differential Scanning Calorimeter).

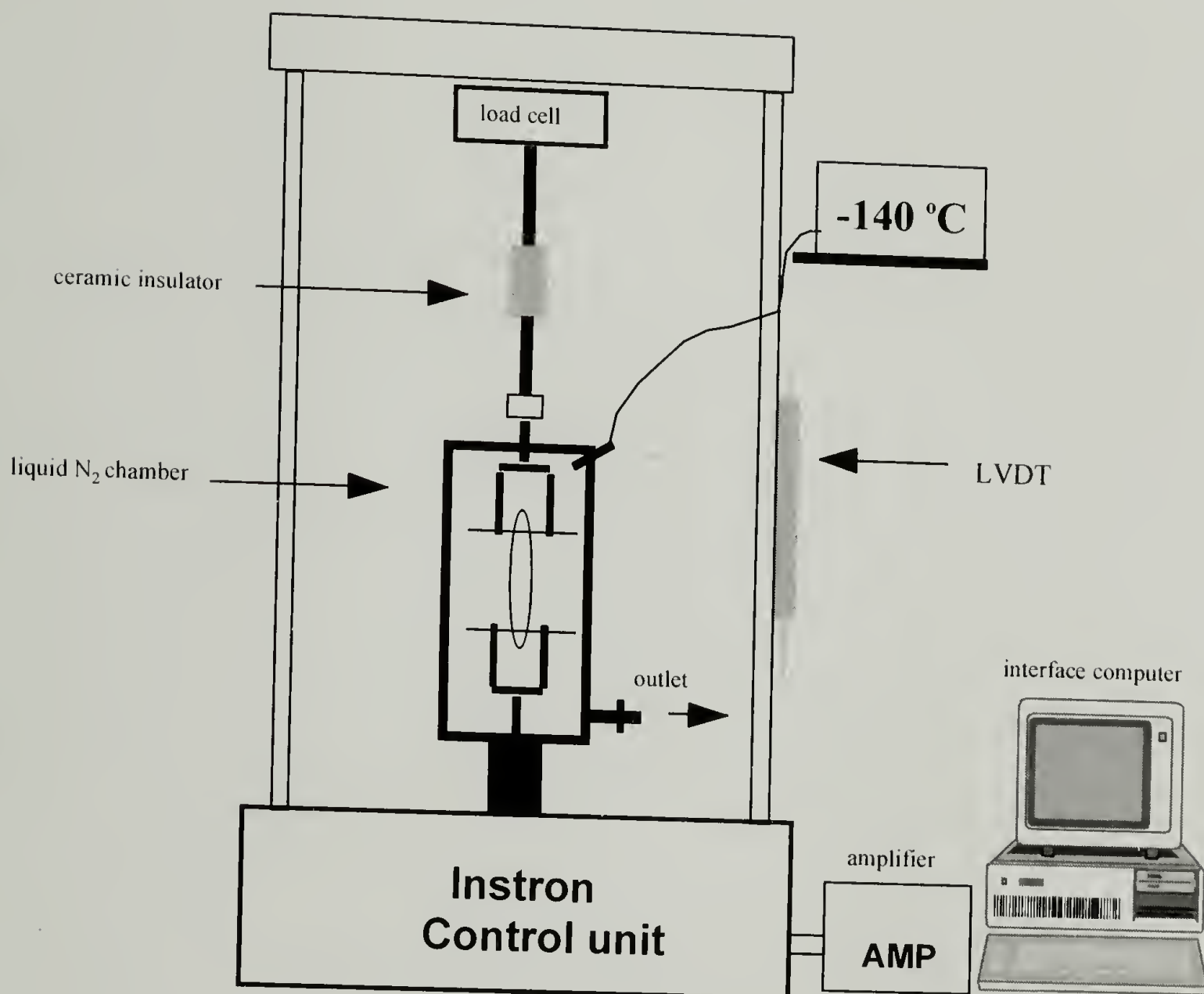


Figure 8.2. A schematic representation of the experimental set-up. The instron tester was modified to accommodate testing at liquid nitrogen temperatures. The recorded temperature (-140 oC) is the temperature immediately above the liquid nitrogen surface.

All DSC experiments were run under nitrogen at a heating rate of 10 °C/min from -100°C to ambient temperatures. Sample sizes were ~10 mg.

A JEOL-35CF scanning electron microscope was used to look at the crack propagation in the polyurethane samples. The broken samples were mounted on aluminum cylinders using double-stick tape and sputter-coated with a thin gold layer.

Polyurethanes: Polyurethane ring shape samples with 33-34 mm diameters and original cross-sectional areas of approximately 0.3 mm² were pre-stretched to predetermined elongations (0 to 640%). The maximum elongation 640% was determined to be the elongation just before the break. Thereafter, and while samples were kept elongated, the temperature was dropped to below -140 °C by filling the container attached to the Instron tester with liquid nitrogen, fig. 8.2. This temperature was determined to be well below the glass transition temperature of these materials, which is -30 °C, as determined by DSC. Therefore Young's elastic moduli, strength and elongation-at-break were determined in their glassy state.

Spandex fibers: There were several different specification Spandex fibers available in our laboratory. The fibers chosen for tensile testing had 280 denier, cross-sectional area $2.6 \times 10^{-3} \text{ cm}^2$ and glass transition of ~ -60 °C. The samples were mounted in a specially made set of grips as shown in fig. 8.3. Spandex fibers, as the other elastomers described above, were similarly pre-stretched to 270% and 630% elongation, and then cooled to -140 °C and tested below their T_g.

Natural Rubber: There were several different type of rubber bands available for testing. They were designated as elastics Light (L10), medium (M6), heavy (H4) and super heavy (SH8). The bands chosen for testing were the medium M6 rubbers which yielded the reported results in this document. The M6 samples have a 6 mm diameter and an original cross-sectional area of 1.0 mm^2 . They were subjected to load and were pre-elongated from 0 to 780% in a similar manner to that previously described for polyurethanes. The glass transition temperature of the rubbers determined by DSC was found to be -60°C , which again was much higher than the testing temperature.

Radiation cross-linked polyethylene: The samples were provided by Raychem Corporation. in the form of a round tube with a diameter about 3 mm and a wall thickness of 0.5 mm. The tube was fitted around a metal rod in order to cut samples more conveniently. Samples of ring shape strips having widths of 2.1-3.1 mm were cut using a razor blade. The sample strips were heated over a hot plate ($150\text{-}160^\circ\text{C}$). The temperature at which the samples were heated was much lower than their decomposition temperature which was determined to be 260°C using TGA. The hot strips were pre-stretched to different elongation from 0 to 230% and while being elongated they were cooled down to room temperature. The pre-stretched cooled rings were placed in the Instron tester where their mechanical properties were determined at room temperature.

8.3 Results and discussion

The results obtained from the testing of the described elastomeric materials confirmed our expectations concerning the relationship between pre-stretching and

mechanical properties. First, in the case of polyurethanes, this relationship is reported in table 8.1. It is clear from these results that the extension of the materials to different extents (when they are in their elastic state-room temperature) greatly affects their moduli. As stated previously, this is because at liquid nitrogen temperatures the chains are forced to retain their orientation. Figure. 8.4 depicts the moduli / pre-elongation relationship. It is apparent that around 600% pre-elongation the modulus increases faster.

The micrographs depicted in Figure 8.5 show that the crack propagates preferably in the direction of the applied load. This observation is due to fibrillation of the rigid rod like chains oriented to the direction of the applied load.

Therefore, the crack propagates by preferentially breaking weak intermolecular forces between the polymer chains and not the stronger covalent bonding within the chain. The mechanism of failure in oriented rubbers, as well as in thermoplastic materials, and the effect of the orientation on crack propagation is described in detail in the literature [5-8]. The predicted linear stress-strain behavior at high elongation is depicted in fig. 8.6. It is clear from the results that the linearity is a function of the pre-elongation and is most pronounced at the maximum extension. Spandex fibers exhibited a similar behavior when tested at the same conditions. The obtained results are summarized in table 8.2 and plotted in fig. 8.7. The observed behavior for the thermoplastic elastomers was not unique. Similar behavior was observed in the case of the natural rubber elastomers. The obtained results are tabulated in table 8.3. The extent of pre-elongation at room temperature proved again to be the factor crucial to the moduli recorded at liquid nitrogen temperatures.

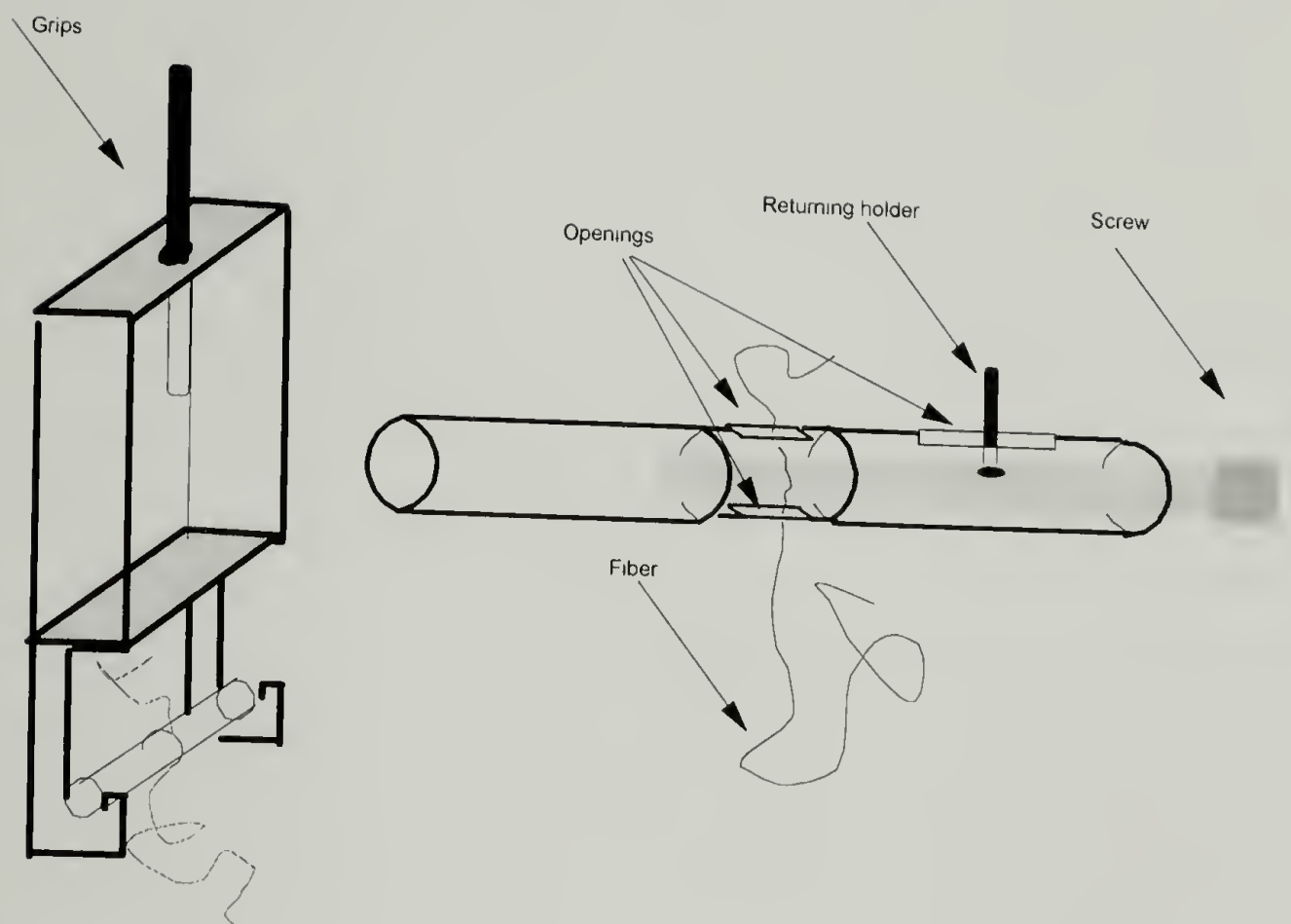


Figure 8.3. Schematic representation of the specially made grips for the testing of the spandex fibers. The fiber was passed through the two perpendicular openings and pressed against the stationary flat aluminum surface with the use of a mobile screw.

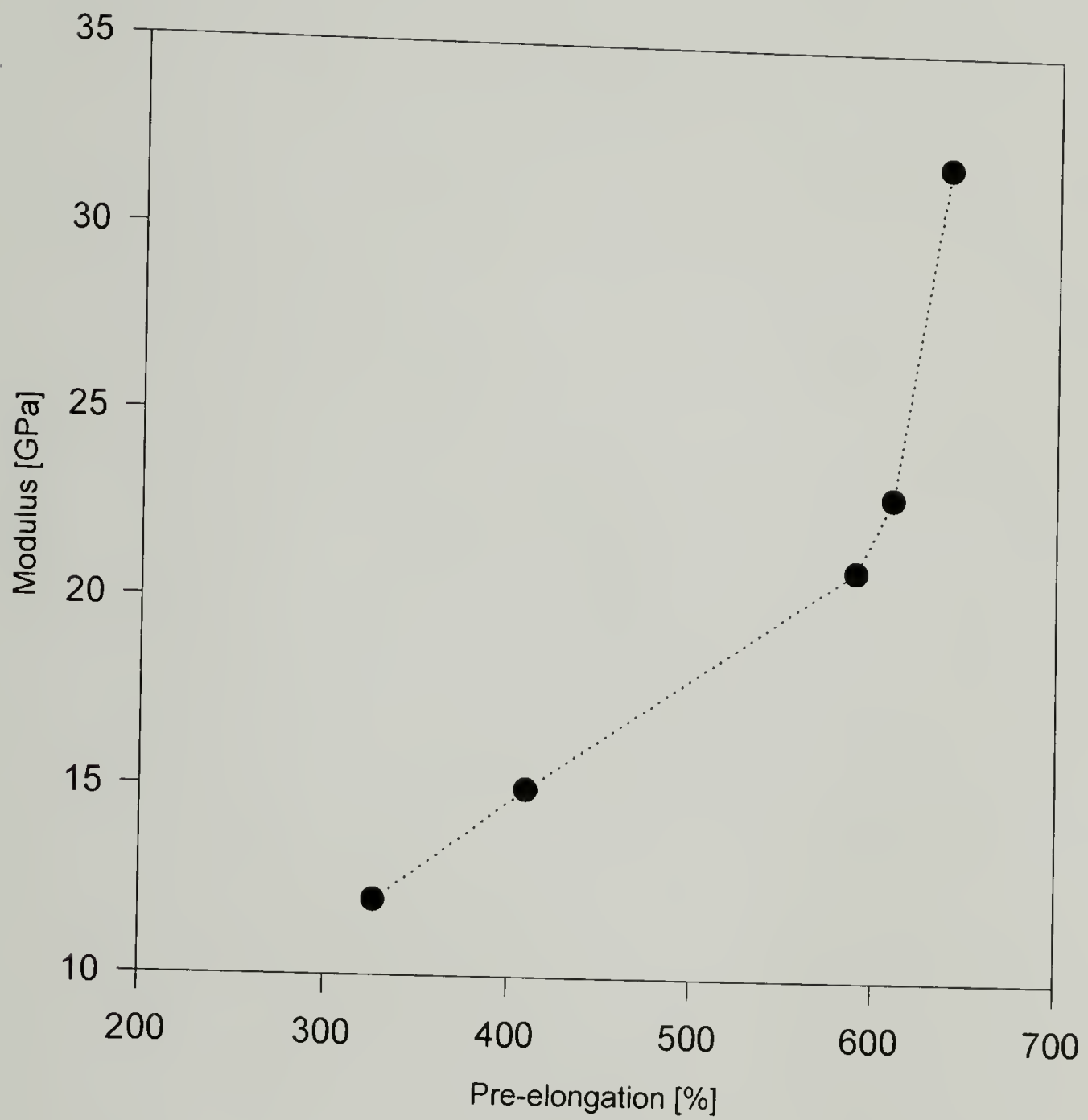


Figure 8.4. The modulus pre-elongation relationship for polyurethane samples tested at liquid nitrogen temperatures.

Table 8.1. Mechanical properties of the polyurethane samples tested at liquid nitrogen temperature. Pre-elongation is the elongation at room temperature, ϵ : the tensile strain at break, σ : the tensile stress at break, E: the elastic modulus.

Pre-elongation [%]	E [GPa]	σ [GPa]	ϵ [%]
0	-	0.025	16.2
327	12	0.61	9.5
410	14	0.68	8.8
590	21	1.01	4.9
610	23	0.94	4.1
640	32	0.98	3.1

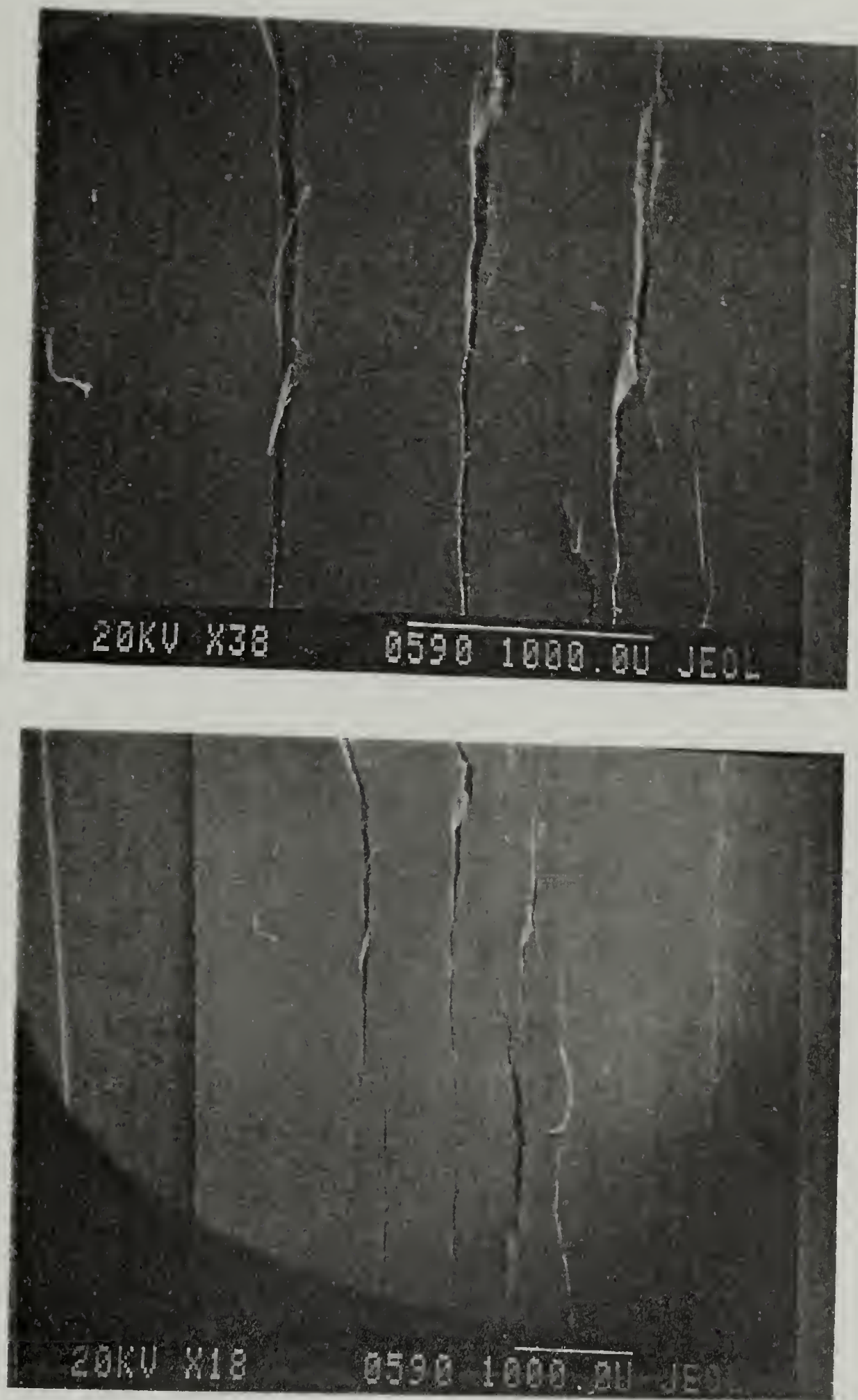


Figure 8.5. SEM micrographs depict the direction of crack propagation in the tested polyurethane samples, pre-elongation was 640% at room temperature. It is shown that the crack propagates preferably in the direction of the applied load. The two micrographs represent the same sample at two different magnifications at room temperature.

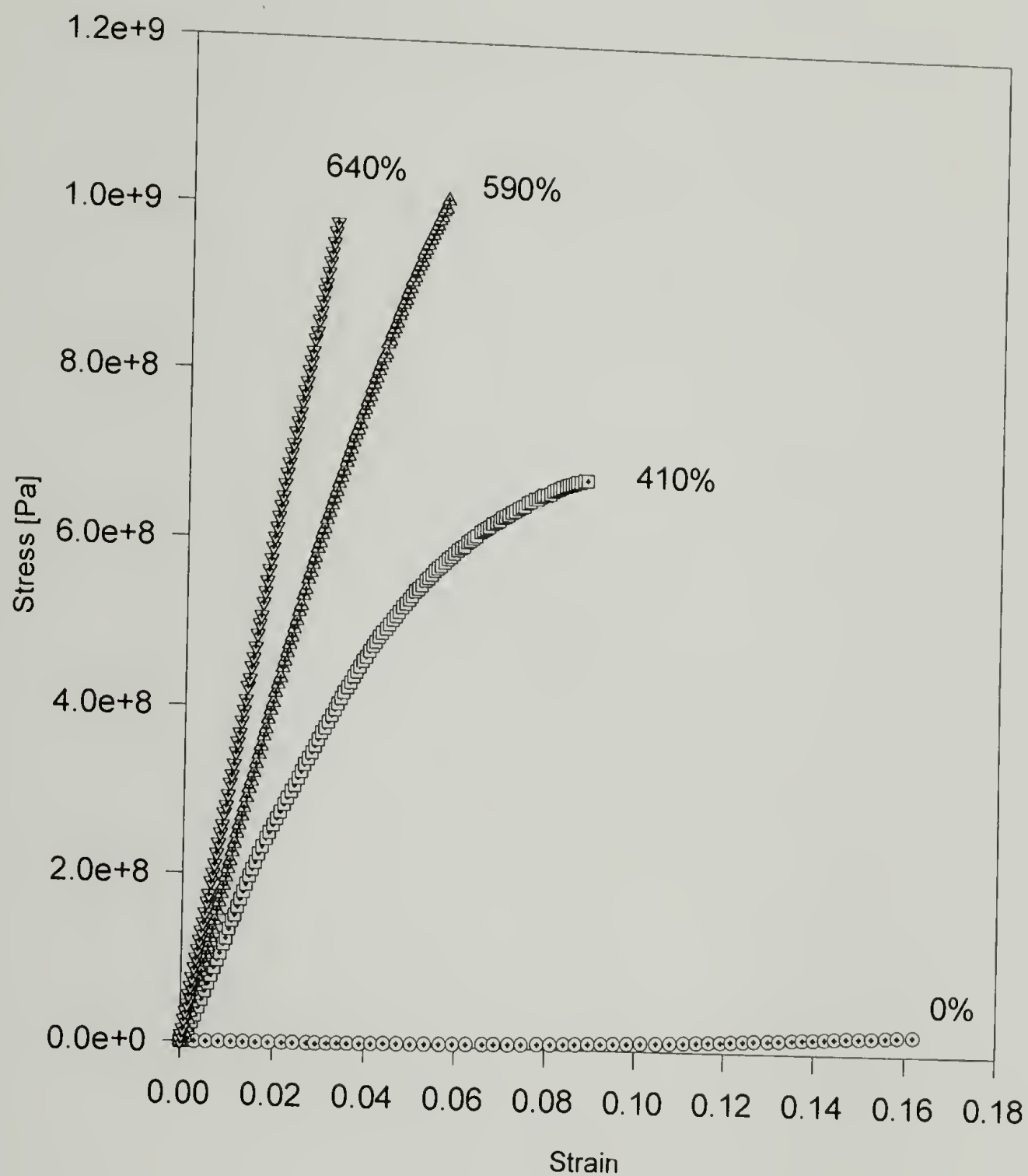


Figure 8.6. Stress-strain curves for the polyurethane samples tested at liquid nitrogen temperature. The different curves correspond to different pre-elongation at ambient temperature. Increase of the pre-elongation increases the linear stress-strain response.

In addition, fig. 8.8 indicates again that the dependence of modulus to pre-elongation is more pronounced at the very high elongation. Linear response is observed for this type of elastomer (fig. 8.9) at the maximum extensions.

In the case of crosslinked polyethylene, the increase of moduli was much lower than was expected. The results for the various pre-elongation are reported in table 8.4. Even though the values obtained seem to be low, it is important to notice from the plot in Fig. 8.10 that for elongation above 180% there is a sudden change in the rate of the increase of modulus with pre-elongation. This result likely indicates that there is not substantial orientation up to this point. In addition, fig. 8.11 shows that even for the maximum (230%) elongation, incomplete linear stress-strain behavior is obtained. This is an indication that the true maximum elongation before the break could not be reached.

8.4 Conclusions and future work

The purpose for the study of the properties of elastomers at low temperatures was to establish the relationship of the modulus with pre-elongation. It was observed that pre-elongation greatly affected the moduli of the elastomeric materials tested at liquid nitrogen temperatures. Another observation was that the stress varied linearly at very high pre-elongation. In addition, the rate of increase of modulus with the imposed pre-elongation shows significant change above a critical pre-elongation. The moduli values obtained for the radiation crosslinked polyethylene were lower than what was expected. Fig. 8.9 indicates that 230% might not be the true maximum pre-elongation.

At this point, it is important to realize that a simple procedure such as stretching an elastomer was adequate to create large differences in the properties of the materials. With this method a low modulus material was forced to assume a high modulus (> 25 GPa) and to behave superior to an engineering plastic (polyethylene terephthalate fiber), table 8.5.

Future tensile testing experiments at low temperatures should include ABA type elastomers (i.e. styrene-polybutadiene rubbers), in order to examine and compare the extension-orientation in triblock systems and the effect on modulus and tensile strength. High molecular weight polyethylene rubbers could also be used in the future to examine the possibility to obtain high modulus at high pre-elongations.

Table 8.2. Mechanical properties of the Spandex fibers tested at liquid nitrogen temperature. Pre-elongation is the elongation at room temperature, ϵ : the tensile strain at break, σ : the tensile stress at break, E: the elastic modulus.

Pre-elongation [%]	Modulus [GPa]	σ [GPa]	ϵ [%]
270	9.6	.41	4.3
630	29.5	1.21	4.2

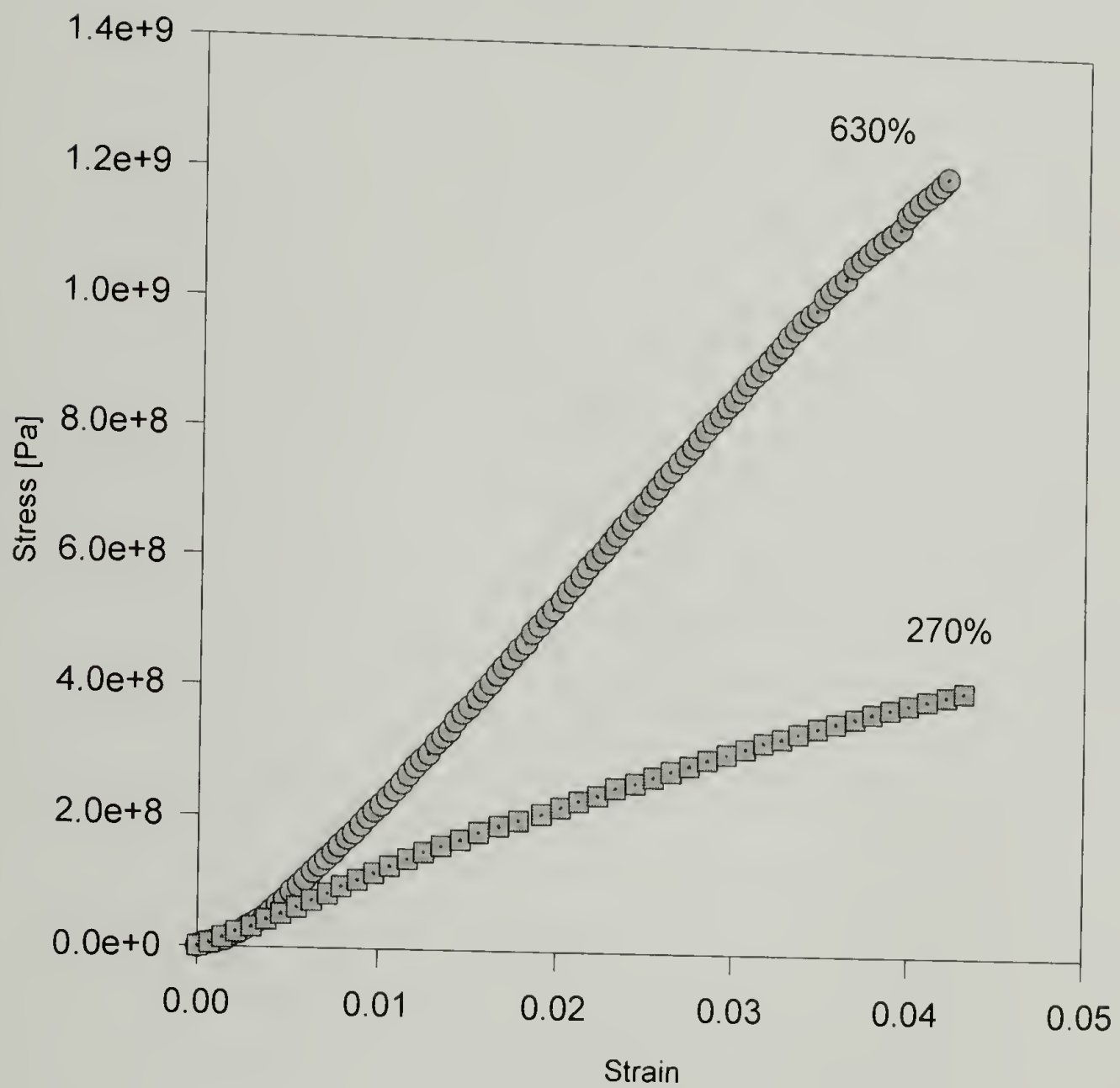


Figure 8.7. Stress-strain curves for the spandex fibers tested at liquid nitrogen temperature. The different curves correspond to different pre-elongation at ambient temperatures. Increase of the pre-elongation increases the linear stress-strain response.

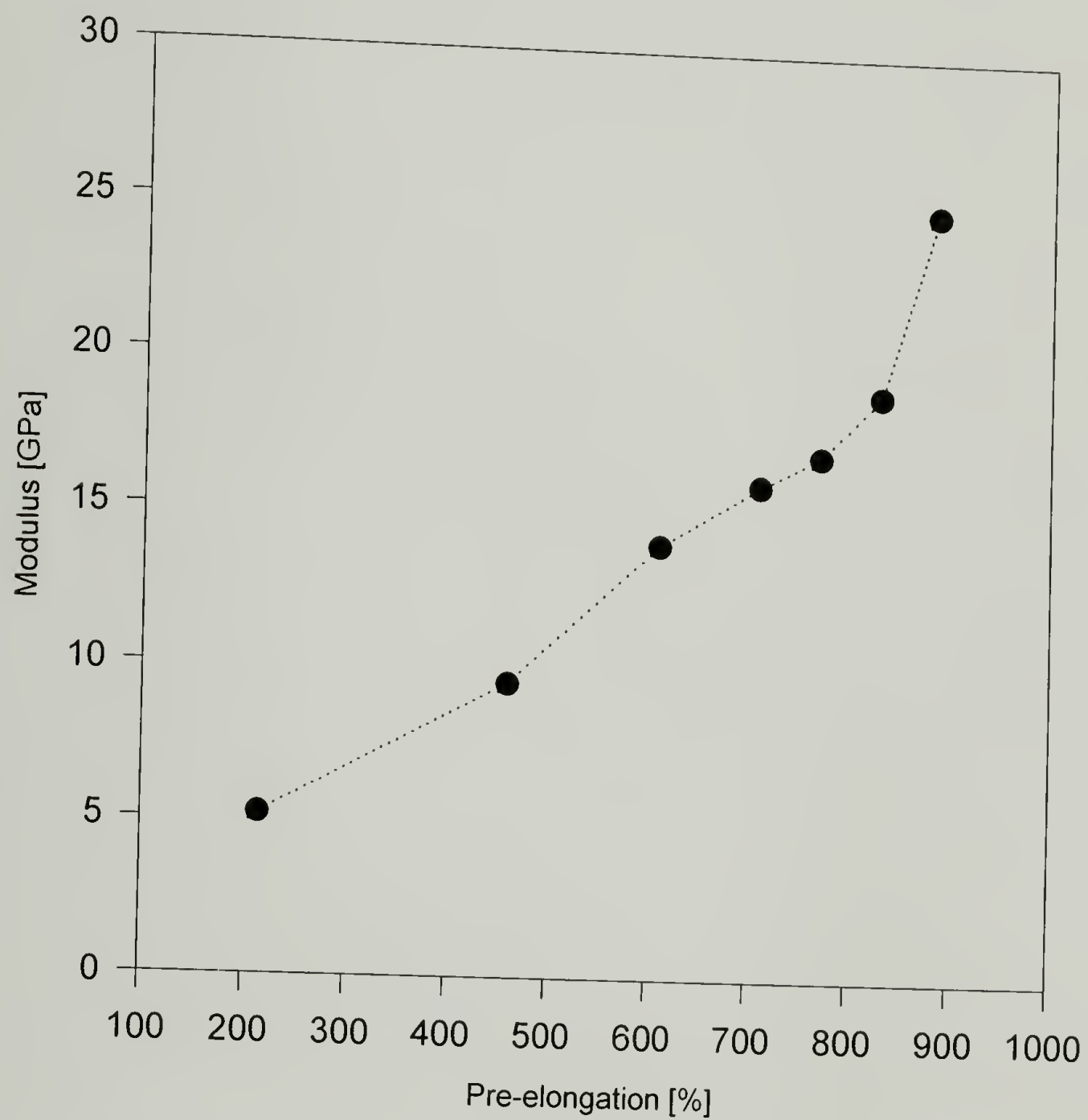


Figure 8.8. The modulus pre-elongation relationship for natural rubber samples tested at liquid nitrogen temperature.

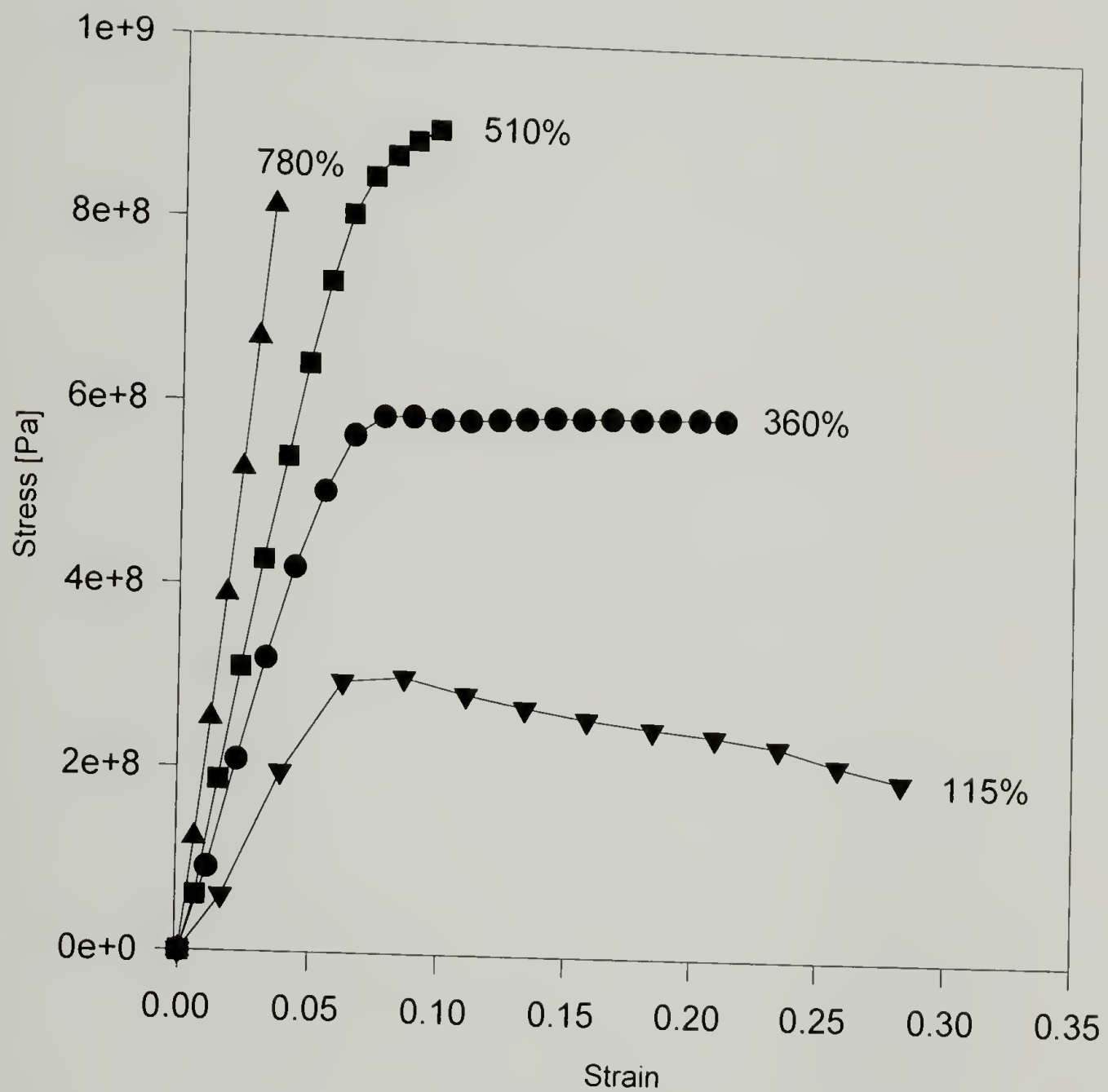


Figure 8.9. Stress-strain curves for the natural rubber samples tested at liquid nitrogen temperature. The different curves correspond to different pre-elongation at ambient temperature. Increase of the pre-elongation increases the linear stress-strain response.

Table 8.3. Mechanical properties of natural rubber samples tested at liquid nitrogen temperature. Pre-elongation is the elongation at room temperature, ϵ : the tensile strain at break, σ : the tensile stress at break, E: the elastic modulus.

Pre-elongation [%]	Modulus [GPa]	σ [GPa]	ϵ [%]
0	-	.05	96.3
115	5.2	0.2	28
360	9.5	0.6	21
510	14	0.9	9.7
610	16	0.61	3.9
670	17	0.67	4.0
730	19	0.84	3.8
780	25	0.82	3.3

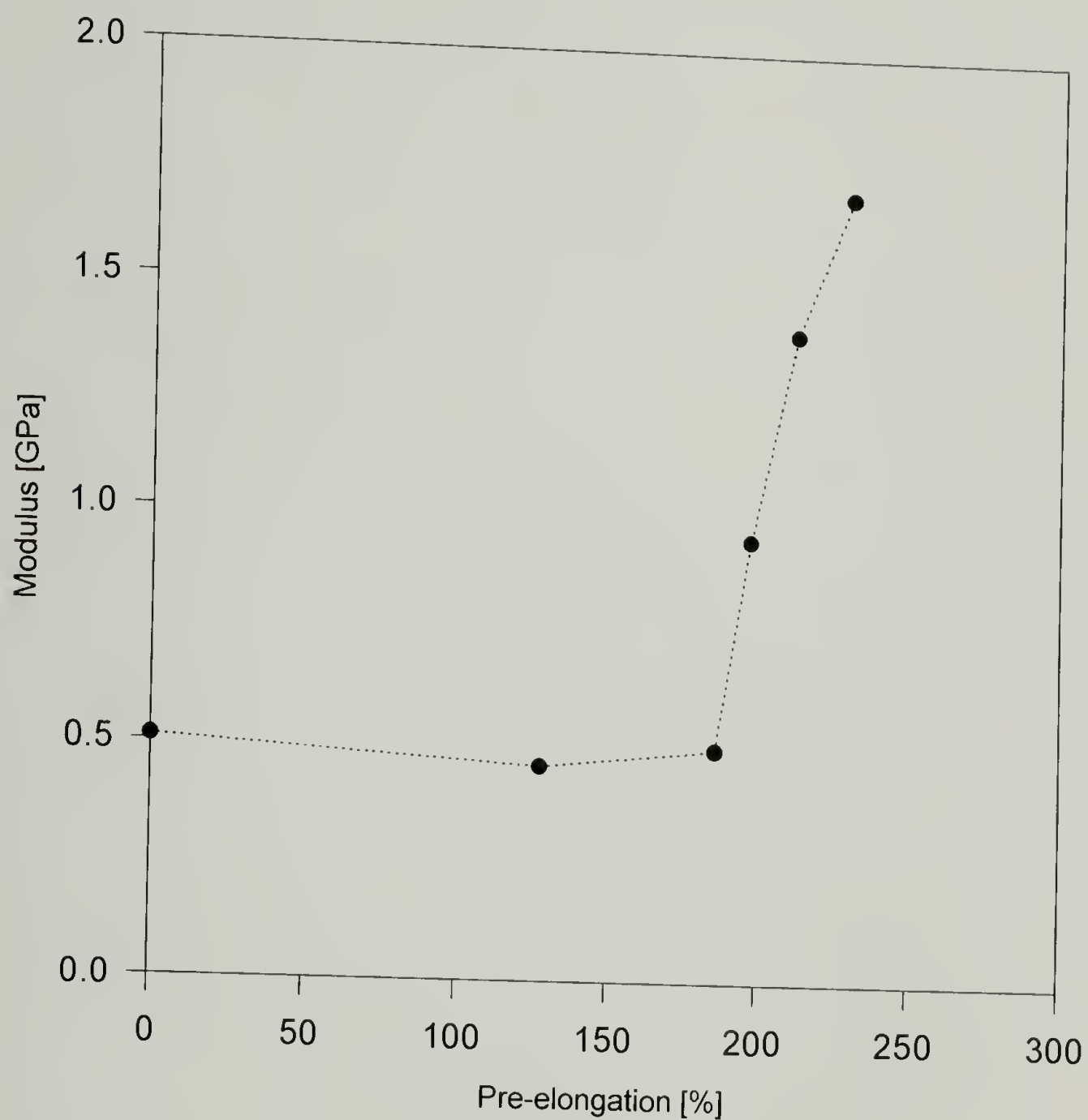


Figure 8.10. The modulus pre-elongation relationship for radiation crosslinked low molecular weight polyethylene samples tested at liquid nitrogen temperature.

Table 8.4. Mechanical properties of low molecular weight radiation crosslinked polyethylene samples tested at liquid nitrogen temperature. Pre-elongation is the elongation at room temperature, ϵ : the tensile strain at break, σ : the tensile stress at break, E: the elastic modulus.

Pre-elongation [%]	Modulus [GPa]	σ [GPa]	ϵ [%]
0	.51	0.1	118
128	.46	0.12	83
186	.5	0.1	42
197	.95	0.19	33
212	1.4	0.24	32
230	1.7	0.21	25

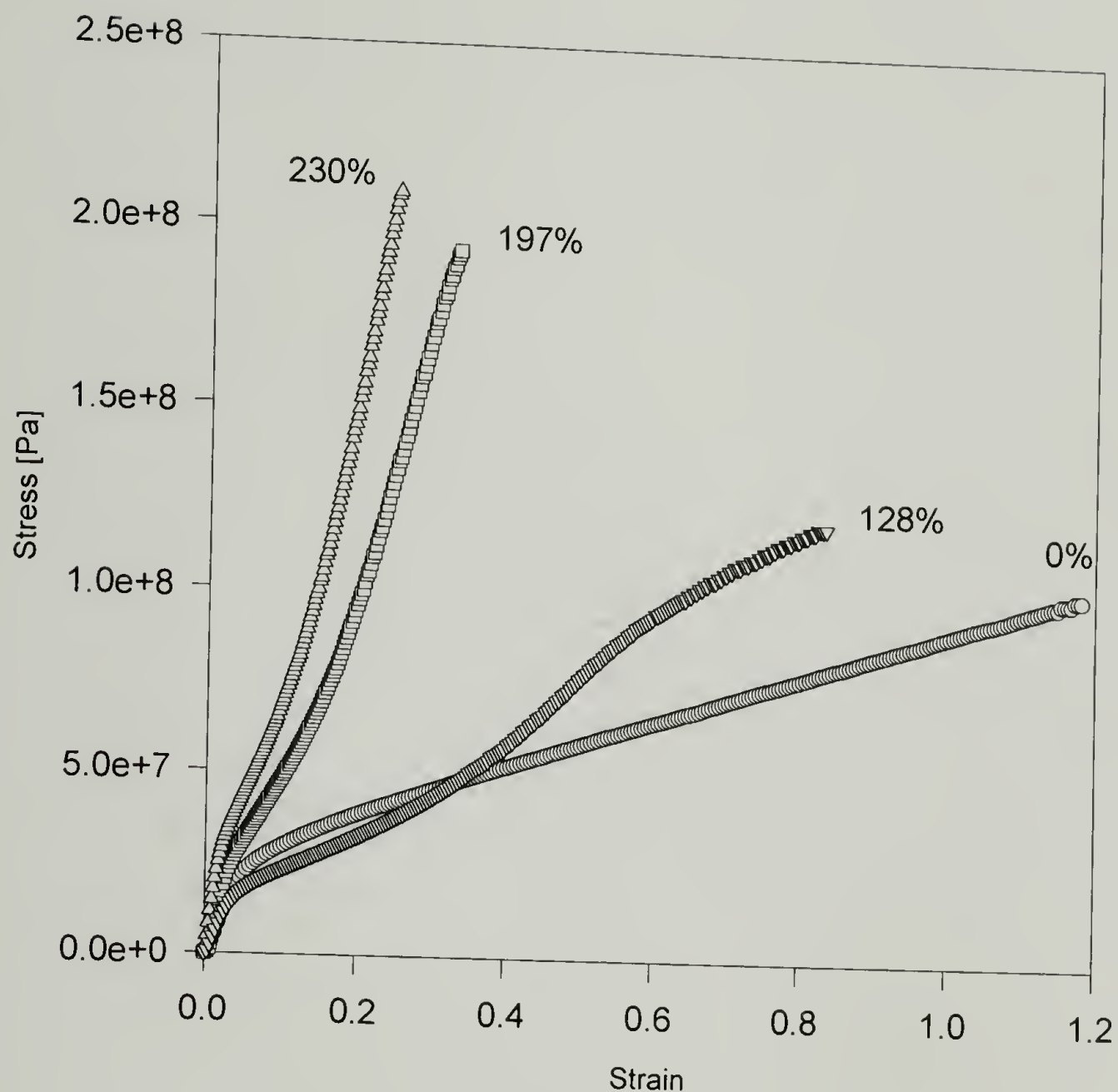


Figure 8.11. Stress-strain curves for the low molecular weight radiation crosslinked polyethylene samples tested at liquid nitrogen temperature. The different curves correspond to different pre-elongation at ambient temperature. Increase of the pre-elongation increases the linear stress-strain response.

Table 8.5. Mechanical properties of some common polymer fibers in comparison with rubber and polyurethanes oriented at ambient and tested at liquid nitrogen temperatures.

Polymer fiber	Young modulus, E [GPa]	Ultimate stress, σ [GPa]
Kevlar 49	124	2.8
Kevlar 29	62	2.8
Vectra	69	2.9
Du Pont nylon type 728	5.5	0.98
Dacron polyester type 68	13.8	1.1
PET	17	1.1
Silk	5	0.6
Nylon	1.4-3	0.05-0.09, 0.8 (oriented)
Polypropylene	9.5	0.71
Polyethylene	120	4.7
PVC	5.5	0.49
PAN	8.6	0.5
Oriented rubber	25	0.8
Oriented polyurethanes	29-32	1.0-1.2

REFERENCES

1. Treloar, G. R. L., "Introduction to Polymer Science", Wykeham Publications, London, 1970, ch. 4 p. 49
2. Aklonis, J. J., and MacKnight, J. W.: "Introduction to Polymer Viscoelasticity", Wiley-Interscience, New York, 1972, ch. 6
3. Malvern, E. L., "Introduction to the Mechanics of a Continuous Medium", Pentice-Hall, N.J., 1969, ch. 4 and 6
4. Bartenev, M. G., and Zuyev, S. Yu.: "Strength and Failure of Viscoelastic Materials," Pergamon Press Ltd., Oxford, 1968
5. Kargin, V. A., V. A. Bartenev, T. V. Gatovskaya Ye. Ya. Yaminskaya, DAN SSSR, **122**, No. 4,668 (1958)
6. Bartenev, V. A., T. V. Gatovskaya, V. A. Kargin, Ye. Ya. Yaminskaya, Viysokom. Soyed. **1**, 373 (1959)
7. Orlova, A. V., V. A. Bartenev, V. A. Kargin, Kauchuk I Rezima, No. **3**, 10 1963
8. Kinloch, A. J., and R. J. Young, "Fracture Behavior of Polymers", Elsevier Applied Science Publishers, N. Y., 1983, ch. 7 and 10

CHAPTER 9

SYNTHESIS AND CHARACTERIZATION OF POLY (ETHERIMIDE-b-STYRENE) ABA TYPE COPOLYMERS

9.1 Introduction

Chapter three describes the behavior of deformed rubber and rubber-like materials (i.e. thermoplastic elastomers) at liquid nitrogen temperatures where they become glassy. It was concluded that the orientation, which was imposed during the pre-elongation and retained by dropping the temperature below -140°C , significantly affects the material's mechanical properties. These materials exhibited moduli comparable to high performance fiber materials e.g. poly(ethylene terephthalate), PET. This was a significant result considering that it was achieved by simply stretching the materials. This, however is not a very practical procedure due to the fact that it was necessary to drop the temperature below -140°C in order to keep the polymer molecules extended. Low temperatures were necessary because rubber-like materials have soft segments with T_g 's below the ambient temperature. In order to be able to exploit the properties observed at more practical conditions, it will be necessary to shift the temperature range at which the transition from rubber to glass occurs. This directed the design of a block copolymer either A-B-A or $(A-B)_n$ type, that has a highly amorphous soft segment with a T_g above room temperature. Therefore, the copolymer that is glassy at ambient

temperatures could be brought to temperatures above the T_g of the soft segment for elongation experiments. When the temperature is increased sufficiently above the transition temperature, the material behaves as an elastomer. This "high temperature elastomer" is subjected to extensive stretching and after the maximum stretching (just before break) has been achieved, the polymer is quenched back to ambient temperature and the orientation of the soft chains (frozen in extended position) is retained to such a degree that a significant improvement in the mechanical properties of the material has been achieved.

9.2 Materials

The potential candidate segments for the design of the desired copolymer should satisfy certain basic requirements. The requirements are somewhat similar to the ones needed for the design of conventional thermoplastic elastomers [1,2]. The soft segment should exhibit a highly amorphous character for good extensibility. In addition, the ability for phase separation is critical in order to form a well defined soft matrix and the dispersed domains [3], fig.9.1. The soft segment also has to have good thermal stability and a decomposition temperature higher than the transition temperatures of the hard segment. On the other hand, the hard segment could be amorphous or crystalline, but it has to have a low enough T_g or T_m for convenient processability. It is also important to mention that the T_g of the soft segment and the T_g or T_m of the hard segment have to be

sufficiently far apart so that a large rubbery plateau will exist to enable adequate stretching.

The chosen soft segment was near monodisperse (1.15 polydispersity index) dicarboxylic acid-terminated polystyrene (~90%) with number molecular weight, ($M_n=69,000$) as determined by size exclusion chromatography. It was purchased in the form of white powder from Scientific Polymer Products, Inc. It was synthesized by anionic polymerization using difunctional catalysts and terminated with gaseous carbon dioxide. The functionalized polystyrene was used as received without any further purification. Polystyrene was chosen because it is a well studied polymer, it is highly amorphous with T_g in acceptable temperature range and with relative good thermal stability. Extensive data about the properties of polystyrene polymers and copolymers can be found in the literature [5-9].

The hard segment was highly diamino-terminated polyetherimide (Ultem) ($M_n=9,000$). The material was kindly provided to our laboratory by the General Electric Corporation. Polyetherimides are the most recently introduced polyimides (General Electric Co., 1982) and have the advantage of good processability. These polymers are synthesized by reaction of dianhydrides containing ether links and diamines [10]. For extensive aminotermination 3% excess of *m*-phenyl diamine was used to terminate the reaction [11].

All the other solvents and catalysts were purchased from Aldrich. Oxalyl chloride, 2.0 M in methylene chloride was packaged under nitrogen. Tetrahydrofuran was freshly distilled from sodium/benzophenone. Dimethylformamide and 4-dimethylamino-pyridine were used as received, while pyridine was freshly distilled from phosphorous pentoxide.

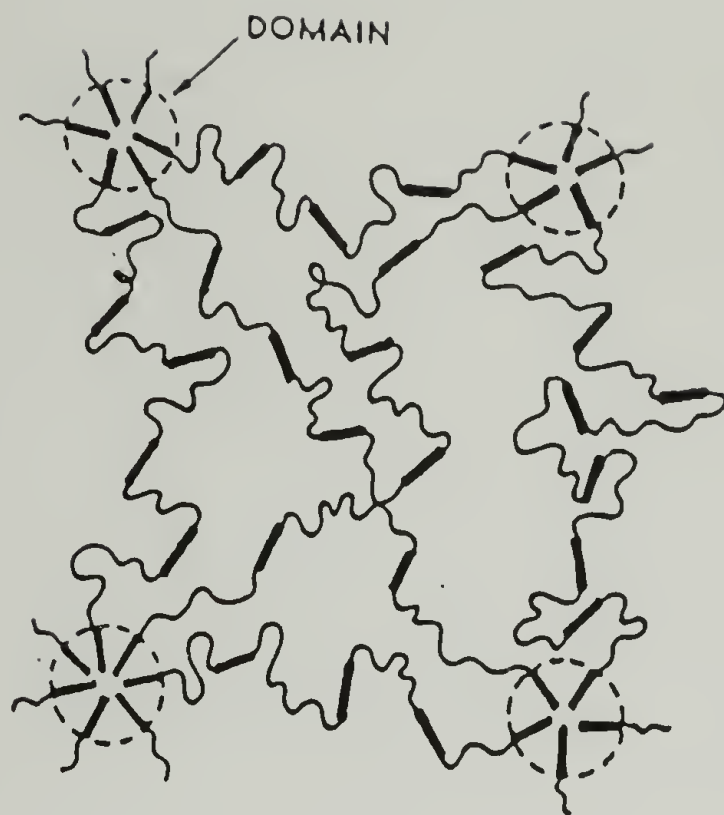


Fig 9.1. A general model for the morphology of $(AB)_n$ type copolymers [4].

9.3 Synthesis of the polyetherimide-b-polystyrene copolymer

The synthesis of the block copolymer involves reaction of carboxylic functional groups with aromatic amino-groups. Many different methods have been proposed for the reaction of these groups. Efforts to apply some of these methods proved to be unsuccessful. First, for the low temperature solution coupling, efforts were made to utilize two coupling agents 1,1-carbonyldiimidazole (CDI) [12-14] and 1,3-dicyclohexylcarbodiimide (DCC) [15-18], widely used in peptide synthesis. The CDI method showed very little activity and the reactions under various conditions produced extremely low yields, while using DCC under several different conditions again produced no reaction. (ntbk-B3, p.12-14, 20-21, 83-85, 95).

The reaction of the ammonium salt at high temperature (solid and molten state) did not work well [19-21]. Many different temperatures from 200 °C up to 300 °C and many different reaction times were used. In each case, however, extensive degradation of the materials was observed regardless of the reaction conditions -under nitrogen, argon, or vacuum- (ntbk-B4, p. 5-7, 10-11, 17, 22).

After the initial unsuccessful attempts it was decided to first convert the carboxylic acids to acyl-chlorides and then react the acid chlorides with the aromatic amines [22-25]. The following is a typical example of the procedure used for the synthesis of the copolymer, scheme 9.1. In the first step, 1 gram dicarboxylic acid-terminated polystyrene (HOOC-PS-COOH) was placed in a 250 ml Erlenmeyer reaction flask equipped with a ground joint and was dissolved with about 20 ml of 2 M oxalyl chloride in methylene chloride. After the polymer was dissolved one to two drops of N,N-dimethylformamide (DMF) were added to catalyze the reaction. The DMF changed the solution immediately from cloudy to clear. The flask was fitted with a reflux condenser and was left to reflux overnight with stirring under dry argon. After the reaction was finished, the excess of oxalyl chloride was removed along with methylene chloride using a water aspirator. The crude ClOC-PS-COCl was dissolved in 50 ml dry THF and approximately 5 ml pyridine was added. The solution was transferred to a 250 ml round bottom flask and was kept under argon until its use. In another 500 ml round bottom flask, 1 gram of diamino-terminated polyetherimide (H₂N-PEI-NH₂) was dissolved in 50 ml THF and 5 ml pyridine was added again along with approximately



Scheme 9.1. Poly(styrene-*b*-etherimide) ABA type copolymer.

0.5 gram of 4-dimethylamino pyridine (DMAP) as catalyst. The solution appeared yellowish and cloudy and contained a small insoluble amount of $\text{H}_2\text{N-PEI-NH}_2$. The solution was vigorously stirred with a magnetic stirrer while the solution of ClOC-PS-COCl was slowly added. The slow transfer of polystyrene ensures an excess of amine in the mixture. After the polystyrene solution was transferred, the flask was fitted with an argon inlet-outlet and was placed in an oil bath at about 60°C . The mixture was left to react under stirring for three days. The major color changes occurred during the first day where the mixture developed a permanent brownish coloration. After the three day period, the mixture was allowed to cool and the insoluble part was filtered from the solution. The filtered solution was placed in a separatory funnel and was washed first with 10% HCl to remove the pyridinium salts and then Na_2CO_3 to remove the excess of acid and finally three times with H_2O . The solution was filtered again to remove some additionally formed insoluble residue and the solvent was evaporated completely in a rotary evaporator and was replaced with methylene chloride. The polymer was precipitated from 90:10 methanol/water, dried under vacuum and re-dissolved in methyl ethyl ketone (MEK). The insoluble excess of $\text{H}_2\text{N-PEI-NH}_2$ was filtered off and the crude copolymer was re-precipitated again from methanol/water mixture and dried in vacuum. The reaction yielded 1 gram of crude copolymer which contained a small amount (5-6 %) of unreacted polystyrene. In an effort to separate the homopolymer from the copolymer, the product was shaken 3-4 times with warm cyclohexane which is a theta solvent for polystyrene at $\sim 35^\circ\text{C}$. The isolated polymer was dried overnight under vacuum and stored in the refrigerator (ntbk-B4, 41-45, 51-53, 62-64).

9.4 Characterization

9.4.1 Thin layer chromatography

Thin Layer Chromatography (TLC) was employed to verify the components in the functionalized samples. The stationary phase was silica gel (Whatman K5F 20x20 cm glass plates). TLC plates were cut into 5 x 10 glass strips and were placed in the oven at ~ 150 °C for a week before their use. Two different solutions (10% in methylene chloride) of the polymers were prepared for chromatographic use. The solvent system used for the functionalized polystyrene was a mixture of 60:40 carbon tetrachloride/methylene chloride. For the amino-terminated polyetherimide the solvent system was 70:30 1,2-dichloroethane/methylene chloride. The spots were visualized using a standard portable UV detector. The materials used for comparison were standard non-functionalized polystyrene and non-functionalized polyetherimide (Ultem). The separation of the applied spot to two distinctive spots, indicated the existence of a mixture of two components in both homopolymers. The two visualized spots for polystyrene indicated the existence of a non dicarboxylic acid-terminated and a dicarboxylic acid-terminated portion. The R_f values were 0 and 0.38 (R_f, distance traveled by substance/distance traveled by solvent). The R_f value for the standard polystyrene was 0.42. It is reported in the literature that during functionalization of the polymer with carbon dioxide some keto-groups are formed [27]. In the case of polyimide two spots were also identified and were attributed to mono- and di- amino-functional components. The R_f values in this case were 0 and 0.6.

9.4.2 Fourier transform infrared spectroscopy (FT-IR)

Infrared spectroscopy was used to examine the structural characteristics of the homopolymers and the block copolymer. The spectra obtained using a Nicolet IR/44 FTIR spectrometer. Solid samples were prepared using potassium bromide (KBr) pellets (~5% sample). Representative spectra of the homopolymers and the isolated copolymer are shown for comparison in fig. 9.2. The copolymer spectrum presented in fig. 9.3 shows the two C=O stretching peaks at 1780 cm^{-1} and at 1724 cm^{-1} attributed to polyetherimide. The aromatic ring C-C stretching peaks at 1584 cm^{-1} and 1602 cm^{-1} (attributed to polystyrene) and 1620 cm^{-1} to polyetherimide. The C-H stretching peaks at 1943 , 1870 , 1803 and 1745 cm^{-1} are the characteristic aromatic overtone patterns.

9.4.3 ^1H NMR spectroscopy

^1H NMR was another analytical technique used to discriminate the copolymer from the homopolymers. The instrument used was a Bruker AC 200 model. Samples were prepared by dissolving approximately 10 mg polymer in 1 ml of deuterated chloroform. The deuterated solvent contained 0.03 % tetramethylsilane as internal standard ($\delta=0\text{ ppm}$).

The ^1H NMR spectra of the homopolymers and the copolymer are depicted in Fig. 9.4. The spectrum obtained from the isolated copolymer shows the CH-H peak at 1.4 ppm and the C-H at 1.8 ppm due to polystyrene. The two sharper peaks at 1.6 and 1.8 ppm are attributed to $[\text{Ar}]_2\text{C}-[\text{CH}_3]_2$ due to bisphenol-A segment of the polyetherimide.

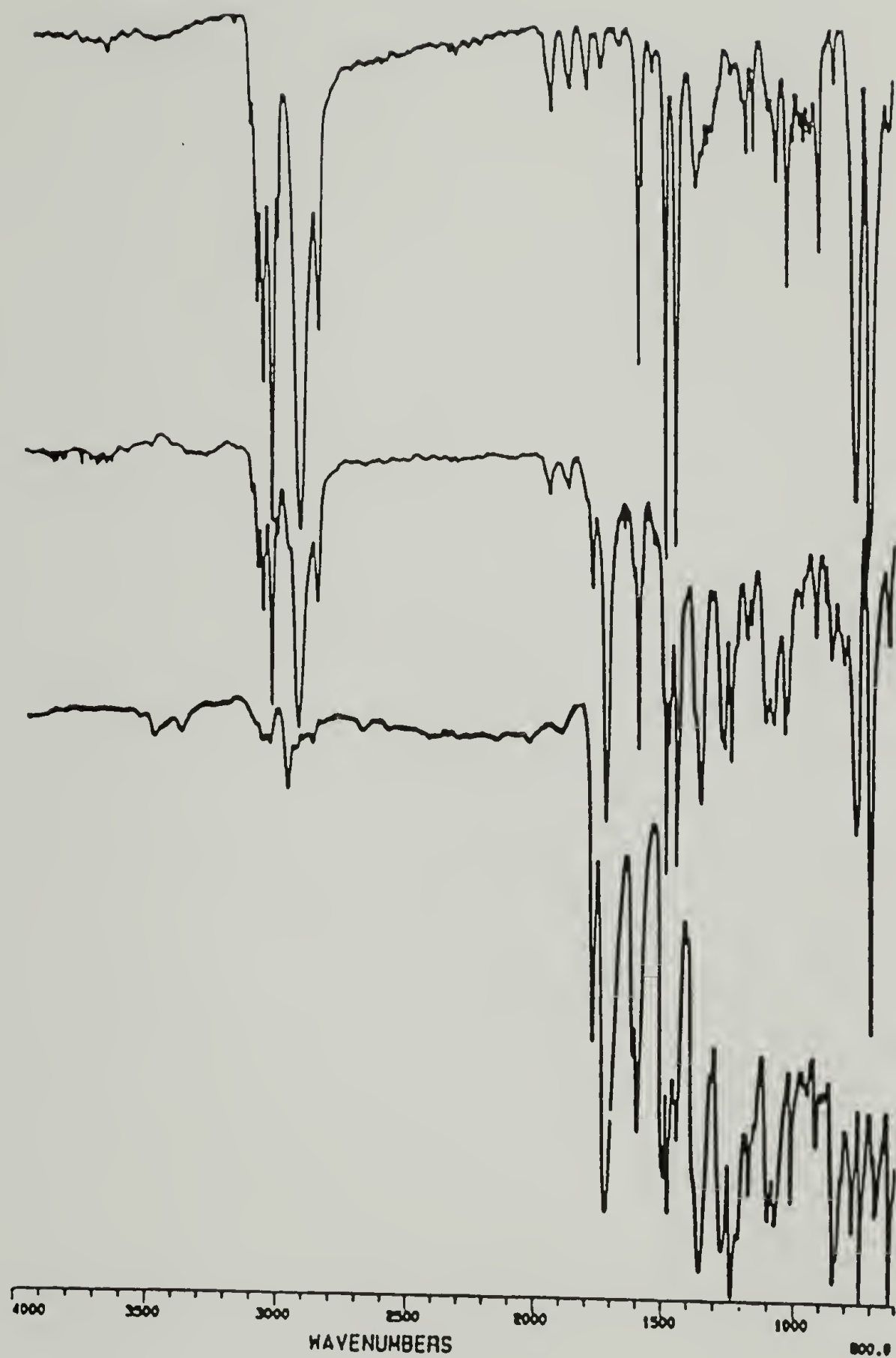


Figure 9.2. FT-IR spectra of the two pure homopolymers and their copolymer. The spectrum shown at the top is taken from the dicarboxyl-terminated polystyrene. The middle spectrum represents the copolymer and the one shown at the bottom is obtained from diamino-terminated polyetherimide.

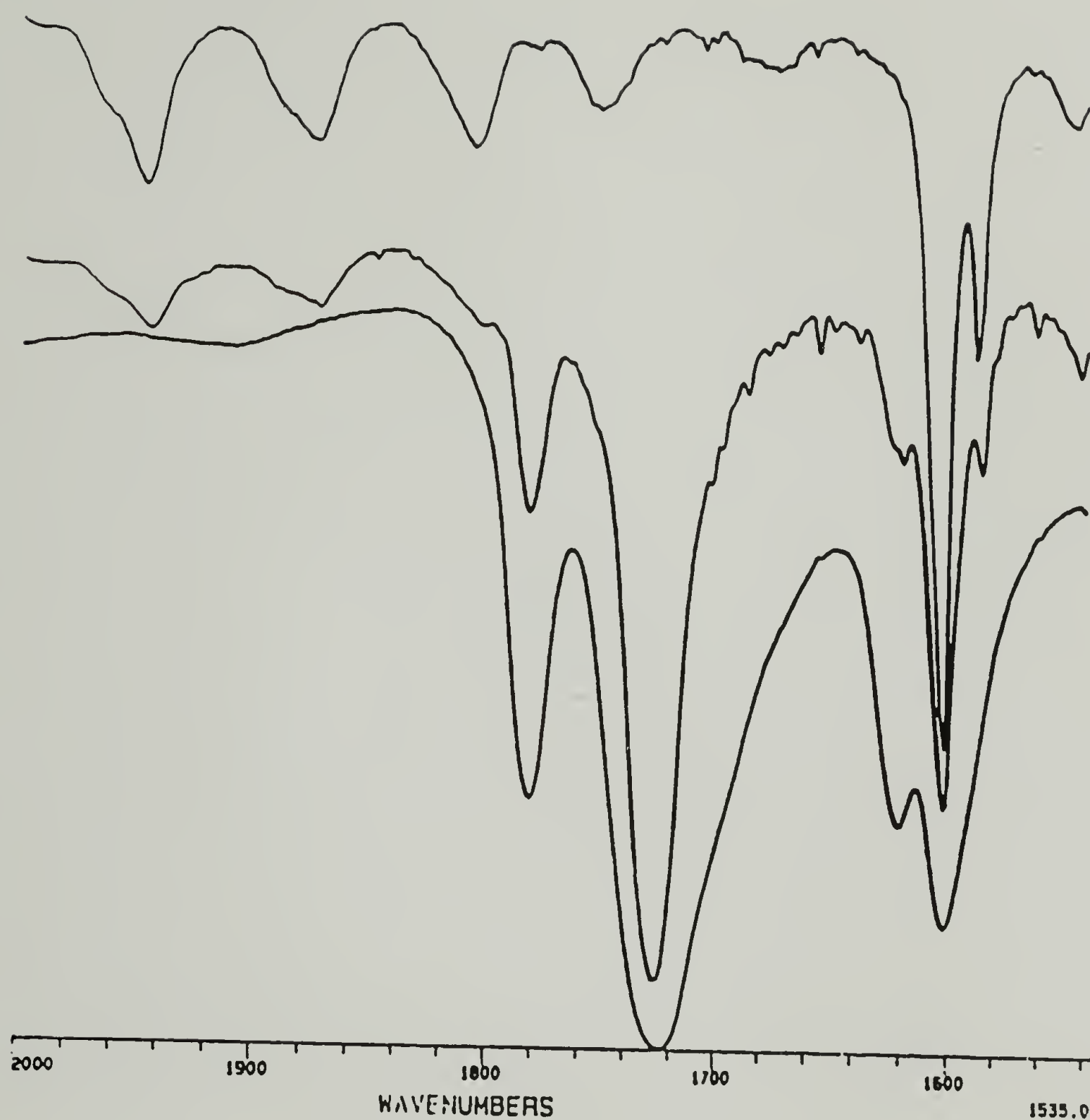


Figure 9.3. FT-IR spectra for the two pure homopolymers and their copolymer . The copolymer spectrum appears in the middle. The carbonyl peaks at 1780 cm^{-1} and 1724 cm^{-1} and the aromatic C-C peak at 1620 cm^{-1} are due to polyimide. The polystyrene segment is identified from the strong overtones and the aromatic C-C at 1584 and 1602 cm^{-1} .

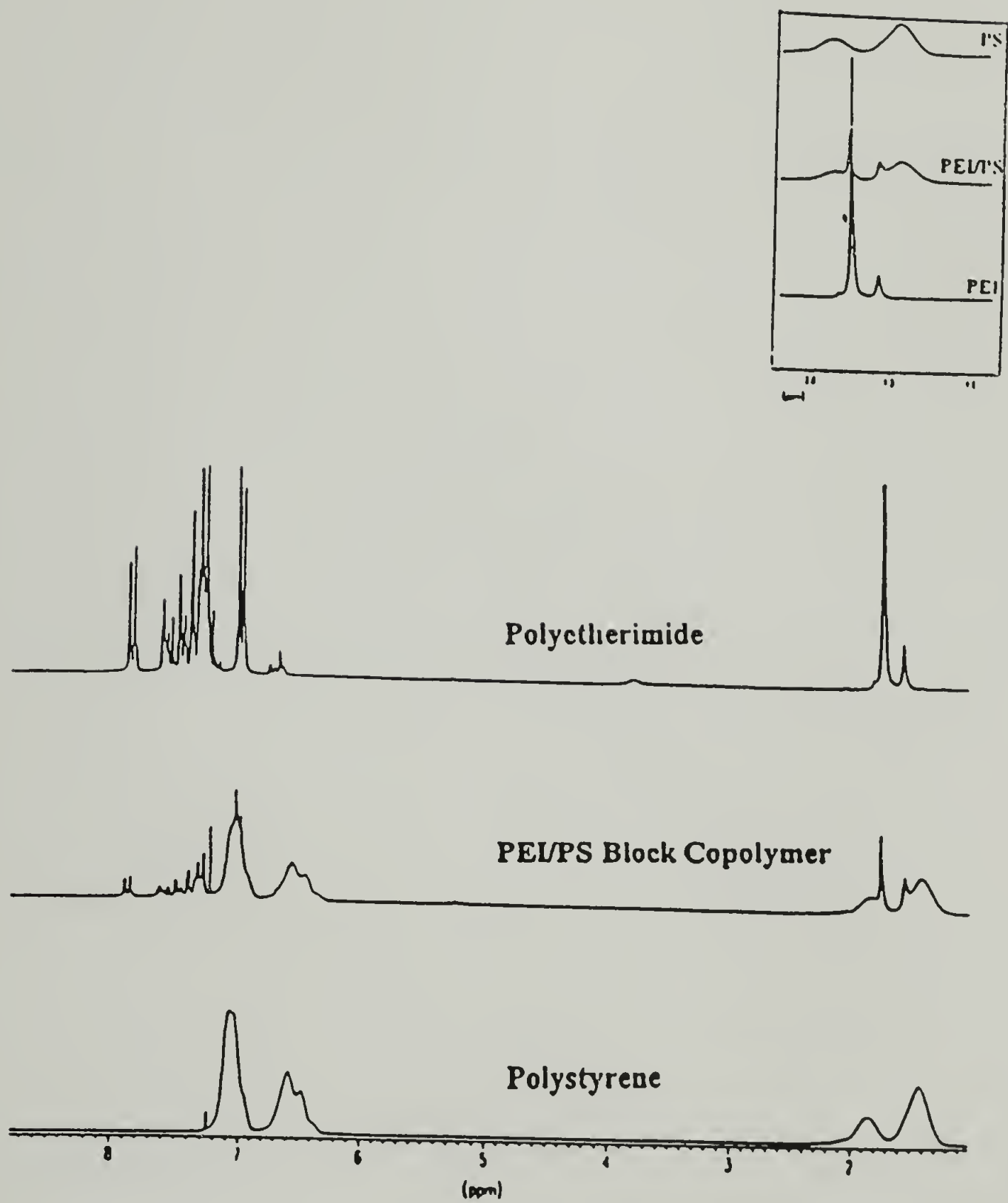


Figure 9.4. ^1H NMR spectra of the two pure homopolymers (polystyrene and polyimide) and their isolated block copolymer.

The observed peaks from 6.5 ppm to 7.9 ppm are due to the protons attached to the aromatic rings. The solvent peak appears at 7.25 ppm.

9.4.4 Solubility characteristics

The solubility of the pure homopolymers, homopolymer blends, and copolymer was examined for two reasons. First, solubility results helped to verify the existence of the block copolymer formed and second, solubility differences were used to separate the different components in the product mixture using solvent non-solvent fractionation. Homopolymer mixtures were very easy to separate using selective solvents. Sequential extraction with selective solvents results in pure homopolymer materials. The copolymer behavior however, was more difficult to explain. The complications arise from the presence of the two dissimilar segments. For a block copolymer A-B-A the relative ability to dissolve in a solvent selective to A or B depends on which segment predominates [28]. For example, if A is the major component, then the copolymer will be completely soluble in A selective solvents. The obtained results are reported in table 9.1.

9.5 Conclusions

The desired copolymer A-B-A poly(etherimide-*b*-styrene) was synthesized. The synthetic method involved the reaction of acid chlorides with aromatic amines. Oxalyl chloride proved to be the most effective reagent for this reaction; more effective than thionyl chloride. The various synthetic methods described in the literature did not

provide satisfactory results. The low reactivity of the aromatic amines created some difficulties. In addition, another serious problem was the sensitivity of amino-terminated polyetherimide to thermal degradation. The isolation of the copolymer was not complicated until the step required for the removal of the unreacted polystyrene from the isolated copolymer., This step, however was not critical as long as the amount of contamination with homopolymer remained small. It is reported in the literature that low impurities of the homopolymer does not affect the properties of the copolymer [5]. For example, the tensile strength of the ABA block copolymer of styrene-b-butadiene is unaffected from the presence of free polystyrene (up to 20% by wt.) and only slightly affected by the presence of free polybutadiene (up to 5% by wt.). Analysis of the copolymer was performed using TLC, FT-IR, and ^1H NMR.

Table 9.1. The solubility characteristics of functionalized polystyrene, polyetherimide and their copolymer. Solubility characteristics were determined using 10 mg/5 ml solvent.

Solvent	HOOC-PS-COOH	H ₂ N-PEI-NH ₂	Copolymer
Methyl ethyl ketone	good	poor	good
Cyclohexane	good (hot)	poor	marginal(hot)
Toluene	good	poor	good
Cyclohexanone	good	good (hot)	marginal (hot)
Dimethyl formamide	good	good	good
Dioxane	good	good (hot)	good
Tetrahydrofuran	good	marginal	marginal
Methylene chloride	good	good	good
Dimethyl sulfoxide	poor	good (hot)	poor

REFERENCES

1. Herburn, C., "Polyurethane Elastomers", Elsevier Applied Science, N. Y., 1992, ch. 3 p. 51
2. Allport, C. D., and Janes, H. W., eds: "Block Copolymers", Halsted Press, New York, 1973, ch. 8c
3. Dawking, V. J., in "Block Copolymers", eds: Allport, C. D. and Janes, H. W., Halsted Press, New York, 1973, ch. 8a
4. LeGrand, D. G., J. Polymer Sci., **B7**, 579 (1969)
5. Allport, C. D., and Janes, H. W., eds: "Block Copolymers", Halsted Press, New York, 1973 ch. 8b, p. 423
6. Harper, A. C., "Handbook of Plastics and Elastomers", McGraw-Hill, Inc., 1975 Ch. 1 p. 94
7. Haward, N. R., ed: "The Physics of Glassy Polymers", John Wiley & Sons N. Y., 1973
8. Yoshida, M., J. J. Ma, K. Min, J. L. White, and R. P. Quirk, Polymer Eng. and Sci., **30**, 30 (1990)
9. Boundy, R. H., R. F. Boyer, eds: "Styrene Its Polymers, Copolymers and Derivatives", part 1-3, Hafner Publishing Co., CT, 1970
10. Saunders, J. K., "Organic Polymer Chemistry", Chapman & Hall, N. Y., 1988 ch. 10 p 220
11. Athanasiou, C., Private Communication, 1995
12. Stabb, H. A., Agnew. Chem. Internat. Edit., 1, 351 (1962)
13. Anderson, G. W., and R. Paul, J. Am. Chem. Soc., **80**, 4423 (1958)
14. Paul, R., and G. W. Anderson, J. Am. Chem. Soc., **82**, 4596 (1960)
15. Khorana, J., Chem. Revs., **53**, 145 (1953)
16. Khorana, J., Chem & Ind. (London), **1955**, 1087.
17. Smith, Moffatt, and Khorana, J. Am. Chem. Soc., **80**, 6204 (1958)

18. Khorana, J., Chem. Soc., **1952**, 2081
19. Kaoru Ozakaki, Asaharu Nakagawa, Yuzaburo Nakayama, and Kenji Sugii, Toyo Rayon Kabushiki Kaisha, Co., Japan 3,493,632, 2.3.70, Japan
20. Braun, D., H. Cherdron and W. Kern, "Practical Macromolecular Organic Chemistry", Hardwood Academic Publishers, N. Y., 1984 ch. 4, p. 257
21. Sorenson, W. R., and T. W. Campbell, "Preparative Methods of Polymer Chemistry", Interscience Publishers, N. Y., 1968 ch. 3
22. Morgan, P. W., and S. L. Kwolek, J. Polymer Sci., **A2**, 181 (1964)
23. Wolfrom, M. L., M. S. Troy, and A. Chaney, J. Am. Chem. Soc., **80**, 6328 (1958)
24. Jablonski, R. J., J. M. Witzel and D. Kruh, Polymer Letters, **8**, 191 (1970)
25. Linstromberg, W. W., and H. E. Baumgarten, "Organic Experiments", D. C. Heath & Co., MA, 1987, p. 285
26. Pavia, D. L., G. M. Lampman, G. S. Kriz, Jr., "Introduction to Organic Laboratory Techniques", W. B. Saunders, Co., PA, 1976, p. 599
27. Iyengar, D. R., Ph.D. Dissertation, University of Massachusetts, **1992**
28. Noshay, A., and J. E. McGrath, eds: "Block Copolymers", Academic Press, New York, 1977, ch. 4, p. 49

CHAPTER 10

THERMAL AND MECHANICAL PROPERTIES OF UNORIENTED POLY (ETHERIMIDE-*b*-STYRENE) ABA COPOLYMER

10.1 Introduction

Chapter four described the synthesis and analysis of the block copolymer. In this chapter the thermal and mechanical properties will be reported, discussed and possible future directions will be suggested. Thermogravimetric analysis data was obtained using a TA Instruments Thermogravimetric Analyzer (TGA). A predetermined amount of sample powder (~10mg) was placed in a platinum sample holder and was heated to 700 °C under nitrogen. The heating rate in all cases was 10 °C/min. The degradation profile was recorded.

Differential Scanning Calorimetry (DSC) was employed to determine the glass transitions of the materials. A TA Instruments calorimeter was again used. Approximately 10 mg of sample was enclosed inside a non-hermetic sample pan and was heated under nitrogen to about fifty degrees above the expected T_g . The heating rate was again 10 °C/min. Two heating cycles (heat-cool) were recorded each time. The second cycle is reported in every case.

Information about the existence of a rubbery plateau was obtained using a Polymer Laboratories Dynamic Mechanical Thermal Analyzer (DMTA). The data was

obtained using single cantilever bending tests [15]. Sample molds were prepared using a Carver Laboratory Press. The polymer powder was placed between two thin polyimide films and the films were placed against two brass plates. The plates were introduced to the preheated press (at 250 °C) and allowed to stay inside for approximately 10 minutes under very slight pressure. Sample dimensions were approximately 0.6x12x20 mm. The prepared sample was placed in an oven head connected to the DMTA and was heated under nitrogen to 250 °C. The heating rate was 2 °C/min. The applied frequency was 10 Hz.

10.2 Thermal properties

Thermogravimetric analysis is considered the most important method to study polymer stability and decomposition [1]. However, there are other unique applications of this technique, among them the determination of additives [2], cross-linking [3] and the characterization of polymer blends and copolymers [4-6]. Thermogravimetry was used here to examine the thermal characteristics of the copolymer and homopolymers, as well as to determine the copolymer composition. The thermograms depicted in fig. 10.1 show the thermal decomposition of the pure homopolymers and of the block copolymer. The various important temperatures are tabulated in table 10.1. It is clear that in the case of the block copolymer decomposition, two distinctive mechanisms are followed which are due to the two different segments. It is also noticeable that the polystyrene segment in the copolymer starts to degrade slower (385 °C) than does the polystyrene homopolymer

Table 10.1. The various decomposition temperatures and the weight loss for the ABA block copolymer and the homopolymers used as A and B segments, T_i : initial decomposition temperature (~ 2 %wt lost), T_d : temperature at the maximum decomposition rate, T_f : the final decomposition temperature. The W_f is the corresponding residual weight percentage. The temperatures enclosed in parenthesis correspond to the polymer blend.

	Polystyrene	Copolymer /(Blend)		Polyetherimide
	homopolymer	A	B	homopolymer
T_i ($^{\circ}\text{C}$)	368	385 (350)	~ 500 (443)	500
T_d ($^{\circ}\text{C}$)	418	430 (410)	525 (511)	533
T_f ($^{\circ}\text{C}$)	448	458 (443)	—	552
W_f (%)	0.67	20	10	65

(368 °C). On the other hand, the polyetherimide segment seems to have thermal stability closer to homopolymer. A comparison of the thermal stability of the block copolymer with a polymer blend of the same components is shown in fig 10.2. The blend was made from dissolution of the two components in methylene chloride (60:40 by wt. polystyrene/polyetherimide).

The composition of the block copolymer can be calculated from the initial sample weight and the relative residual weights of the two components. For example, the initial weight of the sample was 6.1930 mg while the weight loss during the first degradation is due to polystyrene content in the copolymer, fig. 10.1 (5.0163 mg or 7.7×10^{-5} moles). The residual mass left after the first degradation is 1.1767 mg (13.1×10^{-5} moles); this is the polyetherimide content. Therefore, according to the above values, the calculated molecular weight is $M_n=80,247$. The polystyrene to polyetherimide ratio is 1:1.7 implying 85% conversion.

Differential Scanning Calorimetry (DSC) is used mainly to study the physical transitions, although reactions such as degradation [7], polymerization [8,9] and oxidation [10,11] can readily be studied. DSC can be used for heat capacity [12], crystallinity [13] and purity [14] measurements. DSC is used here to determine the glass transitions of the homopolymers and the block copolymer. The thermograms illustrated in figure 10.3 are representative for the corresponding polymers. The copolymer shows two characteristic glass transitions which indicate the phase separation of the two copolymer segments. The first T_g is located at 102 °C and the second at 210 °C. The T_g of pure polystyrene homopolymer was 92 °C and that of the polyetherimide 197 °C.

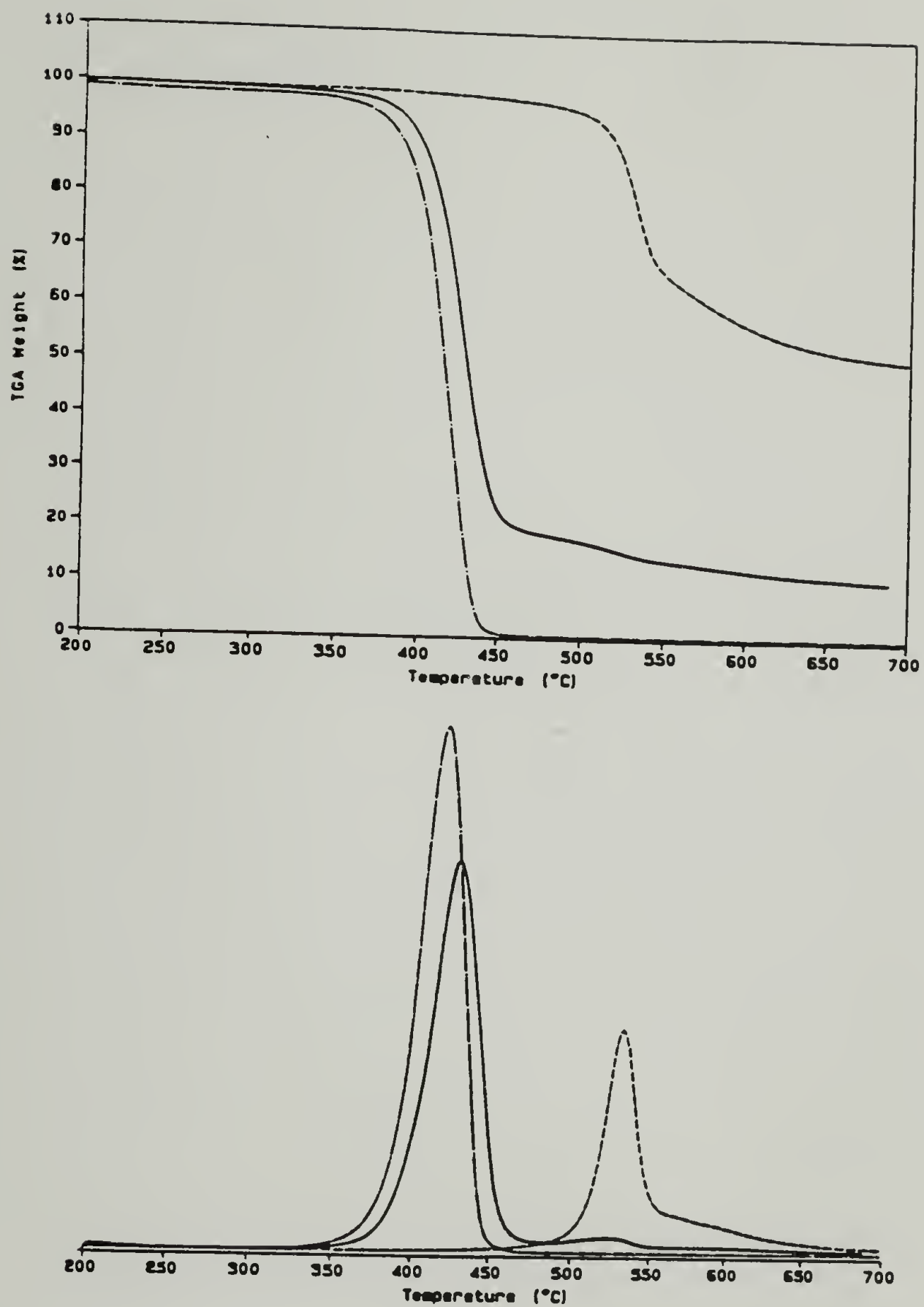


Figure 10.1. At the top are the thermograms (TGs) of the polystyrene homopolymer (—•—), polyetherimide (— —) and the block copolymer (—). At the bottom are the differential thermograms (DTGs) of the same polymers.

10.3 Mechanical properties

Dynamic mechanical thermal analysis (DMTA) of polymers over a wide range of temperature and frequency provides detailed information about the structure (chemical and physical) and their characteristic properties [15]. Variation of the dynamic storage modulus (E' or G') and the damping factor ($\tan \delta$) with temperature and frequency allow characterization of the viscoelastic properties of a particular polymer [16]. DMTA can be used to determine, among other things, the effects of phase type and morphology on properties and performance. This technique is used here as a tool to determine the glass transition temperatures of our polymers and the rubbery region of the copolymer. The copolymer behaves as a glass ($E' < 10^9$ Pa) at ambient temperatures and shows a catastrophic modulus drop ($E' \sim 10^6$ Pa) at the T_{gA} (~ 100 °C). The second transition occurs when the temperature approaches 215 °C which is the T_{gB} , Fig. 10.4. It was concluded from the results shown in fig. 10.4 that the useful temperature gap is from 150 °C to 200 °C. This temperature range will be used to heat the copolymer in order to induce orientation by stretching.

10.3.1 Sample preparation for tensile testing:

Extensive efforts to produce films that would enable mechanical testing proved to be unsuccessful. Two methods were used for the film formation. In the first method the samples were prepared using a Carver Laboratory Press equipped with vacuum capabilities.

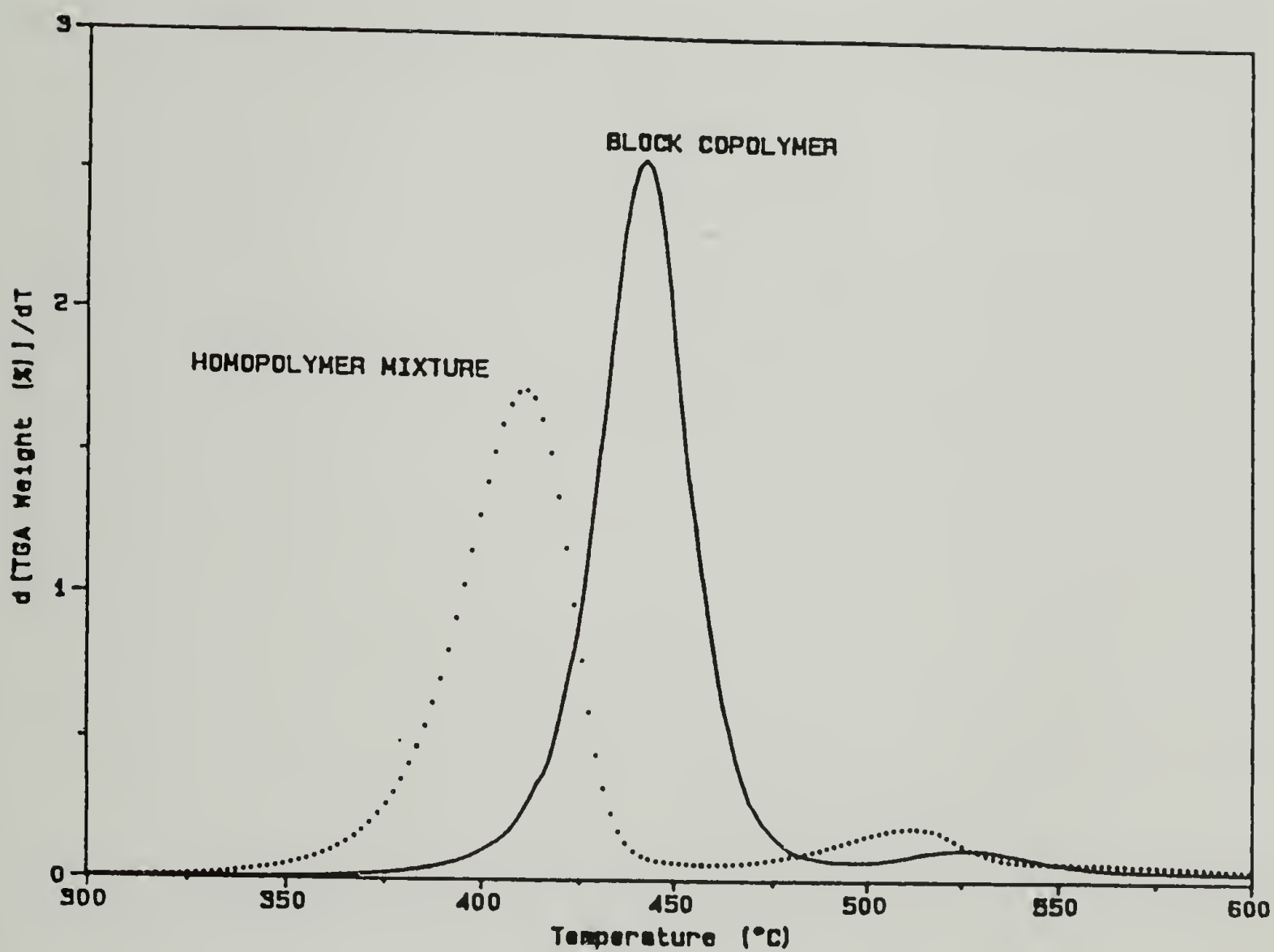


Figure 10.2. Differential thermograms (DTGs) of a dicarboxyl-terminated polystyrene-diamino-terminated polyetherimide blend and of the block copolymer.

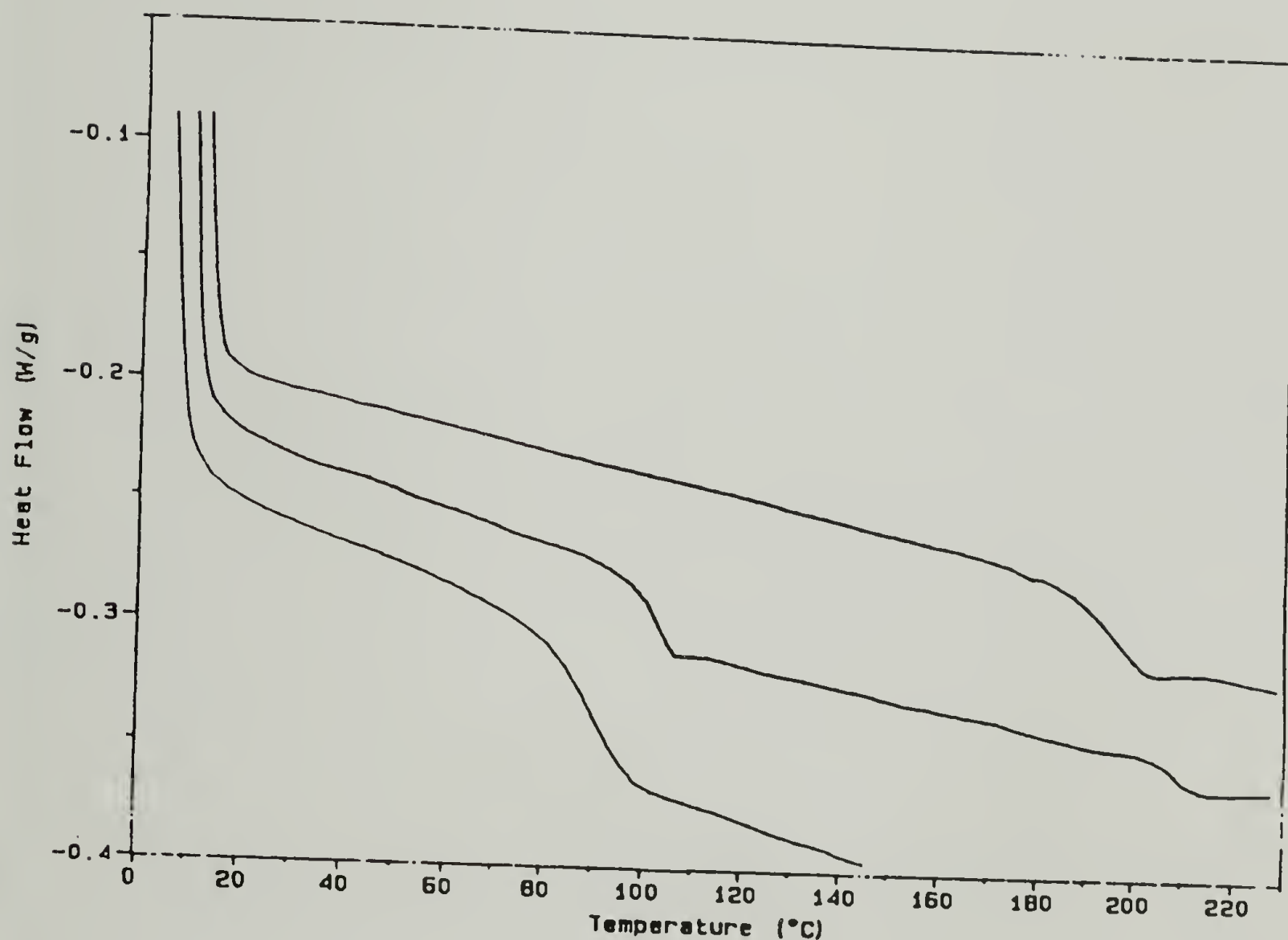


Figure 10.3. DSC thermograms of the two homopolymer components and the block copolymer. The thermogram at the top is obtained from the polyetherimide ($T_g=197\text{ }^{\circ}\text{C}$), the bottom is from the polystyrene ($T_g=92\text{ }^{\circ}\text{C}$) homopolymer. The copolymer thermogram is depicted in the middle ($T_{gA}=102$, $T_{gB}=210$).

The copolymer powder was placed between two thin polyimide films and the films were placed against two brass plates. The plates were introduced in the preheated press (at 250°C) for approximately 5 minutes under vacuum with zero applied pressure. Then minimal pressure was applied for another five to ten minutes. After the pressure and vacuum were released, the samples were allowed to cool slowly before they were removed. The films were extremely brittle and it was almost impossible to detach them from the polyimide films without them developing extensive cracks and eventually breaking in pieces. In the second method, 8 g of the copolymer was dissolved in 50 ml of methylene chloride which is a good solvent for the copolymer. The beaker was left open for the solution to concentrate to a desirable point (thick viscous) and then was closed. The viscous solution was spread inside a glass doubled-open cylinder (60 mm inside diameter) sitting on a teflon sheet. The whole setting was enclosed to allow slow solvent evaporation. The films produced with this method were also very brittle with many cracks and microvoids. In an effort to avoid cracking and produce ring shaped samples, this method was modified. Two systems of two glass cylinders, one inside the other, were used. The outside cylinders had inside diameters 60 mm and 50 mm and the inside cylinders had outside diameters 30 mm and 38 mm. The viscous solution was spread again over a teflon sheet and allowed to sit until the solvent was slowly evaporated to the point where the material was still soft and rubbery. At this point the constraints were removed to allow complete solvent evaporation. Even though the cracks presented a smaller problem with this technique, the voids persisted in spite of efforts to delay the rate of evaporation for as long as possible.

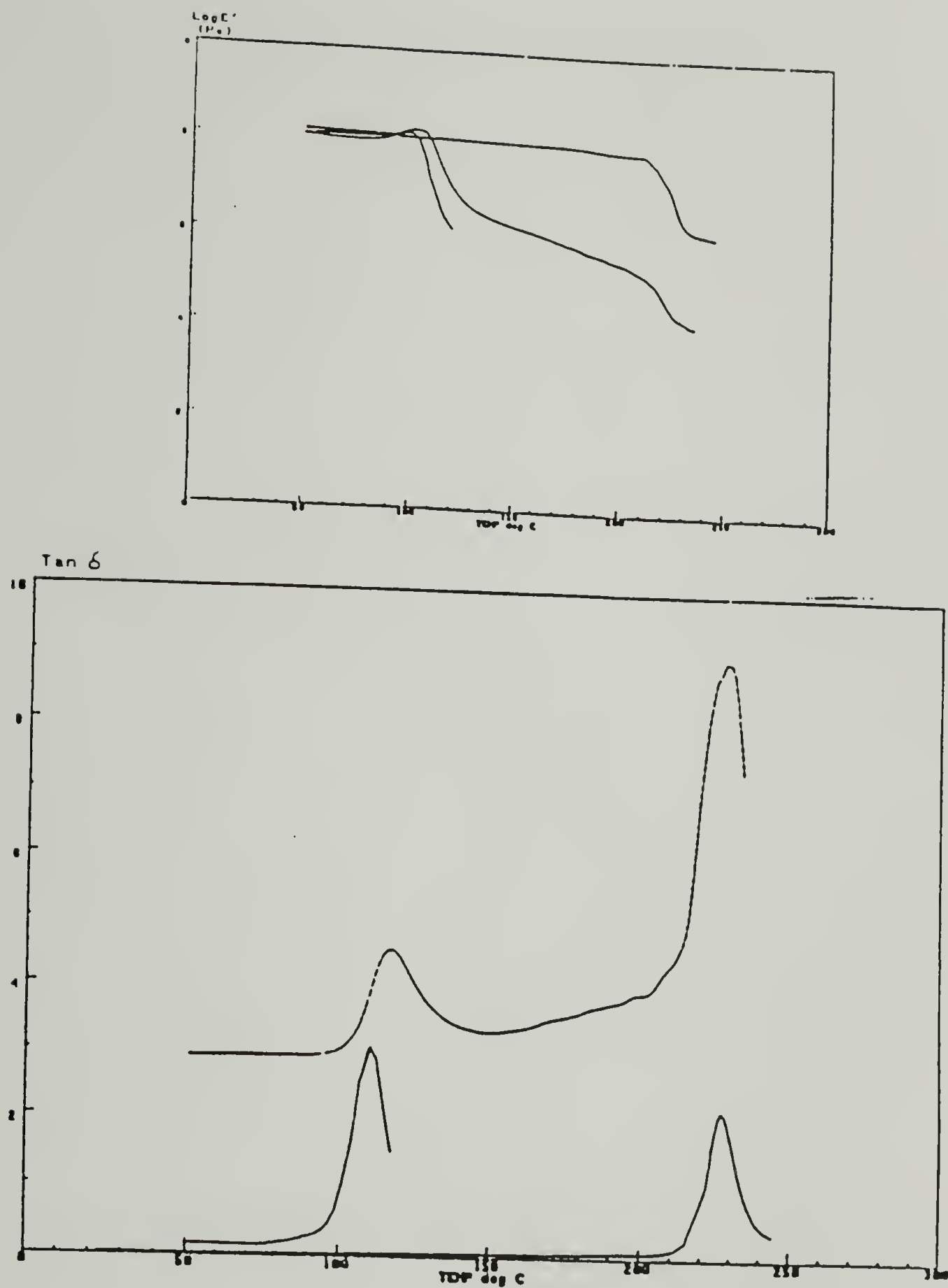


Figure 10.4. Dynamic mechanical thermal analysis (DMTA) of the block copolymer and the two homopolymer segments. The variation of the dynamic moduli is displayed on the top. The change in dumping factor, $\text{tan } \delta$, illustrated at the bottom plot.

It was however possible, to prepare small sample strips, for tensile testing, cut from the cracked films. It was also possible to extend them to a certain degree before testing, but it was impossible to test them as they were very brittle and could not be handle.

The extremely brittle behavior and the weakness of the copolymer films could be attributed to the low molar mass of the soft segment (polystyrene). The effect of molar mass upon the tensile strength and the fracture energy for polystyrene is depicted in fig. 10.5 and 10.6 [17, 18]. Measurements on many glassy polymers have shown that low molar mass polymers have very low tensile strength [17, 19-21] and very low fracture energies [22-24]. The strength and fracture energy, however, increases rapidly as the molar mass increases and levels off at critical molar mass above which the effect is insignificant.

It has been reported in the literature [25] that the “zero” molar mass (M_0), fig. 10.5, for polystyrene is 50,000 (for polyethylene 2,200) and it is correlated with the molar mass at which entanglements start to form, M_e , (35,000 for polystyrene and 1,100 for polyethylene).

The polystyrene molecular weight of 65,000 in this work was selected based on two considerations. First, the molecular weight had to be higher than the reported M_0 but as low as possible to minimize the entanglement effect on the orientation during stretching. If, therefore, the very low fracture energy and strength observed for the copolymer is due to low molar mass, a compromise needs to be made between the entanglement effect and strength.

10.4 Conclusions and future work

The block copolymers showed a decomposition behavior which was consistent with the degradation of the individual segments. Thermogravimetric data also confirmed the relative composition and molecular weight of the block copolymer. Differential scanning calorimetry revealed two glass transition temperatures close to the ones found for the individual components. This was a good indication for phase separation in this system. Dynamic mechanical thermal analysis data suggested that the rubbery region appropriate for pre-elongation of the material was between 150 °C and 200 °C. The preparation of samples for tensile test, however, exposed certain problems. The prepared samples were very weak, brittle and with many voids. Even though both components of the copolymer are glassy and polystyrene is also brittle, the extreme brittle behavior is considered to be unusual and could be attributed to the low molecular weight of the soft segment.

It is suggested, therefore, as a first step in a future direction, to examine the possibility of increasing the molecular weight of the soft segment to a level at which it would not affect the fracture energy and the strength of the material, (fig. 10.5 and 10.6). The use of a different system might be a possibility in future work. A soft segment with high theoretical modulus and strength (i.e. polyethylene, polypropylene etc.) could be a choice.

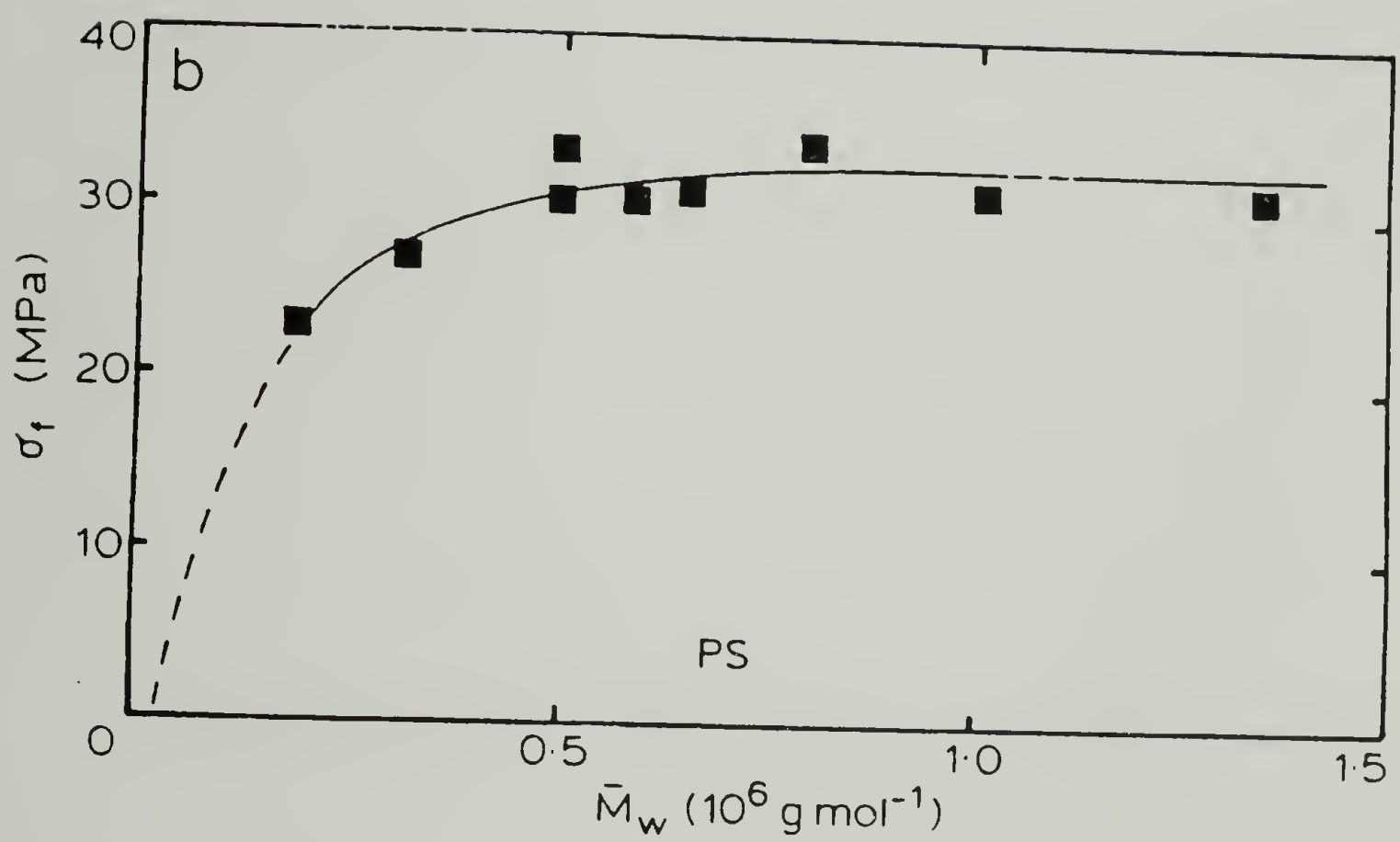


Figure 10.5. Dependence of fracture stress, σ_f , upon molar mass for polystyrene. The “zero” stress molar mass, M_0 , is 50,000.

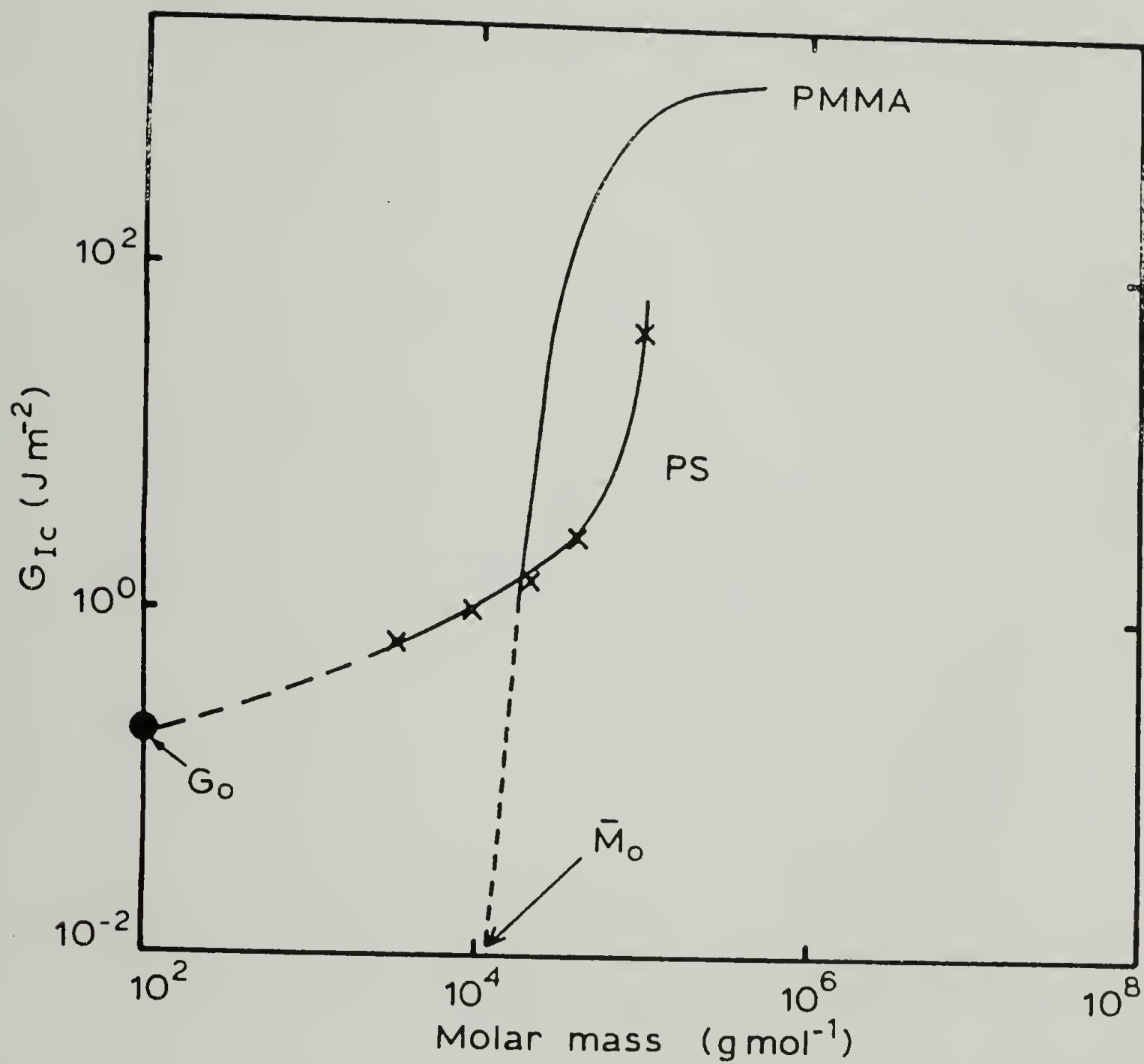


Figure 10.6. Dependence of fracture energy G_i , upon molar mass for polystyrene and poly(methylmethacrylate). M_0 is the "zero" stress molar mass.

REFERENCES

1. Anderson, H. C., in "Thermal Analysis", eds P. E. Slade Jr., L. T. Jenkins, 1966, vol. 1, p. 88
2. Maurer, J. J., Rubber Age (New York), **102** (2),47 (1970)
3. D'Alelio, G. F., D. M. Feigl, H. E. Kieffer, and R. K. Mehta, J. Macromol. Sci., A 2 (6), 1223 (1968)
4. Chiu, J., J. Polym. Sci., C, 8, 27 (1965)
5. Boni, R., B. Filippi, L. Ciceri, and E. Peggion, Biopolymers, 9 (12), 1539 (1970)
6. Mol, G. J., Plastic Des. Process., 11 (12), 20 (1971)
7. Reich, L., Macromol. Rev., 3, 49 (1968)
8. Chiu, J., "Polymer Characterization by Thermal Methods of Analysis", Marcel Dekker, Inc. N. Y., 1974, ch. 1, p. 6
9. Barrett, K. E. J., and H. R. Thomas, Brit. Polym. J., 2 (1-2), 45 (1970)
10. Rudin, A., H. P. Schreiber, and M. H. Waldman, Ind. Eng. Chem., 53, 137 (1961)
11. Wiesener, E., Faserforsch. Textiltech., 21 (12), 514 (1970)
12. Wunderlich, J., Phys. Chem., 69, 2078 (1965)
13. Gray, A. P., Thermochim. Acta, 1, 563 (1970)
14. Plato, C., Anal. Chem., 44, 1531 (1972)
15. Polymer laboratories "Dynamic Mechanical Thermal Analyzer Instruction Manual", England, 1982
16. Aklonis, J. J., and MacKnight, J. W.: "Introduction to Polymer Viscoelasticity", Wiley-Interscience, New York, 1972, ch. 3
17. Golden, J. H., Hammant, B. L and Hazell, E. A. ,J. Polym. Sci., **A2**, 4787
18. Kusy, R. P., and Turner, D. T., Polymer,**17**, 161 (1976)

19. Martin, J. R., Johnson, J. F., Cooper, A. R., J. Macromol. Sci-Revs. Macromol. Chem., **C8**, 57
20. Vincent, R. I., Polymer, **1**, 425 (1960)
21. McCormick, H. W., Brewer, F. M., Kin, L., J. Polym. Sci., **39**, 87 (1959)
22. Robertson, R. E., "Toughness and Brittleness of Plastics," Advances in Chemistry **154**, American Chemical Society, Washington, DC (1976) p. 89
23. Pitman, G. L., Ward, I. M., Polymer, **20**, 895 (1979)
24. Berry, J. P., J. Polym. Sci., **A2**, 4069 (1964)
25. Gent, A. N., Thomas, A. G., J. Polym. Sci., **A-210**, 571 (1972)

